Functional analysis of *Arabidopsis thaliana* lesion mimic mutant *cfs1* in ESCRT complex-related protein trafficking

I n a u g u r a l - D i s s e r t a t i o n

zur

Erlangung des Doktorgrades

der Mathematisch-Naturwissenschaftlichen Fakultät

der Universität zu Köln

vorgelegt von

Arpaporn Sutipatanasomboon

aus Bangkok, Thailand

Köln

2016

Berichterstatter/in: Prof. Dr. Martin Hülskamp

Prof. Dr. Ute Höcker

Prüfungsvorsitzender: Prof. Dr. Kay Hofmann

Tag der mündlichen Prüfung: 1 Dezember 2015

Kurzzusammenfassung

Die Endosomal Sorting Complex Required for Transport (ESCRT) - Maschinerie
besteht aus vier Komplexen, ESCRT-0-III. Diese sortieren am späten Endo-
somen mono-ubiquitinierte Proteine in intraluminale Vesikel, was zur Bildung
eines Multivesikulären Körpers (MVB) führt. Der MVB wird zur Vakuole
transportiert, wo sein Inhalt degradiert wird (Katzmann et al., 2001; Babst
et al., 2002a,b). In *Arabidopsis thaliana* führt der Verlust der ESCRT-I-Komponente
ELCH zu Cytokinese-Defekten (Spitzer et al., 2006); während die Expression
einer dominant-negativen Form der ESCRT-III-Komponente SKD1 zum Ver-
lustes der Vakuole und nachfolgend zum Zelltod führt (Shahriari et al., 2010a).

In dieser Arbeit wird die Funktion des pflanzenspezifischen ELCH-Interaktors
CELL DEATH RELATED FYVE/SYLF DOMAIN CONTAINING 1 (*CFS1*) und
seinen Einfluss auf die ESCRT-Maschinerie analysiert. CFS1 ist ein Phosphatid
ylinositol-3-Phosphat- und Actin-bindendes Protein (Herberth, 2012). Die *cfs1*
Mutanten imitieren Läsionen in der ersten älteste Blatt, das auf die nächste
älteste Blatt verbreiten. Es konnte gezeigt werden, dass die *cfs1*-Mutanten
unter normalen Bedingungen milde Autoimun-Symptome zeigen. Genetische
Analysen zeigen das der Zelltod in *cfs1* keinen funktionalen ESCRT-I-Komplex
voraussetzt, dennoch mildert der Verlust von *CFS1* den Cytokinese-Defekt der
elch-Mutante, was einen Einfluss auf die ESCRT-I-Funktion nahelegt. Auf-
grund einer Reduktion des Autophagosomen-Abbaus akkumuliert die *cfs1*-
Mutante im Laufe ihres Lebens Autophagosomen. Während die Pflanze altert,
triggeren die akkumulierten Autophaogosomen fälschlicherweise die Effektor-
getriggerte Immunität, was in seiner Konsequenz zum Zelltod in *cfs1* führt.
Da die ESCRT-Maschinerie am Transport von Autophagosomen zur Vakuole
beteiligt ist (Gao et al., 2015; Katsiarimpa et al., 2013; Spitzer et al., 2015) und
CFS2, ein CFS1 Homolog mit ATG8 interagiert (Stark et al., 2006), legen die
Ergebnisse dieser Arbeit nahe, dass CFS1 zusammen mit CFS2 eine Funktion
bei der Bindung von reifen Autophagosomen an MVBs übernimmt. An den
MVBs vermittelt die ESCRT-Maschinierie dann die Fusion von Autophago-
somen und MVBs für den nachfolgenden Transport zur Vakuole.

Abstract

The Endosomal Sorting Complex Required for Transport (ESCRT)-complex is composed of four complexes, ESCRT-0-III. They sequentially act on a late endosome to sort mono-ubiquitinated transmembrane proteins into the intralumenal vesicle, forming of a multivesicular body (MVB) that is delivered to vacuole for degradation (Katzmann et al., 2001; Babst et al., 2002a,b). In *Arabidopsis thaliana*, the loss of an ESCRT-I component, *elch* displays a cytokinesis defect (Spitzer et al., 2006); while a dominant negative expression of an ESCRT-III component results in cell death due to vacuolar loss (Shahriari et al., 2010a).

In this work, the function of a plant-specific ELCH-interactor, *CELL DEATH-RELATED FYVE/SYLF DOMAIN CONTAINING 1* (*CFS1*) and its influences on the ESCRT-complex function are investigated. CFS1 is a phosphatidylinositol 3-phosphate- and actin-binding protein (Herberth, 2012). The *cfs1* mutants mimic lesions in the first eldest leaf that propagate to the next eldest one. Genetic analyses have demonstrated that cell death in *cfs1* does not require a functional ESCRT-I component; nevertheless, the loss of *CFS1* alleviates *elch*-cytokinesis defect, suggesting its influence on the ESCRT-I function. Further analyses reveal that *cfs1* accumulates autophagosomes throughout its lifespan due to a decrease in autophagosome degradation, suggesting that as the plant ages, the cumulated autophagosomes falsely trigger effectors-triggered immunity that executes cell death in *cfs1*. As the ESCRT-complex has been demonstrated to be involved in the delivery of autophagosomes to vacuole (Gao et al., 2015; Katsiarimpa et al., 2013; Spitzer et al., 2015) and CFS1 homolog, CFS2 reportedly interacts with ATG8 (Stark et al., 2006), it can be postulated from the results of this work that CFS1 alone or together with CFS2 function in sequestering mature autophagosomes onto MVBs. At the MVBs, the ESCRT-complex then mediates the fusion of autophagosome and MVB for subsequent delivery to vacuole.

For *Mummy*,
my anchor, advisor, therapist and knight in shining armor!

And for *Papa*,
in loving memories (*10 May 1952 - 1 November 2003*).

Acknowledgements

My deepest gratitude goes to *Prof. Dr. Martin Hülskamp* for allowing me the opportunity to work on this project in his lab. I am truly grateful for having been able to spend these last four years with and being one of his lab members. My sincere gratitude goes to *Prof. Dr. Ute Höcker* for accepting to be my second referee in the examination on a rather short-noticed. And also for all her encouragement at the very beginning of my graduate study and her comments and suggestions in the progress seminar throughout the year. I also avail this opportunity to thank *Prof. Dr. Kay Hofmann* for kindly accepting to chair the examination.

My sincere gratitude goes to my supervisor, *Dr. Swen Schellmann* for his time and patience. I genuinely appreciate his support and all the though-provoking discussion. A huge thank you to *Dr. Stefanie Herberth* for her help ever since I first began to work on this project until the very moment I am handing in this thesis. I could only have completed this with my sanity still intact because of her support and encouragement! The same goes to *Britta Müller*, not only for her beautiful sections and TEM pictures but also for her support and encouragement on a professional and personal levels. I am truly grateful for having her next to me in the office and for our break on the balcony.

Thank you *Manuel Osuna-Martinez* and *Julian Müller*, who have produced great results during the internship and BSc thesis. Their findings have saved me time and helped piecing my data together in the discussion. I would like to thank the institute photographer, *Siegfried Werth* who has taken all the photographs of the mutants, particularly his willingness to do so on a short-notice; and the *gardeners* who have put up with my frequent 'bunny invasion' in the greenhouse.

I am extremely grateful to *Jane Parker* of the Max-Planck Institute for Plant Breeding, Cologne for providing the *eds1-2* and SA-biosynthesis mutants, as well as her comments and suggestions she gave during the many SFB635 meetings. Considerable findings in this work only came about because of her the

insights she readily offered. I am also grateful to **Moritz Nowack** of the Ghent University for sharing some of the unpublished developmentally-related cell death marker genes. I also like to thank **John Mundy** of the University of Copenhagen for providing the *laz1-5* and *nahG* seeds.

Thank you to all former and current *Hülskamp lab members*. They have been extremely helpful and supportive in all things science-related and otherwise. Especially, the sweetest & greatest **Alexandra Steffens**, who is *literally, the best office and lab mate anyone could ever ask for*. Thank you for all the help with *everything* lab and non-lab related. I am so thankful for her voluntarily taking her time to teach me and discuss with me. Our late night in the lab or the office are one of the most enjoyable time during the course my PhD.

Another thank you goes to **Marc Jakoby** for his help with the day-to-day work in the lab, suggestions and spontaneous discussions. And most importantly, for all the time that he *'lent'* me the lab gears on his bench. For the beautiful endomembrane system artwork, I would like to thank **Lisa Stephan** - without her original svg file, I would have taken weeks to generate and learn how to use Inkscape for this thesis! Thank you **Uschi Claßen** who bore with my immoderate plastic, chemical and other lab materials consumption in the last few months without a single complaint and for always encouraging me in the time that I needed it most. Also, another big thank you to the wonderful lab manager/waste queen, **Birgit Kernebeck** for her support and understanding during my writing period; and to **Christina Maria Franck & Aurélien Boisson-Dernier** who made my other-than-submission-deadline distress very short-lived; and to **Jessi Pietsch, Ilka Schultheiß, Heike Wolff, Hemal Bhasin and Divykriti Chopra** for always having their ears to let me talk my worries away; and to **Benjamin Jaegle** for his suggestions about dealing the thesis writing and not-quite-being-on-schedule stress.

Ganz herzlichen Dank an **Frauke & Heiner** für Eure Unterstützung, insbesondere in der Schreibenphase. Ich bin sehr dankbar für die Einladungen zu den Familienfeiern und Weihnachtsfesten, sowie für die 'Köln-ist-mir-zu-viel-deswegen-muss-ich-sofort-wegfahren' oder 'Ich-brauche-Zeit-und-Ruhe-damit-

Table of Contents

List of Figures

List of Tables

List of Abbreviations

35s	cauliflower mosaic virus 35s RNA promoter
°C	degree Celsius
μ	micro
A. tumefaciens	*Agrobacterium tumefaciens*
atg	*autophagy-related genes defecient*
E. coli	*Escherichia coli*
nahG	Bacterial enzyme naphthalene hydroxylase G
PstDC3000	*Pseudomonas syringae* pv. tomato DC3000
AAA	ATPase associated with various cellular activities
ACD	Accidental cell death
ACD11	ACCELERATED CELL DEATH 11
ALG2	APOPTOSIS-LINKED GENE 2
ALIX	APOPTOSIS-LINKED GENE-2 INTERACTING PROTEIN-X
AMSH1	ASSOCIATED MOLECULE WITH THE SH3 DOMAIN OF STAM 1
ANOVA	Analysis of Variance
ATG8a	AUTOPHAGY-RELATED 8A
Avr	Avirulent protein
BCL2	B-cell CLL/lymphoma 2
BFN1	BIFUNCTIONAL NUCLEASE 1
BIP1.1	LUMINAL BINDING PROTEIN 1.1
BIP2.1	LUMINAL BINDING PROTEIN 2.1
BIP3.1	LUMINAL BINDING PROTEIN 3.1
BPA1	BINDING PARTNER OF ACD11-1

BSA	Bovine serum albumin
bZIP60	BASIC REGION/LEUCINE ZIPPER MOTIF 60
CAN1	CALCIUM DEPENDENT NUCLEASE 1
CAPS	Cleaved Amplified Polymorphic Sequences
CASA	chaperone-assisted selective autophagy
CC	Coiled-coil domain
cFBPase	cytosolic Fructose-1,6-Bisphosphatase
CFS1	CELL DEATH-RELATED FYVE,SYLF DOMAIN CONTAINING 1
CFS2	CELL DEATH-RELATED FYVE,SYLF DOMAIN CONTAINING 2
CHIP	CARBOXYL TERMINUS OF HSC70 INTERACTING PROTEIN
CHMP1A	CHARGED MULTIVESICULAR BODY PROTEIN 1A
CHMP1B	CHARGED MULTIVESICULAR BODY PROTEIN 1B
CLSM	Confocal laser scanning microscope
Col-0	*Arabidopsis thaliana* ecotype Columbia-0
DAS	Days after sowing
DECP1	double FYVE domain-containing protein 1
DIC	Differential interference contrast microscopy
DMSO	Dimethyl sulfoxide
dNTPs	dideoxynucleotides
Dock4	Dedicator of cytokinesis 4
DUF500	Domanin of unknown function 500
EDS1	ENHANCED DISEASE SUSCEPTIBILITY 1
EDS5	ENHANCED DISEASE SUSCEPTIBILITY 5
EDTA	Ethylenediaminetetraacetic acid
EF1α	ELONGATION FACTOR 1α
eGFP	Enhanced green fluorescent protein

List of Abbreviations

EMS	Ethyl methanesulfonate
ER	Endoplasmic reticulum
ERF1	ETHYLENE RESPONSIVE FACTOR 1
ESCRT	Endosomal Sorting Complex Required for Transport
ETI	Effector-triggered immnunity
FES1A	FACTOR EXCHANGE FOR SSA1 PROTEIN1A
flg22	bacterial PAMP flagellin 22
FLS2	FLAGELLIN SENSING 2
FREE1	FYVE DOMAIN PROTEIN REQUIRED FOR ENDOSOMAL SORTING 1
FYVE	Fab1, YOTB, Vac1 and EEA1
GLY3	GLYOXALASE 3
GUS	β-glucuronidase
HR	Hypersensitive response
HRS	HEPATOCYTE GROWTH FACTOR-REGULATED TYROSINE KINASE SUBSTRATE
ICS1	ISOCHORISMATE SYNTHASE 1
ILV	Intralumenal vesicle
JA	Jasmonic acid
kb	kilobases
LAZ1	LAZARUS 1
LAZ5	LAZARUS 5
LIP5	LYST-INTERACTING PROTEIN 5
LMM	Lesion mimic mutant
LOX2	LIPOXYGENASE 2
M	molar
MC1	METACASPASE 1

MC2   METACASPASE 2

MC9   METACASPASE 9

min   minutes

MS   Murashige and Skoog basal medium

MVB   Multivesicular body

NB-LRR   Nuclear-binding leucin-rich repeats

NBR1   NEXT TO BRCA1 GENE 1

NDR1   NON RACE-SPECIFIC DISEASE RESISTANCE 1

NPR1   NON-EXPRESSOR OF PR GENES 1

PAGE   Polyacrylamide gel electrophoresis

PAMP   Pattern-associated molecular pattern

PBST   phosphate buffered saline Tween-20 solution

PCD   Programmed cell death

PCR   polymerase chain reactions

PDF1.2   PLANT DEFENSIN 1.2

PE   Phosphatidylethanolamines

PI3P   phosphatidylinositol-3-phosphate

PR1   PATHOGENESIS-RELATED GENE 1

PR2   PATHOGENESIS-RELATED GENE 2

PR3   PATHOGENESIS-RELATED GENE 3

PR5   PATHOGENESIS-RELATED GENE 5

PRA1.F3   PRENYLATED RAB ACCEPTOR 1.F3

PRO1   POSITIVE REGULATOR OF SKD1

PRR   Pattern recognition receptor

PTI   PAMPs-triggered immnunity

PVC   Prevacuolar compartment

List of Abbreviations

RCD	Regulated cell death
RD21	RESPONSIVE TO DEHYDRATION 21
RNS	Reaction nitrogen species
RNS3	RIBONUCLEASE 3
ROS	Reactive oxygen species
RT-qPCR	Real-time quantitative reverse transcription PCR
RuBisCO	RIBULOSE-1,5-BISPHOSPHATE CARBOXYLASE/OXYGENASE
SA	Salicylic acid
SAR	Systemic acquired resistance
SDS	Sodium dodecyl sulfate
sec	seconds
SH3P2	SH3 DOMAIN CONTAINING PROTEIN 2
SH3YL1	SH3 domain containing Ysc84-like 1
SID2	SALICYLIC ACID INDUCTION DEFICIENT 2
SKD1	SUPPRESSOR OF K($^+$) TRANSPORT GROWTH DEFECT1
SNARE	Soluble N-ethylmaleimide-sensitive factor Attachment protein REceptor
SYLF	SH3YL1, Ysc84p/Lsb4p, Lsb3p, plant FYVE proteins
SYP	SYNTAXIN OF PLANTS
TEM	Transmission electron microscopy
TIR	Toll-interleukin-1-receptor domain
U	units
UGT74E2	URIDINE DIPHOSPHATE GLYCOSYLTRANSFERASE 74E2
UPR	unfolded protein responses
UPS	ubiquitin/26S proteasome system
UTR	untranslated region

VPE	VACUOLAR PROCESSING ENZYME
vps	vacuolar protein sorting
VSP2	VEGETATIVE STORAGE PROTEIN2
Vta1	Vps20-associated 1
Ws-2	*Arabidopsis thaliana* ecotype Wasilewskaja
YAB	Ysc84 actin binding
YFP	Yellow fluorescent protein

The following nomenclature is used for plants:

- Gene name is written in italics; protein products of the gene in capitals without italics

- Wild-type allele of the gene is written in capitals; mutant allele in lower case letters

- Different alleles of the same gene is indicated by an Arabic number following a hyphen

The following nomenclature is used for yeast:

- Gene name is written in italics. In case of a gene name defined by mutation, dominant trait is written in capitals and recessive in lower case letters.

- Protein product is written as its gene without italics and followed by the suffic 'p'.

1. Introduction

1.1 Cell death as a means to flourish and survive

Cell death is a set of biochemical and molecular processes that lead up to a permanent termination of vital cellular activities (Galluzzi et al., 2014). When cell death occurs in a regulated manner, it facilitates the process of living. Multicellular organisms use cell death as a fundamentality of development and adaptation, including embryogenesis, shape sculpturing, and response to pathogen invasion or other abiotic stimulants (Fuchs and Steller, 2011). The execution of cell death in these processes differs in their natures and can be distinguished by the morphology of the cell corpse, which has been used as a basis for cell death classification (Reape et al., 2008; Galluzzi et al., 2012; van Doorn et al., 2011). Nevertheless, the corpse morphology unavoidably conceals the finer details of the molecular, biochemical or even functional processes that bring about cell death (Galluzzi et al., 2012).

1.1.1 Modes of cell death in animals

Research on cell death in the animal field has been more extensive and defined than in the plant field. Death that results from an unpreventable source is considered an *accidental cell death* (ACD) and can initiate a *regulated cell death* (RCD) event. RCD is controlled and preventable, including death during developmental processes that are collectively termed *programmed cell death* (PCD) (Galluzzi et al., 2014).

RCD mode can now be assigned to the associated biochemical and molecular basis (Galluzzi et al., 2012). *Apoptosis* is the most comprehensive form of cell death that is characterized by the fragmentation of the cell into smaller apoptotic bodies that are eventually engulfed by phagocytes. This mode can be initiated by intrinsic or extrinsic stimuli and is executed by caspase activity and pore-forming activity of the B-cell CLL/lymphoma 2 (BCL2) family mem-

bers (Galluzzi et al., 2014). Opposite to apoptosis is *regulated necrosis* (Vanden Berghe et al., 2014), also termed *necroptosis* (Kaczmarek et al., 2013), that occurs when the cell dies when or while caspase activity is suppressed (Galluzzi et al., 2012). *Autophagic cell death* is another mode of cell death that does not depend on caspase nor BCL2 members activity but on autophagy-mediated lysosome loading. It is distinguished by the presence of a massive lysosome in the cell (Galluzzi et al., 2012) and involves an increase in autophagy activity or degradation of its substrates (Kroemer and Levine, 2008).

1.1.2 Modes of cell death in plants

The mode of cell death in plants is still based on cell and/or cell corpse morphology (Reape et al., 2008; Reape and McCabe, 2008; van Doorn et al., 2011; van Doorn, 2011). The term *plant apoptosis* or *apoptotic-like cell death* has been adopted for plants (Reape et al., 2008; Reape and McCabe, 2008) despite a rigid cell wall that prevents the formation of apoptotic bodies (Lam, 2004) and the lack of a specialized cell that is functionally comparable to animal phagocyte (van Doorn et al., 2011). Furthermore, plants do not have any caspase in the genome that is fundamental to the execution of animal apoptosis (Tsiatsiani et al., 2011; Van Hautegem et al., 2015).

Van Doorn et al. (2011) have proposed the most commonly used terms describing the mode of plant cell death. First, *vacuolar cell death* or *autolytic PCD* (van Doorn, 2011) is the death that leaves an 'empty-walled cell corpse' (Figure 1.1a). Prior to an eventual death, changes in cytoskeletons occur, and cytoplasm slowly shrinks while the volume of lytic vacuole increases. The increased vacuole volume is correlated with autophagic activity (Minina et al., 2014). In the advanced stage, the tonoplast ruptures to release vacuolar content that rapidly clears the cytoplasm and organelles. This type of cell death occurs gradually (van Doorn et al., 2011) and is proposed to reflect a genetically programmed death to allows plant cells to process their own cellular corpse in a developmental PCD (Escamez and Tuominen, 2014).

The second mode of plant cell death is termed 'necrosis' or *non-autolytic* PCD (van Doorn, 2011). Opposite to vacuolar cell death, the dying of this sort
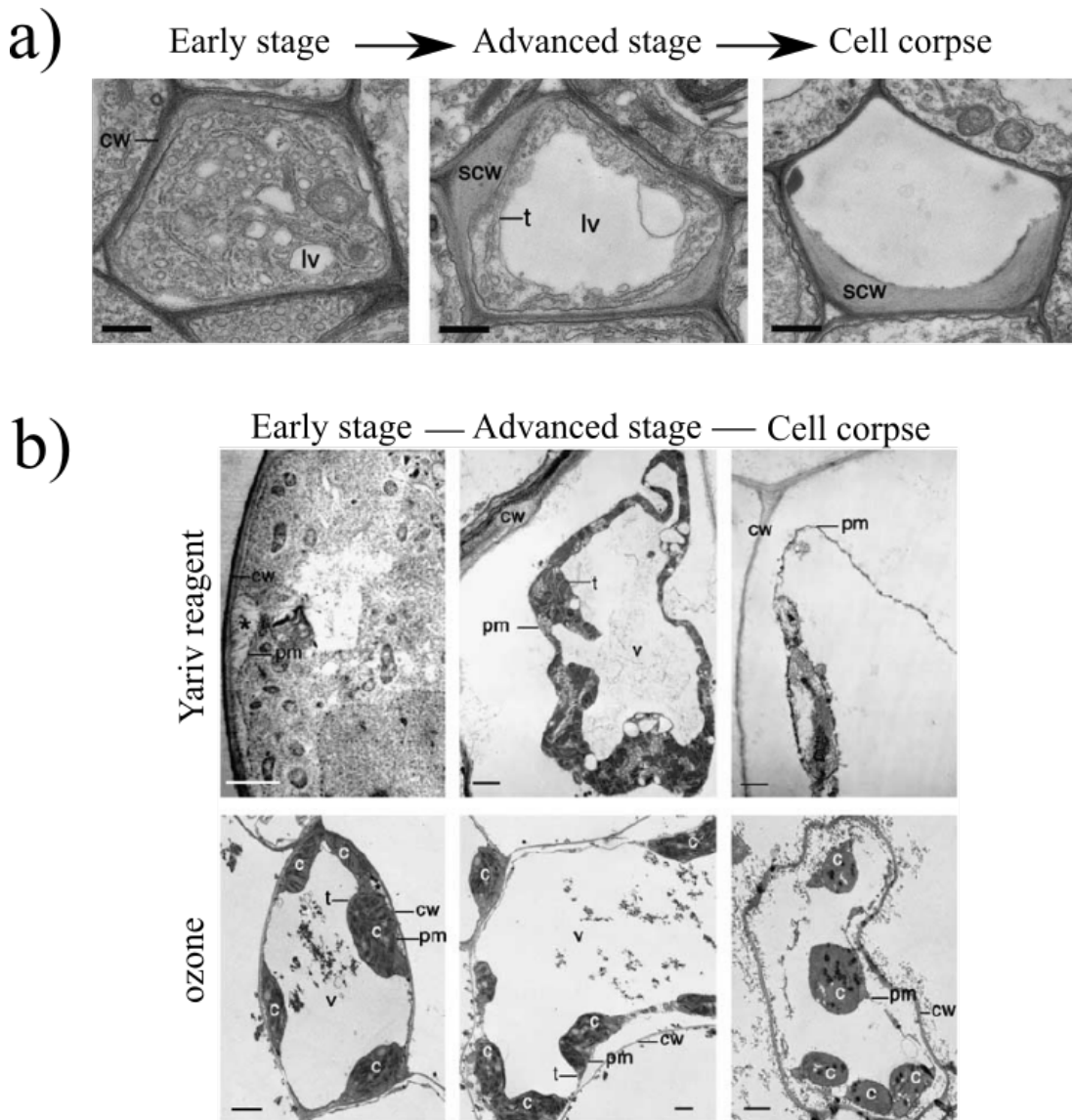
Figure 1.1: **Morphology of cell death in plant** - TEM images of cell death development in
a) Vacuolar cell death in *Arabidopsis* tracheary elements.
b) Necrosis cell death as seen in *Arabidopsis* subjected to by Yariv reagent and ozone treatments. Scale bars are 5μm.
c: chloroplast; cw: cell wall; pm: plasma membrane; scw: secondary cell wall; t: tonoplast; v: vacuole. Pictures are taken from van Doorn et al. (2011).

leaves behind an unprocessed corpse in the cell wall (Figure 1.1b). The most prominent feature preceding cell death is protoplast shrinkage without an increase in vacuolar volume. Frequently, the cell also accumulates reactive oxygen (ROS) and nitrogen (RNS) species. This mode of dying is associated with an acute response to stress, including cell death related to pathogen attack.

Whether vacuolar and necrosis cell death reflect a different underlying molecular mechanism or functional relevance is still much of a discussion (van Doorn et al., 2011; van Doorn, 2011; Reape and McCabe, 2013). For example, a mixture of processed (vacuolar cell death) and unprocessed (necrosis cell death) corpses has been reported in *Papaver* pollen self-incompatibility and victorin-induced cell death (van Doorn et al., 2011). In addition, it has been demonstrated in Norway spruce *(Picea abies)* that vacuolar cell death resulted from an undisturbed *death by autophagy* activity, and the inhibition thereof results in a *death with autophagy* that gives rise to necrosis cell corpse (Minina et al., 2013).

1.1.3   Cell death signals and executors in plants

The decision for a cell to die results from an integration of pro-death and pro-survival signals (Jones, 2001). The irreversible killing of the cell begins when it is overwhelmed with pro-death signals beyond the *point of no return* (Galluzzi et al., 2014). On a physiological level, several phytohormones can serve as a pro-death signal (Lam, 2004). Ethylene, for example, promotes senescence at plant growth completion that results in a collective cell death of an entire organ or plant (Thomas, 2013). Under pathogen attack, jasmonic acid (JA) and salicylic acid (SA) are also integrated into live-or-die decision (Lam et al., 2001).

Cell death can also be triggered on a cellular level. Jones (2001), Hatsugai and Hara-Nishimura (2010) have proposed that vacuolar maintenance and the discharge of its content precipitate cell death. Cell death is executed when tonoplast ruptures and VACUOLAR PROCESSING ENZYME (VPE), a cysteine protease, is released into the cytoplasm. In regard to vacuolar maintenance, cytoskeleton organization is also put forward as an active cell death signal (Smertenko and Franklin-Tong, 2011). Alternatively, vacuolar and plasma membrane can also fuse to release proteasomes into the extracellular space

(Hatsugai et al., 2009).

Analogous to animal cell death, signals derived from mitochondria and its membrane integrity have also been proposed (Lam, 2004). The release of cytochrome *c* from mitochondria occurs prior to the plant cell death (Reape et al., 2015) and interferes with several processes including protein folding, cellular redox maintenance and ROS homeostasis (Martínez-Fábregas et al., 2014). Parallel to mitochondria, the disruption or defects in photosynthetic electron transport chain in chloroplast also changes redox and ROS homeostasis that can induce rapid cell death (Mühlenbock et al., 2008; Bruggeman et al., 2015).

Metacaspase is another group of cystein proteases that recently emerges as functionally comparable to animal caspases (Sanmartín et al., 2005). They have been proposed to act in parallel to and with autophagy after the point of no return to execute cell death in developmental PCD (Minina et al., 2013, 2014) and in PCD after pathogen infection (Coll et al., 2014). *METACASPASE 1* and *2* (*MC1* and *MC2*, respectively) act antagonistically to promote the demise of bacterial-infected cells (Coll et al., 2010). *METACASPASE 9* (*MC9*) is implicated in the corpse clearance of treachery element (Escamez and Tuominen, 2014).

1.2 The plant immune system

Plants have evolved two coping strategies when infected with pathogens (Figure 1.2). The first line of defense involves pattern recognition receptors (PRRs), which are a group of transmembrane receptors that recognize pathogens-associated molecular pattern (PAMP). PRR recognition of PAMP activates *PAMP-triggered immunity* (PTI) (Jones and Dangl, 2006). Adapted pathogens can overcome this line of defense and invade the plant cell by unloading their virulent effectors (Coll et al., 2011), also termed *avirulence factors* or *Avr* proteins (Glazebrook et al., 1997). This activates the second type of defense called *effector-triggered immunity* (ETI) (Jones and Dangl, 2006) or *gene-for-gene resistance* (Glazebrook et al., 1997). Pathogen perception from PTI and ETI result in defense responses at the infection site and a number of cellular events, including a rapid influx of Ca^{2+} ions, transcriptional reprogramming of a defense-related genes and activation of a mitogen-activated protein kinase (MAPK) signaling cascade (Fig-
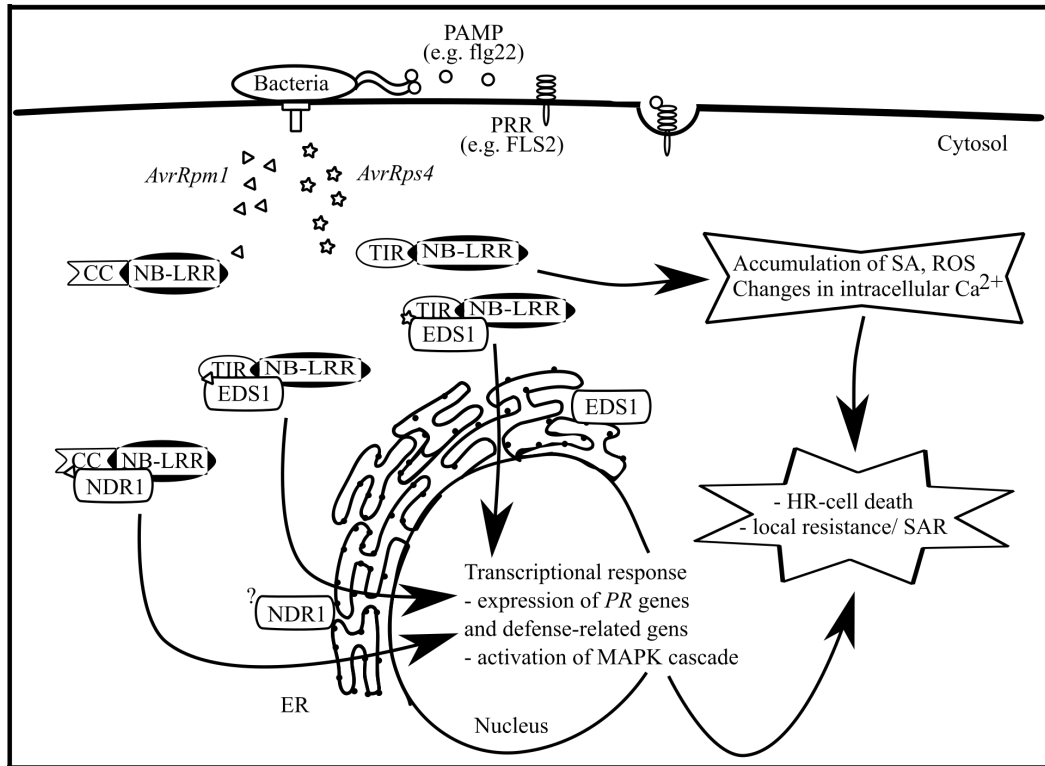
Figure 1.2: **Schematic representation of the two modes of the plant immune system** - PTI is triggered when a PRR recognizes PAMP and undergoes ligand-induced endocytosis. Adapted pathogens that can overcome this line of defense are faced with ETI. Pathogen effectors such as *Pseudomonas syringae AvrRpm1* and *AvrRps4* are recognized by receptor protein CC-NB-LRR and TIR-NB-LRR. The binding of effector and NB-LRR activates NDR1- or EDS1-mediated downstream responses that contribute to HR-cell death and local and systemic resistance. This figure is simplified from a model proposed by Teh and Hofius (2014).

ure 1.2; Dodds and Rathjen, 2010). In *Arabiodopsis thaliana*, PTI is activated at moderately elevated (23-32°C) temperatures while ETI at relatively lower temperatures (10-23°C) (Cheng et al., 2013).

1.2.1 Plant perception of pathogenic entities

The activation of ETI requires the plant ability to distinguish between the self and non-self molecules (Coll et al., 2011). To this end, virulent effectors are

sensed by nuclear-binding leucin-rich repeats (NB-LRR) receptor proteins or *R* genes (Glazebrook et al., 1997) that directly bind to virulent effectors or recognize proteins modified by pathogen effectors (Dodds and Rathjen, 2010). The recognition of compatible effectors activates signaling events that prime the plant for defense responses (Wiermer et al., 2005). Signals generated from NB-LRRs that contain a coiled-coil domain (CC) at the N-terminal are mediated by *NON RACE-SPECIFIC DISEASE RESISTANCE 1* (*NDR1*); while from NB-LRRs containing Toll-interleukin-1-receptor domain (TIR) at the N-terminal is mediated by *ENHANCED DISEASE SUSCEPTIBILITY 1* (*EDS1*) (Aarts et al., 1998). Mutant *ndr1* is susceptible to *Pseudomonas* effector proteins *avrRpt2*, *avrB*, *avrRpm1* and *avrPphB* but *eds1* only to *Pseudomonas syringae* effector protein *avrRps4* (Figure 1.2; Glazebrook et al., 1997; Parker et al., 1996).

1.2.2 Downstream responses of effector-triggered immunity

Signals from ETI can induce a more rapid, broader and stronger response to pathogen than from PTI. It modulates local resistance at the infection site as in PTI and also activates functionally overlapping SA, JA and/or ethylene signaling pathways (Dodds and Rathjen, 2010). The accumulation of SA, transcriptional reprogramming of defense-related genes and synthesis of anti-microbial compounds are essential for a broader *systemic-acquired resistance* (SAR) that affects the whole plant (Figure 1.2; Glazebrook et al., 1997; Coll et al., 2010). Pathogen-induced SA requires a functional *SALICYLIC ACID INDUCTION DEFICIENT 2* (*SID2*) that converts SA precursor, chorismate into isochrorismate (Wildermuth et al., 2001) in chloroplast (Serrano et al., 2013). SA transport into cytosol is mediated by *ENHANCED DISEASE SUSCEPTIBILITY 5* (*EDS5*) (Serrano et al., 2013), which partially contributes to SAR (Nawrath et al., 2002). SAR activation is correlated with the expression of *PATHOGENESIS-RELATED GENE 1, 2, 5* (*PR1*, *PR2* and *PR5*, respectively) (Glazebrook et al., 1997). SA-dependent SAR induction and the expression of *PR1*, *PR2* and *PR5* genes are under the control of *NON-EXPRESSOR OF PR GENES 1* (*NPR1*) (Cao et al., 1994).

1.2.3 Hypersensitive response

Hypersensitive response (HR) is a form of rapid cell death occurrs after plant-microbe interaction (Greenberg, 1996). It is intertwined with, but not equal to ETI and/or SAR (Wiermer et al., 2005; Coll et al., 2011). HR-cell death occurs at the initial infection site and then propagates to the neighboring cells to a certain degree (Greenberg, 1996). It is thought to be invoked only when the defense signal has crossed a certain cellular threshold (Lam et al., 2001; Jones and Dangl, 2006). On a microscopic level, it displays necrosis death mode with some additional features (van Doorn, 2011) such as cell wall thickening and organelle swelling (Dickman and de Figueiredo, 2011).

1.2.3.1 Lesion mimic mutant as a tool to unravel HR

Lesion mimic mutants (LMM) are mutants that display HR-cell death phenotype. LMMs can be classified into *initiation* mutants that spontaneously initiate cell death, or *propagation* mutants that fail to confine death in a local area (Lorrain et al., 2003) - a phenotype that is also referred as *'runaway cell death'* (Jabs et al., 1996; Brodersen et al., 2002). The majority of LMMs display an autoimmune phenotype, in which cell death is accompanied by constitutive expression of pathogen-associated markers (Lorrain et al., 2003; Palma et al., 2010). Identification and characterization of LMMs have untangled the molecular events leading up to HR (Lorrain et al., 2003; Coll et al., 2011). Oxidative stress related to photosynthesis or chloroplast maintenance, influx of ions or ROS and modulation of stress-related gene expression are major mechanisms identified that are directly involved in ETI processes. Another set of mechanisms identified are fatty acids homeostatis and intracellular trafficking (Bruggeman et al., 2015). For instance, the characterization of a LMM *accelerated cell death 11* (*acd11*) reveals that it is involved in regulating phytoceramide level in *Arabidopsis* (Brodersen et al., 2002; Simanshu et al., 2014). The loss of *syntaxin of plants 121* and *122* (*syp121 syp122*) result in a LMM phenotype. Both *syp121* and *syp122* are coat proteins that function in vesicular trafficking in the endomembrane system (Zhang et al., 2008).

1.3 Protein trafficking in the endomembrane system

The endomembrane system is composed of all single membrane-delimited organelles that are connected through a constant donating and receiving of vesicles (Figure 1.3). In the secretory pathway, vesicles containing newly synthesized proteins travel from endoplasmic reticulum (ER), trans-Golgi network (TGN) then plasma membrane or vacuole or lysosome. Conversely, transmembrane proteins or extracellular molecules are endocytosed from the plasma membrane and passed onto endosomes for delivery to vacuole (Bassham et al., 2008).
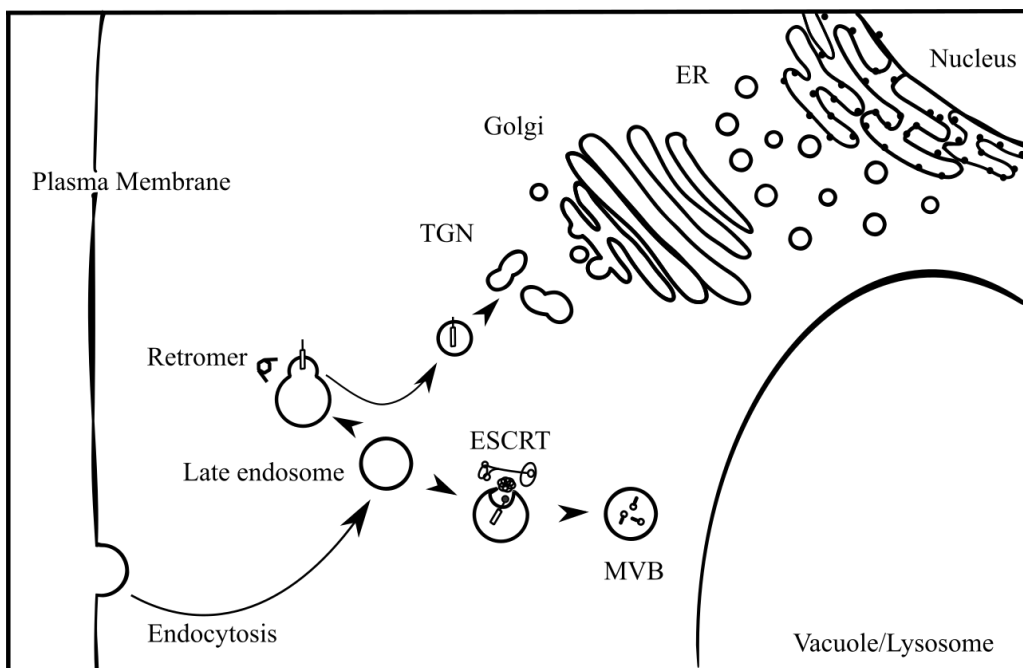
Figure 1.3: **Schematic representation of the protein trafficking in the endomembrane system** - Each organelle in the endomembrane system is connected through a constant donating and receiving of vesicles that are coated with proteins to mediate efficient trafficking. Sorting of endosomal cargo back to TGN requires retromer complex. The ESCRT-complex mediates the sorting of transmembrane proteins into the ILV of a late endosome, giving rise to MVBs that are delivered to vacuole/lysosome for degradation. This figure is modified from Herberth (2012).

Efficient vesicle trafficking relies on a distinctive assemblage of coat proteins on the donor compartment and receptor proteins on the membrane of the receiving organelle (Figure 1.3). For example, the sorting of vacuolar cargo receptor from endosomal compartment back to TGN requires the formation of a *retromer* complex; while the sorting of transmembrane proteins into intralumenal vesicles (ILV) of an endosome is mediated by the Endosomal Sorting Complex Required for Transport (ESCRT) (Schellmann and Pimpl, 2009). At the cargo's destination, cargo and organelle membrane fuse to release the cargo content. This fusion is facilitated by Soluble N-ethylmaleimide-sensitive factor Attachment protein REceptor (SNARE) proteins on the vesicles and a group of SNARE proteins called *syntaxins* on the membrane of targeted organelle (Bassham et al., 2008).

1.3.1 The ESCRT-complex

The ESCRT-complex recognizes and sorts of mono-ubiquitinated or lysin-63-linked polyubiquitinated transmembrane proteins into the ILV of a late endosome, giving rise to a specialized form called multivesicular bodies (MVBs) (Bache et al., 2003b; Babst, 2005). MVBs then travel to vacuole to unload their content for degradation (Katzmann et al., 2001).

1.3.2 The ESCRT-complex machinery

The ESCRT-complex is first identified in budding yeast (*Saccharomyces cerevisiae*) and is made up of four heteromeric complexes named ESCRT 0-III. They interact sequentially to recognize and incorporate its target into an ILV of an MVB (Figure 1.4; Katzmann et al., 2001; Babst et al., 2002a,b). ESCRT-0 initiates the machinery by one of its components, Vacuolar sorting protein27p (Vps27p). Vps27p recognizes its ubiquitinated target (Bache et al., 2003b) and enlists the ESCRT-I complex to the endosome (Raiborg et al., 2001; Bache et al., 2003a) by binding to one of ESCRT-I components, Vps23p (Figure 1.4a; Katzmann et al., 2001, 2003). ESCRT-I further recruits ESCRT-II and creates a cargo-enriched region that initiates membrane invagination (Figure 1.4b). ESCRT-II initiates ESCRT-III formation that in turn facilitates ILV formation and scission
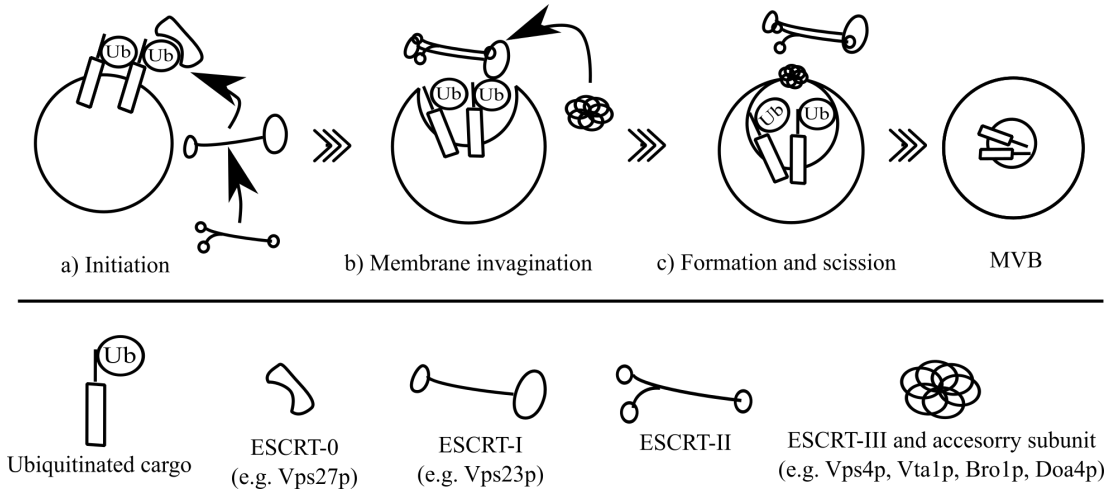
Figure 1.4: **Schematic representation of the ESCRT-complex machinery** - The ESCRT-complex interacts sequentially to form MVB.
a) ESCRT-0 initiates the machinery by recognizing ubiquitinated target. ESCRT-0 recruites the ESCRT-I that in turn enlists the ESCRT-II components.
b) ESCRT-I and ESCRT-II create a cargo-enriched region that facilitates membrane invagination and recruit ESCRT-III complex.
c) ESCRT-III and its accessory subunits remove ubiquitin from cargo and enclose ILV, forming a mature MVB.
The figure is recreated and adapted from Herberth (2012).

by recruiting *accessory ESCRT-III subunits* (Figure 1.4c; Babst et al., 2002a; Babst, 2005). Accessory ESCRT-III subunits, Bro1p recruits Doa4p to remove ubiquitin from the cargo before incorporating into the ILV (Babst et al., 2002b). After cargo has budded off into the MVB, Vps4p interacts with Vps20-associated 1p (Vta1) to dissociate the ESCRT-complex from the MVB membrane for the next sorting event (Babst et al., 1998; Babst, 2005).

In the *Arabidopsis* genome, most of the ESCRT-complex components and its accessory ESCRT-III subunits exist, except for the ESCRT-0 components (Winter and Hauser, 2006). They interact in a similar manner as in the yeast and mammalian system (Shahriari, 2008; Shahriari et al., 2011). For ESCRT-I components, two additional homologues of Vps23p (called *VPS23.1/ELCH*), *VPS23.2* and *VPS23.3* were found as well as another homologue of Vps28p (*VPS28.1* and *VPS28.2*) and Vps37p (*VPS37.1* and *VPS37.2*) (Shahriari, 2008). Additionally, two plant-specific ESCRT components were identified: FYVE

DOMAIN PROTEIN REQUIRED FOR ENDOSOMAL SORTING 1 (FREE1) as a part of ESCRT-I complex (Gao et al., 2014) and POSITIVE REGULATOR OF SKD1 (PRO1) as an interactor of Vps4p and Vta1p plant counterparts, SUPPRESSOR OF K^+ TRANSPORT GROWTH DEFECT 1 (SKD1) and LYST-INTERACTING PROTEIN 5 (LIP5), respectively (Reyes et al., 2014).

1.3.3 Consequences of a dysfunctional ESCRT-complex

In yeast, the components of the ESCRT-complex are among the *Class E vacuolar protein sorting* (*vps*) genes. Yeast lacking these *vps* genes display an accumulation of endosomes seen as a distinctive enlarged late endosome or *prevacuolar compartment* (PVC) that are referred as *class E compartment* (Raymond et al., 1992). Class E compartment reflects the failure to sort cargoes into the ILV of the MVB, which disturbs MVB maturation and its delivery to vacuole (Babst, 2005). In plants, the appearance of class E compartment was reported when the dominant negative version of SKD1 was expressed in tobacco, Arabidopsis cultured (Haas et al., 2007) and trichome cells (Shahriari et al., 2011), and in mutant plant lacking the Doa4p plant counterpart, *apoptosis-linked gene 2 interacting protein-x* (*alix*) (Kalinowska et al., 2015).

The absence of a functional ESCRT-component affects MVB maturation that also disturbs other biological processes. In most cases, the disturbance is a consequence of an endocytic down-regulation of transmembrane signaling receptors (Saksena and Emr, 2009). For example, *Arabidopsis* double mutant of ESCRT-III components, *charged multivesicular body protein 1a and b* (*chmp1a* and *champ1b*, respectively) displays a defective bilateral symmetry and polar differentiation due to the failure to sort auxin transportors, PINFORMED 1 and 2 (PIN1 and PIN2, respectively) and AUXIN-RESISTANT1 (AUX1) into the ILV of the MVB (Spitzer et al., 2009). The ESCRT-I mutant, *vps37.1* and *vps28.2* are impaired in PTI due to a decrease in the endocytosis of a PRR, FLAGELLIN SENSING 2 (FLS2) that perceives the bacterial PAMP, flagellin 22 (flg22) (Spallek et al., 2013).

Another disturbed process reported is the mutant of Vps23p plant counterpart, *elch*. It displays a unique cluster-like trichome phenotype in 2% of the
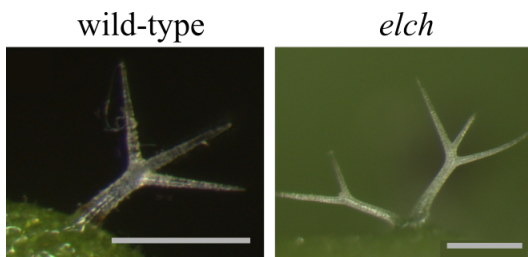
wild-type *elch*

Figure 1.5: **Representatives of wild-type and *elch* trichome** as seen in *elch*. Scale bar: 200µm.

trichomes. This cluster-like *elch*-trichome is an appearance of two trichomes stemming from a single pavement cell (Figure 1.5) that reflects a defect in cytokinesis (Spitzer et al., 2006). The *elch*-trichome phenotype is enhanced in the double and triple mutant of *elch* and other ESCRT-I mutants: *elch vps28.1*, *elch vps28.2*, *elch vps37.1*, *elch vps37.2* and *elch vps28.2 vps37.1* (Keshavaiah, 2008).

1.3.3.1   The ESCRT-complx and cell death

Mutants of most of the ESCRT-components in animal cells develop a *'cell-autonomous death through apoptosis'* phenotype, i.e. they die by apoptosis without any external stimulus (Wegner et al., 2011). This phenomenon was first described in mice lacking the mammalian Vps27p counterpart, HEPATOCYTE GROWTH FACTOR-REGULATED TYROSINE KINASE SUBSTRATE (HRS). Endodermal cells of these mice undergo non-programmed apoptosis causing mislocalized and misformed embryo (Komada and Soriano, 1999). Another example is the mammalian ALIX. It interacts with mammalian Vps23p/ELCH, ESCRT-III complex (Mahul-Mellier et al., 2006) and APOPTOSIS-LINKED GENE2 (ALG2) in a Ca^{2+}-dependent manner (Missotten et al., 1999) to initiate the caspase activity that executes neuronal cell death (Mahul-Mellier et al., 2009).

In *Arabidopsis*, ALIX also interacts with the same components - ELCH and ALG2 (Personal communication S Schellmann, L Kruppe) - and ALIX reduction results in lethality during vegetative growth (Kalinowska et al., 2015). Additionally, the lack of a functional SKD1 (Cai et al., 2014) and the over expression of dominant-negative SKD1 in trichome cells (Shahriari, 2008; Shahriari et al., 2010b) cause the cells to die from vacuole loss or fragmentation.

1.4 An ESCRT-I interactor, CFS1 displays a lesion-mimic phenotype

Another functional link between the ESCRT-complex and cell death in plants came from a phenotypic screening of an ESCRT-I interactor mutant, *cell death-related fyve,sylf domain-containing 1* (*cfs1*) that displays a runaway, lesion-mimic phenotype in both null (*cfs1-1* and *cfs1-2*) and non-null alleles (*cfs1-3*) (Sutipatanasomboon, 2012). CFS1 came up as FYVE2 from a bioinformatic screen for a Vps27p functional equivalence, along with another plant-specific proteins containing a Fab1, YOTB, Vac1 and EEA1 (FYVE) domain, FYVE1 (named CFS2 in this study) (Shahriari, 2008). Protein sequence revealed that FYVE1 and FYVE2 are homologous (Figure 1.6; Herberth 2012) and conserved throughout the plant kingdom (Herberth 2012; Personal communication B Marin).
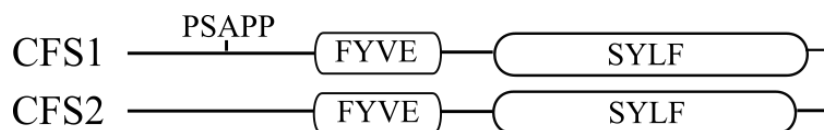
Figure 1.6: **Domain structure of CFS1 and CFS2** -CFS1 is homologous to another plant-specific protein CFS2. Both contain a FYVE domain at the N-terminal and a SYLF domain at the C-terminal. Only CFS1 has a PSAPP-motif that facilitates its interaction with ELCH. This figure is modified from Herberth, 2012

Both CFS1/FYVE2 and CFS2/FYVE1 possess a domain of an unknown function 500 (DUF500) (Figure 1.6; Herberth, 2012) that is homologous to an actin binding domain, Ysc84 actin binding (YAB) in yeast (Robertson et al., 2009; Herberth, 2012) and a phosphatidylinositol (3,4,5)-trisphosphate (PI(3,4,5)P(3)) binding domain named SH3YL1, Ysc84p/Lsb4p, Lsb3p, plant FYVE proteins (SYLF) in mammals (Hasegawa et al., 2011). Only CFS1 contains a PSAP-motif in the N-terminal that binds to ELCH and VPS23.2 (Shahriari, 2008; Herberth, 2012).

Biochemical characterization of FYVE2 revealed that its DUF500 domain binds to actin and phosphatidylinositol 3-phosphate (PI3P). This binding is

instrumental in the protein localization on late endosomes (Herberth, 2012). However, the lack of ubiquitin-binding property (Herberth, 2012) and FYVE2 influence on ELCH localization (Sutipatanasomboon, 2012) negate the hypothesis that FYVE2 acts as a plant Vps27p. Taken the biochemical findings and the mutant phenotype into consideration, *FYVE2* is therefore renamed to *CFS1*.

1.5 Aims of this study

Screening in Yeast-2-Hybrid and bimolecular fluorescence complementation have revealed CFS1 interactions with proteins involved in heat stress response such as CARBOXYL TERMINUS OF HSC70 INTERACTING PROTEIN (CHIP) and biotic stress response such as BINDING PARTNER OF ACD11 1 (BPA1) (Ulbricht, 2011). BPA1 binds to another lesion-mimic protein, ACD11 (Brodersen et al., 2002; Petersen et al., 2009). Mutant *acd11* displays an autoimmune phenotype, i.e. a runaway cell death phenotype without any pathogen perception and constitutive activation of a defense response (Brodersen et al., 2002; Palma et al., 2010). The phenotypic resemblance of *cfs1* and *acd11* phenotype, together with *CFS1* protein interaction network suggest its involvement in HR-cell death and implies a connection between the ESCRT-complex and immunity-related cell death (Sutipatanasomboon, 2012).

To provide a framework on how the ESCRT-complex factors in the plant HR-cell death, this study is aimed to unravel the role *CFS1* plays in plant cell death. To this end, the cell death phenotype in *cfs1* is characterized to investigate *CFS1* involvement in HR and the effect of its absence to ESCRT-complex protein trafficking.

2. Materials and Methods

2.1 Molecular cloning

For the purpose of plasmid amplification, *Escherichia coli* (*E. coli*) strain DH5α was employed. *E. coli* strain DB3.1 was used to amplify vectors containing *ccdB* operon. All *Agrobacterium tumefaciens* used in this study was of the strain GV3101 containing binary Ti plasmid pMP90RK (pTiC58Δ T-DNA). The chromosomal background was resistant to 25μM rifampicin; the binary Ti plasmid was resistant to 25μM gentamicin and 25-50μM kanamycin.

2.1.1 Cloning of *CFS1* promoter and genomic region

Genomic sequence of *CFS1* (AT3G43230) and its upstream region were retrieved from Seqviewer of The Arabidopsis Information Resource (November 2012 Release). Several oligonucleotides (Sigma-Aldrich) were designed to cover from 4.862kilobases (kb) upstream of *CFS1* until 0.380kb downstream of translation termination codon, 0.052kb of which was annotated as a part a 5′-untranslated region (UTR) of the next gene (AT3G43240) (Figure2.1, Table 2.1). The AscI and XhoI restriction sites were introduced to the 5′-end of primer ASU59 and ASU207 to facilitate subcloning (Figure 2.1).

Genomic DNA of *Arabidopsis thaliana* ecotype Columbia-0 (Col-0) was used as a template for polymerase chain reactions (PCR)-amplification. The region was split into three fragments, and each fragment was PCR-amplified in a 25μL reaction (1xHF-buffer, 0.5μM dideoxynucleotides (dNTPs), 1pmole forward and reverse primers each, 0.4U of High-Fidelity DNA Polymerases (Fermentas)) using the following condition: 2mins of initial denaturation at 98°C followed by 35 cycles of denaturation step at 98°C for 45sec, annealing at 55°C for 45sec and extension at 72°C for 1.5min, then final extension at 72°C for 5 minutes. PCR products were purified by column from GeneJET PCR purification kit (Fermentas) and ligated to pJET1.2 cloning vector from CloneJET
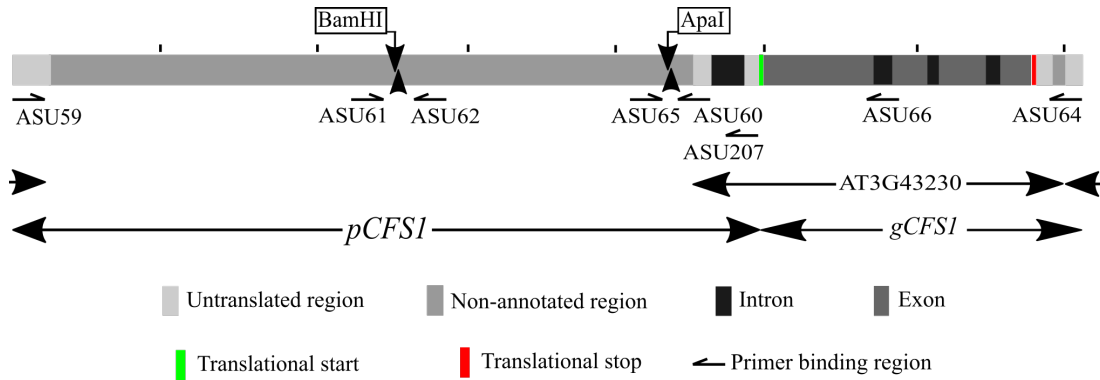
Figure 2.1: **Schematic representation of *AT3G43230* in the genome** - *CFS1* genomic region (*gCFS1*) and the upstream region considered as a promoter region (*pCFS1*). Primer sequences is listed in Table 2.1

Table 2.1: List of primers used in cloning of *CFS1* promoter and genomic region

Primer ID	Description	Primer
ASU59	3′UTR of AT3G43220 with AscI	GGCGCGCCaaaacgaagctcggatttca
ASU60	5′UTR of CFS1 with XhoI	CTCGAGcgatttatgggattgaagaa
ASU61	Promoter second fragment fwd	cataaggaaagtccaaagca
ASU62	Promoter second fragment rev	aagcaaaatcaagatttgaggat
ASU64	5′UTR of AT3G43240	cttggaaccaaatgattgat
ASU65	Promoter third fragment fwd	aaagatagaccgcatgaaaa
ASU66	genomic *CFS1* rev	cgatttatgggattgaagaa
ASU207	UTR CFS1 before ATG fwd with XhoI	CTCGAGgccttaaaaaatgaaacttcac

Non-native sequences are written in capital letters.

PCR Cloning kit (Fermentas) following the manufacturer's protocols. Plasmid DNA from ligation-positive transformant was sequenced in a 10µL reaction using BigDye® Terminator v3.1 Cycle Sequencing Kit (Applied Biosystems) with either 2.5µM pJET1.2 forward or reverse primer using the following condition: 2min of denaturation at 96°C followed by 35 cycles of denaturation at 96°C for 10sec, annealing at 55°C for 5sec and extension at 60°C for 4min. Capillary electrophoresis was performed by Cologne Center for Genomics. Obtained chromatograms were visualized and corrected using FinchTV (Geospiza) and sequences were aligned to template using CLC Main Workbench 7 (QIAGEN Aarhus A/S).

The first two fragments that contain the promoter region were fused via BamHI in *CFS1* sequence and XhoI site. The fused fragments were subcloned to pAM-PAT:2x35s::GUS, via its AscI and XhoI site to generate pCFS1::GUS. GUS in pCFS1::GUS was replaced by gCFS1 via ApaI site in pCFS1 and NotI site in pAMPAT.

2.1.2   Construction of genes tagged with fluorescent protein

Construction of a gene of interest tagged with a fluorescent protein was done using GATEWAY® recombination technology (Invitrogen) that enables the transfer of a specific DNA fragment to a binary vector using homologous recombination instead of ligation. By flanking the fragment with a specific attachment (*att*) site, the reading frame of the gene is maintained throughout the process.

First, the DNA sequence of interest is flanked by $attB_1$ and $attB_2$ sites from amplification with gene-specific primers. The obtained PCR product is incorporated to a donor vector via BP reaction. A donor vector contains an $attP_1$ and $attP_2$ site flanking the lethal *ccdB* gene that is disrupted after homologous recombination at the $attP_1$ and $attP_2$ sites. Successful recombination of DNA sequence into the donor vector is termed entry clone and is selected by the growth of *E.coli* DH5α on selection medium and subsequent restriction digestion of plasmid DNA, positive clones were chosen. Plasmid DNA from entry clones is sequenced to confirm the integrity of amplified sequence as described in the previous section. Finally, LR reaction is perform to transfer the DNA

2. MATERIALS AND METHODS

Table 2.2: List of vectors and their features

Vector name	Features	Plasmid selection (μM)
Cloning vectors		
pDONR201 (Invitrogen)	Contains attP-sites flanking *ccdB* operon	Kanamycin 25-50
pDONR207 (Invitrogen)	Contains attP-sites flanking *ccdB* operon	Gentamicin 25
pJET1.2 (Fermentas)	Contains multiple cloning sites in the *eco47IR* gene that is lethal to *E.coli* when expressed	Ampicilin 100 or Carbenicillin 50
Binary vectors		
pAMARENA-mCherry (Marc Jakoby)	Contains 2 cauliflower mosaic virus 35s RNA (2x35s) promoter, mCherry and Strep tag at the N-terminal of the attL-site flanking the *ccdB* gene and *BAR* gene cassette, encoding glufosinate resistance in plants	Ampicilin 100 or Carbenicillin 50
pAMPAT (GenBank: AY436765.1)	Contains 2x35s and attL-sites flanking the *ccdB* gene and *BAR* gene cassette, encoding glufosinate resistance in plants	Ampicilin 100 or Carbenicillin 50
pBatTL-eGFP (Joachim Uhrig)	Contains 35s promoter, eGFP tag at the C-terminal of the attL-site flanking the *ccdB* gene and *BAR* gene cassette, encoding glufosinate resistance in plants	Spectinomycin 50
pCFS1	Originated from pAMPAT but contains instead *CFS1* promoter region	Ampicilin 100 or Carbenicillin 50
pEarleyGate104 (Earley et al., 2006)	Contains 35s promoter, YFP tag at the N-terminal of the attL-site flanking the *ccdB* gene and *BAR* gene cassette, encoding glufosinate resistance in plants	Kanamycin 25-50
pENSG-YFP (Feys et al., 2005)	Destination vector containing 2x35s promoter, YFP tag at the N-terminal of the attL-site flanking the *ccdB* gene and *BAR* gene cassette, encoding glufosinate resistance in plants	Ampicilin 100 or Carbenicillin 50

fragment to a destination vector, a binary vector containing a promoter, $attL_1$ and $attL_2$ sites and the fluorescent tag such as enhance green fluorescent protein (eGFP), yellow fluorescent protein (YFP) or mCherry. Successful recombination is selected by the growth of *E.coli* DH5α on selection medium, followed by restriction digestion of plasmid DNA.

All donor and destination vectors used in this study are listed in Table 2.2. Entry and expression clones used in this study are listed in Table 2.3.

Table 2.3: List of constructs used in this study

Construct name	AGI code	Vector
mCherry-ARA7	AT4G19640	pAMARENA (Herberth, 2012)
YFP-ATG8a	AT4G21980	pENSG-YFP (Alexandra Steffens)
pCFS1-gCFS1	AT3G43230	pCFS1
CFS1 +stop		pDONR201 (Herberth, 2012)
GUS		pAMPAT
pCFS1:GUS		pCFS1
ELCH +stop	AT3G12400	pDONR201 (Spitzer et al., 2006)
YFP-ELCH		pEarleyGate104
SYP61 +stop	AT1G28490	pDONR207 (Florian Hessner)
mCherry-SYP61		pAMARENA
mCherry-VTI12	AT1G28490	pAMARENA (Marc Jakoby)

2.1.3 Transformation into host and plasmid DNA preparation

2.1.3.1 Transformation into *E.coli*

Desired constructs were introduced to *E. coli* DH5α or DB3.1 cells by heat shock transformation as follows: 50µL of competent cells were incubated with the construct at 42°C for 2 minutes, then 350µL of iced-cold liquid LB medium were immediately added to the cells then cultured at 37°C. After incubation for at least 30 minutes, the culture was spread on 1.5% agar- LB medium with the corresponding antibiotics listed in Table2.2 and grown overnight at 37°C.

2.1.3.2 Transformation into *Agrobacterium*

The construct was mixed with iced-cold chemically competent *Agrobacterium* and heat shock at 42°C for 2min, then 350µL iced-cold liquid YEB medium was immediately added to the cells and cultured at 28°C for two hours. One third of the culture was selected at 28°C for 48 - 72 hours on 1.5% agar-YEB medium containing the respective antibiotics listed in Table 2.2.

Plasmid DNA from transformed *E. coli* and *A. tumefaciens* were prepared by using the spin column-based GeneJET Plasmid Miniprep Kit (Fermentas). In case of *A. tumefaciens*, purified plasmid was introduced to *E. coli* DH5α as described, and the plasmid DNA obtained from *E. coli* was used for selection by restriction digestion.

2.2 Mutants and transgenic lines

All mutants used in this study, their corresponding locus, ecotype background and molecular markers are listed in Table 2.4. Mutant *cfs1-1*, *cfs1-2* and *cfs1-3* are *Agrobacterium* transferred DNA (T-DNA) insertion lines (Alonso et al., 2003) and were obtained from The Nottingham Arabidopsis Stock Centre. Britta Müller provided seeds of *elch, vps28.2, vps37.1* and *elch vps28.2 vps37.1 (i^3)*. Ethyl methanesulfonate (EMS)-mutagenized *esd1-2*, *eds5-1* and *sid2-1* were from Jane Parker (Max Planck Institute for Plant Breeding Research Cologne). John Mundy (University of Copenhagen) provided the *laz1-5* T-DNA insertion line (Malinovsky et al., 2010).

Stable transgenic plants used in this study were in Col-0 ecotype background and are listed in Table 2.5. Plants expressing bacterial enzyme naphthalene hydroxylase G (*nahG*) were obtained from John Mundy (University of Copenhagen) and Lifeact-eGFP (Riedl et al., 2008) from Alexandra Steffens (Steffens et al., 2014). Other transgenic lines were generated by Agrobacterium-mediated transformation using floral-dip method (Clough and Bent, 1998) or crossing to an existing transgenic line.

Table 2.4: List of mutants used in this study and the corresponding locus, ecotype background and molecular marker

Mutant name	Locus	Ecotype		Molecular markers
cfs1-1 (SALK_018265)	AT3G43230	Col-0	wild-type	PCR: primers ASU79 and ASU80
			mutant	PCR: primers ASU80 and ASU9
cfs1-2 (SALK_024058)	AT3G43230	Col-0	wild-type	PCR prrimers, ASU49 and ASU50
			mutant	PCR: primers ASU49 and ASU9
cfs1-3 (SALK_068647)	AT3G43230	Col-0	wild-type	PCR primers, ASU10 and ASU11
			mutant	PCR, primers ASU49 and ASU9
eds1-2 (Aarts et al., 1998)	AT3G48090	Col-0	wild-type	PCR: primers ASU83 and ASU84 resulted in 1.3 kb product
			mutant	PCR: primers ASU83 and ASU84 resulted in 0.4kb product
eds5-1 (Nawrath et al., 2002)	AT4G39030	Col-0	wild-type	CAPS: primers ASU157 and ASU158 then cleaved by LweI
			mutant	CAPS: primers ASU157 and ASU158, cannot be cleaved by LweI
elch (Spitzer et al., 2006)	AT3G12400	Wasilewskaja (Ws-2)	wild-type	PCR: primers BM-P20 and BM-P22 (Keshavaiah, 2008)
			mutant	PCR: primers BM-P20 and BM-P21 (Keshavaiah, 2008)
laz1-5 (SALK_034193) (Malinovsky et al., 2010)	AT4G38360	Col-0	wild-type	PCR: primer ASU81 and ASU82
			mutant	PCR: primer ASU81 and ASU9
nahG (Brodersen et al., 2005)		Col-0	mutant*	PCR: primer LK-P180 and LK-P181
sid2-1 (Wildermuth et al., 2001)	AT1G74710	Col-0	wild-type	CAPS: primers ASU155 and ASU156, cleaved by MunI
			mutant	CAPS: primers ASU155 and ASU156, cannot be cleaved by MunI
vps28.2 (SAIL_690_E05) (Keshavaiah, 2008)	AT4G05000	Col-0	wild-type	PCR: primers BM-P205 and BM-P206 (Keshavaiah, 2008)
			mutant	PCR: primers BM-P204 and BM-P205 (Keshavaiah, 2008)
vps37.1 (SAIL_97_H04) (Keshavaiah, 2008)	AT3G53120	Col-0	wild-type	PCR: primers BM-P208 and BM-P209 (Keshavaiah, 2008)
			mutant	PCR: primers BM-P207 and BM-P208 (Keshavaiah, 2008)

*domonant marker

The corresponding primer sequences are list in Table 2.6.

22

Table 2.5: List of transgenic lines used in this study

Transgenic line	Genotype	AGI code	Vector
Lifeact-eGFP	Col-0		pBaTL-eGFP (Phillip Thomas; Steffens et al., 2014)
Lifeact-eGFP	*cfs1-2*[c]		
mCherry-ARA7	Col-0[t]	AT4G19640	pAMARENA
	cfs1-2[c]		
mCherry-SYP61	Col-0[t]	AT1G28490	pAMARENA
	cfs1-2[c]		
mCherry-VTI12	Col-0[t]	AT1G28490	pAMARENA
	cfs1-2[c]		
nahG	Col-0		(Brodersen et al., 2005)
	cfs1-2[c]		
pCFS1:GUS	Col-0[t]	AT3G43230	pCFS1
pCFS1-gCFS1	*cfs1-1*[t]	AT3G43230	pCFS1
pCFS1-gCFS1	*cfs1-2*[t]	AT3G43230	pCFS1
pCFS1-gCFS1	*cfs1-3*[t]	AT3G43230	pCFS1

[t] generated by Agrobacterium-mediated transformation
[c] generated by crossing to an existing transgenic line

2.2.1 Crossing

Crossing was done by emasculating flowers of *cfs1* plants under a stereo microscope with a fine tweezer, and subsequent pollination was within 12-42 hours. F1 progeny were selected by the detection of a fluorescent signal or by resistance to glufosinate. Positive transformants were pooled for F2 seeds. Homozygous plants were selected in F2 generation as listed in Table 2.4, and phenotypic analysis was performed in F3. In case of dominant marker as in *nahG*, progeny of at eight F2 individuals were selected in the F3 generation.

2.2.2 Floral dip

Single transformed *Agrobacterium* clone was selected and cultured in 250mL YEB medium supplemented with antibiotics at 28°C for 48 - 72hours. Immature young flower buds of plants were dipped in overnight culture containing 5%(w/v) sucrose and 0.05%(v/v) of surfactant Silwet L-77 (Clough and Bent, 1998). Transformed plants were placed horizontally in darkness for 12-24 hours before transferring to the greenhouse. Transformed plants were selected

in T1 generation after cotyledons were fully opened for glufosinate resistance by spraying with 0.01%(v/v) Basta solution (Aventis) containing 0.001%(v/v) Tween-20.

2.2.3   Selection with molecular markers

PCR-amplification or Cleaved Amplified Polymorphic Sequences (CAPS) was employed for selection of individuals having homozygous loci (Table 2.4). All primers were designed using the Primer3 software (Untergasser et al., 2012). Their sequences are listed in Table 2.6.

2.2.3.1   DNA extraction

DNA for genotype determination was extracted from a 1-2cm leaf disc. The disc was crushed in a 2mL microcentrifuge tube using a QIAGEN Tissue Lyser for 1.5 minutes at 30Hz. Ground samples were briefly centrifuged, and 125µL of extraction buffer (25mM NaCl, 20mM Tris/HCl (pH = 8.0), 25mM ethylene-diaminetetraacetic acid (EDTA) (pH = 8), 0.5%(v/v) sodium dodecyl sulfate (SDS)) was added to the sample. The tube was inverted several times and 36.5µL of 3M sodium acetate (pH = 5.5) was added and centrifuged at maximum speed for 2 minutes. Supernatant was transferred to a new microcentrifuge tube, mixed with 125 µL isopropanol and centrifuged for 10 minutes at maximun speed. Supernatant was gently removed, and pellet was wash with 500µL absolute ethanol then centrifuged for 2 minutes at maximum speed twice. Supernatant was removed and air-dried and resuspended in 50µL sterile water.

Table 2.6: List of primer sequences used for genotyping

Primer ID	Description	Primer sequence (5' - 3')	Annealing temperature (°C)
ASU9	Lbb1.3	ATTTTGCCGATTTCGGAAC	
ASU10	Salk_068647 LP	AATCCCATAAATCGGATTTGC	56.5
ASU11	Salk_068647 RP	AACAGGGAGATTCAACCATCC	
ASU155	sid2-1fwd	TGCTTCTAGTGCTCGTGATA	55
ASU156	sid2-1rev	CACTCTGAAGATGGGTCACT	
ASU157	eds5-1fwd	CTGCACCTGTTTTATCTCC	55
ASU158	eds5-1rev	AATCTTCTCCACCGTGTATG	
ASU49	Salk_024058RP	CGGAAAAGCTTCTCCGTATTC	56.5
ASU50	Salk_024058LP	GCTCGACTAAGAACAGCATGC	
ASU79	Salk_018265LP	GAAGTTGAGATGGGGAAAACC	55
ASU80	Salk_018265RP	TTCGAAATGTTTCGTTTCTTGG	
ASU81	laz1-5 fwd	TCGCCAAAGTGTAGAAGAAGC	55
ASU82	laz1-5 rev	AGGGAAGAGAGGAGAGCAATG	
ASU83	eds1-2 fwd	CCCTTTCTAGTTTCCTTGAGCTAAG	55
ASU84	eds1-2 rev	TCAGGTATCTGTTATTTCATCCATC	
BM-P205	VPS28-2_RP	GACAAACGCGAAAGAGAGATG	58
BM-P206	VPS28-2_LP	TCAAATTAATAAAATTTCACGGTCC	
BM-P207	SAIL_LB	GCCTTTTCAGAAATGGATAAATAGCCCTTGCTTCC	58
BM-P208	VPS37-1_RP	TCCTGAGTTCATCCACGCTAC	58
BM-P209	VPS37-1_LP	TGGAGGATCTGATGGAGAATG	
BM-P20	elch rev	ATGGTTCCCCGCCGTCTAAT	58
BM-P21	elch mut fwd	TCAAAAAAGCACGTTCGGC	
BM-P22	elch WT fwd	CGATTCTCAGGCCCTGATCC	
LK-P180	nahG fwd	GCCTTAGCACTGGAACTCTG	55
LK-P181	nahG rev	TCGGTGAACAGCACTTGCAC	

2.2.3.2   PCR-amplification and CAPS

To determine the genotype of an individual with PCR, a 20µL PCR reaction was performed using DreamTaq™ Green PCR master mix (Fermentas) with 1pmole of each forward and reverse primer. The PCR condition was as follows: 2 minutes of initial denaturation at 94°C, followed by 35 cycles of denaturation at 94°C for 45 seconds, annealing for 45 seconds at the temperature indicated in Table 2.6, extension at 72°C for 1.5 minutes. Final extension was performed at 72°C for 5 minutes. The PCR products were separated and visualized in 1%(w/v) agarose gel electrophoresis stained with 0.1%(v/v) 10 mg/ml ethidium bromide.

For CAPS, the same PCR condition was used, but the reaction performed contained 1xDreamTaq™ PCR buffer, 1pmole of each forward and reverse primer, 1µM dNTPs and one unit of DreamTaq™ DNA polymerase (Fermentas). Afterwards, 10µL of PCR product was digested with 5 unit of restriction enzyme (Fermentas) as listed in Table 2.4. Digested product was separated and visualized in 2%(w/v) agarose gel electrophoresis stained with 0.1%(v/v) 10 mg/ml ethidium bromide.

2.2.4   Biolistic transformation

Biolistic transformation was employed to transiently express a gene of interested tagged with fluorescent protein in epidermal leaf cells. Coated particles were prepared as described in Mathur et al. (2003) with some modifications. For each transformation, approximately 1200ng of DNA was coated to 60mg of gold particles. 20µL of 2.5M $CaCl_2$ and 8µL of 0.1M spermidine were added to the coated gold particles. The mixture was filled up to 50µL by sterile water and vortexed for 10min. Coated particles were pelleted by centrifugation at 10,000rpm for 5sec. Supernatant was discarded by pipetting, and pellet was washed with 100µL 70%(v/v) ethanol, centrifuged and washed again with 40µL of absolute ethanol. Coat particles were then resuspend in 12µL absolute ethanol, spotted on a macrocarrier and air-dried. Each construct was bombarded to several epidermal cells using biolistic PDS-1000 He System (Biorad) with the following parameters: 900psi rupture disc pressure, 26-inch Hg

vacuum. After transformation, samples were incubated for 14-16 hours in the dark before observation.

2.3 Plant growth condition

Seeds were sown on 0.8%(w/v) agar half strength Murashige and Skoog basal (MS) medium (Duchefa Biochemie bv) or on soil, stratified at 4°C for 1-3 days and grown in greenhouse or growth chamber under long day condition (16 hours light, 8 hours dark) at 22°C, approximately 60% relative humidity, 150-300nmol light intensity. At elevated temperature, plants were grown in growth cabinet (SANYO versatile environmental test chamber, MLR-350) at 28°C under the same conditions as in growth chamber.

2.3.1 Surface sterilization

Seeds were sterilized by gently shaking in 70% ethanol for 5 minutes, followed by bleach solution (4%(v/v) sodium hyprochlorite, 0.1%(v/v) Triton™-X100) for 15 minutes. Seeds were washed at least three times with sterile water, suspended in 0.15% plant agar solution and plated on medium.
Alternatively, vapor-phase seeds sterilization was adopted by placing seeds in a desiccator next to chlorine gas. The gas was generated by mixing hydrochloric acid to 10% sodium hypochlorite solution (Carl-Roth) in 3:100 ratio.

2.3.2 Induction of nutrients starvation condition

To simulate nutrient starvation condition, components of MS medium were prepared as five separate stocks as listed in Table 2.7. Nitrogen source was removed from medium by replacing NH_4NO_3 and KNO_3 in stock A1 with equal mole of KCl. Seedlings were first germinated on 0.8%(w/v) agar MS medium prepared from stock A1, A2, B, C and D as described in Table 2.7. 7-10 day-old seedlings were transferred to either complete darkness or to MS medium lacking nitrogen supplemented with 1%(w/v) sucrose and grown for 10 days.

Table 2.7: Components of MS medium stock solutions

Component	Stock concentration	Working concentration
STOCK A1 (100x SALTS)		
NH_4NO_3	411.6 mmol	20.88 mmol
KNO_3	375.2 mmol	18.76 mmol
$CaCl_2 \cdot 2H_2O$	59.8 mmol	2.99mmol
KH_2PO_4	24.95 mmol	1.25 mmol
H_3BO_3	2.007 mmol	0.1 mmol
$MnSO_4 \cdot H_2O$	2.08 mmol	0.104 mmol
$ZnSO_4 \cdot 7H_2O$	0.6 mmol	0.03 mmol
KI	0.1 mmol	0.00498 mmol
$Na_2MoO_4 \cdot 2H_2O$	0.021 mmol	0.001037 mmol
STOCK A2 (100x)		
$CuSO_4 \cdot 5H_2O$	40 µmol	0.1 µmol
$CoCl_2 \cdot 6H_2O$	42 µmol	0.105 µmol
STOCK B (100x)		
$MgSO_4 \cdot 7H_2O$	15 mmol	1.498 mmol
STOCK C (200x)		
$Fe \cdot Na - EDTA$	1.998 mmol	0.0999 mmol
STOCK D (10000x)		
Thiamine hydrochloride	29.65 µmol	0.3 µmol
Glycine	2704 µmol	27.04 µmol
Nicotinic acid	406.154 µmol	4.074 µmol
Pyridoxine HCl	243.1434 µmol	2.439 µmol

Full-strength MS-medium is prepared by combining stock A1, A2, B, C and D then 0.56mmol myo-inositol is added. Medium is adjusted to pH = 5.8 with KOH

2.4 Real-time quantitative reverse transcription PCR

2.4.1 RNA preparation

Leaf 1 and 2 from five 28-30 days-old plants after germination were collected, pooled and frozen in liquid nitrogen. Samples were ground in liquid nitrogen using a mortar. Total RNA was extracted using RNeasy™ Plant Mini kit (QIAGEN) following the manufacturer's protocol. DNase digestion was perform with extracted total RNA using 1 unit of DNAseI (Fermentas) at 37°C for 30 minutes. DNAseI was inactivated by adding 2mM EDTA and incubated at 65°C for 10 minutes. The integrity of extracted RNA was tested by separation in 1.5 %(w/v) formaldehyde agarose gel stained with 0.1 %(v/v) 10 mg/ml ethidium bromide solution. The quantity of extracted RNA was determined by GE NanoVue Spectrophotometer.

2.4.2 First strand cDNA synthesis and RT-qPCR

After quantification, equal amount of total RNA were reverse-transcribed with an oligo(dT) primer and SuperScript™III reverse transcriptase (Invitrogen) following the manufacturer's instructions. Subsequent quantitative real-time PCR was performed with Power SYBR Green PCR Master Mix (Applied Biosystems) in an Applied Biosystems 7300 Real-Time PCR System. All reactions were performed in 10μL reaction using a two-step protocol as follows: initiation at 50°C for 2 minutes, 95°C for 10 minutes, 40 cycles of 95°C for 15 seconds, 60 °C for 1 minute, followed by a dissociation step at 95°C for 15 seconds, 60°C for 20 seconds then then 95°C for 15 seconds, 60°C for 15 seconds. Gene-specific primers used are listed in Table 2.8.

All data were from three biological replicates with two to three technical replicates each. Fold change in expression was calculated using $2^{\Delta\Delta C_T}$ method (Livak and Schmittgen, 2001) with *ELONGATION FACTOR-1ALPHA* (*EF1α*) as an endogenous control (Czechowski et al., 2005). Normality test was performed using Shapiro-Wilk normality test, and difference between groups were tested by the analysis of variance (ANOVA) or Kruskal-Wallis rank sum.

Table 2.8: List of gene-specific primer sequences used for RT-qPCR

Primer ID	Description	Primer sequence (5' - 3')	AGI code	Reference
RB70	ACT2_qPCR rev	ATCATACTCGGCCTTGGAGA	AT3G18780	Zhao et al. 2008
RB69	ACT2_qPCRfwd	TCCATTCTTGCTTCCCTCAG		
ASU285	ACT8_qPCRfwd	TCAGCACTTTCCAGCAGATG	AT1G49240	Mishiba et al. 2013
ASU286	ACT8_qPCRrev	ATGCCTGGACCTGCTTCAT		
ASU165	ATG8a_qPCRfwd	TAACCCTCTCGAGGCAAGG	AT4G21980	Katsiarimpa et al. 2013
ASU166	ATG8a_qPCRrev	TGTCAGGAACATCACTTTGTCC		
ASU167	ATG8b_qPCRfwd	TTCAAGCTTTCTAATCCTCTGGA	AT4G0462	Katsiarimpa et al. 2013
ASU168	ATG8b_qPCRrev	TCCAGCTTTTTCCACAATCAC		
ASU769	ATG8c_qPCRfwd	TTTCAAGTTGGAACACCCACTA	AT1G62040	Katsiarimpa et al. 2013
ASU170	ATG8c_qPCRrev	AGCTCTCTACGATCACTGGAA		
ASU173	ATG8e_qPCRfwd	ACCCTGATCGAATTCCTGTG	AT2G45170	Katsiarimpa et al. 2013
ASU174	ATG8e_qPCRrev	TTAGGTCTGATGGCACAAGGT		
ASU175	ATG8f_qPCRfwd	TCCTGATAGGATTCCGGTGA	AT4G16520	Katsiarimpa et al. 2013
ASU176	ATG8f_qPCRrev	AAACTGCCCCACAGTCAGAT		
ASU177	ATG8g_qPCRfwd	CCCAAACATTGACAAGAAGAAA	AT3G60640	Katsiarimpa et al. 2013
ASU178	ATG8g_qPCRrev	CATACACAAACTGGCCTACCG		
ASU179	ATG8h_qPCRfwd	GGGGATTGTTGTCAAGTCTTTC	AT3G06420	Katsiarimpa et al. 2013
ASU180	ATG8h_qPCRrev	TGCGTTTGAATATTTCTCAATGAT		
ASU181	ATG8i_qPCRfwd	CGCTAAGTACCCTACTCGGATTC	AT3G15580	Katsiarimpa et al. 2013

Table 2.8: List of gene-specific primer sequences used for RT-qPCR – *continued from previous page*

Primer ID	Description	Primer sequence (5' - 3')	AGI code	Reference
ASU182	ATG8i_qPCRrev	TCTCTTGGAACCAGAAACTTCTTT		
ASU301	BFN1_qPCR fwd	ATCGCTTGTCCACACAAGTATGC	AT1G11190	
ASU302	BFN1_qPCRrev	ACCAGACTTGACGCCTTTGTATCC		
ASU267	BIP1.1_qPCR fwd	TCAGTCCTGAGGAGATTAGTGCT	AT5G28540.1	Mishiba et al. 2013
ASU268	BIP1.1_qPCRrev	TGCCTTTGAGCATCATTGAA		
ASU271	BIP2.1_qPCR fwd	GGAAATTCGACCTCACTGGA	AT5G42020.1	Mishiba et al. 2013
ASU272	BIP2.1_qPCR rev	GCCTTGTCCTCTGCTTTCAC		
ASU269	BIP3.1_qPCR fwd	CGAAACGTCTGATTGGAAGAA	AT1G09080	Mishiba et al. 2013
ASU270	BIP3.1_qPCR rev	GGCTTCCCATCTTTGTTCAC		
ASU273	bZIP60s spliced fwd	AAGCAGGAGTCTGCTGTTGG	AT1G42990.1	Mishiba et al. 2013
ASU274	bZIP60s spliced rev	TTTGTGTGGGACATATAAGGGAAT		
ASU275	bZIP60 unspliced fwd	AGTCTGCTGTGCTCTTGTTGG		
ASU276	bZIP60u unspliced rev	GCAACACTTTGTGTGGGACATA		
ASU318	CAN1_qPCRfwd	ACTTCGAGACCACTTCTCAGGTTC	AT3G56170	
ASU319	CAN1_qPCRrev	TTTGGGAAGACACAACGTAACTCC		
ASU337	EF1alpha_qPCRfwd	TGAGCACGCTCTTCTTGCTTTCA	AT5G60390	Czechowski et al. 2005
ASU336	EF1alpha_qPCRrev	GGTGGTGGCATCCATCTTGTTACA		
ASU279	ERF1_qPCRfwd	TCGGCGATTCTCAATTTTTC	AT3G23240.1	Tintor et al. 2013
ASU280	ERF1_qPCRrev	ACAACCGGAGAACAACCATC		

Continued on next page

Table 2.8: List of gene-specific primer sequences used for RT-qPCR – *continued from previous page*

Primer ID	Description	Primer sequence (5′ - 3′)	AGI code	Reference
ASU314	FES1A_qPCRfwd	CCCAGGCTCTTGGCGCAATATCATC	AT3G09350.1	Hackenberg et al. 2013
ASU315	FES1A_qPCRrev	GGCAAGCTTGAAAGCCGTTACTC		
ASU308	GLY3_qPCRfwd	ACCTTGAGGTTCGTGCTACACC	AT1G53580	
ASU309	GLY3_qPCRrev	GATCAGCTCCTTCACCAGTCAC		
ASU281	LOX2_qPCRfwd	GATGCCCCAGTTCTCATTAACAGGG	AT3G45140	Danisman et al. 2012
ASU282	LOX2_qPCRrev	CGGGTCTAGTTTGCTTATTAACGGC		
ASU302	MC1_qPCRfwd	TGCTTGCCATAGTGGTACCGTTC	AT1G02170	
ASU303	MC1_qPCRrev	ACACATACTGCCCAGCTCTGTTC		
ASU326	MC9_qPCRfwd	AGGCAGTCCTTGACCACTTGAG	AT5G04200	
ASU327	MC9_qPCRrev	TGTGTGCCGATGTCGGAAGTTG		
ASU334	NBR1_qPCRfwd	GAGGAAATGGGTTTCAAGGA	AT4G24690	Zhou et al. 2013
ASU335	NBR1_qPCRrev	ATTGGATCCCACTCGCTAAC		
ASU122	PDF1.2_qPCRfwd3	TGCTTCCATCATCACCCTTA	AT5G44420	
ASU123	PDF1.2_qPCRrev3	CCTGACCATGTCCCACTTG		
ASU184	PR1_qPCRrev	TTCACATAATTCCCACGAGGA	AT2G14610	Katsiarimpa et al. 2013
ASU183	PR1_qRTfwd	GATGTGCCAAAGTGAGGTGTAA		
ASU95	PR2_qPCRfwd	GTCTGAATCAAGGAGCTTAGCC	AT3G57260	
ASU96	PR2_qPCRrev	AGCATACTCCGATTTGTCCAG		
ASU283	PR3-qPCRfwd	ACGGAAGAGGACCAATGCAA	AT3G12500.1	Abe et al. 2013

Continued on next page

Table 2.8: List of gene-specific primer sequences used for RT-qPCR – *continued from previous page*

Primer ID	Description	Primer sequence (5' - 3')	AGI code	Reference
ASU284	PR3_qPCRrev	GTTGGCAACAAGGTCAGGGT		
ASU185	PR5_qPCRfwd	GACTGTGGCGGTCTAAGATGT	AT1G75040	Katsiarimpa et al. 2013
ASU186	PR5_qPCRrev	TGAATTCAGCCAGAGTGACG		
ASU306	RD21_qPCRfwd	GCTCATCAACCCATTAGCATTGCCA	AT1G47128	
ASU307	RD21_qPCRrev	ACCCGAATCATAGAGCTGGAACG		
ASU304	RNS3_qPCRfwd	AAGCTGGTCTCAAGCTCAAACAG	AT1G26820	
ASU305	RNS3_qPCRrev	TCCGGTTTGATCCCAGCATTGG		
ASU93	SAG12_qPCRfwd	TGCTTTGCCGGTTCTGT	AT5G45890	
ASU94	SAG12_qPCRrev	TGAAAAGCGCCAACAACAT		
ASU189	SAG13_qPCRfwd	AGGAAAACTCAACATCCTCGTC	AT2G29350	Katsiarimpa et al. 2013
ASU190	SAG13_qPCRrev	GCTGACTCGAGATTTGTAGCC		
ASU310	UGT87E_qPCRfwd	CGAGTCGACATAGTGTTGTGC	AT1G05680	Hackenberg et al. 2013
ASU311	UGT87E2_qPCRrev	CACAAGCTTTGGACCCATTTCA		
ASU277	VSP2_qPCRfwd	TCAGTGACCGTTGGAAGTTGTG	AT5G24770.1	Tintor et al. 2013
ASU278	VSP2_qPCRrev	GTTCGAACCATTAGGCTTCAATATG		
ASU91	WRKY53_qPCRfwd	CGGAAGTCCGAGAAGTGAAG	AT4G23810	
ASU92	WRKY53_qPCRrev	TCTGACCACTTTGGTAACATCTTT		

2.5   Histology and microscopy

2.5.1   Trypan blue staining

The degree of dead cells in the leaf was quantify by area of cells positivly stained by trypan blue. Staining procedure were performed with some modification from Bowling et al. (1997). Leaves were detached and submerged in 70°C trypan blue staining solution (2.5mg/ml trypan blue, 25%(w/v) lactic acid, 23%(v/v), saturated phenol, 25%(v/v) glycerol). The staining solution were vacuum infiltrated for 5 minutes and boiled for 2 minutes. Specimens were removed after solution has cooled and destained several times in 2.5g/mL chloral hydrate until cleared and equilibrated in 70%(v/v) glycerol. Images of stained samples were taken with a stereo microscope (Leica MZ16F Binocular UV microscope).

2.5.2   Vacuolar staining

To visualize vacuoles, 5-7-days old seedlings were stained with flouresceine diacetate (FDA), 2',7'-Bis-(2-Carboxyethyl)-5-(and-6)-Carboxyfluorescein, Acetoxymethyl Ester (BCECF-AM) and *N*-(3-Triethylammoniumpropyl)-4-(6-(4-(Diethylamino) Phenyl) Hexatrienyl) Pyridinium Dibromide (FM4-64).
FDA solution was prepared as a 5mg/ml stock in acetone and kept in 4°C until used. FDA stock solution was diluted in 1:1000 in half-strength MS medium and incubated with seedlings for 30 minutes. Before visualization, seedlings were washed three times to remove excess dye with half-strength MS medium. Samples were excited with 494nm laser line, and emission collection was set at 505-525nm.
BCECF-AM was prepared as a 10mM stock solution and diluted in 1:1000 in half-strength MS medium for staining. Seedlings were incubated with staining solution for 20 minutes. Seedlings were washed twice with half-strength MS medium. Samples were excited with 488nm laser line and detectiong length was 520-550nm.
FM4-64 was prepared as a 0.5%(w/v) stock solution in DMSO and diluted

in 1:1000 in half-strength MS medium for staining. Seedlings were incubated with ice-cold staining solution for 5 minutes and at room temperature for 20-30 minutes. Seedlings were washed twice with half-strength MS medium. Samples were excited with 488nm laser line, and signal was detected at 625-665nm.

2.5.3   Pavement cell complexity measurement

Pavement cell complexity measurements were performed by preparing epidermal agarose imprints as described in Mathur and Koncz (1997). Cotyledons were placed on setting 3%(w/v) low-melting agarose (Biozym Scientific) in water and refrigerated until completely set. The imprints were visualized and imaged using differential interference contrast microscopy (DIC) (Leica DM5000B). Measurements were taken from four cells each from five plants using circularity function built in ImageJ (Schneider et al., 2012).

2.5.4   GUS-staining

Transgenic *pCFS1::GUS* plants were plated on half strength MS medium for several time points to examine β-glucuronidase (GUS) expression driven by *CFS1* promoter. Plant materials were incubated in GUS staining solution (50mM sodium phosphate buffer (pH = 7.2), 2mM potassium ferrocyanide, 2mM potassium ferricyanide, 2mM X-Gluc, 0.2% Triton X-100) and gently vacuum infiltrated for 15 minutes. Samples were incubated in staining solution at 37°C for 6-24 hours.

To observation the staining pattern with stereo microscope, chlorophyll of stained samples were cleared by rinsing with water and incubate in increasing concentration of ethanol (20%(v/v), 35%(v/v), 50%(v/v), 70%(v/v)) each for 2 hours at room temperature.

2.5.5   *elch*-trichome analysis

The number of wild-type and *elch* trichome were observed with stereo microscope and counted manually. The difference in the ratio of *elch*-trichomes to

all trichomes between genotypes was tested using Fisher's exact test and Pearson's χ^2 test of independence.

2.5.6 Fluorescence microscopy

Fluorescent signal from transiently expressed plants and stable transgenic lines were screened with a stereo microscope (Leica MZ16F) and a fluorescent microscope (Leica DMRA2).

2.5.7 Confocal laser scanning microscopy

All observations made with confocal laser scanning microscopy (CLSM) were done using either Leica TSC SPE or Leica TSC SP8. Subsequent image analysis was perform with ImageJ2/Fiji software (Schindelin et al., 2012, 2015).

2.5.8 Transmission electron microscopy

For transmission electron microscopy (TEM), leaf 1 and 2 from Col-0 and *cfs1* from 25-30 day-old plants were collected, immediately fixed in fixation solution (2.5%(v/v) glutaraldehyde, 2%(v/v) paraformaldehyde, 80mM HEPES buffer pH =7.0) and washed three times in the HEPES buffer.
Britta Müller performed all the processes after fixation. Postfixation was conducted in 1% OsO_4 in 80mM HEPES buffer (pH =7) for 2 hours at room temperature followed by washing 3 times in the HEPES buffer and treated with 1% (w/v) uranylacetate in HEPES buffer overnight in the dark at 4°C. Dehydration was achieved by washing in increasing acetone concentration (10%(v/v), 20%(v/v), 30%(v/v), 50%(v/v), 70%(v/v), 90%(v/v), 95%(v/v), 100% (v/v) acetone) on ice. SPURR resin (SPURR:acetone in 1:3, 1:1, 3:1, 1:0) were infiltrated to samples for 2h for each combination and for 1:0 SPURR:acetone, dehydrated samples were polymerized overnight at 70°C (Spurr, 1969). Semi-thin sections (1μM) and 60-80 nm ultra-thin sections were prepared with a Leica EM UC7 microtome equipped with a DiATOME diamond knife at 45°angle. Semi-thin sections were stained with a 1%(v/v) toludine blue in 1% Borax: 1% Pyronin G solution (5 : 1). Ultrathin sections were mounted on pioloform cov-

ered with 1mm copper grids, contrasted with Reynolds lead citrate (Reynolds, 1963) for one minute and observed with a Philips CM10 TEM. Micrographs were taken with an Orius SC200W CCD camera equipped with the DigitalMicrograph software (Gatan Inc.).

2.6 Biochemical methods

2.6.1 Sample preparation

Samples for western blot were prepared according to Zhou et al. (2013) with some modifications. Plant materials from various stages were collected and ground in liquid nitrogen using a mortar. Detergent protein extraction buffer (100mM Tris/HCl (pH = 8.0), 10mM NaCl, 1mM EDTA (pH = 8.0), 1%(v/v) Triton X-100, 0.2% β-mercaptoethanol, 25mM N-Ethylmaleimide) was immediately added to the sample, and the lysate was filtered through 210µm and 70µm nylon mesh to obtain crude extract.

To ensure equal amount of total protein for subsequent experiments, crude extract was mixed with Laemmli buffer (50mM Tris/HCl (pH=6.8), 2%(w/v) SDS, 10%(v/v) glycerol, 0.01%(w/v) bromophenol blue, 100mM DTT), heated for 5 minutes at 95°C and separated by SDS-Polyacrylamide gel electrophoresis (PAGE) at constant 25mA per gel. Polyacrylamide gels were rinsed several time with distilled water and stained with colloidal Coomassie blue solution (10%(w/v) ammonium sulfate, 0.1% Coomassie Brilliant Blue G-250, 3%(v/v) $ortho$-phosphoric acid, 20%(v/v) ethanol) for 4-16 hours. The gels were destained several times in water. Total protein amount was quantified and adjusted with Laemmli buffer according to an area size of an approximately 55kDa RIBULOSE-1,5-BISPHOSPHATE CARBOXYLASE/OXYGENASE (RuBisCO) band. Calculation was performed using Gel analysis function in ImageJ2/Fiji software (Schindelin et al., 2012, 2015).

2.6.2 Western blot

Separated proteins on polyacrylamide gels were transferred to PVDF membrane in semi-dry condition. The transfer was performed at constant 2.5 mA per transfer hour at 4°C. The presence of PageRuler™prestained protein ladder (Thermo Scientific) on membrane was used to determine successful and complete transfer of proteins onto membranes.

Table 2.9: List of antibodies used in this study

Antibody	Clonality	Predicted size (kDa)	Host	Dilution	Lot number
Primary antibody					
anti-ATG8a (abcam; ab77003)	Polyclonal	14	rabbit	1:500	GR193264-1
anti-cFBPase (Agrisera; AS04 043)	Polyclonal	45/37	rabbit	1:5000	1104
anti-NBR1 (Agrisera; AS14 2805)	Polyclonal	100/75	rabbit	1:2000	1410
anti-Ub(P4D1) (Santa Cruz; sc-8017)	Monoclonal		mouse	1:500	G0913
Secondary antibody					
anti-mouse (JacksonImmuno; 115-035-003)	Polyclonal		goat	1:5000	107936
anti-rabbit (Sigma-Aldrich; A6154)	Polyclonal		goat	1:5000	SLBK2462V

For detection with anti-Ub(P4D1), proteins blotted onto membrane were denatured by incubating in denaturating buffer (6M Guanidine hydrochloride, 20mM Tris, 5mM β-mercaptoethanol and 1mM phenylmethylsulfonyl fluoride) for 30 minutes at 4°C under agitation. The membrane was washed in phosphate buffered saline Tween-20 (PBST) solution (137mM NaCl, 12mM Phosphate, 2.7mM KCl, 1%(v/v) Tween-20, pH = 7.4) for 15 minutes three times at room temperature. Blocking was done with 3%(w/v) bovine serum albumin (BSA) in PBST for one hour at room temperature under agitation.

For anti-cytosolic FRUCTOSE-1,6-BISPHOSPHATASE (cFBPase) and anti-NBR1 detection, membranes were blocked with 3%(w/v) skimmed milk powder in PBST for one hour at room temperature under agitation. Anti-ATG8a

detection were blocked in 5%BSA(w/v) in PBST for two hours at room temperature under agitation. Primary antibody was diluted in PBST (see Table 2.9) and incubated with membranes for one hour at room temperature under agitation. The membranes were washed in PBST three times, each for 15 minutes under agitation. Anti-mouse and anti-rabbit conjugated with horse radish peroxidase (HRP) were diluted in PBST (see Table 2.9) and incubated with the membranes for one hour at room temperature under agitation. The membranes were washed in PBST for 15 minutes three times before adding chemiluminescent substrate from SuperSignal® West Femto Maximum Sensitivity Substrate kit (Thermo Scientific). HRP signal was exposed and recorded every 10 seconds in increment by a light-sensitive CCD camera (Fujifilm LAS-4000mini).

2.7 Statistical analysis and graphical representation

All descriptive statistics and statistical tests were performed using R statistical programming language 3.2.1 "World-Famous Astronaut" (R Core Team, 2014) in RStudio environment (RStudio Team, 2015). The following additional R-programming packages were used: *plyr* package (Wickham, 2011) for summary of descriptive statistics; *reshape2* package for data organization (Wickham, 2007); *multcomp* package and its dependencies (Hothorn et al., 2008) for Tukey's honest significance difference test after ANOVA analysis. All graphical representation was generated using *ggplot2* package (Wickham, 2009). The package *scales* was used for y-axis-transformation (Wickham, 2015). Figures are complied using the Inkscape 0.91.

3. Results

CFS1 emerged along with *CFS2* from a previous bioinformatic screen as a potential plant ESCRT-0 component that could recognize ubiquitinated proteins and recruit ELCH, the core ESCRT-I component, to late endosomes (Shahriari, 2008). CFS1 interacts with ELCH (Herberth, 2012) but has no influences on ELCH localization on endosomes (Sutipatanasomboon, 2012). Its SYLF domain binds to PI3P and actin instead of ubiquitin, negating the ESCRT-0 equivalence hypothesis (Herberth, 2012). As several dysfunctional ESCRT-component mutants in yeast and mammalian system show an autonomous cell death phenotype (Wegner et al., 2011), the cell death phenotype in *cfs1* mutants offered an alternative explanation for its ESCRT-related function.

3.1 *pCFS1-gCFS1* can complement *cfs1* phenotype

In my MSc thesis, I could show that the lesion mimic phenotype could be rescued by expressing *CFS1* under the control of 35s promoter in both null (*cfs1-1* and *cfs1-2*) and non-null (*cfs1-3*) mutants (Sutipatanasomboon, 2012). To ascertain that the endogenous level of *CFS1* expression is sufficient to complement the cell death phenotype in *cfs1*, the genomic region including the upstream promotor region (Figure 2.1) was introduced to *cfs1-2* mutants (*pCFS1-gCFS1* in *cfs1-2*).

In *cfs1-2* background, 12 T1 plants were isolated by glufosinate resistance, and four lines were analyzed in the T2 generation. In all lines studied, the majority were wild-type like, while the minority still showed lesions (Figure 3.1 and Table 3.1). This minor fraction were all susceptible to glufosinate, and the number of individuals in each line did not deviated from 25% (p-value = 0.6703, 0.1693, 0.8163 and 0.93 for each line respectively. Statistical test is shown in Appendix A). This demonstrate that the lesion mimic phenotype in *cfs1* is recessive and was caused by the lack of functional *CFS1*.
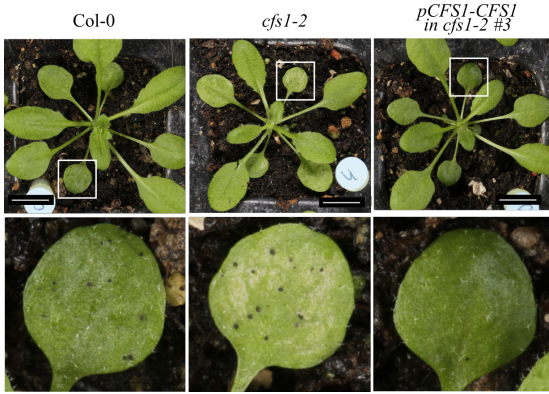
Figure 3.1: ***pCFS1-gCFS1* complements the *cfs1-2* mutant phenotype** - Representative of 30-day old Col-0, *cfs1-2* and *cfs1-2* mutant complemented with *pCFS1-gCFS1*. Boxed regions are digitally magnified in the figures below. Scale bars: 1cm.

Table 3.1: Number of T2 *cfs1-2* plants complemented by *pCFS1-gCFS1*

Line	N_{WT}	N_{lesion}	N_{all}
1	45	9	54
2	46	3	49
3	24	6	30
4	40	12	52

N_{WT}: Number of plants wild-type like plants
N_{lesion}: Number of plants showing lesions
N_{all}: Total number of plants analyzed

3.2 Cell death in *cfs1* mutants

The cell phenotype was characterized in details to discern which type of cell death occurred in *cfs1* mutant, which could reveal the possible pathway *CFS1* is involved in. The development of *cfs1* leaves was phenotypically analyzed to rule out a possible defect in leaf development. Seeds of Col-0, *cfs1-1*, *cfs1-2*, *cfs1-3* and *cfs1* non-null homologue, *cfs2* were randomly grown in the same tray. Total leaf numbers and that of leaf showing lesions were recorded every two days until flower bud started to form.

At all observation points, total leaf number of plants were comparable in every genotype (Figure 3.2b). Nevertheless, after *cfs1* mutants started to produce leaf 5 or 6, lesions surrounding the leaf veins became visible in leaf 1 and in some cases, leaf 2; while the first and second leaf of Col-0 and *cfs2* appeared healthy (Figure 3.2). Over time, lesion formation progressed to leaves 3 and 4 until flower buds started to be appear. By the time all plants have flowered (33 days after sowing), lesions did not progress beyond the last observation point and were visible in 100% of *cfs1-1* (n=15), 92.31% of *cfs1-2* (n=13) and

a)

b)
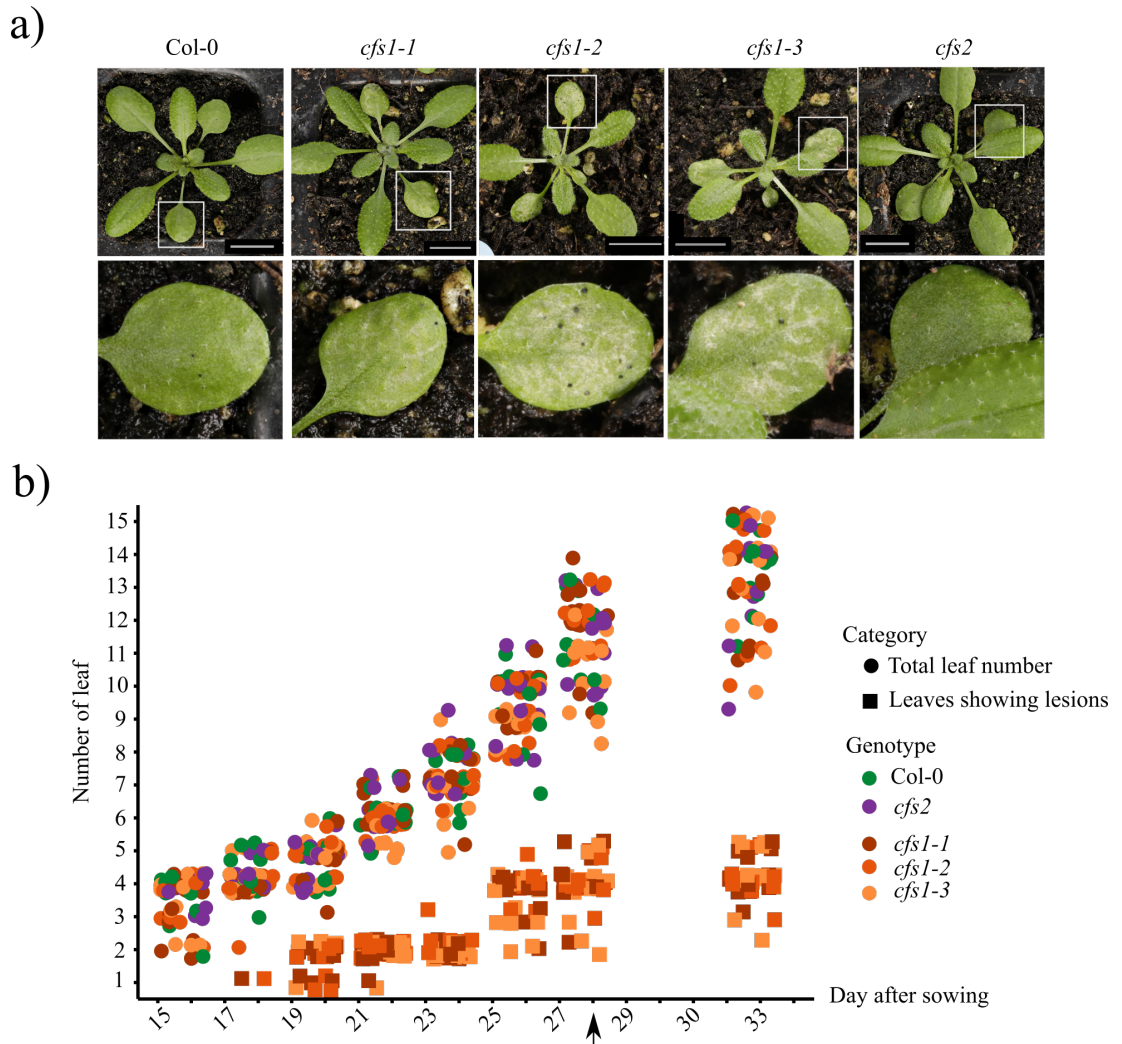
Figure 3.2: **All *cfs1* mutants form lesions before flowering** -
a) Representatives of 23-days old Col-0, *cfs1-1*, *cfs1-2*, *cfs1-3* and *cfs2* plants.
Boxed regions are digitally magnified in the figures below. Scale bars: 1 cm.
Photos were taken by Siegfried Werth.
b) Graphical representation of Col-0, *cfs1-1*, *cfs1-2*, *cfs1-3* and *cfs2* leaf development. The genotypes are represented by colors, total leaf numbers by circle and the number of leaves showing lesions by square. The arrow indicates the day flower bud formation was visible. The complete data set and its summary are shown in Appendix B.

100% of *cfs1-3* (n=15) plants. (See Table B.2 for a summary of each observation point). Altogether, this establishes that, apart from lesion formation in the eldest leaves, *cfs1* mutants do not develop differently than Col-0 under the condition studied.

3.2.1 Cell death in *cfs1* only occurs in palisade cells

To illustrate where cell death in *cfs1* mutants occurs and in which cell type, *cfs1* leaves showing lesions were stained with trypan blue (Figure 3.3a) and toludine blue for sectioning (Figure 3.3b). Trypan blue staining showed that cell death in *cfs1* mutants occurred in the non-epidermal layer (Figure 3.3a). Semi-thin sections stained with toludine blue revealed that cell death was restricted to the mesophyll layer and occurred only in palisade cells (Figure 3.3b), which corroborated the observation seen by trypan blue staining.
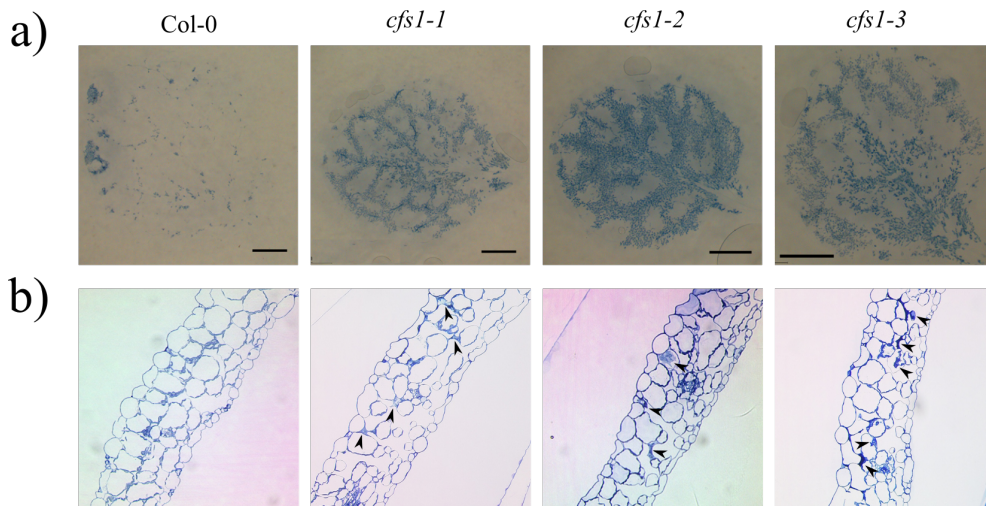
Figure 3.3: **Cell death in *cfs1* mutants occurs in palisade cells -**
a) Trypan blue staining of leaf 1 or 2 of Col-0, *cfs1-1*, *cfs1-2* and *cfs1-3*. Scale bar: 1mm.
b) Toludine blue staining of leaf 1 or 2 of Col-0, *cfs1-1*, *cfs1-2* and *cfs1-3* semi-thin sections. Arrowheads indicate stained dead cells. Sectioning and imaging were performed by Britta Müller.

3.2.2   *CFS1* promoter activity changes in an age-dependent manner

The specificity of cell death in *cfs1* mutants poses the question whether *CFS1* activity is restricted to the palisade cells. To address this, a GUS reporter gene driven by *pCFS1* was introduced to Col-0 plants. The promoter activity was observed 25 days after sowing (DAS), the time point that lesions were visible in all leaf 1 and 2 of *cfs1* mutants (Table B.2). Staining pattern showed that in leaves 1 and 2, the promoter activity was restricted to the leaf veins (Figure 3.4, leaf 2 in line 1 and leaf 1 in line 2). Whereas in younger and emerging true leaves, the activity was observed in all layers and cell types (Figure 3.4, leaf 8 in line 1 and leaf 5 in line 2).
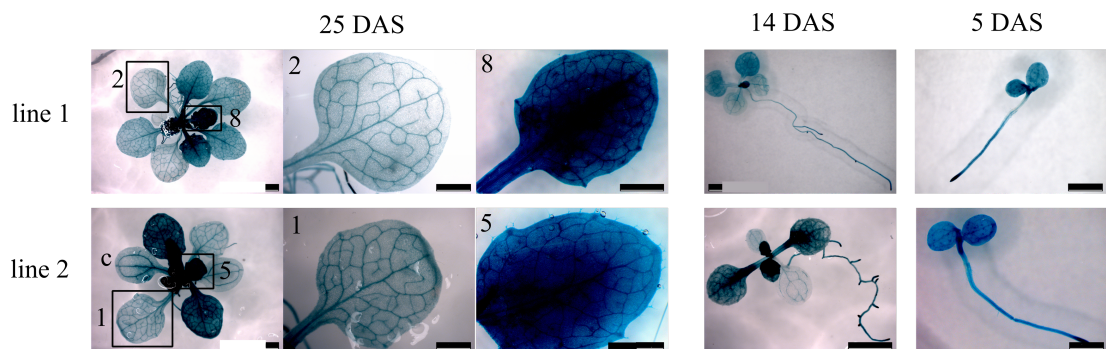
Figure 3.4: **GUS activity of *pCFS1*** - GUS staining of pCFS1-GUS in Col-0 at 25, 14 and 5 DAS. Boxed leaves are magnified and shown next to the figure with the number indicating the leaf number. Cotyledons are indicated as c. Scale bar: 1mm.

At a younger age (14 DAS), the promoter activity in leaves 1 and 2 was similar to leaves 3 and 4 of an older stage; while promoter activtiy was indistinguishable between leaves 3 and 4 to those of the emerging leaves of an older stage (Figure 3.4, 14 DAS). In seedling stage, the GUS expression in cotyledon was ubiquitous, in contrast to those in the older stage (Figure 3.4, 5 DAS). Taken all stages together, the pattern of GUS activity driven by *pCFS1* shows that *CFS1* expression is not restricted to palisade cells and differs in an age-dependent manner.

3.2.3 Cell death in *cfs1* show HR-cell death characteristics

To distinguish whether cell death observed in *cfs1* mutants is associated with developmental or stress-response processes, dead *cfs1-2* cells were visualized in a higher magnification using transmission electron microscopy (TEM). In all *cfs1-2* dead cells, cell remnant was present (Figure 3.5a), opposite to an 'empty-walled cell corpse' that is typical of a developmental-related cell death (van Doorn et al., 2011; van Doorn, 2011). Furthermore, the cell wall between lived and dead *cfs1-2* cells has thickened (Figure 3.5b), which is a characteristics of hypersensitive response (HR)-cell death (Dickman and de Figueiredo, 2011).
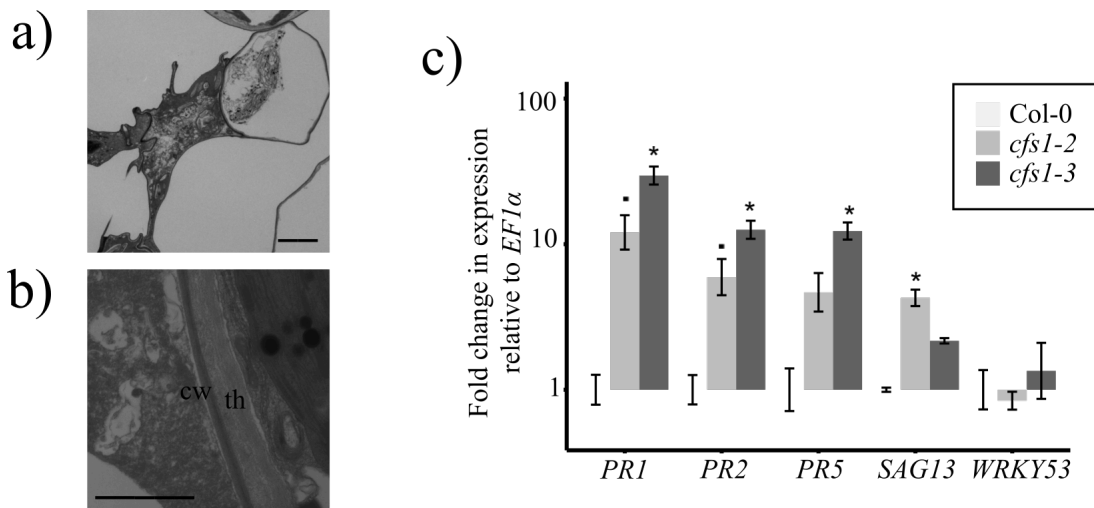
Figure 3.5: *cfs1* **mutants show HR-cell death characteristics** -
a) TEM image of dead *cfs1-2* palisade cells. Scale bar is 2μm.
b) TEM image of the cell wall between lived (left) and dead (right) *cfs1-2* palisade cells. Scale bar is 1 μm. cw: cell wall; th: cell wall thickening.
Britta Müller performed postfixation, sectioning and imaging of Figure 3.5a, b.
c) Comparative transcript levels of *PR1*, *PR2*, *PR5*, *SAG13* and *WRKY53* in leaves 1 and 2 of *cfs1-2* and *cfs1-3* showing lesions. The expression was normalized with *EF1α* and calibrated to Col-0 of the same age. Y-axis is plotted in log10 scale. Error bars represent standard error. Asterisks indicate a significant difference at $p \leqslant 0.05$ level and squares at $p \leqslant 0.1$ level. Statistical tests are shown in Appendix C.

To further test if cell death in *cfs1* mutants is related to HR, the expression of HR-related genes, *PATHOGENESIS-RELATED GENE 1,2,5* (*PR1, PR2 and PR5*, respectively) and *SENESCENCE-ASSOCIATED-GENE 13* (*SAG13*) (Brodersen et al., 2002) were examined by Real-time quantitative reverse transcription PCR (RT-qPCR). In *cfs1-2* and *cfs1-3* leaves 1 and 2 showing lesions, transcript levels of *PR1, PR2, PR5* and *SAG13* were slightly up-regulated, ranging from 10-35, 5-15, 3-15 and 2-5 fold, respectively (Figure 3.5c; fold change for each allele is shown in Table C.2). For *cfs1-3*, the expression of *PR1, PR2* and *PR5* were significantly different from Col-0 ($p = 0.0145$, $p = 0.0177$, $p = 0.0353$, respectively.) In case of *SAG13*, the expression in *cfs1-2* is significantly different from Col-0 ($p = 0.0446$). Conversely, the transcript levels of an age-dependent senescence gene, *WRKY53* (Hinderhofer and Zentgraf, 2001) were not differentially expressed in *cfs1-2* or *cfs1-3* when compared to Col-0 (Figure 3.5c; fold change is shown in Table C.2 and statistical analysis in Appendix C). The HR-cell death and the constitutive expression of *PR1, PR2* and *PR5* establish that *cfs1* is a lesion-mimic mutant (LMM) that displays an autoimmune phenotype (Lorrain et al., 2003; Palma et al., 2010).

3.2.4   The involvement of *CFS1* in HR-cell death

The microscopic morphology of dead *cfs1* cells (Figure 3.5a, b), and the slight up-regulation of HR-related marker genes (Figure 3.5c) suggest an involvement of *CFS1* in cell death following HR. An additional connection to HR-cell death comes from CFS1 interactions with PRENYLATED RAB ACCEPTOR 1.F3 (PRA1.F3) and with BINDING PARTNER OF ACD11-1 (BPA1) (Herberth, 2012), both known as interactors of another LLM protein, ACCELERATED CELL DEATH 11 (ACD11) (Petersen et al., 2009).

Mutant *acd11* also exhibits autoimmune phenotype (Palma et al., 2010). It displays a 'runaway cell death', in which death propagates to the neighboring healthy cells and engulfs the entire leaf before the plant can flower (Brodersen et al., 2002). The phenotype is identical to plants over-expressing *APOPTOSIS-LINKED GENE 2-INTERACTING PROTEIN X* (*ALIX*) (Personal communication S Schellmann), an accessory ESCRT-III subunit that interacts with mam-

malian ELCH counterpart, TUMOUR SUSCEPTIBILITY GENE 101 (TSG101) (Mahul-Mellier et al., 2006). Similar to *cfs1*, the transcript levels of *PR1*, *PR2*, *PR5* and *SAG13* are also up-regulated in *acd11* (Brodersen et al., 2002). Taken the phenotypic similarities of ALIX over-expression and *cfs1* plants to *acd11* into account and ALIX interaction with mammalian ELCH homologue, I hypothesized that the involvement of the ESCRT-complex in plant cell death is through the ACD11-related cell death pathway. Hence, cell death seen in *cfs1* mutants could be a reflection of a less severe *acd11* runaway cell death.

3.2.4.1 Cell death in *cfs1* is dependent on EDS1-activated effector-triggered immunity

If cell death in *cfs1* was a milder form of *acd11* cell death, the *cfs1* phenotype would then be dependent on functional *acd11* suppressors. To test this hypothesis, *cfs1-2* was crossed to two of the *acd11* cell death suppressors *lazarus1* (*laz1*) and *enhanced disease susceptibility 1* (*eds1*) (Malinovsky et al., 2010; Brodersen et al., 2002). Under a normal greenhuse condition, neither *cfs1-2 laz1-5* nor *cfs1-2 eds1-2* developed visible lesions when *cfs1* did (Figure 3.6a).

EDS1 is a lipase-like protein that activates effector-triggered immunity (ETI) (Aarts et al., 1998; Wiermer et al., 2005). When ETI is activated, it results in HR and other overlapping cellular responses (Wiermer et al., 2005; Coll et al., 2011). ETI responses are inhibited at ambient elevated temperatures (28-32°C) that in turn significantly reduce HR-cell death (Cheng et al., 2013; Wang et al., 2009). To further establish whether HR-cell death in *cfs1* is attested to ETI, *cfs1* mutants were shifted to 28°C after germination. As a result, at 30 DAS, 100% in *cfs1-1* (n = 19), 95% in *cfs1-2* (n = 20) and 100% in *cfs1-3* (n = 19) still had not developed lesions (Figure 3.6b), demonstrating that HR-cell death in *cfs1* mutants results from the activation of ETI.

3.2.4.2 Cell death in *cfs1* does not require SA signaling

HR occurs in concert with several signaling cascades and molecular events. Together, they kill uninjured cells surrounding the compromised cells and prime the plants to cope with and fight against pathogen attack (Wiermer
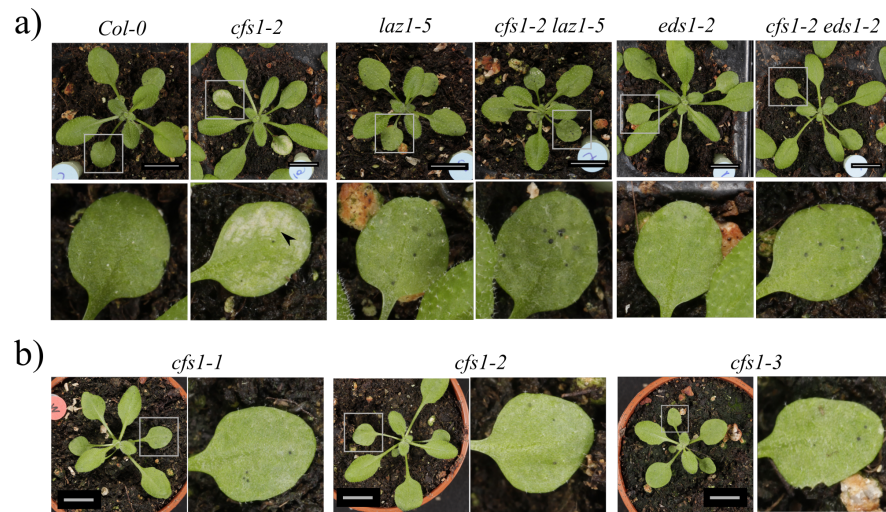
Figure 3.6: **Cell death in *cfs1-2* mutants requires a functional EDS1 signaling pathway** -
a) Representatives of 27-days old Col-0, *cfs1-2*, *laz1-5*, *cfs1-2 laz1-5*, *eds1* and *cfs1-2 eds1-2* grown in greenhouse condition.
b) Representatives of 27-days old cfs1-1, cfs1-2 and cfs1-3 grown at 28°C.
Scale bar: 1cm. All images were taken by Siegfried Werth.

et al., 2005; Coll et al., 2011). In *acd11*-related cell death, this murderous command relies, in most part, on a SA-signaling cascade (Brodersen et al., 2002, 2005). The expression of the bacterial enzyme naphthalene hydroxylase G (*nahG*) that degrades SA and other isochorismate-derived compounds (Serrano et al., 2013) completely restores *acd11* to wild-type phenotype (Brodersen et al., 2002). It was also demonstrated that the *acd11* runaway cell death phenotype is depended on a functional SA biosynthesis enzyme, *ISOCHORISMATE SYNTHASE 1* (*ICS1*) encoded by *SALICYLIC ACID INDUCTION DEFICIENT 2* (*SID2*) but not *ENHANCED DISEASE SUSCEPTIBILITY 5* (*EDS5*)-dependent SA export to cytoplasm (Brodersen et al., 2005).

To investigate if functional SA signaling is necessary for the execution of cell death in *cfs1* mutant, *nahG* was introduced to *cfs1-2*, and double mutant *cfs1-2 sid2-1* and *cfs1-2 eds5-1* were generated. As a result, none of the SA-deficient *cfs1-2* plants showed phenotype suppression (Figure 3.7), demonstrating that the execution of cell death in the *cfs1* mutant does not require functional SA signaling as in *acd11*.

Col-0   cfs1-2   nahG/Col-0   nahG/cfs1-2

sid2-1   cfs1-2 sid2-1   eds5-1   cfs1-2 eds5-1

Figure 3.7: **Cell death in *cfs1-2* mutants is independent of SA-signalling** - Representatives of 25 DAS Col-0, *cfs1-2*, nahG in Col-0 (nahG/Col-0), nahG in *cfs1-2* (nahG/*cfs1-2*), *sid2-1*, *cfs1-2 sid2-1*, *eds5-1* and *cfs1-2 eds5-1* grown in the greenhouse condition.
Scale bar: 1 mm.
Images were taken by Siegfried Werth.

The independence of *cfs1* cell death on the SA-signaling pathway contradicts the hypothesis that *cfs1* cell death is a milder manifestation of *acd11* cell death and poses the question which signaling pathway brings about *cfs1* cell death. Because EDS1 also assists in a crosstalk between SA to ethylene and jasmonic acid (JA)-signaling pathways (Wiermer et al., 2005), I checked for possible deregulation of both pathways in *cfs1* mutant using *ETHYLENE RESPONSIVE FACTOR 1* (*ERF1*) (Tintor et al., 2013) and *PATHOGENESIS-RELATED GENE 3* (*PR3*) (Abe et al., 2013) as ethylene-responsive marker genes. *VEGETATIVE STORAGE PROTEIN2* (*VSP2*) and *PLANT DEFENSIN 1.2* (*PDF1.2*) served as JA and ethylene-reponsive marker genes (Lorrain et al., 2003), while *LIPOXYGENASE 2* (*LOX2*) responses only to JA (Danisman et al., 2012).

In *cfs1-2* and *cfs1-3* leaves 1 and 2 showing lesions, the transcript levels of *ERF1*, *LOX2*, and *VSP2* were comparable to Col-0 leaves 1 and 2 of the same age (Figure 3.8a; fold change in each allele are shown in Table D.2). For *PR3* and *PDF1.2*, the expression in *cfs1-2* were slightly up-regulated, but only *PR3* was significantly different from Col-0 ($p = 0.00674$); however, this is likely a side-effect of SA-accumulation as both markers have been reported to also response to SA-accumulation (Yoshimoto et al., 2009).

In addition to JA and ethylene crosstalk signaling, it is also possible that

a)

b)

c)
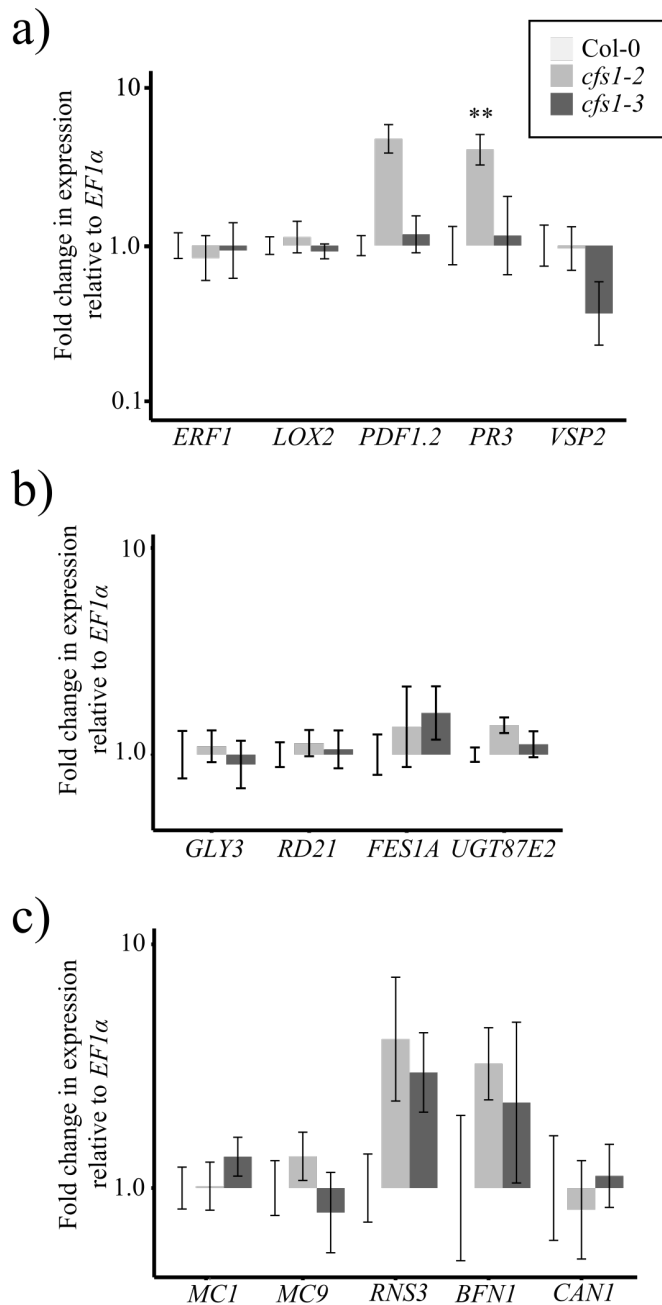
Figure 3.8: **JA, ethylene, ROS and cell death executor transcript levels in *cfs1*** - Fold change expression of leaves 1 and 2 of *cfs1-2* and *cfs1-3* compared to that of Col-0 using
a) *ERF1*, *LOX2*, *PDF1.2*, *PR3* and *VSP2* as JA and ethylene-responsive marker genes.
b) *GLY3*, *RD21*, *FES1A* and *UGT87E2* as oxidative stress genes.
c) *MC1*, *MC9*, *RNS3*, *BFN1* and *CAN1* as cell death execution genes.
The expression levels were normalized to *EF1α*. Y-axis is plotted in log10 scale; error bars represent standard error.
Two asterisks indicate a significant difference at $p \leqslant 0.01$ level. Statistical tests for Figure 3.8a are shown in Appendix D and Figure 3.8b,c in Appendix E.

cfs1 cell death relies on other signaling branches that are concurrent to HR-cell death, for example, the generation of reactive oxygen species (ROS) and the initiation of caspase-like protease activity that execute cell death (Coll et al., 2011). To check for any indication of *cfs1* cell death involvement to these signaling branches, the expression of oxidative stress response marker genes, *GLY-*

OXALASE 3 (*GLY3*), *RESPONSIVE TO DEHYDRATION 21* (*RD21*) (Martínez-Fábregas et al., 2014), *FACTOR EXCHANGE FOR SSA1 PROTEIN1A* (*FES1A*) and *URIDINE DIPHOSPHATE GLYCOSYLTRANSFERASE 74E2* (UGT74E2) (Hackenberg et al., 2013) were examined to check for an increase in ROS production. *METACASPASE 1* and *9* (*MC1, MC9*, respectively) (Coll et al., 2011), *RIBONUCLEASE 3* (*RNS3*), *BIFUNCTIONAL NUCLEASE 1* (*BFN1*) and *CALCIUM DEPENDENT NUCLEASE 1* (*CAN1*) are cell death executor genes that served as marker genes for the initiation of caspase-like protease activity (Van Hautegem et al. 2015; Personal communtiation M Nowack). None of the marker genes investigated showed a differential expression when compared to Col-0 (Figure 3.8b, c; see Appendix E for fold change of each marker gene and statistical tests)

To sum up, the examination of JA, ethylene, oxidative stress and caspase-like proteases marker genes showed no indication that *cfs1* cell death command came from or was executed by any of these signaling branches.

3.3 *CFS1* function in ESCRT-related trafficking

Due to the lack of any indication which signaling pathway is involved in *cfs1*, I turn to consider it from the ESCRT-related trafficking perspective. To undertake this, two main questions were put forward. First, if the lack of functional *cfs1* has an impact on ESCRT-related trafficking; and second, how and if cell death in *cfs1* mutant is influenced by the function of the ESCRT-I complex.

3.3.1 *cfs1* mutants show normal endomembrane architecture

Because CFS1 has been shown to bind specifically to PI3P, which is associated with endosomes (Herberth, 2012), the endomembrane architecture was examined for aberrant endosomes similar to *class E* compartment (Raymond et al., 1992) to address the first question. Non-colocalizing endosomal markers, mCherry-VTI12 and mCherry-SYP61 and co-localizing markers, mCherry-ARA7 were stably expressed and YFP-ELCH (Herberth, 2012) were transiently expressed and imaged in *cfs1-2* and Col-0. In none of endosomal markers ex-

amined was there any obvious aberrant endosomes similar to *class E* compartment observed in *cfs1-2* (Figure 3.9).
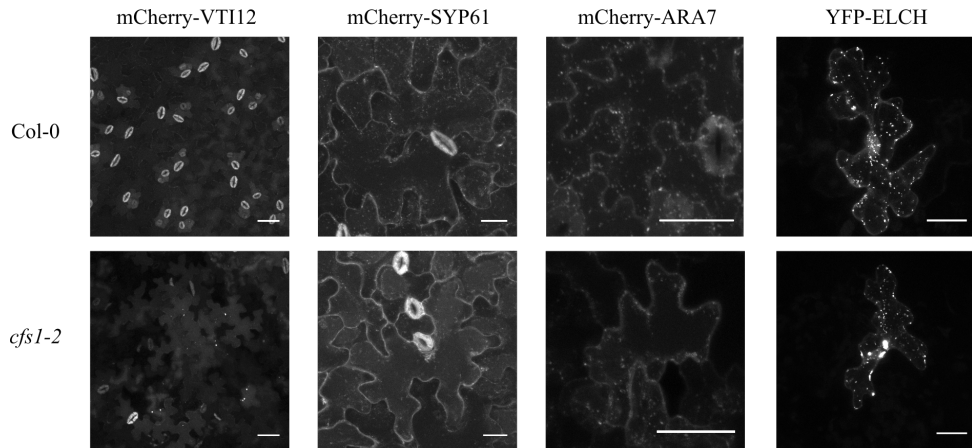
Figure 3.9: **Lack of functional *CFS1* does not affect endomembrane architechture** - CLSM images of endosomal markers VTI12, SYP61 and ARA7 were stably expressed, and fluorescent ESCRT-I component ELCH was transiently expressed in Col-0 and *cfs1-2*. Scale bar: 25μm.

In addition to the connection to endosomes, the ESCRT-complex is also linked to vacuole maintenance (Shahriari et al., 2010b; Michaillat and Mayer, 2013; Cai et al., 2014; Kalinowska et al., 2015). One striking example is SUPPRESSOR OF K($^+$) TRANSPORT GROWTH DEFECT1 (SKD1) that disassembles the ESCRT-complex from the endosomal membrane (Haas et al., 2007). Lack of a functional SKD1 (Cai et al., 2014) and the overexpression of its dominant-negative form in tobacco cells, *Arabidopsis* cell culture (Haas et al., 2007) and trichome cell (Shahriari, 2008; Shahriari et al., 2010b) result in cell death following vacuole loss or fragmentation. To check if this is also the case in *cfs1-2* cell death, vacuoles were stained using BCECF-AM (direct staining), FDA and FM4-64 (indirect stainings). None of these vacuolar staining methods reveal an abnormal vacuole morphology in *cfs1-2* mutants (Figure 3.10).

3.3.2   No alteration in actin cytoskeleton in *cfs1* mutants

Another biochemical property of CFS1 is the actin binding its SYLF domain (Herberth, 2012). As actin dynamics have been proposed to play an active role
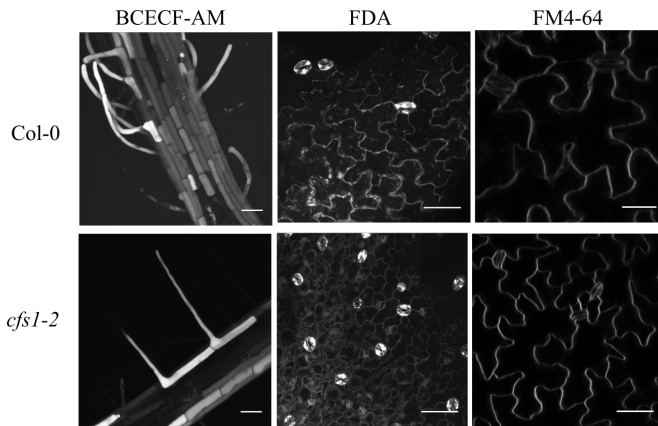
Figure 3.10: **Lack of functional *CFS1* does not affect vacuole maintenance** - CLSM images of Col-0 and *cfs1-2* seedlings stained with BCECF-AM, FDA and FM4-64 show intact vacuole. Scale bar: 50μm.

in cell-death signaling (Smertenko and Franklin-Tong, 2011), possible changes in actin cytoskeleton morphology were screened by analyzing the localization of Lifeact-eGFP and by pavement cell complexity in *cfs1-2* and *cfs1-3*. Neither methods showed any obvious alteration of the actin cytoskeleton when *CFS1* function was removed (Figure 3.11).
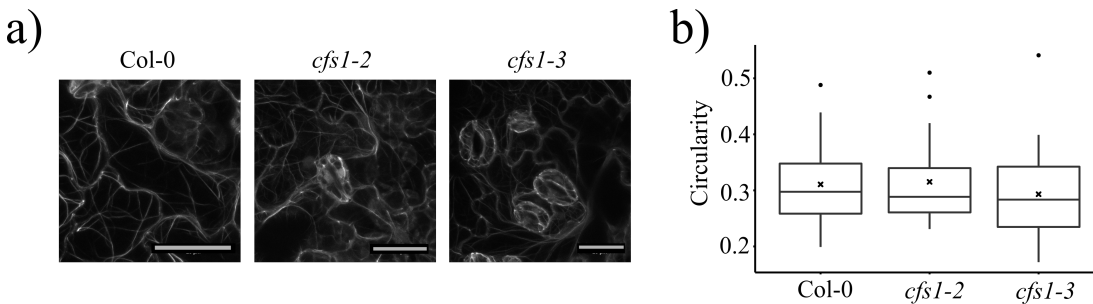
Figure 3.11: **Lack of functional *CFS1* does not affect actin cytoskeleton** - No abnormality in actin cytoskeleton in compared to Col-0 as shown in
a) stable expression of Lifeact-eGFP in Col-0, *cfs1-2* and *cfs1-3*. Scale bar: 25μm.
b) the pavement cell complexity of Col-0, *cfs1-2* and *cfs1-3*. The box plot summarizes the circularity of 20 cells from each genotype. Dots indicate outliers and crosses the mean of circularity. Circularity values and descriptive statistics are shown in Appendix F.

3.3.3 Cytokinesis defects are alleviated in *cfs1-2 elch*

One of the *Arabidopsis* ESCRT-I core components, *elch* shows a defect in cytokinesis that is translated into the formation of the *elch*-trichome (Spitzer et al.,

2006). The *elch*-trichome is an appearance of two trichomes stemming from a single pavement cell (Figure 1.5 and Spitzer et al. 2006). The phenotype is only present in about 2% of all trichomes in *elch* and is enhanced when additional ESCRT-I components are mutated (Spitzer et al., 2006; Keshavaiah, 2008). To further address if lack of functional CFS1 plays a role in the ESCRT-I function, the level of deficiency in cytokinesis in *cfs1-2 elch* mutant was inspected.

Table 3.2: Wild-type and *elch* trichome number in Col-0, *cfs1-2*, *cfs1-2 elch*, *elch* and Ws-2

Genotype	Trichome$_{Wild-type}$	Trichome$_{elch}$	All trichomes	%*elch*	N$_{WT}$	N$_{elch}$	N$_{all}$
Col-0	2353	0	2353	0.000	22	0	22
cfs1-2	2633	0	2633	0.000	24	0	24
cfs1-2 elch	3819	16	3835	0.417	36	12	36
elch	4014	47	4061	1.157	30	21	30
Ws-2	1733	0	1733	0.000	14	0	14

%*elch*: Percentage of the number of *elch* trichomes to the number of all trichomes
N$_{WT}$: Number of leaves showing wild-type trichomes
N$_{elch}$: Number of leaves showing *elch* trichomes
N$_{all}$: Number of all leaves counted
Data in the table are a summary of Table H.1. Summary by leaf number is displayed in Table H.2. All statistical tests are shown in Appendix H.

In *cfs1-2 elch* mutant, only 0.42% of *elch*-trichome were present in contrast to 1.16% in *elch*. Two statistical analyses (Fisher's exact test and Pearson's χ^2 test of independence) showed that 0.42% and 1.16% are not equal (p=$3.666e^{-05}$ and p=0.0002228, respectively) but 0.42% is less (p =$2.428e^{-05}$ and p = 0.0002228, respectively) than 1.16% (Table 3.2). This shows that the lack of *cfs1* function alleviates cytokinesis effect in *elch* and suggests an influence of *CFS1* on *ELCH* function.

3.3.4   Cell death in *cfs1* is not dependent on ESCRT-I function

To address whether the ESCRT-I complex function influences cell death in *cfs1*, *cfs1-2* mutant was crossed to its ESCRT-I interactor *elch*, and other non-interacting ESCRT-I components, *vps28.2* and *vps31.7*. At 20 DAS, 63.6% of *cfs1-2* (n = 33) , 64.5% of double mutant *cfs1-2 vps28.2* (n=35) and 52.5% of *cfs1-*

2 vps37.1 (n=34) developed lesions in leaves 1 and 2 (Figure 3.12). In *cfs1-2 elch* at 20DAS, however, no visible lesions were observed (n=35; Figure 3.12 and Table G.2). At 25 DAS, 90.9% of *cfs1-2*, 82.5% of *cfs1-2 vps28.2* and 100% of *cfs1-2 vps37.1* have formed lesion, but only 42.9% of *cfs1-2 elch* showed the cell death phenotype (Figure 3.12 and Table G.2). According to Pearson's χ^2 test of independence, the fraction of *cfs1-2 elch* plants showing lesions at 25 DAS is significantly different from the fraction of *cfs1-2* plants (90.2%) showing lesions at the same stage ($p = 2.841e^{-05}$). By 30 DAS, however, 82.86% of *cfs1-2 elch* showed the cell death phenotype, which is comparable to the percentage of *cfs1-2* plants showing cell death phenotype at the same stage ($p = 0.1563$; Table G.2). This illustrates that cell-death in *cfs1* mutant does not require a fully functional ESCRT-I complex. Nevertheless, the lack of a functional *ELCH* may impact how *cfs1-2* cell death progresses.
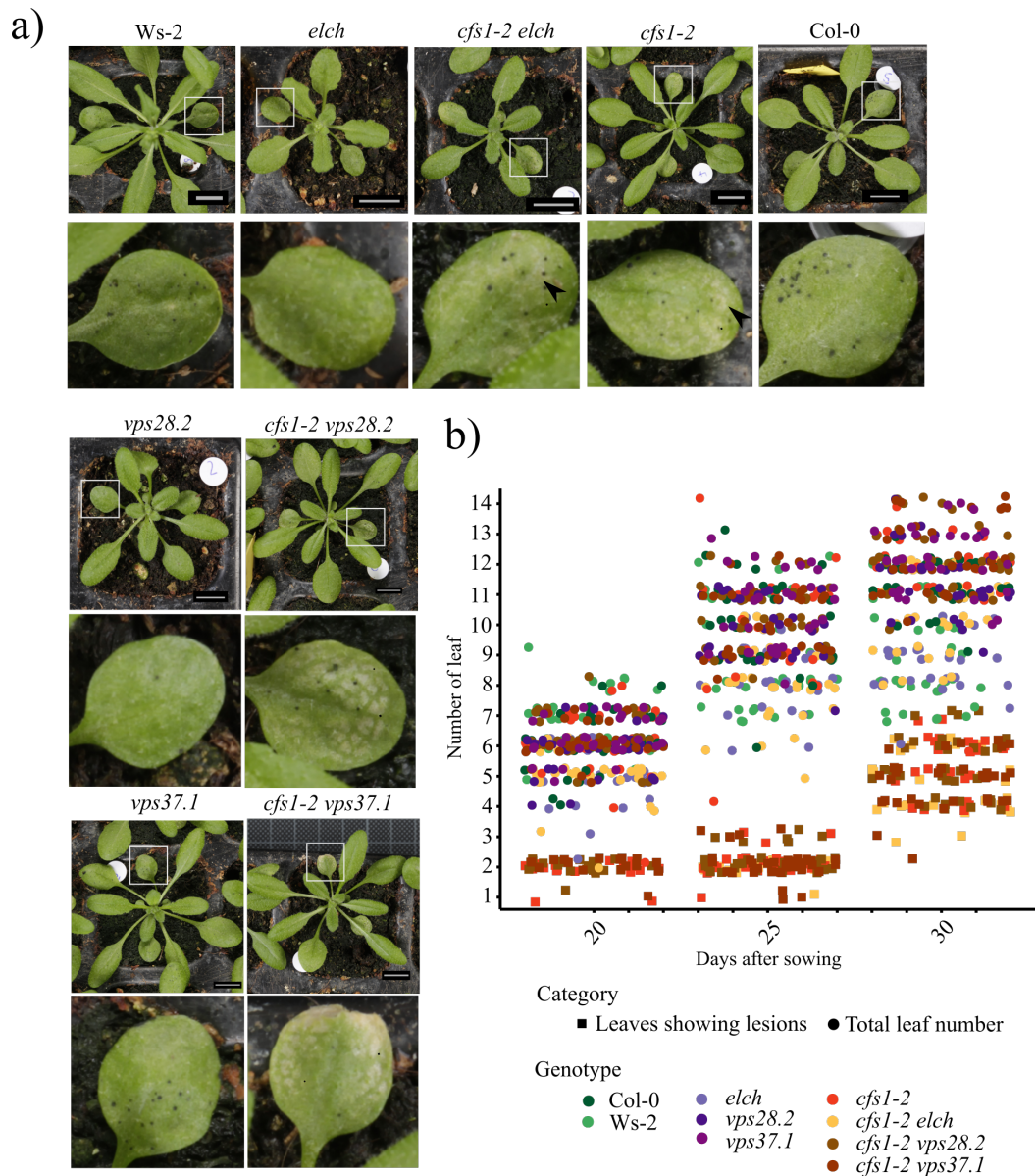
Figure 3.12: **Cell death in *cfs1* mutants is independent of a functional ESCRT-I component** -
a) Representatives of 25-days old Ws-2, *elch*, *cfs1-2 elch*, Col-0, *vps28.2*, *cfs1-2 vps28.2*, *vps37.1* and *cfs1-2 vps37.1* plants. Boxed regions are magnified in the figures below. Scale bar: 1cm. All photos were taken by Siegfried Werth.
b) Graphical representation of the total number of Ws-2, *elch*, *cfs1-2 elch*, Col-0, *vps28.2*, *cfs1-2 vps28.2*, *vps37.1* and *cfs1-2 vps37.1* leaves and those of leaves showing lesions. Circle represents total leaf number and square the number of leaves showing lesions. Each genotype is represented by color. The complete data set and its summary are shown in Appendix G.

3.3.5   Mature *cfs1* mutants accumulate ubiquitinated proteins

The principle function of the ESCRT-complex is to target ubiquitinated proteins and sort them into late endosomes, forming multivesicular bodies (MVBs) that are subsequently delivered to vacuole for degradation (Katzmann et al., 2001). It has been demonstrated in *elch* and *elch vps28.2 vps37.1* (i^3) mutants that the deficiency of the ESCRT-I complex resulted in an accumulation of ubiquitinated proteins (Personal communication S Schellmann). To answer if *CFS1* influences the role of ELCH in this aspect, *cfs1* and *cfs1-2 elch* were probed with ubiquitin antibody (anti-Ub(P4D1)) for ubiquitinated proteins accumulation (Figure 3.13).
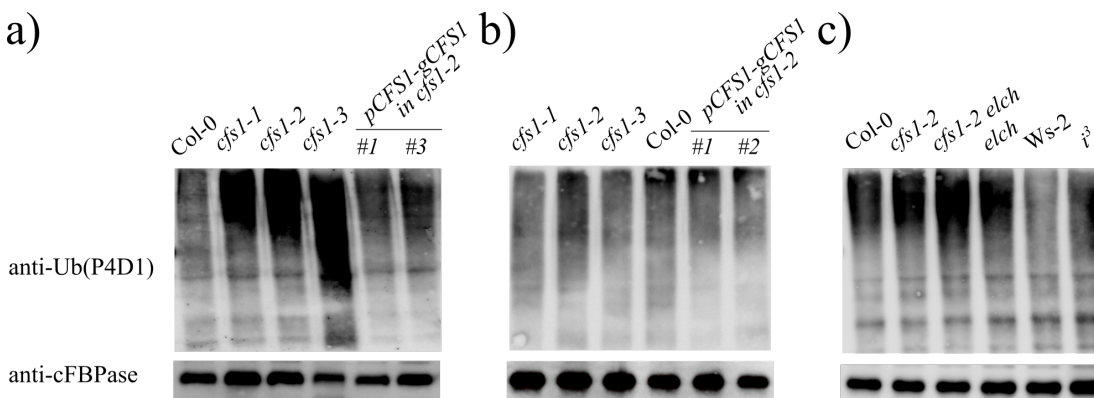
Figure 3.13: **Only *cfs1* leaves with lesions accumulate ubiquitinated proteins** - Immunodetection of ubiquitinated proteins in
a) leaves of *cfs1* mutants showing lesions and of Col-0, *pCFS1-gCFS1* in *cfs1-2* of the same age.
b) younger *cfs1* mutants whose lesions had yet to be formed and of Col-0 and *pCFS1-gCFS1* in *cfs1-2* plants of the same age.
c) younger *cfs1* mutants whose lesions had yet to be formed and of Col-0, *cfs1 elch*, *elch*, Ws-2 and i^3 of the same age.
Anti-cFBPase served as a loading control. All experiments were performed with four biological replicates (Figures I.1 to I.3).

In *cfs1* leaves showing lesions, a marked accumulation of ubiquitinated proteins was observed in all samples when compared to wild-type and the complementation lines (*pCFS1-gCFS1* in *cfs1-2*) (Figure 3.13a). In younger *cfs1* plants, however, the level of ubiquitinated proteins detected was comparable to that in wild-type and in the complementation lines (Figure 3.13b), and no

obviouse change in the accumulation of ubiquitinated proteins in *cfs1-2 elch* was observed in comparison to *elch* (Figure 3.13c).

3.3.6 *cfs1* mutants accumulate autophagosomes during their lifespan

Because *cfs1* mutants only accumulated ubiquitinated proteins after cell death had already occurred (Figure 3.13a and b) and *cfs1-2 elch* did not accumulate ubiquitinated proteins beyond that of *elch* (Figure 3.13c), I inferred that the accumulation of ubiquitinated proteins in *cfs1* leaves with lesions (Figures 3.13a) is a consequence of cell death rather than a deficiency in the ESCRT-complex function.

Alternative to the insufficiency of an ESCRT-mediated ubiquitinated proteins degradation, Munch et al. (2014) have proposed that deficiencies in autophagy could also lead to an accumulation of ubiquitinated proteins and eventually uncontrolled cell death. For this reason, autophagy malfunction in *cfs1* mutants was investigated by immunoblotting against an autophagosomal membrane marker, AUTOPHAGY-RELATED 8A (ATG8a) (Thompson et al., 2005; Bassham, 2015) and a selective autophagy substrate, NEXT TO BRCA1 GENE 1 (NBR1) (Svenning et al., 2011).

When compared to wild-type, mature *cfs1* leaves showing lesions showed a drastic accumulation of ATG8a and NBR1, ranging from 5 to 45 fold from 0.6 to 23 fold, respectively. In the complemented lines (*pCFS1-gCFS1* in *cfs1-2*), the level of accumulation was reduced to 1.7 - 2.3 fold and to 0.2 - 17 fold for ATG8a and NBR1, respectively (Figure 3.14a,b). To exclude the possibility that accumulation of ATG8a and NBR1 in mature plants resulted from a higher number of dead cells in *cfs1* than in wild-type, I also checked the level of ATG8a and NBR1 accumulation in growing plants without lesions (14-days old) and in young seedlings (7-days old).

In 14-days old *cfs1* mutants, the detected level of ATG8a and NBR1 was 1.7 - 8.1 fold and 0.2 - 4.2 fold in compared to wild-type of the same age, respectively, which were higher than that of the complemented lines of the same age (Figure 3.14c-d). In young seedlings, the level of ATG8a and NBR1 varied
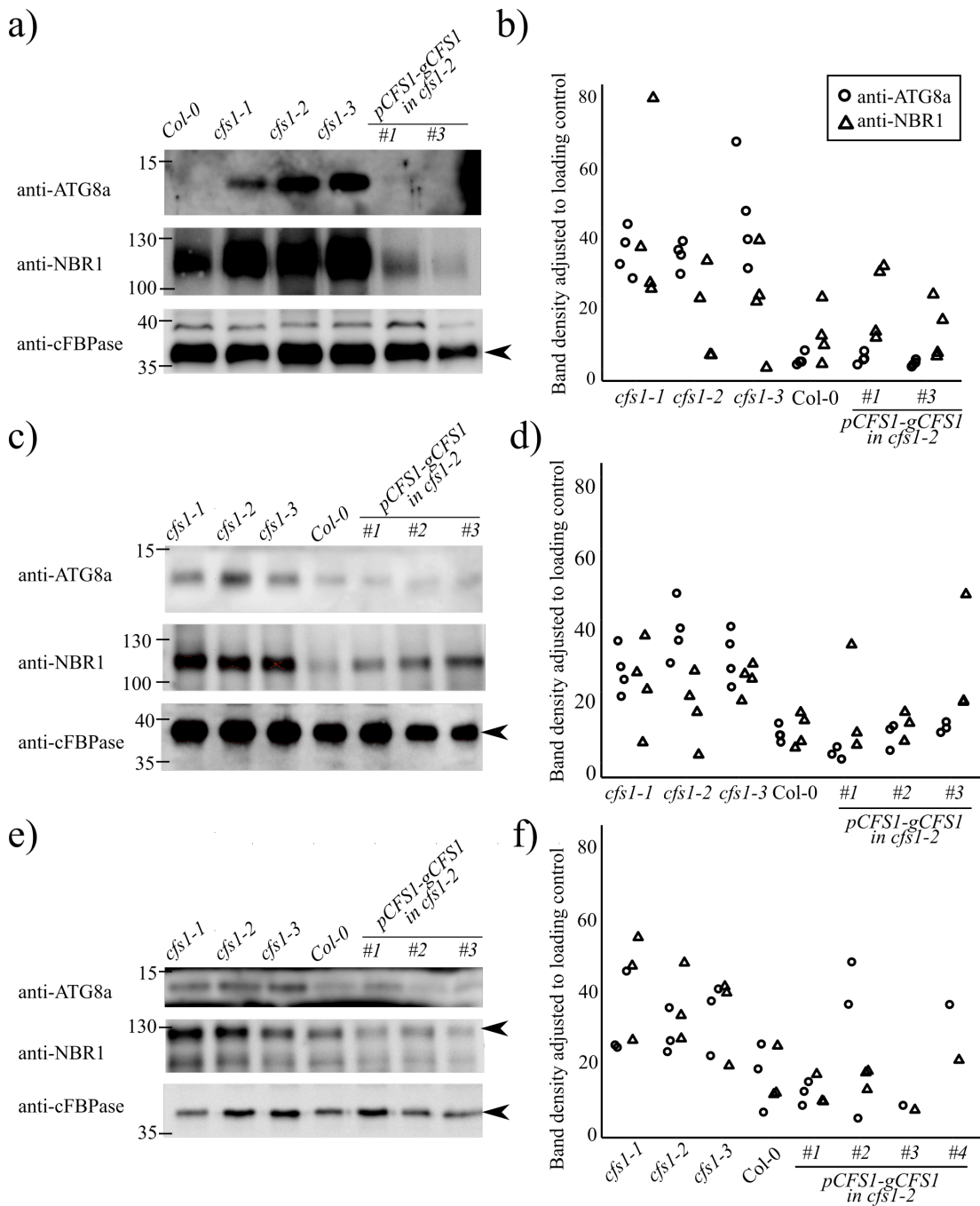
Figure 3.14: *cfs1* **mutants accumulate autophagosomes during their lifespan** - Immunodetection of autophagosomes with anti-ATG8 and anti-NBR1.

from 0.96 -14 fold and 0.7 - 6.1 fold when compared to wild-type, respectively. In the complemented lines of the same age, the level of ATG8a and NBR1 accumulation was reduced to 0.49 - 2.96 fold and 0.29 - 2.2 fold, respectively when compared to Col-0 (Figure 3.14e-f). Altogether, this demonstrates that the lack of functional *CFS1* causes an accumulation of autophagosomal components associated with ATG8a and in most cases, NBR1. This accumulation occurs at the early stage of the plant life and becomes more obvious as the plants age.

Under an optimal condition, autophagy transpires at a low level to facilitate basal autophagy activity (Sláviková et al., 2005). When stress occurs, ATG genes are upregulated to increase the formation of autophagosomes (Pu and Bassham, 2013). In developing autophagosome, ATG8 is modified and decorated (Yoshimoto et al., 2004; Thompson et al., 2005; Li and Vierstra, 2012). Mature ATG8-decorated autophagosomes are then transported to the vacuole for degradation (Li and Vierstra, 2012). For this reason, an increased ATG8a accumulation in *cfs1* could point to either a misregulation of basal autophagy or to an incomplete autophagosome formation or degradation.

Figure 3.14: ***cfs1* mutants accumulate autophagosomes during their lifespan** - Immunodetection of autophagosomes with anti-ATG8 and anti-NBR1 in

a) leaves of *cfs1* mutants showing lesions and of Col-0, *pCFS1-gCFS1* in *cfs1-2* of the same age. The intensity of detected anti-ATG8a and anti-NBR1 band of all four biological replicates (Figures J.1 to J.4) are depicted in **b)**.

c) 14-days old *cfs1* mutants, Col-0 and *pCFS1-gCFS1* in *cfs1-2* plants. The intensity of detected anti-ATG8a and anti-NBR1 band of all four biological replicates (Figures J.5 to J.8) are depicted in **d)**.

e) young seedlings of *cfs1* mutants, Col-0 and *pCFS1-gCFS1* in *cfs1-2* plants. The intensity of detected anti-ATG8a and anti-NBR1 band of all three biological replicates (Figures J.9 to J.11) are depicted in **f)**.

Anti-cFBPase served as a loading control. Arrowhead denotes the band selected for calculation.

3.3.6.1 No misregulation of *ATG8* and *NBR1* in *cfs1* mutants

To assess whether basal autophagy is misregulated in *cfs1*, the level of ATG8 genes and NBR1 transcripts were assessed in both null (*cfs1-2*) and non-null (*cfs1-3*) alleles in compared to wild-type. In neither null nor non-nulll *cfs1* alleles was the expression of *ATG8* genes or *NBR1* significantly different from that of Col-0 (Figure 3.15 and Appendix K). This indicates a normal regulation of ATG8 genes and NBR1.
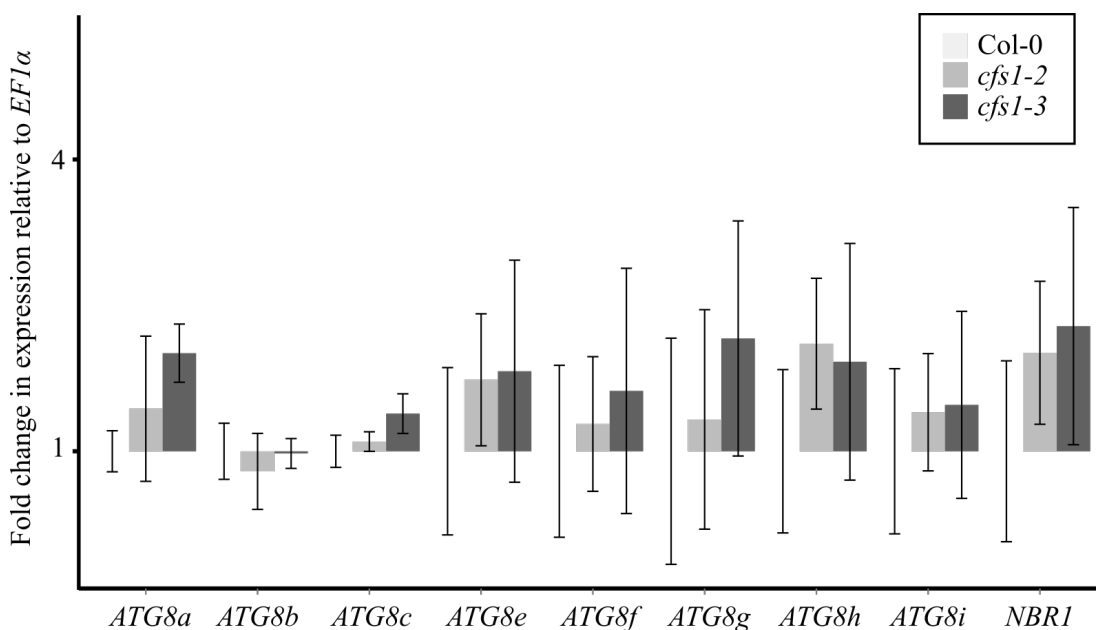
Figure 3.15: **No misregulation of ATG8 genes or NBR1 in *cfs1*** - Transcript levels of *ATG8* genes and *NBR1* in *cfs1-2* and *cfs1-3* leaves showing lesions were similar to that of Col-0. The expression levels were normalized to *EF1α* and calibrated to Col-0 of the same age. Y-axis is plotted in log2 scale. Error bars represent standard error. Fold change and statistical tests are shown in Appendix K.

3.3.6.2 No misregulation of ER-stress marker genes in *cfs1* mutants

In addition to ATG-induced autophagosome formation (Li and Vierstra, 2012), autophagosomes could also be induced under ER-stress (Pu and Bassham, 2013), or vice versa (Munch et al., 2014). To attend to this possibility, I checked if *cfs1* mutants are under ER-stress by comparing the level unfolded protein
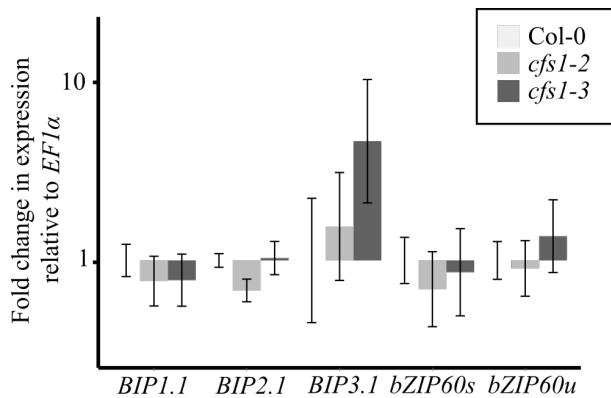
Figure 3.16: **No upregulation of ER-stress marker genes in *cfs1*** - Comparative transcript levels of ER-stress marker genes, *BIP1.1*, *BIP2.1*, *BIP3.1* and *bZIP60* spliced and unspliced variants (*bZIP60s* and *bZIP60u*, respectively) in *cfs1-2* and *cfs1-3* leaves showing lesions to Col-0 of the same age.

Y-axis is plotted in log10 scale. Error bars represent standard error. Fold change of each marker genes and statistical tests are shown in Appendix L.

responses (UPR)-related genes, *LUMINAL BINDING PROTEIN 1.1* (*BIP1.1*), *LUMINAL BINDING PROTEIN 2.1* (*BIP2.1*), and *LUMINAL BINDING PROTEIN 3.1* (*BIP3.1*) that are up-regulated during ER-stress and the level of *BASIC REGION/LEUCINE ZIPPER MOTIF 60* (*bZIP60*) that is spliced to activate the up-regulation of UPR-related genes (Liu et al., 2012; Pu and Bassham, 2013). In both null and non-null alleles of *cfs1*, no significant difference in the transcript levels of these genes was observed when compared to wild-type (Figure 3.16 and Appendix L).

3.3.6.3 Autophagosomes are formed in *cfs1-2*

The usual transcript levels of *ATG8* genes, *NBR1* and ER-stress markers genes in *cfs1* mutants demonstrate that autophagosome accumulation in *cfs1* is not due to misregulation of basal autophagy (Figure 3.15)or higher ER-stress (Figure 3.16). Hence, only defective autophagosome formation or degradation remain as a probable cause of autophagosome accumulation in *cfs1* mutants. Defective autophagosome formation can be translated into failure to form ATG8-punctated structures after induction (Sláviková et al., 2005) and lower tolerance to nutrient starvation (Doelling et al., 2002; Thompson et al., 2005).

When YFP-ATG8a was transiently expressed, YFP signals were present in cytosolic form and dot-like structures in both Col-0 and *cfs1-2* (Figure 3.17a).
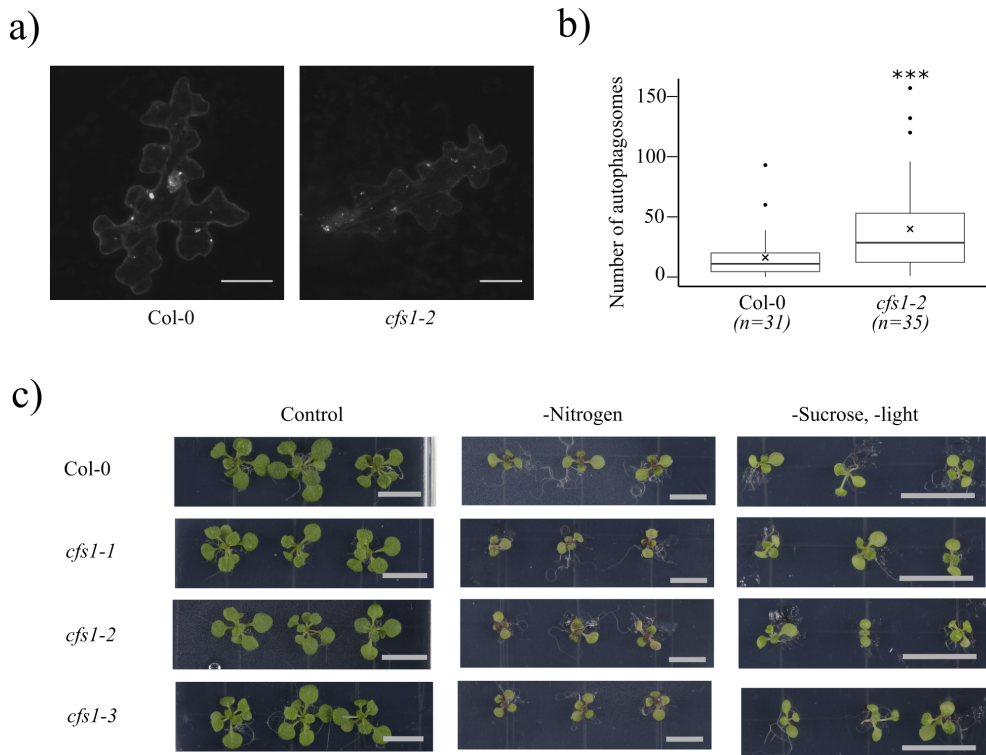
Figure 3.17: **Autophagosomes can be initiated in *cfs1* mutant** - Autophago-
somes formation in Col-0 and *cfs1-2* mutant was initiated by
a) transient expression of YFP-ATG8a in Col-0 and *cfs1-2*. The number of punc-
tated structures (Tables M.1 and M.2) is summarized in the boxplot in **b)**. Scale
bar: 25µm. Crosses indicate the average number of punctated stucture. Dots
indicate outliers. Three asterisks indicate a significant difference at $p \leqslant 0.001$
level.
c) 10 days-carbon and nitrogen starvation subjected to 7-days old Col-0 and
cfs1 seedlings. Scale bar: 1cm.

The average number of punctated YFP-ATG8 structures in *cfs1-2* was signifi-
cantly more than in Col-0 (p= 0.0005894, Figure 3.17b; Statistical test is shown
in Appendix M). On a phenotypic level, no obvious difference was observed
when 7-days old wild-type and *cfs1* seedlings were starved from nitrogen and
carbon source for 10 days (Figure 3.17c). Both approaches substantiate a nor-
mal autophagosome formation in *cfs1*. Greater number of YFP-ATG8a punc-
tated structure in *cfs1-2* suggests, instead, a faulty autophagosome degrada-
tion.

3.3.6.4 Autophagosome accumulation in *cfs1-2* is independent of EDS1 or ELCH function

The accumulation of autophagosomes in *cfs1-2* mutants and the lack thereof in the complemented lines (Figure 3.14) propose that it could be the cause of HR-cell death seen in *cfs1-2*. As it has been demonstrated that autophagosomes accumulate following infection by *Pseudomonas syringae* pv. tomato DC3000 (*PstDC3000*) *AvrRps4* in an *EDS1*-dependent manner (Hofius et al., 2009), it is interesting to see if autophagosome accumulation in *cfs1* mutants would also rely on a functional EDS1.

Both growing *cfs1* and *cfs1-2 eds1-2* plants accumulated 2.35 -3.77 fold and 1.99-4.25 fold of ATG8a in comparison to wild-type, respectively. In *eds1-2* mutants of the same age, the accumulation was 1.18 - 2.98 in comparison to wild-type. The level of NBR1 accumulation was 1.01-2.06 fold, 1.22-2.40 fold and 0.81-1.14 fold in compared to wild-type for *cfs1-2*, *cfs1-2 eds1-2* and *eds1-2*, respectively (Figure 3.18a, b). Altogether, this shows that autophagosome accumulation in *cfs1-2* is, unlike its cell death phenotype, independent of *EDS1* function.

Since cell death in *cfs1-2 elch* progressed slower than in *cfs1-2* (Figure 3.12), it seems likely that the lack of a functional *ELCH* may affect autophagosome accumulation in *cfs1-2*. To tackle this, 14 days old plants (approximately 20 DAS, without an appearance of lesions in *cfs1-2* and *cfs1-2 elch*) were detected for ATG8a and NBR1 accumulation. The accumulation of ATG8 was 2.09 -4.59 fold, 1.99 -5.38 fold in comparison to Col-0 in *cfs1-2* and *cfs1-2 elch*, respectively and 0.78 - 4.27 fold in comparison to Ws-2 in *elch*. As for NBR1, *cfs1-2* and *cfs1-2 elch* accumulated 1.31-2.19 fold and 1.09-2.30 fold in comparison to Col-0, respectively and 0.88-6.29 fold in comparison to Ws-2 in *elch* (Figure 3.18c,d). All in all, this shows that the lack of functional *ELCH* does not drastically affect autophagosome accumulation in *cfs1-2*.
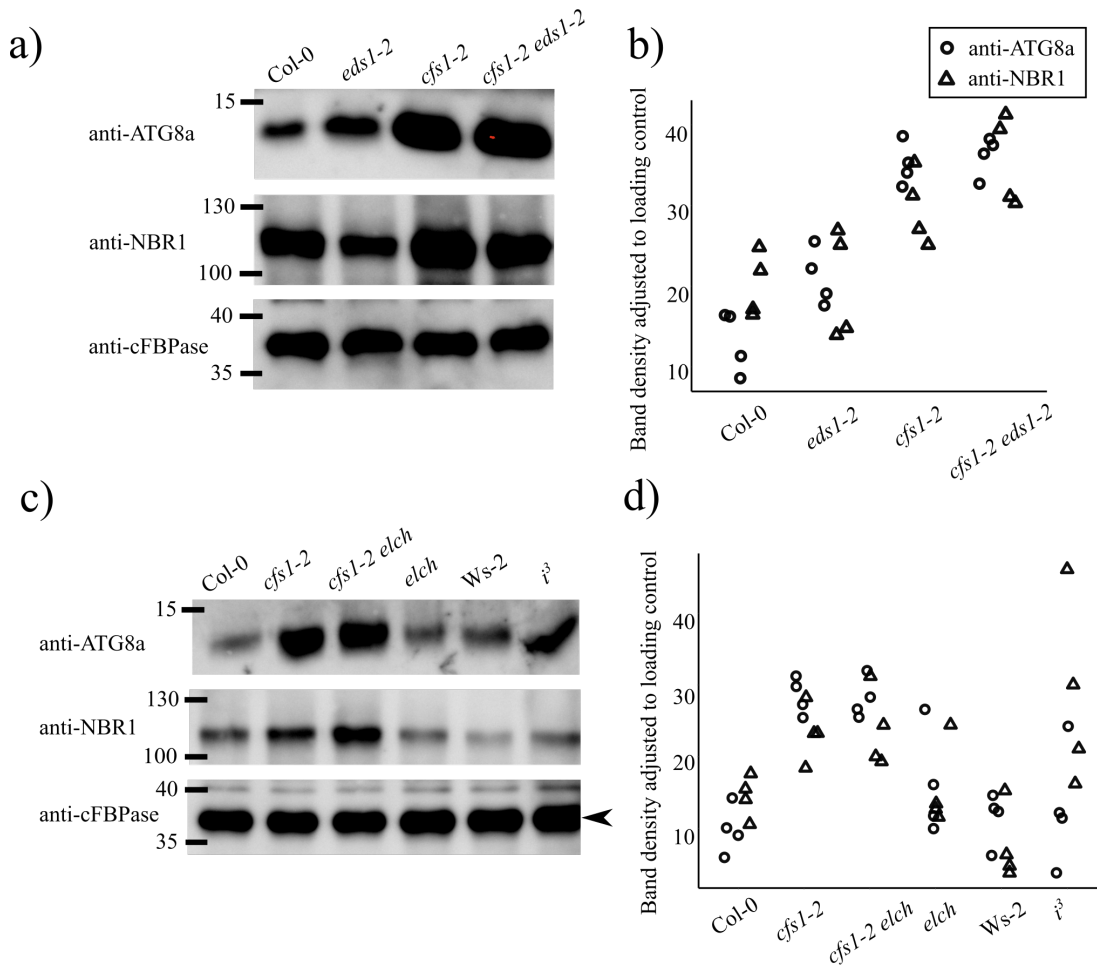
Figure 3.18: **Neither lack of *EDS1* nor *ELCH* function affect autophagosomes accumulation in *cfs1*** - Immunodetection of autophagosomes with anti-ATG8 and anti-NBR1 in

a) 14-days old Col-0, *eds1-2*, *cfs1-2* and *cfs1-2 eds1-2*. The intensities of detected anti-ATG8a and anti-NBR1 bands of all four biological replicates (Figures J.16 to J.19) are depicted in **b)**.

c) 14-days old Col-0, *cfs1*, *cfs1 elch*, *elch*, Ws-2 and i^3. The intensities of detected anti-ATG8a and anti-NBR1 bands of all four biological replicates (Figures J.12 to J.15) are depicted in **d)**.

Anti-cFBPase served as a loading control.

4. Discussions

CFS1 is a plant specific actin- and PI3P-binding protein that interacts with the ESCRT-I component, ELCH (Herberth, 2012). The mutant of this gene mimics lesion formation (Sutipatanasomboon, 2012). The characterization of *cfs1* phenotype reveals that it displays a mild autoimmune symptoms (Figures 3.2, 3.3 and 3.5) and starts to accumulate autophagosomes from the seedlings stage (Figure 3.14). Genetic analyses have demonstrated that HR-cell death in *cfs1* is independent of a functional ESCRT-I component (Figure 3.12) but requires a functional EDS1-induced ETI (Figure 3.6). Although cell death phenotype is lost in *cfs1-2 eds1-2* (Figure 3.6), the mutant still accumulates autophagosomes (Figure 3.18), indicating a separate contribution of *CFS1* to autophagosomes accumulation and of *EDS1* to HR-cell death. Correspondingly, these findings raise the question of how HR-cell death is triggered in *cfs1*; how does CFS1 contribute to autophagy; and how theses processes are connected to the ESCRT-complex related trafficking.

4.1 The cause of death in *cfs1*

Autophagy is a conserved degradative mechanism that sequesters cellular constituents and damaged organelles and delivers them to the vacuole or lysosomes for degradation (Klionsky and Emr, 2000). Under an optimal condition in plants, autophagy activity is basal to maintain cellular homeostasis (Sláviková et al., 2005). Under stress condition, the autophagy genes are transcriptionally up-regulated (Liu and Bassham, 2010; Liu et al., 2012) to increase autophagy degradation that accommodates cellular responses for homeostasis maintenance (Li and Vierstra, 2012; Babst and Odorizzi, 2013).

The autophagosome accumulation in *cfs1* started at the early stage and became more obvious as the plants aged (Figure 3.14). Considering the promoter activity that was depleted as the leaf aged (Figure 3.4), the increasing accumu-
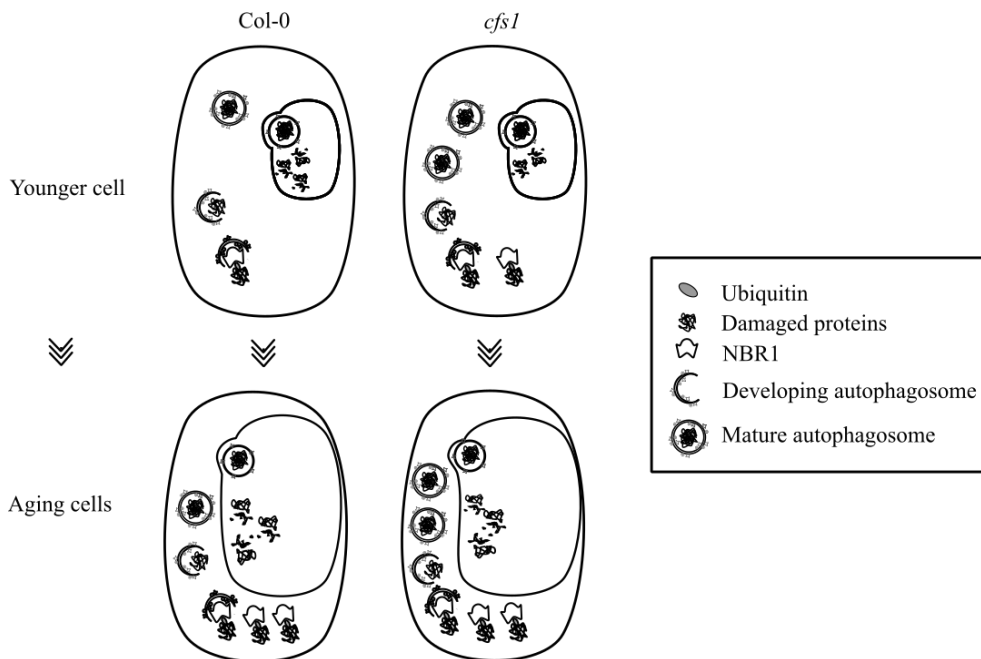
Figure 4.1: **Schematic representation of younger and aging wild-type and cfs1 palisade cell** - In younger cells, autophagosomes start to accumulates in *cfs1* when compared to wild-type at the same age. As the cell ages, damaged proteins and organelles increase, causing a homeostasis imbalace in *cfs1* due to cumulated autophagosomes from the earlier stage.

lation possibly reflects the cumulating lack of *CFS1* activity (Figure 4.1). In the embryogenesis of *Picea abies*, down-regulation of autophagic components disrupts vacuolar cell death in suspensor cells and causes premature necrosis cell death (Minina et al., 2013). In a similar manner, a hindered autophagy activity in *cfs1* can be translated into the appearance of HR-cell death (Figure 3.2). In this regard, cell death in *cfs1* is a cumulative rather than a first-hand occurrence and is likely precipitated by the accumulation of autophagosomes. At the earlier stage, the effect of autophagosome accumulation in *cfs1* to protein homeostasis is propably small and tolerable; however, as the plant ages and is constantly subjected to more stress (Figure 4.1; Coll et al., 2014), the little disturbance cumulates and becomes a crucial factor that breaches the point of no return for homeostasis perturbation. The propagation aspect of *cfs1* phenotype can be explained by the cellular threshold for protein homeostasis that is breached in the older cells before younger cells.

4.1.1 How *CFS1* disruption falsely triggers ETI

Effector-triggered immunity (ETI) is a defensive strategy plants have developed against adapted pathogens that have infected the plants (Wiermer et al., 2005). The centrality of ETI revolves around the plants ability to perceive and distinguish the presence of pathogenic molecules in the cells (Coll et al., 2011). This perception activates downstream defense responses that are mediated by EDS1 or NDR1 (Wiermer et al., 2005). In case of EDS1-mediated ETI, the signal comes from the binding of TIR-NB-LRR *R*-protein to virulent effectors (Aarts et al., 1998). Alternatively, *R*-protein can indirectly perceive pathogen presence by sensing a modification of its binding partner that originates from pathogen effector (Dodds and Rathjen, 2010). This is reflected in several autoimmune mutants whose gene functions are not directly involved in HR-cell death but have been proposed to be targeted by pathogen effectors (Palma et al., 2010; Bruggeman et al., 2015). For example ACD11, another LMM in CFS1 protein interaction network, is a ceramide-1-phosphate transfer protein that regulates the level of cellular phytoceramides (Simanshu et al., 2014) and also interacts with TIR-NB-LRR-like *R* protein, LAZARUS5 (LAZ5) (Palma et al., 2010). It has been proposed that in *acd11*, the disturbance in ceramide level causes an imbalance in death-promoting phytoceramides that may mimic a non-self environment similar to when pathogen effectors modify ACD11 (Munch et al., 2015).

Downstream signaling of ETI results in several cellular responses. One of them is to induce autophagy for the execution of HR-cell death (Hofius et al., 2011; Coll et al., 2014). It has been demonstrated in *Arabidopsis* infected with *PstDC3000 AvrRpm1* and *AvrRpm4* that autophagosomes were initiated in concert with a global transcriptional defense responses mediated by EDS1 (Hofius et al., 2009). In younger *autophagy-related genes defecient* (*atg*) mutants, HR-cell death was suppressed following *PstDC3000 AvrRpm1* and *AvrRpm4* infection (Yoshimoto et al., 2009; Hofius et al., 2009; Coll et al., 2014). This effect, however, disappeared when the *atg* plants became older and worsened as runaway cell death was developed a few days after infection (Yoshimoto et al., 2009). Nevertheless, HR-cell death suppression was restored again when ER stress

(Munch et al., 2014) or SA-accumulation (Yoshimoto et al., 2009) was relieved. The phenotype in older plants suggests that the accumulated cellular garbage in older *atg* mutants is so overwhelming that it masks the autophagy role in HR-cell death (Hofius et al., 2011; Coll et al., 2014) and also hints at the feedback amplification loop through homeostasis perturbation and SA-signaling (Zhou et al., 2014a).

The requirement of a functional EDS1 and ETI for *cfs1* HR-cell death (Figure 3.6) places *CFS1* at the same functional level as TIR-NB-LRRs, which trigger *EDS1*-mediated ETI following pathogen perception (Wiermer et al., 2005). The detection of autophagosomes in the HR-cell death suppressed *cfs1-2 eds1-2* (Figure 3.18a) separates the cell death signaling from autophagosome accumulation and suggests that it triggers EDS1-signaling. By drawing the same rationale as in *acd11*, the cumulated homeostasis perturbation in *cfs1* might be perceived as a non-self environment that falsely invokes HR-cell death. Unlike *acd11*, however, no known NB-LRR protein has been found in the CFS1-interactor proteomic screen (Personal communication S Herberth) nor does *cfs1* phenotype require the presence of SA (Figure 3.7). These suggest that autophagosome accumulation in *cfs1* may trigger an EDS1-ETI feedback mechanism through homeostasis perturbation that is proposed to function in parallel to SA-induced SAR (Bartsch et al., 2006; Breitenbach et al., 2014). In this case, ETI induction in *cfs1* may be suppressed by up-regulating another the degradation pathway and may be unspecific to EDS1 because NDR1 also partially contributes to *PstDC3000 AvrRpm1*-induced HR (Aarts et al., 1998) that partly relies on autophagy machinery for HR-cell death execution (Coll et al., 2014).

4.2   How does CFS1 contribute to autophagy?

Several lines of evidence from this study indicate that the disruption of *CFS1* interferes with autophagosome degradation. First, the level of ER and oxidative-stress marker genes, which can induce autophagy, (Xiong et al., 2007; Munch et al., 2014) were comparable to wild-type (Figures 3.8 and 3.16). Second, the transcript levels of autophagosome component genes and its selective substrate, *NBR1* in *cfs1* were similar to wild-type (Figure 3.15). Lastly, ATG8-

associated punctated structures were formed in *cfs1*, and the nutrient-starvation induced autophagy degradation was functional to a certain degree (Figure 3.17). Therefore, autophagy interference in *cfs1* is not in the initiation of or degradation by autophagy per se but in the degradation of mature autophagosomes (Figure 4.1).

4.2.1 CFS1 could contribute to autophagy via its PI3P and actin binding propety

In developing autophagosomes, PI3P is adhered, and the residing phosphatidylethanolam (PE) is attached to ATG8, providing a unique mark for a developing phagophore and a docking platform for ATG8-interacting proteins (Li and Vierstra, 2012). This that drives autophagosome maturation, selective cargo recruitment and delivery to vacuole (Johansen and Lamark, 2011). Several PI3P-binding proteins have been reported to aid autophagosome maturation. For example, a PI3P binding protein in mammals, double FYVE domain-containing protein 1 (DFCP1) has been shown to translocate from the ER or TGN after nutrient starvation induction to the growing ATG8-punctated structures (Burman and Ktistakis, 2010). PI3P and ATG8-PE on autophagosomal membrane can also be recognized by a class of conserved FYVE and CC domain-containing protein (FYCO) that interacts with ATG8 (Li and Vierstra, 2012). In mammalian cell, FYCO1 transports autophagosomes to vacuole via microtubule plus end- directed movement. FYCO1 depletion is mirrored by an accumulation of ATG8-punctated structure (Pankiv et al., 2010), similar to that in *cfs1-2* (Figure 3.17).

These two examples, together with a report of the actin influence on autophagosome maturation (Aguilera et al., 2012) suggest that a possible autophagic disturbance in *cfs1* likely results from the lack of PI3P and actin-binding that is mediated by the FYVE and/or SYLF domain of the protein. The YAB/SYLF domain functions in the inward movement of the endocytotic cargo in budding yeast (Robertson et al., 2009) and contributes to the interaction with Dedicator of cytokinesis 4 (Dock4) that promotes cancer cell migration (Kobayashi et al., 2014). Interestingly, CFS2 interacts with its only homolog CFS1 (Herberth, 2012), whose interaction with ATG8 has been reported

in the BioGRID database (Stark et al., 2006). In a transient expression assay, CFS2 localization was largely cytoplasmic with low numbers of dots (J Müller BSc thesis, 2014), similar to the the localization of ATG8 under a non-induced condition (Bassham, 2015). In the light of a revealed CFS1 connection to autophagosomes, the localization of CFS1, CFS2 and ELCH should be examined under normal and stress-induced condition with an emphasis on how they are related to ATG8. The interaction between CFS1, CFS2 and ATG8 should also be tested, and the phenotype in a null *cfs2* should be analyzed.

4.2.2 CFS1 could contribute to autophagosome degradation from its interaction with the ESCRT-I component

The ESCRT-complex has been shown to be involved in autophagy initiation, maturation and degradation in budding yeast, *Caenorhabditis elegans*, *Drosophila melanogaster* and various types of mammalian cells (Metcalf and Isaacs, 2010). Therefore, it is foreseeable that CFS1 contribution to autophagy is also through its interaction with the ESCRT-complex component. Although *elch* and i^3 showed the same level of autophagosomes accumulation as in wild-type (Figure 3.18), there have been several reports on the accumulation of autophagosomes from organisms that only have one gene for ELCH/VPS23 and VPS28 (Manil-Segalén et al., 2012; Teis et al., 2009), suggesting the effect in *elch* and i^3 reported here might be concealed by the other functional ESCRT-I components.

Nevertheless, autophagosomes accumulation was reported in *free1*, a plant-specific ESCRT-I component (Gao et al., 2015). FREE1 was shown to regulate ILV formation into the MVB (Gao et al., 2014). When induced by SA agonist, *free1* accumulated higher number of autophagosomes co-localizing with MVBs although less autophagosomes were found in the vacuole. This can be inferred that in plants, apart from the direct delivery of autophagosomes to vacuole, they can also fuse to late endosomes or MVB beforehand (Gao et al., 2015), forming an *amphisome* as reported in budding yeast and various types of mammalian cell (Metcalf and Isaacs, 2010; Manil-Segalén et al., 2012). This concept is supported by a similar phenotype in the later ESCRT components: ESCRT-III components, CHMP1A and CHMP1B (Spitzer et al., 2015)

and an accessory ESCRT-III subunit, ASSOCIATED MOLECULE WITH THE SH3 DOMAIN OF STAM 1 (AMSH1) (Katsiarimpa et al., 2013). Double mutant of ESCRT-III subunits, *chmp1a chmp1b* delivered lesser plastids-containing autophagosome to vacuole (Spitzer et al., 2015). Similarly, under nutrient-starved condition, *amsh1* accumulated autophagosomes, but lesser autophagosomes were detected in the vacuoles of *amsh1* than that of wild-type (Katsiarimpa et al., 2013).
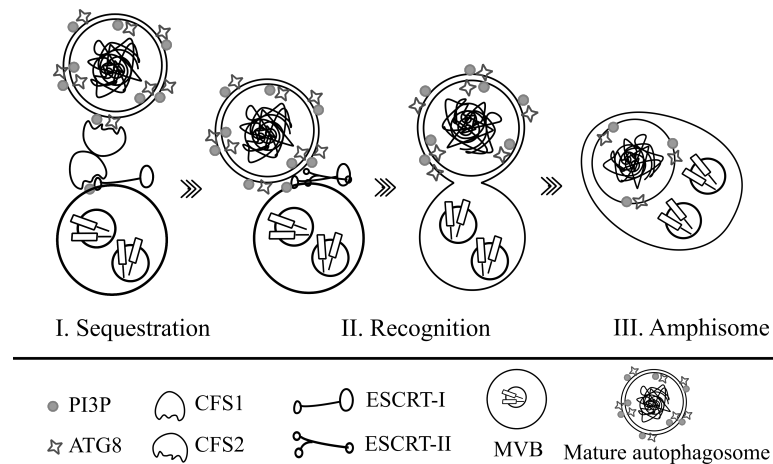
Figure 4.2: **Proposed model of how CFS1 contributes to autophagosome degradation** - CFS1 can contribute to autophagosome degradation through its interaction with CFS2 and ELCH/ESCRT-I component. Together with CFS2, CFS1 sequesters mature autophagosome to the MVB surface. The ESCRT-I components then initiates the fusion of MVB and autophagosome, forming an amphisome.

The accumulation of autophagosomes in *free1*, *chmp1a chmp1b* and *amsh1* indicate that the ESCRT-complex mediates amphisome formation and/or their subsequent delivery to vacuole. Taken the sequential nature of the ESCRT-complex action together with the specificity of CFS1 interaction to ELCH (Herberth, 2012), it is proposed here that CFS1 together with CFS2 function in bridging a mature autophagosome to a MVB where the ESCRT-complex resides to facilitate amphisome formation (Figure 4.2).

4.3   Concluding remarks

The findings that *CFS1* deficiency interferes with autophagosome degradation (Figure 3.14) and affects ETI-induced HR-cell death connect the ESCRT-complex to autophagosome degradation and emphasize the importance of protein homeostasis maintenance in the cell. This is demonstrated in the recent proteomic analysis in nutrient-starved budding yeasts that reveals a coordinated action of MVB and autophagy-mediated degradation. In the early phase of starvation, MVB action provides building blocks for autophagy degradation by selectively degrading transmembrane protein (Müller et al., 2015). Therefore, it is not too far-fetched to speculate that such coordination between the two pathways also exist in plants, and that they are crucial in the developmental processes and adaptation to stress.

Intriguingly, other than autophagy that emerges from this study, CFS1 has been shown to be involved in ubiquitin/26S proteasome system (UPS) through its interaction with XBAT35 and CHIP - both an E3 ligase (Ulbricht, 2011). CHIP interacts with molecular chaperones to ubiquitinate misfolded proteins for degradation by UPS (Lee et al., 2009) in an anti-proteotoxic pathways complementary to NBR1 (Zhou et al., 2014b). NBR1 targets ubiquitined protein aggregates (Kirkin et al., 2009; Zhou et al., 2013) and act as a substrate for selective autophagy degradation (Svenning et al., 2011). It has been demonstrated that prolonged heat stress increases misfolded proteins. Due to a limited capacity of UPS, these increased misfolded proteins aggregate and are targeted by NBR1 for selective autophagy degradation (Figure 4.3; Zhou et al., 2014b; Kirkin et al., 2009). CFS1 interaction with CHIP and XBAT35 suggest an involvement of CFS1 in modulating UPS and autophagy-mediated degradation, also known as chaperone-assisted selective autophagy (CASA) (Johansen and Lamark, 2011), which has not been dissected in plants (Figure 4.3; Li and Vierstra, 2012).

Alternatively, it has been recently demonstrated in fission yeast (*Schizosaccharomyces pombe*) that the ESCRT-complex directly sorts NBR1-bound cargo into the MVB (Liu et al., 2015). Thus, it could be speculated that CFS1 would be involved in this process if similar pathway existed in plants (Figure 4.3).
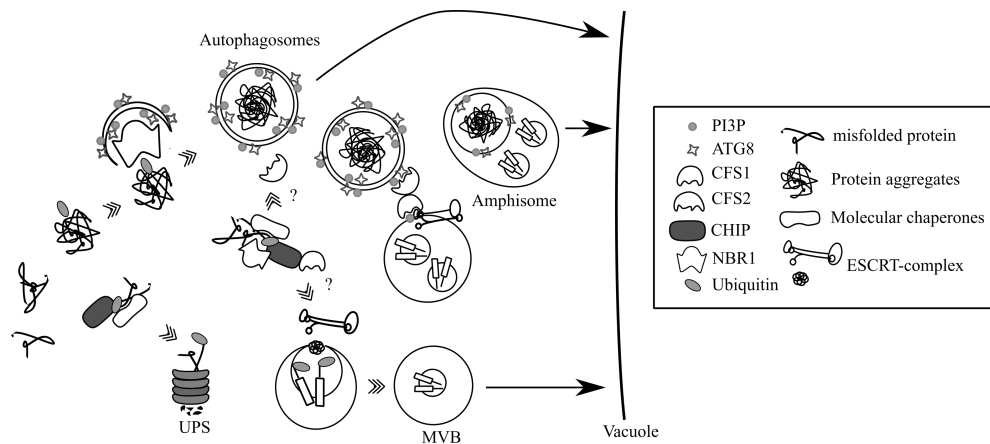
Figure 4.3: **Functional landscape of CFS1 in the endomembrane system** - Misfolded proteins are recognized and ubiquitinated by CHIP and molecular chaperones for the degradation by UPS. Misfolded proteins aggregate when subjected to prolonged stress. Protein aggregates are ubiquitinated and recognized by NBR1 that acts as a substrate for selective autophagy. Together with CFS2 and the ESCRT-complex, it is proposed that CFS1 functions in sequestering mature autophagosome to MVB where amphisome is formed before subsequent delivery to vacuole. Whether CFS1 interaction with CHIP facilitates misfolded protein degradation via CASA or ESCRT-mediated MVB-pathway remains to be explored.

All things considered, this study provides a functional landscape of *CFS1* in the ESCRT-complex related protein trafficking (Figure 4.3). CFS1 functions, possibly together with CFS2, in sequestering mature autophagosomes to late endosomes where the ESCRT-complex resides. This interaction is crucial for a proper degradation of autophagosomes. Considering that CFS1 also interacts with other two E3 ligases, it is feasible that CFS1 also influences CASA. To further explore this possibility, the function of CFS1 in relation to autophagy, CHIP and XBAT35, as well as CFS2 to ATG8 should be investigated. By the same token, the effect of up- or down-regulating UPS and MVB-pathways on autophagosomes degradation and HR-cell death phenotype in *cfs1* should also be examined.

References

Nicole Aarts, Matthew Metz, EB Holub, Brian J Staskawicz, Michael J Daniels, and Jane E Parker. Different requirements for EDS1 and NDR1 by disease resistance genes define at least two R gene-mediated signaling pathways in Arabidopsis. *Proceedings of the National Academy of Sciences of the United States of America*, 95(17):10306–10311, 1998. doi: 10.1073/pnas.95.17.10306.

Hiroshi Abe, Ken Tateishi, Shigemi Seo, Soichi Kugimiya, Masami Yokota Hirai, Yuji Sawada, Yoshiyuki Murata, Kaori Yara, Takeshi Shimoda, and Masatomo Kobayashi. Disarming the Jasmonate-Dependent Plant Defense Makes Nonhost Arabidopsis Plants Accessible to the American Serpentine Leafminer. *Plant physiology*, 163(3):1242–53, November 2013. doi: 10.1104/pp.113.222802.

Milton Osmar Aguilera, Walter Berón, and María Isabel Colombo. The actin cytoskeleton participates in the early events of autophagosome formation upon starvation induced autophagy. *Autophagy*, 8(11):1590–1603, 2012. doi: 10.4161/auto.21459.

José M Alonso, Anna N Stepanova, Thomas J Leisse, Christopher J Kim, Huaming Chen, Paul Shinn, Denise K Stevenson, Justin Zimmerman, Pascual Barajas, Rosa Cheuk, Carmelita Gadrinab, Collen Heller, Albert Jeske, Eric Koesema, Cristina C Meyers, Holly Parker, Lance Prednis, Yasser Ansari, Nathan Choy, Hashim Deen, Michael Geralt, Nisha Hazari, Emily Hom, Meagan Karnes, Celene Mulholland, Ral Ndubaku, Ian Schmidt, Plinio Guzman, Laura Aguilar-Henonin, Markus Schmid, Detlef Weigel, David E Carter, Trudy Marchand, Eddy Risseeuw, Debra Brogden, Albana Zeko, William L Crosby, Charles C Berry, and Joseph R Ecker. Genome-wide insertional mutagenesis of Arabidopsis thaliana. *Science (New York, N.Y.)*, 301(5633):653–657, 2003. doi: 10.1126/science.1086391.

Markus Babst. A Protein s Final ESCRT. *Traffic*, pages 2–9, 2005. doi: 10.1111/j.1600-0854.2005.00246.x.

Markus Babst and Greg Odorizzi. The balance of protein expression and degradation: an ESCRTs point of view. *Current opinion in cell biology*, pages 3–8, June 2013. ISSN 1879-0410. doi: 10.1016/j.ceb.2013.05.003.

Markus Babst, Beverly Wendland, Eden J. Estepa, and Scott D. Emr. The Vps4p AAA ATPase regulates membrane association of a Vps protein complex required for normal endosome function. *EMBO Journal*, 17(11):2982–2993, June 1998. doi: 10.1093/emboj/17.11.2982.

Markus Babst, David J Katzmann, Eden J Estepa-Sabal, Timo Meerloo, and Scott D Emr. ESCRT-III: an endosome-associated heterooligomeric protein complex required for mvb sorting. *Developmental cell*, 3(2):271–82, August 2002a. ISSN 1534-5807.

Markus Babst, David J Katzmann, William B Snyder, Beverly Wendland, and Scott D Emr. Endosome-associated complex, ESCRT-II, recruits transport machinery for protein sorting at the multivesicular body. *Developmental cell*, 3(2):283–9, August 2002b. ISSN 1534-5807.

Kristi G Bache, Andreas Brech, Anja Mehlum, and Harald Stenmark. Hrs regulates multivesicular body formation via ESCRT recruitment to endosomes. *The Journal of cell biology*, 162(3): 435–42, August 2003a. ISSN 0021-9525. doi: 10.1083/jcb.200302131.

Kristi G Bache, Camilla Raiborg, Anja Mehlum, and Harald Stenmark. STAM and Hrs are subunits of a multivalent ubiquitin-binding complex on early endosomes. *The Journal of biological chemistry*, 278(14):12513–21, April 2003b. ISSN 0021-9258. doi: 10.1074/jbc.M210843200.

Michael Bartsch, Enrico Gobbato, Pawel Bednarek, Svenja Debey, Joachim L Schultze, Jaqueline Bautor, and Jane E Parker. Salicylic acid-independent ENHANCED DISEASE SUSCEPTIBILITY1 signaling in Arabidopsis immunity and cell death is regulated by the monooxygenase FMO1 and the Nudix hydrolase NUDT7. *The Plant cell*, 18(4):1038–1051, March 2006. ISSN 1040-4651. doi: 10.1105/tpc.105.039982.1.

Diane C. Bassham. Methods for analysis of autophagy in plants. *Methods*, 75:181–188, March 2015. ISSN 10462023. doi: 10.1016/j.ymeth.2014.09.003.

Diane C. Bassham, Federica Brandizzi, Marisa S Otegui, and Anton A Sanderfoot. The Secretory System of Arabidopsis, January 2008. ISSN 1543-8120.

S. A. Bowling, J D Clarke, Y Liu, D F Klessig, and X Dong. The cpr5 mutant of Arabidopsis expresses both NPR1-dependent and NPR1-independent resistance. *The Plant cell*, 9(9): 1573–1584, September 1997. doi: 10.1105/tpc.9.9.1573.

Heiko H Breitenbach, Marion Wenig, Finni Wittek, Lucia Jordá, Ana M Maldonado-Alconada, Hakan Sarioglu, Thomas Colby, Claudia Knappe, Marlies Bichlmeier, Elisabeth Pabst, David Mackey, Jane E Parker, and a Corina Vlot. Contrasting Roles of the Apoplastic Aspartyl Protease APOPLASTIC, ENHANCED DISEASE SUSCEPTIBILITY1-DEPENDENT1 and LEGUME LECTIN-LIKE PROTEIN1 in Arabidopsis Systemic Acquired Resistance. *Plant physiology*, 165(2):791–809, 2014. doi: 10.1104/pp.114.239665.

Peter Brodersen, Morten Petersen, Helen M Pike, Brian Olszak, Sø ren Skov, Niels Odum, Lise Bolt Jø rgensen, Rhoderick E Brown, and John Mundy. Knockout of Arabidopsis accelerated-cell-death11 encoding a sphingosine transfer protein causes activation of programmed cell death and defense. *Genes & development*, 16(4):490–502, February 2002. ISSN 0890-9369. doi: 10.1101/gad.218202.

REFERENCES

Peter Brodersen, Frederikke Gro Malinovsky, Kian Hématy, Mari-anne Newman, and John Mundy. The role of salicylic acid in the induction of cell death in Arabidopsis acd11. *Plant physiology*, 138(2):1037–1045, June 2005. ISSN 0032-0889. doi: 10.1104/pp.105.059303.

Quentin Bruggeman, CÃcile Raynaud, Moussa Benhamed, and Marianne Delarue. To die or not to die? Lessons from lesion mimic mutants. *Frontiers in Plant Science*, 6(January):1–22, 2015. ISSN 1664-462X. doi: 10.3389/fpls.2015.00024.

Chloe Burman and Nicholas T Ktistakis. Regulation of autophagy by phosphatidylinositol 3-phosphate. *FEBS letters*, 584(7):1302–12, April 2010. ISSN 1873-3468. doi: 10.1016/j.febslet. 2010.01.011.

Yi Cai, Xiaohong Zhuang, Caiji Gao, Xiangfeng Wang, and Liwen Jiang. The Arabidopsis Endosomal Sorting Complex Required for Transport III Regulates Internal Vesicle Formation of the Prevacuolar Compartment and Is Required for Plant Development. *Plant physiology*, 165(3):1328–1343, 2014. ISSN 1532-2548. doi: 10.1104/pp.114.238378.

Hui Cao, SA Scott A Sa Bowling, AS Susan Gordon, and X. Dong. Characterization of an Arabidopsis Mutant That Is Nonresponsive to Inducers of Systemic Acquired Resistance. *The Plant cell*, 6(11):1583–1592, November 1994. ISSN 1040-4651. doi: 10.1105/tpc.6.11. 1583. URL http://www.pubmedcentral.nih.gov/articlerender.fcgi?artid=160545& tool=pmcentrez&rendertype=abstract.

Cheng Cheng, Xiquan Gao, Baomin Feng, Jen Sheen, Libo Shan, and Ping He. Plant immune response to pathogens differs with changing temperatures. *Nature communications*, 4(May): 2530, September 2013. ISSN 2041-1723. doi: 10.1038/ncomms3530.

Steven J. Clough and Andrew F. Bent. Floral dip: A simplified method for Agrobacterium-mediated transformation of Arabidopsis thaliana. *Plant Journal*, 16(6):735–743, December 1998. doi: 10.1046/j.1365-313X.1998.00343.x.

Nuria S Coll, Dominique Vercammen, Andrea Smidler, Charles Clover, Frank Van Breusegem, Jeffery L Dangl, and Petra Epple. Arabidopsis type I metacaspases control cell death. *Science (New York, N.Y.)*, 330(6009):1393–1397, 2010. ISSN 0036-8075. doi: 10.1126/science.1194980.

Nuria S Coll, P Epple, and J L Dangl. Programmed cell death in the plant immune system. *Cell death and differentiation*, 18(8):1247–56, August 2011. ISSN 1476-5403. doi: 10.1038/cdd. 2011.37.

Nuria S Coll, A Smidler, M Puigvert, C Popa, M Valls, and J L Dangl. The plant metacaspase AtMC1 in pathogen-triggered programmed cell death and aging: functional linkage with autophagy. *Cell death and differentiation*, pages 1–10, May 2014. ISSN 1476-5403. doi: 10. 1038/cdd.2014.50.

Tomasz Czechowski, Mark Stitt, Thomas Altmann, Michael K Udvardi, and Wolf-Rüdiger Scheible. Genome-wide identification and testing of superior reference genes for transcript normalization in Arabidopsis. *Plant physiology*, 139(1):5–17, September 2005. ISSN 0032-0889. doi: 10.1104/pp.105.063743.

S. Danisman, F. van der Wal, S. Dhondt, R. Waites, S. de Folter, A. Bimbo, A. D. van Dijk, J. M. Muino, L. Cutri, M. C. Dornelas, G. C. Angenent, and R. G. H. Immink. Arabidopsis Class I and Class II TCP Transcription Factors Regulate Jasmonic Acid Metabolism and Leaf Development Antagonistically. *Plant Physiology*, 159(4):1511–1523, August 2012. ISSN 0032-0889. doi: 10.1104/pp.112.200303.

Martin B. Dickman and Paul de Figueiredo. Comparative Pathobiology of Fungal Pathogens of Plants and Animals. *PLoS Pathogens*, 7(12):e1002324, December 2011. ISSN 1553-7374. doi: 10.1371/journal.ppat.1002324.

Peter N. Dodds and John P. Rathjen. Plant immunity: towards an integrated view of plant-pathogen interactions. *Nature Reviews Genetics*, 11(8):539–548, August 2010. ISSN 1471-0056. doi: 10.1038/nrg2812.

Jed H. Doelling, Joseph M. Walker, Eric M. Friedman, Allison R Thompson, and Richard D Vierstra. The APG8/12-activating enzyme APG7 is required for proper nutrient recycling and senescence in Arabidopsis thaliana. *Journal of Biological Chemistry*, 277(36):33105–33114, August 2002. ISSN 00219258. doi: 10.1074/jbc.M204630200.

Keith W Earley, Jeremy R Haag, Olga Pontes, Kristen Opper, Tom Juehne, Keming Song, and Craig S Pikaard. Gateway-compatible vectors for plant functional genomics and proteomics. *The Plant journal : for cell and molecular biology*, 45(4):616–629, 2006. doi: 10.1111/j.1365-313X.2005.02617.x.

Sacha Escamez and Hannele Tuominen. Programmes of cell death and autolysis in tracheary elements: When a suicidal cell arranges its own corpse removal. *Journal of Experimental Botany*, 65(5):1313–1321, 2014. ISSN 14602431. doi: 10.1093/jxb/eru057.

Bart J Feys, Marcel Wiermer, Riyaz A Bhat, Lisa J Moisan, Nieves Medina-Escobar, Christina Neu, Adriana Cabral, and Jane E Parker. Arabidopsis SENESCENCE-ASSOCIATED GENE101 stabilizes and signals within an ENHANCED DISEASE SUSCEPTIBILITY1 complex in plant innate immunity. *The Plant cell*, 17(9):2601–13, September 2005. doi: 10.1105/tpc.105.033910.

Yaron Fuchs and Hermann Steller. Programmed Cell Death in Animal Development and Disease. *Cell*, 147(4):742–758, November 2011. ISSN 00928674. doi: 10.1016/j.cell.2011.10.033.

REFERENCES

L Galluzzi, I Vitale, J M Abrams, E S Alnemri, E H Baehrecke, M V Blagosklonny, T M Dawson, V L Dawson, W S El-Deiry, S Fulda, E Gottlieb, D R Green, M O Hengartner, O Kepp, R a Knight, S Kumar, S a Lipton, X Lu, F Madeo, W Malorni, P Mehlen, G Nuñez, M E Peter, M Piacentini, D C Rubinsztein, Y Shi, H-U Simon, Peter Vandenabeele, E White, J Yuan, B Zhivotovsky, G Melino, and Guido Kroemer. Molecular definitions of cell death subroutines: recommendations of the Nomenclature Committee on Cell Death 2012. *Cell death and differentiation*, 19(1):107–20, January 2012. ISSN 1476-5403. doi: 10.1038/cdd.2011.96.

L Galluzzi, J M Bravo-San Pedro, I Vitale, S a Aaronson, J M Abrams, D Adam, E S Alnemri, L Altucci, D Andrews, M Annicchiarico-Petruzzelli, E H Baehrecke, N G Bazan, M J Bertrand, K Bianchi, M V Blagosklonny, K Blomgren, C Borner, D E Bredesen, C Brenner, M Campanella, E Candi, F Cecconi, F K Chan, N S Chandel, E H Cheng, J E Chipuk, J a Cidlowski, A Ciechanover, T M Dawson, V L Dawson, V De Laurenzi, R De Maria, K-M Debatin, N Di Daniele, V M Dixit, B D Dynlacht, W S El-Deiry, G M Fimia, R a Flavell, S Fulda, C Garrido, M-L Gougeon, D R Green, H Gronemeyer, G Hajnóczky, J M Hardwick, M O Hengartner, H Ichijo, B Joseph, P J Jost, T Kaufmann, O Kepp, D J Klionsky, R a Knight, S Kumar, J J Lemasters, B Levine, A Linkermann, S a Lipton, R a Lockshin, C López-Otín, E Lugli, F Madeo, W Malorni, J-C Marine, S J Martin, J-C Martinou, J P Medema, P Meier, S Melino, N Mizushima, U Moll, C Muñoz Pinedo, G Nuñez, A Oberst, T Panaretakis, J M Penninger, M E Peter, M Piacentini, P Pinton, J H Prehn, H Puthalakath, G a Rabinovich, K S Ravichandran, R Rizzuto, C M Rodrigues, D C Rubinsztein, T Rudel, Y Shi, H-U Simon, B R Stockwell, G Szabadkai, S W Tait, H L Tang, N Tavernarakis, Y Tsujimoto, Tom Vanden Berghe, Peter Vandenabeele, A Villunger, E F Wagner, H Walczak, E White, W G Wood, J Yuan, Z Zakeri, B Zhivotovsky, G Melino, and Guido Kroemer. Essential versus accessory aspects of cell death: recommendations of the NCCD 2015. *Cell Death and Differentiation*, 22 (1):58–73, 2014. ISSN 1350-9047. doi: 10.1038/cdd.2014.137.

Caiji Gao, Ming Luo, Qiong Zhao, Renzhi Yang, Yong Cui, Yonglun Zeng, Jun Xia, and Liwen Jiang. A Unique Plant ESCRT Component, FREE1, Regulates Multivesicular Body Protein Sorting and Plant Growth. *Current Biology*, 24(21):2556–2563, November 2014. ISSN 09609822. doi: 10.1016/j.cub.2014.09.014.

Caiji Gao, Xiaohong Zhuang, Yong Cui, Xi Fu, Yilin He, Qiong Zhao, Yonglun Zeng, Jinbo Shen, Ming Luo, and Liwen Jiang. Dual roles of an Arabidopsis ESCRT component FREE1 in regulating vacuolar protein transport and autophagic degradation. *Proceedings of the National Academy of Sciences*, 112(6):1886–1891, February 2015. ISSN 0027-8424. doi: 10. 1073/pnas.1421271112.

J Glazebrook, E E Rogers, and F M Ausubel. Use of Arabidopsis for genetic dissection of plant defense responses. *Annual review of genetics*, 31:547–569, 1997. ISSN 0066-4197. doi: 10.1146/annurev.genet.31.1.547.

Jean T Greenberg. Programmed cell death: a way of life for plants. *Proceedings of the National Academy of Sciences of the United States of America*, 93(22):12094–7, 1996. ISSN 0027-8424. doi: 10.1073/pnas.93.22.12094.

Thomas J Haas, Marek K Sliwinski, Dana E Martínez, Mary Preuss, Kazuo Ebine, Takashi Ueda, Erik Nielsen, Greg Odorizzi, and Marisa S Otegui. The Arabidopsis AAA ATPase SKD1 is involved in multivesicular endosome function and interacts with its positive regulator LYST-INTERACTING PROTEIN5. *The Plant cell*, 19(4):1295–1312, 2007. ISSN 1040-4651. doi: 10.1105/tpc.106.049346.

T. Hackenberg, T. Juul, A. Auzina, S. Gwizdz, A. Malolepszy, K. van der Kelen, S. Dam, S. Bressendorff, A. Lorentzen, P. Roepstorff, K. Lehmann Nielsen, J.-E. Jorgensen, Daniel Hofius, F Breusegem, M. Petersen, and S. U. Andersen. Catalase and NO CATALASE ACTIVITY1 Promote Autophagy-Dependent Cell Death in Arabidopsis. *The Plant Cell*, 25(11): 4616–4626, November 2013. ISSN 1040-4651. doi: 10.1105/tpc.113.117192.

Junya Hasegawa, Emi Tokuda, Takeshi Tenno, Kazuya Tsujita, Haruko Sawai, Hidekazu Hiroaki, Tadaomi Takenawa, and Toshiki Itoh. SH3YL1 regulates dorsal ruffle formation by a novel phosphoinositide-binding domain. *The Journal of Cell Biology*, 193(5):901–916, May 2011. ISSN 0021-9525. doi: 10.1083/jcb.201012161.

Noriyuki Hatsugai and Ikuko Hara-Nishimura. Two vacuole-mediated defense strategies in plants. *Plant signaling & behavior*, 5(12):1568–70, December 2010. ISSN 1559-2324. doi: 10.4161/psb.5.12.13319.

Noriyuki Hatsugai, Shinji Iwasaki, Kentaro Tamura, Maki Kondo, Kentaro Fuji, Kimi Ogasawara, Mikio Nishimura, and Ikuko Hara-Nishimura. A novel membrane fusion-mediated plant immunity against bacterial pathogens. *Genes & Development*, 23(21):2496–2506, November 2009. ISSN 0890-9369. doi: 10.1101/gad.1825209.

Stefanie Herberth. *ESCRT-0 in Arabidopsis thaliana ? Biochemische und zellbiologische Analyse von FYVE2*. Inaugural-dissertation, Universität zu Köln, 2012.

Katrin Hinderhofer and Ulrike Zentgraf. Identification of a transcription factor specifically expressed at the onset of leaf senescence. *Planta*, 213(3):469–473, July 2001. ISSN 0032-0935. doi: 10.1007/s004250000512.

Daniel Hofius, Torsten Schultz-Larsen, Jan Joensen, Dimitrios I. Tsitsigiannis, Nikolaj H T Petersen, Ole Mattsson, Lise Bolt Jø rgensen, Jonathan D G Jones, John Mundy, and Morten Petersen. Autophagic Components Contribute to Hypersensitive Cell Death in Arabidopsis. *Cell*, 137(4):773–783, May 2009. ISSN 00928674. doi: 10.1016/j.cell.2009.02.036.

REFERENCES

Daniel Hofius, David Munch, S Bressendorff, John Mundy, and M Petersen. Role of autophagy in disease resistance and hypersensitive response-associated cell death. *Cell Death and Differentiation*, 18(8):1257–1262, 2011. ISSN 1350-9047. doi: 10.1038/cdd.2011.43.

Torsten Hothorn, Frank Bretz, and Peter Westfall. Simultaneous Inference in General Parametric Models. *Biometrical Journal*, 50(3):346–363, June 2008. ISSN 03233847. doi: 10.1002/bimj.200810425.

T Jabs, R a Dietrich, and J L Dangl. Initiation of runaway cell death in an Arabidopsis mutant by extracellular superoxide. *Science (New York, N.Y.)*, 273(5283):1853–6, September 1996. ISSN 0036-8075.

Terje Johansen and Trond Lamark. Selective autophagy mediated by autophagic adapter proteins. *Autophagy*, 7(3):279–296, March 2011. ISSN 1554-8627. doi: 10.4161/auto.7.3.14487.

a M Jones. Programmed cell death in development and defense. *Plant physiology*, 125(1):94–7, January 2001. ISSN 0032-0889.

Jonathan D G Jones and Jeffery L Dangl. The plant immune system. *Nature*, 444(7117):323–329, 2006. ISSN 0028-0836. doi: 10.1038/nature05286.

Agnieszka Kaczmarek, Peter Vandenabeele, and Dmitri V. Krysko. Necroptosis: The Release of Damage-Associated Molecular Patterns and Its Physiological Relevance. *Immunity*, 38(2): 209–223, 2013. ISSN 10747613. doi: 10.1016/j.immuni.2013.02.003.

Kamila Kalinowska, Marie-Kristin Nagel, Kaija Goodman, Laura Cuyas, Franziska Anzenberger, Angela Alkofer, Javier Paz-Ares, Pascal Braun, Vicente Rubio, Marisa S. Otegui, and Erika Isono. Arabidopsis ALIX is required for the endosomal localization of the deubiquitinating enzyme AMSH3. *Proceedings of the National Academy of Sciences*, page 201510516, August 2015. ISSN 0027-8424. doi: 10.1073/pnas.1510516112.

Anthi Katsiarimpa, Kamila Kalinowska, Franziska Anzenberger, Corina Weis, Maya Ostertag, Chie Tsutsumi, Claus Schwechheimer, Frédéric Brunner, Ralph Hückelhoven, and Erika Isono. The Deubiquitinating Enzyme AMSH1 and the ESCRT-III Subunit VPS2.1 Are Required for Autophagic Degradation in Arabidopsis. *The Plant cell*, pages 1–18, June 2013. ISSN 1532-298X. doi: 10.1105/tpc.113.113399.

David J Katzmann, Markus Babst, and S D Emr. Ubiquitin-dependent sorting into the multivesicular body pathway requires the function of a conserved endosomal protein sorting complex, ESCRT-I. *Cell*, 106(2):145–55, July 2001. ISSN 0092-8674.

David J Katzmann, Christopher J Stefan, Markus Babst, and Scott D Emr. Vps27 recruits ESCRT machinery to endosomes during MVB sorting. *The Journal of cell biology*, 162(3):413–23, August 2003. ISSN 0021-9525. doi: 10.1083/jcb.200302136.

Channa Keshavaiah. *Molecular and Functional Characterization of the Arabidopsis ESCRT-I complex*. Inaugural-dissertation, Universität zu Köln, 2008.

Vladimir Kirkin, Trond Lamark, Yu-Shin Sou, Geir Bjø rkøy, Jennifer L. Nunn, Jack-Ansgar Bruun, Elena Shvets, David G. McEwan, Terje H. Clausen, Philipp Wild, Ivana Bilusic, Jean-Philippe Theurillat, Aud Ø vervatn, Tetsuro Ishii, Zvulun Elazar, Masaaki Komatsu, Ivan Dikic, and Terje Johansen. A Role for NBR1 in Autophagosomal Degradation of Ubiquitinated Substrates. *Molecular Cell*, 33(4):505–516, 2009. ISSN 10972765. doi: 10.1016/j.molcel.2009.01.020.

D J Klionsky and S D Emr. Autophagy as a regulated pathway of cellular degradation. *Science (New York, N.Y.)*, 290(5497):1717–21, 2000. ISSN 0036-8075. doi: 10.1126/science.290.5497. 1717.

Masakazu Kobayashi, Kohei Harada, Manabu Negishi, and Hironori Katoh. Dock4 forms a complex with SH3YL1 and regulates cancer cell migration. *Cellular signalling*, 26(5):1082–8, 2014. ISSN 1873-3913. doi: 10.1016/j.cellsig.2014.01.027.

Masayuki Komada and Philippe Soriano. Hrs, a FYVE finger protein localized to early endosomes, is implicated in vesicular traffic and required for ventral folding morphogenesis. *Genes and Development*, 13(11):1475–1485, 1999. ISSN 08909369. doi: 10.1101/gad.13.11.1475.

Guido Kroemer and Beth Levine. Autophagic cell death: the story of a misnomer. *Nature Reviews Molecular Cell Biology*, 9(12):1004–1010, December 2008. ISSN 1471-0072. doi: 10. 1038/nrm2529.

Eric Lam. Controlled cell death, plant survival and development. *Nature Reviews Molecular Cell Biology*, 5(4):305–315, April 2004. ISSN 1471-0072. doi: 10.1038/nrm1358.

Eric Lam, Naohiro Kato, and Michael Lawton. Programmed cell death, mitochondria and the plant hypersensitive response. *Nature*, 411(June):848–853, 2001. ISSN 00280836. doi: 10.1038/35081184.

Sookjin Lee, Dong Wook Lee, Yongjik Lee, Ulrike Mayer, York-Dieter Stierhof, Sumin Lee, Gerd Jürgens, and Inhwan Hwang. Heat shock protein cognate 70-4 and an E3 ubiquitin ligase, CHIP, mediate plastid-destined precursor degradation through the ubiquitin-26S proteasome system in Arabidopsis. *The Plant cell*, 21(12):3984–4001, 2009. ISSN 1532-298X. doi: 10.1105/tpc.109.071548.

Faqiang Li and Richard D Vierstra. Autophagy: A multifaceted intracellular system for bulk and selective recycling. *Trends in Plant Science*, 17(9):526–537, 2012. ISSN 13601385. doi: 10.1016/j.tplants.2012.05.006.

REFERENCES

Xiao-Man Liu, Ling-ling Sun, Wen Hu, Yue-he Ding, Meng-qiu Dong, and Li-Lin Du. ESCRTs Cooperate with a Selective Autophagy Receptor to Mediate Vacuolar Targeting of Soluble Cargos. *Molecular Cell*, 59(6):1035–1042, September 2015. ISSN 10972765. doi: 10.1016/j.molcel.2015.07.034.

Y. Liu, J. S. Burgos, Y. Deng, R. Srivastava, S. H. Howell, and Diane C. Bassham. Degradation of the Endoplasmic Reticulum by Autophagy during Endoplasmic Reticulum Stress in Arabidopsis. *The Plant Cell*, 24(11):4635–4651, November 2012. ISSN 1040-4651. doi: 10.1105/tpc.112.101535.

Yimo Liu and Diane C. Bassham. TOR Is a Negative Regulator of Autophagy in Arabidopsis thaliana. *PLoS ONE*, 5(7):e11883, July 2010. ISSN 1932-6203. doi: 10.1371/journal.pone.0011883.

Kenneth J. Livak and T D Schmittgen. Analysis of relative gene expression data using real-time quantitative PCR and the 2(-Delta Delta C(T)) Method. *Methods (San Diego, Calif.)*, 25 (4):402–8, December 2001. doi: 10.1006/meth.2001.1262.

Séverine Lorrain, Fabienne Vailleau, Claudine Balagué, and Dominique Roby. Lesion mimic mutants: keys for deciphering cell death and defense pathways in plants? *Trends in plant science*, 8(6):263–71, June 2003. ISSN 1360-1385. doi: 10.1016/S1360-1385(03)00108-0.

Anne-Laure Mahul-Mellier, Fiona J Hemming, Béatrice Blot, Sandrine Fraboulet, and Rémy Sadoul. Alix, making a link between apoptosis-linked gene-2, the endosomal sorting complexes required for transport, and neuronal death in vivo. *The Journal of neuroscience : the official journal of the Society for Neuroscience*, 26(2):542–549, January 2006. ISSN 0270-6474. doi: 10.1523/JNEUROSCI.3069-05.2006.

Anne-Laure Mahul-Mellier, Flavie Strappazzon, Christine Chatellard-Causse, Béatrice Blot, David Béal, Sakina Torch, Fiona Hemming, Anne Petiot, Jean-Marc Verna, Sandrine Fraboulet, and Rémy Sadoul. Alix and ALG-2 make a link between endosomes and neuronal death. *Biochemical Society transactions*, 37(Pt 1):200–3, February 2009. ISSN 1470-8752. doi: 10.1042/BST0370200.

Frederikke G Malinovsky, Peter Brodersen, Berthe Katrine Fiil, Lea Vig McKinney, Stephan Thorgrimsen, Martina Beck, H Bjø rn Nielsen, Stefano Pietra, Cyril Zipfel, Silke Robatzek, Morten Petersen, Daniel Hofius, and John Mundy. Lazarus1, a DUF300 protein, contributes to programmed cell death associated with arabidopsis acd11 and the hypersensitive response. *PLoS ONE*, 5(9):1–11, January 2010. doi: 10.1371/journal.pone.0012586.

Marion Manil-Segalén, Christophe Lefebvre, Emmanuel Culetto, Renaud Legouis, Marion Manil-segalén, Christophe Lefebvre, Emmanuel Culetto, and Renaud Legouis. Need an

ESCRT for autophagosomal maturation? *Communicative and Integrative Biology*, 5(6):566–571, 2012. ISSN 19420889. doi: 10.4161/cib.21522.

J Martínez-Fábregas, I Díaz-Moreno, K González-Arzola, A Díaz-Quintana, and M A De la Rosa. A common signalosome for programmed cell death in humans and plants. *Cell Death and Disease*, 5(7):e1314, July 2014. ISSN 2041-4889. doi: 10.1038/cddis.2014.280.

Jaideep Mathur and Csaba Koncz. Method for preparation of epidermal imprints using agarose. *BioTechniques*, 22:280–282, 1997. ISSN 07366205.

Jaideep Mathur, Neeta Mathur, Victor Kirik, Birgit Kernebeck, Bhylahalli Purushottam Srinivas, and Martin Hülskamp. Arabidopsis CROOKED encodes for the smallest subunit of the ARP2/3 complex and controls cell shape by region specific fine F-actin formation. *Development (Cambridge, England)*, 130(14):3137–3146, July 2003. ISSN 0950-1991. doi: 10.1242/dev.00549.

Daniel Metcalf and Adrian M. Isaacs. The role of ESCRT proteins in fusion events involving lysosomes, endosomes and autophagosomes. *Biochemical Society Transactions*, 38(6):1469–1473, 2010. ISSN 0300-5127. doi: 10.1042/BST0381469.

Lydie Michaillat and Andreas Mayer. Identification of Genes Affecting Vacuole Membrane Fragmentation in Saccharomyces cerevisiae. *PLoS ONE*, 8(2), 2013. ISSN 19326203. doi: 10.1371/journal.pone.0054160.

Elena A Minina, Lada H Filonova, Kazutake Fukada, Eugene I Savenkov, Vladimir Gogvadze, David Clapham, Victoria Sanchez-Vera, Maria F Suarez, Boris Zhivotovsky, Geoffrey Daniel, Andrei Smertenko, and Peter V Bozhkov. Autophagy and metacaspase determine the mode of cell death in plants. *The Journal of cell biology*, 203(6):917–27, December 2013. ISSN 1540-8140. doi: 10.1083/jcb.201307082.

Elena A Minina, Peter V Bozhkov, and Daniel Hofius. Autophagy as initiator or executioner of cell death. *Trends in Plant Science*, pages 1–6, August 2014. ISSN 13601385. doi: 10.1016/j.tplants.2014.07.007.

Kei-ichiro Mishiba, Yukihiro Nagashima, Eiji Suzuki, Noriko Hayashi, Yoshiyuki Ogata, Yukihisa Shimada, and Nozomu Koizumi. Defects in IRE1 enhance cell death and fail to degrade mRNAs encoding secretory pathway proteins in the Arabidopsis unfolded protein response. *Proceedings of the National Academy of Sciences of the United States of America*, 110(14):5713–8, April 2013. ISSN 1091-6490. doi: 10.1073/pnas.1219047110.

M Missotten, A Nichols, K Rieger, and R Sadoul. Alix, a novel mouse protein undergoing calcium-dependent interaction with the apoptosis-linked-gene 2 (ALG-2) protein. *Cell death and differentiation*, 6(2):124–9, February 1999. ISSN 1350-9047. doi: 10.1038/sj.cdd.4400456.

REFERENCES

Per Mühlenbock, Magdalena Szechynska-Hebda, Marian Plaszczyca, Marcela Baudo, Alfonso Mateo, Philip M Mullineaux, Jane E Parker, Barbara Karpinska, and Stanislaw Karpinski. Chloroplast signaling and LESION SIMULATING DISEASE1 regulate crosstalk between light acclimation and immunity in Arabidopsis. *The Plant cell*, 20(9):2339–56, September 2008. ISSN 1040-4651. doi: 10.1105/tpc.108.059618.

Martin Müller, Oliver Schmidt, Mihaela Angelova, Klaus Faserl, Sabine Weys, Leopold Kremser, Thaddäus Pfaffenwimmer, Thomas Dalik, Claudine Kraft, Zlatko Trajanoski, Herbert Lindner, and David Teis. The coordinated action of the MVB pathway and autophagy ensures cell survival during starvation. *eLife*, 4:1–25, April 2015. ISSN 2050-084X. doi: 10.7554/eLife.07736.

David Munch, Eleazar Rodriguez, Simon Bressendorff, Ohkmae K Park, Daniel Hofius, and Morten Petersen. Autophagy deficiency leads to accumulation of ubiquitinated proteins, ER stress, and cell death in Arabidopsis. *Autophagy*, 10(9):1–9, July 2014. ISSN 1554-8635. doi: 10.4161/auto.29406.

David Munch, Ooi-Kock Teh, Frederikke Gro Malinovsky, Qinsong Liu, Ramesh R. Vetukuri, Farid El Kasmi, Peter Brodersen, Ikuko Hara-Nishimura, Jeffery L. Dangl, Morten Petersen, John Mundy, and Daniel Hofius. Retromer contributes to immunity-associated cell death in Arabidopsis. *The Plant cell*, 27(2):463–79, 2015. ISSN 1532-298X. doi: 10.1105/tpc.114.132043.

Christiane Nawrath, Silvia Heck, Nonglak Parinthawong, and Jean-Pierre Métraux. EDS5, an Essential Component of Salicylic AcidDependent Signaling for Disease Resistance in Arabidopsis, Is a Member of the MATE Transporter Family. *The Plant Cell*, 14(1):275–286, 2002.

Kristoffer Palma, Stephan Thorgrimsen, Frederikke Gro Malinovsky, Berthe Katrine Fiil, H. Bjørn Bjorn Nielsen, Peter Brodersen, Daniel Hofius, Morten Petersen, and John Mundy. Autoimmunity in Arabidopsis acd11 is mediated by epigenetic regulation of an immune receptor. *PLoS pathogens*, 6(10):12, January 2010. ISSN 1553-7374. doi: 10.1371/journal.ppat.1001137.

S. Pankiv, E. a. Alemu, A. Brech, J.-a. Bruun, T. Lamark, A. Overvatn, G. Bjorkoy, and Terje Johansen. FYCO1 is a Rab7 effector that binds to LC3 and PI3P to mediate microtubule plus end-directed vesicle transport. *The Journal of Cell Biology*, 188(2):253–269, 2010. ISSN 0021-9525. doi: 10.1083/jcb.200907015.

Jane E Parker, EB B Holub, LN N Frost, A Falk, N D Gunn, and M J Daniels. Characterization of eds1, a mutation in Arabidopsis suppressing resistance to Peronospora parasitica specified by several different RPP genes. *The Plant cell*, 8(11):2033–2046, 1996. ISSN 1040-4651. doi: 10.1105/tpc.8.11.2033.

Nikolaj H T Petersen, Jan Joensen, Lea V McKinney, Peter Brodersen, Morten Petersen, Daniel Hofius, and John Mundy. Identification of proteins interacting with Arabidopsis ACD11. *Journal of plant physiology*, 166(6):661–6, April 2009. ISSN 1618-1328. doi: 10.1016/j.jplph. 2008.08.003.

Yunting Pu and Diane C. Bassham. Links between ER stress and autophagy in plants. *Plant Signaling & Behavior*, 8(6):e24297, June 2013. ISSN 1559-2324. doi: 10.4161/psb.24297.

R Core Team. R: A Language and Environment for Statistical Computing, 2014. URL `http://www.r-project.org/`.

Camilla Raiborg, B Bremnes, A Mehlum, D J Gillooly, A D'Arrigo, E Stang, and H Stenmark. FYVE and coiled-coil domains determine the specific localisation of Hrs to early endosomes. *Journal of cell science*, 114(Pt 12):2255–63, June 2001. ISSN 0021-9533.

C K Raymond, I Howald-Stevenson, C A Vater, and T H Stevens. Morphological classification of the yeast vacuolar protein sorting mutants: evidence for a prevacuolar compartment in class E vps mutants. *Molecular biology of the cell*, 3(12):1389–402, December 1992. ISSN 1059-1524.

Theresa J. Reape and Paul F. McCabe. Apoptotic-like programmed cell death in plants, 2008. ISSN 0028646X.

Theresa J Reape and Paul F McCabe. Commentary: the cellular condensation of dying plant cells: programmed retraction or necrotic collapse? *Plant science : an international journal of experimental plant biology*, 207:135–9, June 2013. ISSN 1873-2259. doi: 10.1016/j.plantsci. 2013.03.001.

Theresa J Reape, Elizabeth M Molony, and Paul F McCabe. Programmed cell death in plants: distinguishing between different modes. *Journal of experimental botany*, 59(3):435–44, January 2008. ISSN 1460-2431. doi: 10.1093/jxb/erm258.

Theresa J Reape, Joanna Kacprzyk, Niall Brogan, Lee Sweetlove, and Paul F McCabe. Mitochondrial Markers of Programmed Cell Death in Arabidopsis thaliana. In *Methods in molecular biology (Clifton, N.J.)*, volume 1305, pages 211–221. 2015. doi: 10.1007/978-1-4939-2639-8\ _15.

Francisca C. Reyes, Rafael a. Buono, Hannetz Roschzttardtz, Simone Di Rubbo, Li Huey Yeun, Eugenia Russinova, and Marisa S. Otegui. A Novel Endosomal Sorting Complex Required for Transport (ESCRT) Component in Arabidopsis thaliana Controls Cell Expansion and Development. *The Journal of biological chemistry*, 289(8):4980–8, February 2014. ISSN 1083-351X. doi: 10.1074/jbc.M113.529685.

REFERENCES

E S Reynolds. The use of lead citrate at high pH as an electron-opaque stain in electron microscopy. *The Journal of cell biology*, 17:208–212, 1963. doi: 10.1083/jcb.17.1.208.

Julia Riedl, Alvaro H Crevenna, Kai Kessenbrock, Jerry Haochen Yu, Dorothee Neukirchen, Michal Bista, Frank Bradke, Dieter Jenne, Tad A Holak, Zena Werb, Michael Sixt, and Roland Wedlich-Soldner. Lifeact: a versatile marker to visualize F-actin. *Nature methods*, 5(7):605–7, July 2008. ISSN 1548-7105. doi: 10.1038/nmeth.1220.

Alastair S Robertson, Ellen G Allwood, Adam P C Smith, Fiona C Gardiner, Rosaria Costa, Steve J Winder, and Kathryn R Ayscough. The WASP homologue Las17 activates the novel actin-regulatory activity of Ysc84 to promote endocytosis in yeast. *Molecular biology of the cell*, 20(6):1618–28, March 2009. ISSN 1939-4586. doi: 10.1091/mbc.E08-09-0982.

RStudio Team. RStudio: Integrated Development Environment for R, 2015. URL `http://www.rstudio.com/`.

Suraj Saksena and Scott D Emr. ESCRTs and human disease. *Biochemical Society transactions*, 37(Pt 1):167–72, February 2009. ISSN 1470-8752. doi: 10.1042/BST0370167.

Maite Sanmartín, Lukasz Jaroszewski, Natasha V Raikhel, and Enrique Rojo. Caspases. Regulating death since the origin of life. *Plant physiology*, 137(3):841–847, February 2005. ISSN 0032-0889. doi: 10.1104/pp.104.058552.

Swen Schellmann and Peter Pimpl. Coats of endosomal protein sorting: retromer and ESCRT. *Current Opinion in Plant Biology*, 12(6):670–676, December 2009. ISSN 13695266. doi: 10.1016/j.pbi.2009.09.005.

Johannes Schindelin, Ignacio Arganda-Carreras, Erwin Frise, Verena Kaynig, Mark Longair, Tobias Pietzsch, Stephan Preibisch, Curtis Rueden, Stephan Saalfeld, Benjamin Schmid, Jean-Yves Tinevez, Daniel James White, Volker Hartenstein, Kevin Eliceiri, Pavel Tomancak, and Albert Cardona. Fiji: an open-source platform for biological-image analysis, 2012.

Johannes Schindelin, Curtis T Rueden, Mark C Hiner, and Kevin W Eliceiri. The ImageJ ecosystem: An open platform for biomedical image analysis., 2015. ISSN 1098-2795.

Caroline A Schneider, Wayne S Rasband, and Kevin W Eliceiri. NIH Image to ImageJ: 25 years of image analysis. *Nature Methods*, 9(7):671–675, June 2012. ISSN 1548-7091. doi: 10.1038/nmeth.2089.

Mario Serrano, Bangjun Wang, Bibek Aryal, Christophe Garcion, Eliane Abou-Mansour, Silvia Heck, Markus Geisler, Felix Mauch, Christiane Nawrath, and Jean-Pierre Métraux. Export of salicylic acid from the chloroplast requires the multidrug and toxin extrusion-like transporter EDS5. *Plant physiology*, 162(4):1815–21, 2013. ISSN 1532-2548. doi: 10.1104/pp.113.218156.

Mojgan Shahriari. *Molecular and cell biological analysis of the ESCRT system in Arabidopsis thaliana*. Inaugural-dissertation, Universität zu Köln, 2008.

Mojgan Shahriari, Martin Hülskamp, and Swen Schellmann. Seeds of Arabidopsis plants expressing dominant-negative AtSKD1 under control of the GL2 promoter show a transparent testa phenotype and a mucilage defect. *Plant Signaling & Behavior*, 5(10):1308–1310, October 2010a. ISSN 1559-2324. doi: 10.4161/psb.5.10.13134.

Mojgan Shahriari, Channa Keshavaiah, David Scheuring, Aneta Sabovljevic, Peter Pimpl, Rainer E Häusler, Martin Hülskamp, and Swen Schellmann. The AAA-type ATPase AtSKD1 contributes to vacuolar maintenance of Arabidopsis thaliana. *The Plant journal : for cell and molecular biology*, 64(1):71–85, October 2010b. ISSN 1365-313X. doi: 10.1111/j.1365-313X.2010.04310.x.

Mojgan Shahriari, Klaus Richter, Channa Keshavaiah, Aneta Sabovljevic, Martin Huelskamp, and Swen Schellmann. The Arabidopsis ESCRT protein-protein interaction network. *Plant molecular biology*, 76(1-2):85–96, May 2011. ISSN 1573-5028. doi: 10.1007/s11103-011-9770-4.

Dhirendra K. Simanshu, Xiuhong Zhai, David Munch, Daniel Hofius, Jonathan E. Markham, Jacek Bielawski, Alicja Bielawska, Lucy Malinina, Julian G. Molotkovsky, John W. Mundy, Dinshaw J. Patel, and Rhoderick E. Brown. Arabidopsis accelerated cell death 11, ACD11, Is a ceramide-1-phosphate transfer protein and intermediary regulator of phytoceramide levels. *Cell Reports*, 6(2):388–399, January 2014. ISSN 22111247. doi: 10.1016/j.celrep.2013.12.023.

Silvia Sláviková, Galia Shy, Youli Yao, Rina Glozman, Hanna Levanony, Shmuel Pietrokovski, Zvulun Elazar, and Gad Galili. The autophagy-associated Atg8 gene family operates both under favourable growth conditions and under starvation stresses in Arabidopsis plants. *Journal of experimental botany*, 56(421):2839–49, October 2005. ISSN 0022-0957. doi: 10.1093/jxb/eri276.

A Smertenko and V E Franklin-Tong. Organisation and regulation of the cytoskeleton in plant programmed cell death. *Cell death and differentiation*, 18(8):1263–70, August 2011. ISSN 1476-5403. doi: 10.1038/cdd.2011.39.

Thomas Spallek, Martina Beck, Sara Ben Khaled, Susanne Salomon, Gildas Bourdais, Swen Schellmann, and Silke Robatzek. ESCRT-I mediates FLS2 endosomal sorting and plant immunity. *PLoS genetics*, 9(12):e1004035, December 2013. ISSN 1553-7404. doi: 10.1371/journal.pgen.1004035.

Christoph Spitzer, Swen Schellmann, Aneta Sabovljevic, Mojgan Shahriari, Channa Keshavaiah, Nicole Bechtold, Michel Herzog, Stefan Müller, Franz-Georg Hanisch, and Martin

REFERENCES

Hülskamp. The Arabidopsis elch mutant reveals functions of an ESCRT component in cytokinesis. *Development (Cambridge, England)*, 133(23):4679–89, December 2006. ISSN 0950-1991. doi: 10.1242/dev.02654.

Christoph Spitzer, Francisca C Reyes, Rafael Buono, Marek K Sliwinski, Thomas J Haas, and Marisa S Otegui. The ESCRT-related CHMP1A and B proteins mediate multivesicular body sorting of auxin carriers in Arabidopsis and are required for plant development. *The Plant cell*, 21(3):749–66, March 2009. ISSN 1040-4651. doi: 10.1105/tpc.108.064865.

Christoph Spitzer, Faqiang Li, Rafael Buono, Hannetz Roschzttardtz, Taijoon Chung, Min Zhang, Katherine W. Osteryoung, Richard D Vierstra, and Marisa S. Otegui. The Endosomal Protein CHARGED MULTIVESICULAR BODY PROTEIN1 Regulates the Autophagic Turnover of Plastids in Arabidopsis. *The Plant Cell Online*, 27(2):391–402, 2015. ISSN 1040-4651. doi: 10.1105/tpc.114.135939.

A R Spurr. A low-viscosity epoxy resin embedding medium for electron microscopy. *Journal of ultrastructure research*, 26(1):31–43, 1969. ISSN 00225320. doi: 10.1016/S0022-5320(69)90033-1.

Chris Stark, Bobby-Joe Breitkreutz, Teresa Reguly, Lorrie Boucher, Ashton Breitkreutz, and Mike Tyers. BioGRID: a general repository for interaction datasets. *Nucleic acids research*, 34 (Database issue):D535–9, 2006. ISSN 1362-4962. doi: 10.1093/nar/gkj109.

Alexandra Steffens, Benjamin Jaegle, Achim Tresch, Martin Hülskamp, Marc Jakoby, M. Hulskamp, and Marc Jakoby. Processing-Body Movement in Arabidopsis Depends on an Interaction between Myosins and DECAPPING PROTEIN1. *PLANT PHYSIOLOGY*, 164(4): 1879–1892, April 2014. ISSN 0032-0889. doi: 10.1104/pp.113.233031.

Arpaporn Sutipatanasomboon. *Analysis of FYVE2 function and its relation to the Arabidopsis thaliana ESCRT-complex*. Master of science thesis, Universität zu Köln, 2012.

Steingrim Svenning, Trond Lamark, Kirsten Krause, and Terje Johansen. Plant NBR1 is a selective autophagy substrate and a functional hybrid of the mammalian autophagic adapters NBR1 and p62/SQSTM1. *Autophagy*, 7(9):993–1010, 2011. ISSN 15548627. doi: 10.4161/auto.7.9.16389.

Ooi-Kock Teh and Daniel Hofius. Membrane trafficking and autophagy in pathogen-triggered cell death and immunity. *Journal of experimental botany*, pages 1–16, January 2014. ISSN 1460-2431. doi: 10.1093/jxb/ert441.

David Teis, Suraj Saksena, and Scott D. Emr. SnapShot: the ESCRT machinery. *Cell*, 137(1): 182–182.e1, April 2009. ISSN 1097-4172. doi: 10.1016/j.cell.2009.03.027.

Howard Thomas. Senescence, ageing and death of the whole plant. *New Phytologist*, 197(3): 696–711, February 2013. ISSN 0028646X. doi: 10.1111/nph.12047.

Allison R Thompson, Jed H Doelling, Anongpat Suttangkakul, and Richard D Vierstra. Autophagic nutrient recycling in Arabidopsis directed by the ATG8 and ATG12 conjugation pathways. *Plant physiology*, 138(4):2097–2110, 2005. ISSN 0032-0889. doi: 10.1104/pp.105. 060673.

Nico Tintor, Annegret Ross, Kazue Kanehara, Kohji Yamada, Li Fan, Birgit Kemmerling, Thorsten Nürnberger, Kenichi Tsuda, and Yusuke Saijo. Layered pattern receptor signaling via ethylene and endogenous elicitor peptides during Arabidopsis immunity to bacterial infection. *Proceedings of the National Academy of Sciences of the United States of America*, 110 (15):6211–6, April 2013. ISSN 1091-6490. doi: 10.1073/pnas.1216780110.

L Tsiatsiani, Frank Van Breusegem, P Gallois, a Zavialov, Eric Lam, and P V Bozhkov. Metacaspases. *Cell death and differentiation*, 18(8):1279–1288, 2011. ISSN 1350-9047. doi: 10.1038/cdd.2011.66.

Milena Franciska Ulbricht. *Charakterisierung von Protein-Protein Interaktionen der Arabidopsis ESCRT Regulatoren FYVE-2, EAL1 und AtALIX*. Staatexam, Universität zu Köln, 2011.

A. Untergasser, I. Cutcutache, T. Koressaar, J. Ye, B. C. Faircloth, M. Remm, and S. G. Rozen. Primer3–new capabilities and interfaces. *Nucleic Acids Research*, 40(15):e115–e115, August 2012. ISSN 0305-1048. doi: 10.1093/nar/gks596.

Wouter G van Doorn. Classes of programmed cell death in plants, compared to those in animals. *Journal of experimental botany*, 62(14):4749–61, October 2011. ISSN 1460-2431. doi: 10.1093/jxb/err196.

Wouter G van Doorn, E P Beers, J L Dangl, V E Franklin-Tong, P Gallois, Ikuko Hara-Nishimura, A M Jones, M Kawai-Yamada, Eric Lam, John Mundy, L a J Mur, M Petersen, A Smertenko, M Taliansky, Frank Van Breusegem, T Wolpert, E Woltering, B Zhivotovsky, and P V Bozhkov. Morphological classification of plant cell deaths. *Cell death and differentiation*, 18(8):1241–6, August 2011. ISSN 1476-5403. doi: 10.1038/cdd.2011.36.

Tom Van Hautegem, Andrew J. Waters, Justin Goodrich, and Moritz K. Nowack. Only in dying, life: programmed cell death during plant development. *Trends in Plant Science*, 20(2): 102–113, 2015. ISSN 13601385. doi: 10.1016/j.tplants.2014.10.003.

Tom Vanden Berghe, Andreas Linkermann, Sandrine Jouan-Lanhouet, Henning Walczak, and Peter Vandenabeele. Regulated necrosis: the expanding network of non-apoptotic cell death pathways. *Nature reviews. Molecular cell biology*, 15(2):135–47, 2014. ISSN 1471-0080. doi: 10.1038/nrm3737.

REFERENCES

Yi Wang, Zhilong Bao, Ying Zhu, and Jian Hua. Analysis of temperature modulation of plant defense against biotrophic microbes. *Molecular plant-microbe interactions : MPMI*, 22(5):498–506, 2009. ISSN 0894-0282. doi: 10.1094/MPMI-22-5-0498.

Catherine Sem Wegner, Lina M W Rodahl, and Harald Stenmark. ESCRT proteins and cell signalling. *Traffic*, 12(10):1291–1297, 2011. ISSN 13989219. doi: 10.1111/j.1600-0854.2011. 01210.x.

Hadley Wickham. Reshaping Data with the {reshape} Package. *Journal of Statistical Software*, 21(12):1–20, 2007.

Hadley Wickham. *ggplot2: elegant graphics for data analysis*. Springer New York, New York, NY, 2009. ISBN 978-0-387-98140-6. doi: 10.1007/978-0-387-98141-3.

Hadley Wickham. The Split-Apply-Combine Strategy for Data Analysis. *Journal of Statistical Software*, 40(1):1–29, 2011.

Hadley Wickham. scales: Scale Functions for Visualization, 2015.

Marcel Wiermer, Bart J. Feys, and Jane E Parker. Plant immunity: The EDS1 regulatory node. *Current Opinion in Plant Biology*, 8(4):383–389, 2005. ISSN 13695266. doi: 10.1016/j.pbi.2005. 05.010.

M C Wildermuth, Julia Dewdney, Gang Wu, and F M Ausubel. Isochorismate synthase is required to synthesize salicylic acid for plant defence. *Nature*, 414(6863):562–565, 2001. doi: 10.1038/417571a.

Verena Winter and Marie-Theres Hauser. Exploring the ESCRTing machinery in eukaryotes. *Trends in plant science*, 11(3):115–23, March 2006. ISSN 1360-1385. doi: 10.1016/j.tplants. 2006.01.008.

Yan Xiong, Anthony L. Contento, Phan Quang Nguyen, and Diane C. Bassham. Degradation of oxidized proteins by autophagy during oxidative stress in Arabidopsis. *Plant physiology*, 143(1):291–9, 2007. ISSN 0032-0889. doi: 10.1104/pp.106.092106.

Kohki Yoshimoto, Hideki Hanaoka, Shusei Sato, Tomohiko Kato, Satoshi Tabata, Takeshi Noda, and Yoshinori Ohsumi. Processing of ATG8s, ubiquitin-like proteins, and their deconjugation by ATG4s are essential for plant autophagy. *The Plant cell*, 16(11):2967–2983, November 2004. ISSN 1040-4651. doi: 10.1105/tpc.104.025395. URL `http://www.plantcell.org/cgi/doi/10.1105/tpc.104.025395`.

Kohki Yoshimoto, Y. Jikumaru, Y. Kamiya, M. Kusano, C. Consonni, R. Panstruga, Y. Ohsumi, and K. Shirasu. Autophagy Negatively Regulates Cell Death by Controlling NPR1-Dependent Salicylic Acid Signaling during Senescence and the Innate Immune Response

in Arabidopsis. *the Plant Cell Online*, 21(9):2914–2927, 2009. ISSN 1040-4651. doi: 10.1105/tpc.109.068635.

Ziguo Zhang, Andrea Lenk, Mats X. Andersson, Torben Gjetting, Carsten Pedersen, Mads E. Nielsen, Mari Anne Newman, Bi Huei Hou, Shauna C. Somerville, and Hans Thordal-Christensen. A lesion-mimic syntaxin double mutant in Arabidopsis reveals novel complexity of pathogen defense signaling. *Molecular Plant*, 1(3):510–527, 2008. ISSN 16742052. doi: 10.1093/mp/ssn011.

Mingzhe Zhao, Kengo Morohashi, Greg Hatlestad, Erich Grotewold, and Alan Lloyd. The TTG1-bHLH-MYB complex controls trichome cell fate and patterning through direct targeting of regulatory loci. *Development*, 135(11):1991–1999, April 2008. ISSN 0950-1991. doi: 10.1242/dev.016873.

Jie Zhou, Jian Wang, Yuan Cheng, Ying-Jun Chi, Baofang Fan, Jing-Quan Yu, and Zhixiang Chen. NBR1-Mediated Selective Autophagy Targets Insoluble Ubiquitinated Protein Aggregates in Plant Stress Responses. *PLoS Genetics*, 9(1):e1003196, 2013. ISSN 1553-7404. doi: 10.1371/journal.pgen.1003196.

Jie Zhou, Jing-Quan Yu, and Zhixiang Chen. The perplexing role of autophagy in plant innate immune responses. *Molecular Plant Pathology*, 15(6):637–645, 2014a. ISSN 14646722. doi: 10.1111/mpp.12118.

Jie Zhou, Yan Zhang, Jingxia Qi, Yingjin Chi, Baofang Fan, Jing-Quan Yu, and Zhixiang Chen. E3 Ubiquitin Ligase CHIP and NBR1-Mediated Selective Autophagy Protect Additively against Proteotoxicity in Plant Stress Responses. *PLoS Genetics*, 10(1):e1004116, January 2014b. ISSN 1553-7404. doi: 10.1371/journal.pgen.1004116.

Appendices

Appendix A   Statistical analysis of *pCFS1-gCFS1* in cfs1-2 plants

Pearson's χ^2 test of independence was performed using *prop.test* function without continuity correction.

For **line 1**:

two-sided test:

χ^2 = 0.18125, df = 1, p-value = 0.6703

95 percent confidence interval: -0.5191644, 0.3524977

sample estimates: prop 1 = 0.1666667; prop 2 = 0.2500000

For **line 2**:

two-sided test:

χ^2 = 1.8887, df = 1, p-value = 0.1693

95 percent confidence interval: -0.6183967, 0.2408456

sample estimates: prop 1 = 0.06122449; prop 2 = 0.25000000

For **line 3**:

two-sided test:

χ^2 = 0.053968, df = 1, p-value = 0.8163

95 percent confidence interval: -0.497835, 0.397835

sample estimates: prop 1 = 0.20; prop 2 = 0.25

For **line 4**:

two-sided test:

χ^2 = 0.0077061, df = 1, p-value = 0.93

95 percent confidence interval: -0.4587557, 0.4202941

sample estimates: prop 1 = 0.2307692; prop 2 = 0.2500000

Appendix B Analysis of lesion formation in *cfs1* mutants

Appendix B.1: Number of true leaf and true leaf showing lesions in *cfs1* mutant, *cfs2* and Col-0

ID	DAS Genotype	15 all	15 le	17 all	17 le	19 all	19 le	21 all	21 le	23 all	23 le	25 all	25 le	27 all	27 le	32 all	32 le
13	*cfs1-1*	4	0	4	0	5	2	6	2	7	2	9	3	10	4	11	4
24	*cfs1-1*	2	0	4	0	5	2	7	2	7	2	9	4	11	4	14	4
25	*cfs1-1*	4	0	5	0	6	2	7	2	8	2	10	4	12	4	14	4
26	*cfs1-1*	4	0	4	0	5	2	6	2	7	2	10	4	14	5	15	5
29	*cfs1-1*	4	0	4	0	5	0	6	2	7	2	10	4	12	4	15	4
30	*cfs1-1*	4	0	4	0	5	1	7	2	8	2	9	3	12	5	13	5
36	*cfs1-1*	4	0	4	0	5	0	6	2	7	2	10	4	12	4	15	4
40	*cfs1-1*	4	0	4	0	5	0	6	2	7	2	9	4	12	4	11	4
42	*cfs1-1*	2	0	4	0	5	0	6	2	7	2	10	4	12	4	14	4
47	*cfs1-1*	4	0	4	0	5	2	6	2	7	2	10	4	12	4	14	4
50	*cfs1-1*	4	0	4	0	5	0	7	2	8	2	10	0	13	5	13	4
60	*cfs1-1*	4	0	5	0	5	1	7	2	8	2	11	4	10	4	11	4
69	*cfs1-1*	4	0	4	0	4	2	6	2	8	2	9	4	13	4	17	5
71	*cfs1-1*	4	0	4	0	3	2	6	2	7	2	10	4	13	4	13	5
4	*cfs1-1*	4	0	4	1	4	1	5	1	5	2	9	2	9	2	13	3
18	*cfs1-2*	4	0	5	0	5	1	6	2	8	3	8	4	11	5	11	5
23	*cfs1-2*	4	0	4	0	5	2	6	2	7	2	8	3	11	5	12	5
27	*cfs1-2*	3	0	4	0	5	0	6	2	7	2	9	4	11	4	13	4
28	*cfs1-2*	3	0	5	0	6	0	6	2	7	2	10	5	12	5	15	4
32	*cfs1-2*	4	0	2	0	4	0	5	0	7	0	8	0	11	0	13	0
41	*cfs1-2*	4	0	4	0	5	0	6	0	7	0	9	3	12	4	11	4
53	*cfs1-2*	4	0	4	0	4	0	6	0	6	0	8	4	12	4	15	4
54	*cfs1-2*	4	0	4	0	5	2	6	2	7	2	9	4	12	5	14	4
56	*cfs1-2*	2	0	4	0	5	2	6	2	8	2	9	4	13	4	14	4

Continued on next page

Appendix B.1: Number of true leaf and true leaf showing lesions in *cfs1* mutant, *cfs2* and Col-0 –*continued from previous page*

ID	DAS Genotype	15 all	le	17 all	le	19 all	le	21 all	le	23 all	le	25 all	le	27 all	le	32 all	le
61	*cfs1-2*	4	0	4	0	5	1	6	2	7	2	10	4	13	4	15	4
72	*cfs1-2*	2	0	5	0	4	2	6	2	7	2	10	4	13	4	13	4
73	*cfs1-2*	4	0	4	0	4	2	6	2	7	2	10	4	12	4	15	4
8	*cfs1-2*	3	0	4	1	5	1	7	2	8	2	10	3	10	3	10	3
5	*cfs1-3*	4	0	4	0	4	0	5	2	7	2	8	3	10	3	14	4
15	*cfs1-3*	4	0	5	0	6	2	6	2	9	2	9	4	13	4	15	5
17	*cfs1-3*	4	0	5	0	5	0	5	2	8	2	9	4	11	4	14	4
22	*cfs1-3*	4	0	4	0	4	2	6	2	7	2	9	2	9	2	10	2
44	*cfs1-3*	4	0	4	0	4	2	6	2	6	2	8	4	10	4	11	4
45	*cfs1-3*	4	0	4	0	5	1	6	2	7	2	9	3	11	4	12	4
46	*cfs1-3*	4	0	4	0	5	2	6	2	6	2	9	4	11	4	15	4
48	*cfs1-3*	2	0	4	0	5	0	6	2	7	2	9	4	9	5	14	5
55	*cfs1-3*	3	0	4	0	5	0	5	2	6	2	9	4	11	4	15	4
57	*cfs1-3*	2	0	4	0	5	0	5	2	7	2	9	2	8	2	12	3
59	*cfs1-3*	4	0	4	0	5	2	6	2	5	2	9	3	11	4	14	4
62	*cfs1-3*	4	0	4	0	5	0	5	2	7	2	10	4	12	5	14	5
63	*cfs1-3*	3	0	4	0	4	2	5	2	7	2	9	3	10	4	13	4
64	*cfs1-3*	4	0	4	0	4	2	6	2	7	2	9	4	12	4	15	5
2	*cfs1-3*	4	0	4	0	5	0	6	1	7	2	8	4	11	4	14	4
11	*cfs2*	4	0	4	0	5	0	6	0	8	0	9	0	11	0	11	0
16	*cfs2*	4	0	4	0	5	0	6	0	7	0	10	0	13	0	14	0
20	*cfs2*	3	0	5	0	5	0	7	0	9	0	11	0	10	0	12	0
21	*cfs2*	3	0	4	0	5	0	6	0	8	0	8	0	10	0	13	0
37	*cfs2*	3	0	4	0	5	0	6	0	7	0	10	0	13	0	13	0
43	*cfs2*	3	0	4	0	4	0	6	0	7	0	8	0	10	0	9	0
49	*cfs2*	4	0	4	0	5	0	6	0	8	0	10	0	12	0	14	0
51	*cfs2*	2	0	4	0	5	0	6	0	7	0	9	0	13	0	14	0
58	*cfs2*	3	0	4	0	5	0	6	0	7	0	10	0	12	0	16	0

ID	DAS Genotype	15 all	15 le	17 all	17 le	19 all	19 le	21 all	21 le	23 all	23 le	25 all	25 le	27 all	27 le	32 all	32 le
65	*cfs2*	3	0	5	0	5	0	7	0	8	0	11	0	12	0	18	0
66	*cfs2*	4	0	4	0	4	0	5	0	7	0	8	0	12	0	14	0
68	*cfs2*	4	0	4	0	4	0	7	0	8	0	10	0	10	0	11	0
75	*cfs2*	4	0	4	0	4	0	6	0	7	0	9	0	12	0	15	0
10	*cfs2*	2	0	4	0	6	0	6	0	8	0	10	0	11	0	15	0
6	Col-0	4	0	4	0	6	0	6	2	8	0	9	0	13	0	16	0
9	Col-0	4	0	4	0	5	0	6	0	7	0	9	0	10	0	14	0
19	Col-0	4	0	4	0	4	0	6	0	6	0	9	0	12	0	13	0
33	Col-0	2	0	5	0	5	0	7	0	8	0	10	0	11	0	14	0
34	Col-0	3	0	3	0	4	0	5	0	6	0	7	0	9	0	11	0
35	Col-0	3	0	5	0	5	0	6	0	8	0	8	0	11	0	13	0
38	Col-0	4	0	5	0	5	0	6	0	8	0	10	0	13	0	12	0
39	Col-0	4	0	5	0	5	0	7	0	7	0	11	0	13	0	14	0
52	Col-0	4	0	4	0	5	0	6	0	6	0	10	0	12	0	15	0
67	Col-0	4	0	4	0	4	0	6	0	7	0	9	0	10	0	14	0
70	Col-0	4	0	4	0	4	2	6	2	8	2	12	3	13	4	13	4
74	Col-0	4	0	4	0	4	0	6	0	8	0	10	0	13	0	15	0

DAS: date after sowing

all: number of true leaf

les: number of true leaf showing lesions

The number of individuals showing lesions from Table B.1 is summarized in Table B.2.

Appendix B.2: Summary of the number of Col-0, *cfs1* mutants and *cfs2* showing spontaneous lesions formation

Genotype	DAS	N_{lesion}	N_{all}	%phenotype
Col-0	15	0	11	0

Appendix B.2: Summary of the number of Col-0, *cfs1* mutants and *cfs2* showing spontaneous lesion formation –*continued from previous page*

Genotype	DAS	N_{lesion}	N_{all}	%phenotype
	17	0	11	0
	19	0	11	0
	21	0	11	0
	23	0	11	0
	25	0	11	0
	27	0	11	0
	32	0	11	0
cfs1-1	15	0	15	0
	17	1	15	6.67
	19	10	15	66.67
	21	15	15	100
	23	15	15	100
	25	15	15	100
	27	15	15	100
	32	15	15	100
cfs1-2	15	0	13	0
	17	1	13	7.69
	19	8	13	61.54
	21	10	13	76.92
	23	10	13	76.92
	25	12	13	92.31
	27	12	13	92.31
	32	12	13	92.31
cfs1-3	15	0	15	0
	17	0	15	0
	19	8	15	53.33
	21	15	15	100
	23	15	15	100
	25	15	15	100

Continued on next page

Appendix B.2: Summary of the number of Col-0, *cfs1* mutants and *cfs2* showing spontaneous lesion formation –*continued from previous page*

Genotype	DAS	N_{lesion}	N_{all}	%phenotype
	27	15	15	100
	32	15	15	100
cfs2	15	0	14	0
	17	0	14	0
	19	0	14	0
	21	0	14	0
	23	0	14	0
	25	0	14	0
	27	0	14	0
	32	0	14	0

DAS: Day after sowing

N_{lesion}: Number of individuals showing lesions

N_{all} : Number of individuals observed

Appendix C   Analysis of SA-responsive marker genes

Ct values from each technical and biological replicates are listed in Table C.

Appendix C.1: Ct values of *EFα1* and SA-responsive marker genes

Replication		Target	Samples			
biological	technical		*cfs1-3*	Col-0	*cfs1-2*	water
1	1	*EFalpha1*	19.911	19.468	18.798	NA
1	2	*EFalpha1*	20.186	19.566	19.315	NA
2	1	*EFalpha1*	19.596	21.073	19.997	NA
2	2	*EFalpha1*	19.426	20.477	19.346	32.723
3	1	*EFalpha1*	21.496	19.332	19.589	35.032
3	2	*EFalpha1*	21.793	19.777	20.05	NA
1	1	*PR1*	19.971	22.649	21.526	NA
1	2	*PR1*	19.821	22.485	21.387	NA
2	1	*PR1*	20.326	25.009	20.54	NA
2	2	*PR1*	20.39	25.116	20.559	NA
3	1	*PR1*	19.896	25.764	19.475	NA
3	2	*PR1*	20.08	26.075	19.472	NA
1	1	*PR2*	21.42	23.491	21.862	NA
1	2	*PR2*	21.429	23.378	22.005	NA
2	1	*PR2*	19.778	24.716	22.27	37.558
2	2	*PR2*	19.544	24.673	22.194	NA
3	1	*PR2*	22.104	24.454	19.407	NA
3	2	*PR2*	22.012	24.764	19.716	38.562
1	1	*PR5*	23.112	24.173	23.957	39.799
1	2	*PR5*	23.082	23.776	24.261	33.869
2	1	*PR5*	21.337	26.504	22.723	35.134
2	2	*PR5*	21.264	26.695	22.826	34.861
3	1	*PR5*	22.25	26.076	21.194	36.335
3	2	*PR5*	22.424	25.261	21.585	NA
1	1	*SAG13*	21.386	21.841	20.88	35.193
1	2	*SAG13*	21.382	21.941	20.859	32.133
2	1	*SAG13*	21.206	22.492	20.705	32.009
2	2	*SAG13*	21.308	22.473	21.161	31.805
3	1	*SAG13*	22.611	24.145	20.427	30.578

Continued on next page

Appendix C.1: Ct values of *EFα1* and SA-responsive marker genes –*continued from previous page*

Replication		Target	Samples			
biological	technical		*cfs1-3*	Col-0	*cfs1-2*	water
3	2	*SAG13*	22.501	24.204	20.483	33.065
1	1	*EFalpha1*	20.231	19.91	19.44	
1	2	*EFalpha1*	20.216	19.981	19.436	
2	1	*EFalpha1*	19.085	19.936	19.331	
2	2	*EFalpha1*	19.116	19.723	19.304	
3	1	*EFalpha1*	21.211	19.241	19.337	
3	2	*EFalpha1*	21.098	19.199	19.219	
1	1	*WRKY53*	22.651	22.246	22.418	
1	2	*WRKY53*	22.674	22.177	22.267	
2	1	*WRKY53*	21.888	22.645	23.062	
2	2	*WRKY53*	21.915	23.907	22.707	
3	1	*WRKY53*	23.283	22.145	22.254	
3	2	*WRKY53*	23.263	22.174	22.161	

NA: undetected

All Shapiro-Wilk normality tests were performed using *shapiro.test* function. ANOVA was performed using *aov* function. Post-hoc analysis was performed using Tukey Honest Significant Difference test with *glht* function from *multcomp* package. ΔC_t values were subjected to statistical test as follows:

For **PR1**:

Shapiro-Wilk normality test: normality accepted
(W = 0.96188, p-value = 0.8178)

ANOVA:

	Df	Sum Sq	Mean Sq	F Value	Pr($> F$)	
genotype	2	38.47	19.234	9.178	0.0149	*
Residuals	6	12.57	2.096			

Signif. codes: 0 *** 0.001 ** 0.01 * 0.05 . 0.1 1

Tukey Honest Significant Difference test:

Test	Estimate Std.	Error	t value	Pr($> |t|$)	
cfs1-3 - cfs1-2	-1.298	1.182	-1.098	0.5493	
Col-0 - cfs1-2	3.590	1.182	3.037	0.0520	.
Col-0 - cfs1-3	4.888	1.182	4.136	0.0145	*

—

Signif. codes: 0 *** 0.001 ** 0.01 * 0.05 . 0.1   1

(Adjusted p values reported – single-step method)

For *PR2*:

Shapiro-Wilk normality test: normality accepted

(W = 0.93565, p-value = 0.537)

ANOVA:

	Df	Sum Sq	Mean Sq	F Value	Pr($> F$)	
genotype	2	21.102	10.551	8.275	0.0188	*
Residuals	6	7.651	1.275			

—

Signif. codes: 0 *** 0.001 ** 0.01 * 0.05 . 0.1   1

Tukey Honest Significant Difference test:

Test	Estimate Std.	Error	t value	Pr($> |t|$)	
cfs1-3 - cfs1-2	-1.080	0.922	-1.171	0.5103	
Col-0 - cfs1-2	2.571	0.922	2.788	0.0705	.
Col-0 - cfs1-3	3.651	0.922	3.960	0.0177	*

—

Signif. codes: 0 *** 0.001 ** 0.01 * 0.05 . 0.1   1

(Adjusted p values reported – single-step method)

For *PR5*:

Shapiro-Wilk normality test: normality accepted

(W = 0.94043, p-value = 0.5865)

ANOVA:

	Df	Sum Sq	Mean Sq	F Value	Pr($> F$)	
genotype	2	20.02	10.01	5.75	0.0403	*
Residuals	6	10.4	1.74			

—

Signif. codes: 0 *** 0.001 ** 0.01 * 0.05 . 0.1   1

Tukey Honest Significant Difference test:

Test	Estimate Std.	Error	t value	Pr($>|t|$)	
cfs1-3 - cfs1-2	-1.398	1.077	-1.298	0.4463	
Col-0 - cfs1-2	2.224	1.077	2.065	0.1779	
Col-0 - cfs1-3	3.622	1.077	3.363	0.0353	*

Signif. codes: 0 *** 0.001 ** 0.01 * 0.05 . 0.1 1

(Adjusted p values reported – single-step method)

For *SAG13*:

Shapiro-Wilk normality test: normality accepted

(W = 0.91106, p-value = 0.3233)

ANOVA:

	Df	Sum Sq	Mean Sq	F Value	Pr($>F$)	
genotype	2	6.604	3.302	4.991	0.0529	.
Residuals	6	3.970	0.662			

Signif. codes: 0 *** 0.001 ** 0.01 * 0.05 . 0.1 1

Tukey Honest Significant Difference test:

Test	Estimate Std.	Error	t value	Pr($>|t|$)	
cfs1-3 - cfs1-2	0.9798	0.6641	1.475	0.3657	
Col-0 - cfs1-2	2.0968	0.6641	3.157	0.0446	*
Col-0 - cfs1-3	1.1170	0.6641	1.682	0.2863	

Signif. codes: 0 *** 0.001 ** 0.01 * 0.05 . 0.1 1

(Adjusted p values reported – single-step method)

For *WRKY53*:

Shapiro-Wilk normality test: normality accepted

(W = 0.93836, p-value = 0.5647)

ANOVA:

	Df	Sum Sq	Mean Sq	F Value	Pr($>F$)
genotype	2	0.5356	0.2678	1.116	0.387
Residuals	6	1.4401	0.2400		

Signif. codes: 0 *** 0.001 ** 0.01 * 0.05 . 0.1 1

Fold change in relative to Col-0 and its corresponding minimum and maximum fold change is listed in Table C.2

Appendix C.2: Fold change in expression of SA-responsive marker genes

Target	Genotype	Fold change		
		minimum	average	maximum
EFalpha1	*cfs1-2*	0.681	1.000	1.467
EFalpha1	*cfs1-3*	0.834	1.000	1.200
EFalpha1	Col-0	0.731	1.000	1.369
PR1	*cfs1-2*	9.176	12.043	15.807
PR1	*cfs1-3*	25.683	29.613	34.145
PR1	Col-0	0.789	1.000	1.267
PR2	*cfs1-2*	4.461	5.941	7.912
PR2	*cfs1-3*	10.884	12.559	14.493
PR2	Col-0	0.793	1.000	1.261
PR5	*cfs1-2*	3.444	4.670	6.334
PR5	*cfs1-3*	10.751	12.311	14.097
PR5	Col-0	0.714	1.000	1.401
SAG13	*cfs1-2*	3.756	4.278	4.872
SAG13	*cfs1-3*	2.079	2.169	2.263
SAG13	Col-0	0.967	1.000	1.034
WRKY53	*cfs1-2*	0.748	0.841	0.946
WRKY53	*cfs1-3*	1.059	1.270	1.524
WRKY53	Col-0	0.695	1.000	1.438

Appendix D   Analysis of JA and ethylene-responsive marker genes

Ct values from each technical and biological replicates are listed in Table D.1.

Appendix D.1: Ct values of *EFα1*, JA-, and ethylene-responsive marker genes

| Replication | | Target | Samples | | |
biological	technical		*cfs1-3*	Col-0	*cfs1-2*
1	1	*EF1alpha*	20.621	20.148	19.629
1	2	*EF1alpha*	20.766	20.231	19.634
2	1	*EF1alpha*	19.268	19.788	19.122
2	2	*EF1alpha*	19.121	19.889	19.44
3	1	*EF1alpha*	21.108	19.145	19.748
3	2	*EF1alpha*	21.097	19.412	19.525
1	1	*ERF1*	26.78	26.631	26.299
1	2	*ERF1*	28.033	26.746	26.635
2	1	*ERF1*	26.324	26.123	26.48
2	2	*ERF1*	27.383	26.203	27.029
3	1	*ERF1*	27.317	27.06	26.258
3	2	*ERF1*	28.101	27.496	27.174
1	1	*LOX2*	22.261	20.179	20.196
1	2	*LOX2*	22.197	20.354	20.818
2	1	*LOX2*	19.201	20.499	19.961
2	2	*LOX2*	19.347	20.861	20.13
3	1	*LOX2*	22.561	21.315	20.3
3	2	*LOX2*	22.634	21.016	20.096
1	1	*PDF1.2*	27.598	24.584	24.071
1	2	*PDF1.2*	26.536	24.964	24.028
2	1	*PDF1.2*	25.065	25.981	21.977
2	2	*PDF1.2*	25.17	25.654	22.4
3	1	*PDF1.2*	26.048	26.687	23.166
3	2	*PDF1.2*	25.78	26.516	23.202
1	1	*PR3*	28.052	26.949	24.073

Continued on next page

Appendix D.1: Ct values of *EFα1*, JA-, and ethylene-responsive marker genes
–continued from previous page

| Replication | | Target | Samples | | |
biological	technical		*cfs1-3*	Col-0	*cfs1-2*
1	2	*PR3*	25.825	27.067	24.001
2	1	*PR3*	25.505	25.306	23.528
2	2	*PR3*	25.211	25.271	23.055
3	1	*PR3*	27.409	25.52	24.018
3	2	*PR3*	27.27	25.328	23.707
1	1	*VSP2*	29.262	24.469	25.551
1	2	*VSP2*	28.84	24.215	25.898
2	1	*VSP2*	26.14	25.145	25.296
2	2	*VSP2*	27.001	25.31	26.457
3	1	*VSP2*	28.456	29.893	26.502
3	2	*VSP2*	29.056	28.627	26.061

All statistical analyses were performed using the functions described in Appendices C and E. ΔC_t values were subjected to statistical test as follows:

For **ERF1**:
Shapiro-Wilk normality test: normality accepted
(W = 0.90237, p-value = 0.26618)
ANOVA:

	Df	Sum Sq	Mean Sq	F Value	Pr($>$ F)
genotype	2	0.103	0.0515	0.11	0.897
Residuals	6	2.804	0.4673		

Signif. codes: 0 *** 0.001 ** 0.01 * 0.05 . 0.1 1

For **LOX2**:
Shapiro-Wilk normality test: normality accepted
(W = 0.95331, p-value = 0.7264)
ANOVA:

	Df	Sum Sq	Mean Sq	F Value	Pr(> F)
genotype	2	0.1364	0.0682	0.13	0.88
Residuals	6	3.1351	0.5225		

Signif. codes: 0 *** 0.001 ** 0.01 * 0.05 . 0.1 1

For *PDF1.2*:

Shapiro-Wilk normality test: normality accepted
(W = 0.96671, p-value = 0.8652)

ANOVA:

	Df	Sum Sq	Mean Sq	F Value	Pr(> F)	
genotype	2	9.039	4.519	4.215	0.0719	.
Residuals	6	6.434	1.072			

Signif. codes: 0 *** 0.001 ** 0.01 * 0.05 . 0.1 1

For *PR3*:

Shapiro-Wilk normality test: normality accepted
(W = 0.91031, p-value = 0.318)

ANOVA:

	Df	Sum Sq	Mean Sq	F Value	Pr(> F)	
genotype	2	7.295	3.647	14.29	0.00523	**
Residuals	6	1.532	0.255			

Signif. codes: 0 *** 0.001 ** 0.01 * 0.05 . 0.1 1

Tukey Honest Significant Difference test:

Test	Estimate Std.	Error	t value	Pr(> $|t|$)	
cfs1-3 - cfs1-2	1.7961	0.4126	4.354	0.01112	*
cfs1-2 - Col-0	-2.0061	0.4126	-4.863	0.00674	**
cfs1-3 - Col-0	-0.2100	0.4126	-0.509	0.86981	

Signif. codes: 0 *** 0.001 ** 0.01 * 0.05 . 0.1 1
(Adjusted p values reported – single-step method)

For *VSP2*:

Shapiro-Wilk normality test: normality accepted

(W = 0.99124, p-value = 0.9975)

ANOVA:

	Df	Sum Sq	Mean Sq	F Value	Pr($> F$)
genotype	2	3.862	1.931	0.592	0.583
Residuals	6	19.569	3.261		

—

Signif. codes: 0 *** 0.001 ** 0.01 * 0.05 . 0.1   1

Fold change in relative to Col-0 and its corresponding minimum and maximum fold change is listed in Table D.2 .

Appendix D.2: Fold change in expression of JA- and ethylene-responsive marker genes

Target	Genotype	Fold change		
		maximum	average	minimum
EF1alpha	Col-0	0.902	1.000	1.109
EF1alpha	cfs1-2	0.795	1.000	1.258
EF1alpha	cfs1-3	0.874	1.000	1.144
ERF1	Col-0	0.830	1.000	1.204
ERF1	cfs1-2	0.603	0.835	1.156
ERF1	cfs1-3	0.623	0.931	1.393
LOX2	Col-0	0.880	1.000	1.136
LOX2	cfs1-2	0.900	1.132	1.423
LOX2	cfs1-3	0.826	0.920	1.024
PDF1.2	Col-0	0.865	1.000	1.156
PDF1.2	cfs1-2	3.828	4.705	5.783
PDF1.2	cfs1-3	0.901	1.178	1.540
PR3	Col-0	0.757	1.000	1.320
PR3	cfs1-2	3.220	4.017	5.011
PR3	cfs1-3	0.656	1.157	2.040
VSP2	Col-0	0.742	1.000	1.347
VSP2	cfs1-2	0.699	0.959	1.315
VSP2	cfs1-3	0.236	0.374	0.592

Appendix E Analysis of cell death executioner and oxidative stress marker genes

Ct values from each technical and biological replicates are listed in Table E.1.

Appendix E.1: Ct values of *EFα1*, cell death executioner and oxidative stress marker genes

| Replication | | Target | Samples | | |
biological	technical		Col-0	*cfs1-2*	*cfs1-3*
1	1	*BFN1*	34.406	28.349	35.514
1	2	*BFN1*	31.82	27.656	33.084
2	1	*BFN1*	28.263	28.097	32.559
2	2	*BFN1*	28.372	28.695	30.851
2	3	*BFN1*	28.443	28.042	31.491
3	1	*BFN1*	33.601	31.718	31.121
3	2	*BFN1*	32.111	30.972	30.227
3	3	*BFN1*	32.602	31.952	31.218
1	1	*CAN1*	30.402	29.139	30.82
1	2	*CAN1*	30.224	29.02	30.356
1	3	*CAN1*	29.533	29.014	30.256
2	1	*CAN1*	30.471	28.752	29.693
2	2	*CAN1*	30.749	30.022	29.684
2	3	*CAN1*	30.023	28.826	28.928
3	1	*CAN1*	30.234	30.713	31.06
3	2	*CAN1*	31.328	31.045	30.417
1	1	*EFalpha1*	19.482	19.652	21.498
1	2	*EFalpha1*	19.471	19.594	21.515
1	3	*EFalpha1*	19.619	19.863	21.346
2	1	*EFalpha1*	20.394	19.693	19.517
2	2	*EFalpha1*	20.579	20.066	19.789
2	3	*EFalpha1*	20.567	20.033	19.855
3	1	*EFalpha1*	21.444	20.09	21.182
3	2	*EFalpha1*	21.874	20.296	21.097

Continued on next page

Appendix E.1: Ct values of *EFα1*, cell death executioner and oxidative stress marker genes *–continued from previous page*

| Replication | | Target | Samples | | |
biological	technical		Col-0	*cfs1-2*	*cfs1-3*
3	3	*EFalpha1*	21.498	20.263	20.9
1	1	*FES1A*	27.039	26.694	28.216
1	2	*FES1A*	27.262	25.936	27.302
1	3	*FES1A*	26.91	26.292	27.709
2	1	*FES1A*	27.604	27.833	26.877
2	2	*FES1A*	28.072	25.86	26.151
2	3	*FES1A*	27.612	26.669	27.068
3	1	*FES1A*	28.323	26.708	27.084
3	2	*FES1A*	28.728	27.171	27.502
3	3	*FES1A*	27.98	26.956	27.363
1	1	*GLY3*	22.478	22.33	24.385
1	2	*GLY3*	22.591	22.634	25.268
1	3	*GLY3*	22.701	22.479	24.513
2	1	*GLY3*	23.396	22.738	23.111
2	2	*GLY3*	23.376	23.063	23.105
2	3	*GLY3*	23.027	22.893	23.133
3	1	*GLY3*	24.25	23.038	23.484
3	2	*GLY3*	25.302	23.167	24.028
1	1	*MC1*	23.612	22.893	23.982
1	2	*MC1*	23.708	23.781	24.477
1	3	*MC1*	23.317	23.136	24.108
2	1	*MC1*	24.018	23.268	23.117
2	2	*MC1*	24.698	23.511	23.32
2	3	*MC1*	24.222	23.435	23.215
3	1	*MC1*	24.954	23.681	24.498
3	2	*MC1*	25.203	23.992	24.618
3	3	*MC1*	24.79	23.671	24.198
1	1	*MC9*	31.06	29.537	33.157
1	2	*MC9*	31.359	28.982	34.807

Continued on next page

Appendix E.1: Ct values of *EFα1*, cell death executioner and oxidative stress marker genes –*continued from previous page*

| Replication | | Target | Samples | | |
biological	technical		Col-0	*cfs1-2*	*cfs1-3*
1	3	*MC9*	31.399	29.885	34.674
2	1	*MC9*	30.023	29.257	31.145
2	2	*MC9*	29.279	29.128	31.061
2	3	*MC9*	29.981	28.589	30.238
3	1	*MC9*	32.021	30.851	31.258
3	2	*MC9*	31.504	30.582	31.167
1	1	*RD21*	19.624	19.499	21.073
1	2	*RD21*	19.515	19.289	21.475
1	3	*RD21*	19.693	19.273	21.025
2	1	*RD21*	20.556	19.736	19.665
2	2	*RD21*	20.207	19.508	19.675
2	3	*RD21*	20.334	19.36	19.456
3	1	*RD21*	21.338	19.897	21.192
3	2	*RD21*	21.214	19.99	20.605
3	3	*RD21*	21.176	20.058	20.498
1	1	*RNS3*	32.046	30.533	33.494
1	2	*RNS3*	32.416	31.631	34.918
1	3	*RNS3*	31.017	29.873	35.037
2	1	*RNS3*	NA	30.073	30.219
2	2	*RNS3*	31.976	29.703	29.781
2	3	*RNS3*	31.881	29.996	30.299
3	1	*RNS3*	34.541	30.016	31.369
3	2	*RNS3*	34.48	30.546	31.068
1	1	*UGT87E2*	27.17	25.311	27.6
1	2	*UGT87E2*	27.272	25.126	27.658
1	3	*UGT87E2*	27.051	25.259	27.801
2	1	*UGT87E2*	25.526	25.693	26.836
2	2	*UGT87E2*	25.264	25.802	26.899
2	3	*UGT87E2*	25.417	25.803	26.304

Continued on next page

Appendix E.1: Ct values of *EFα1*, cell death executioner and oxidative stress marker genes *–continued from previous page*

Replication		Target	Samples		
biological	technical		Col-0	*cfs1-2*	*cfs1-3*
3	1	*UGT87E2*	26.141	26.55	25.895
3	2	*UGT87E2*	26.19	26.399	25.759
3	3	*UGT87E2*	26.265	26.633	25.826

All statistical analyses were performed using the functions described in Appendix C. Function *kruskal.test* was used for Kruskal-Wallis rank sum test. ΔC_t values were subjected to statistical test as follows:

For *MC1*:

Shapiro-Wilk normality test: normality accepted

(W = 0.85064, p-value = 0.07573)

ANOVA:

	Df	Sum Sq	Mean Sq	F Value	Pr($>$ F)
genotype	2	0.3447	0.17237	1.873	0.233
Residuals	6	0.5521	0.092		

—

Signif. codes: 0 *** 0.001 ** 0.01 * 0.05 . 0.1   1

For *PR2*:

Shapiro-Wilk normality test: normality rejected

(W = 0.75987, p-value = 0.007054)

Kruskal-Wallis rank sum test:

Kruskal-Wallis chi-squared = 0.2735, df = 2, p-value = 0.8722

For *RNS3*:

Shapiro-Wilk normality test: normality rejected

(W = 0.81643, p-value = 0.0314)

Kruskal-Wallis rank sum test:

Kruskal-Wallis chi-squared = 2.4615, df = 2, p-value = 0.2921

For *BFN1*:

Shapiro-Wilk normality test: normality accepted

(W = 0.95104, p-value = 0.7015)

ANOVA:

	Df	Sum Sq	Mean Sq	F Value	Pr($> F$)
genotype	2	4.504	2.252	0.808	0.489
Residuals	6	16.732	2.789		

Signif. codes: 0 *** 0.001 ** 0.01 * 0.05 . 0.1   1

For *CAN1*:

Shapiro-Wilk normality test: normality accepted

(W = 0.91294, p-value = 0.337)

ANOVA:

	Df	Sum Sq	Mean Sq	F Value	Pr($> F$)
genotype	2	0.3296	0.1648	0.496	0.632
Residuals	6	1.9917	0.3319		

Signif. codes: 0 *** 0.001 ** 0.01 * 0.05 . 0.1   1

For *GLY3*:

Shapiro-Wilk normality test: normality rejected

(W = 0.82849, p-value = 0.04295)

Kruskal-Wallis rank sum test:

Kruskal-Wallis chi-squared = 2.4615, df = 2, p-value = 0.2921

For *FES1A*:

Shapiro-Wilk normality test: normality rejected

(W = 0.81127, p-value = 0.02745)

Kruskal-Wallis rank sum test:

Kruskal-Wallis chi-squared = 7.3846, df = 2, p-value = 0.02491

For *UGT87E2*:

Shapiro-Wilk normality test: normality rejected

(W = 0.65775, p-value = 0.0004549)

Kruskal-Wallis rank sum test:

Kruskal-Wallis chi-squared = 1.1852, df = 2, p-value = 0.5529

For *RD21*:

Shapiro-Wilk normality test: normality rejected
(W = 0.72058, p-value = 0.002467)
Kruskal-Wallis rank sum test:
Kruskal-Wallis chi-squared = 0.82051, df = 2, p-value = 0.6635

Fold change in relative to Col-0 and its corresponding minimum and maximum fold change is listed in Table E.2

Appendix E.2: Fold change in expression of cell death executioner and oxidative stress marker genes

Target	Genotype	Fold change		
		maximum	average	minimum
BFN1	*cfs1-2*	2.300	3.234	4.547
BFN1	*cfs1-3*	1.049	2.242	4.791
BFN1	Col-0	0.503	1.000	1.987
CAN1	*cfs1-2*	0.512	0.814	1.295
CAN1	*cfs1-3*	0.833	1.122	1.512
CAN1	Col-0	0.610	1.000	1.639
EFalpha1	*cfs1-2*	0.887	1.000	1.127
EFalpha1	*cfs1-3*	0.881	1.000	1.136
EFalpha1	Col-0	0.824	1.000	1.213
FES1A	*cfs1-2*	1.005	1.249	1.552
FES1A	*cfs1-3*	1.318	1.670	2.117
FES1A	Col-0	0.770	1.000	1.300
GLY3	*cfs1-2*	1.037	1.245	1.495
GLY3	*cfs1-3*	0.836	1.133	1.534
GLY3	Col-0	0.708	1.000	1.413
MC1	*cfs1-2*	0.812	1.018	1.278
MC1	*cfs1-3*	1.120	1.345	1.616
MC1	Col-0	0.820	1.000	1.219
MC9	*cfs1-2*	1.075	1.350	1.695
MC9	*cfs1-3*	0.543	0.793	1.159

Continued on next page

Appendix E.2: Fold change in expression of cell death executioner and oxidative stress marker genes –*continued from previous page*

Target	Genotype	Fold change		
		maximum	**average**	**minimum**
MC9	Col-0	0.772	1.000	1.295
RD21	*cfs1-2*	0.935	1.042	1.162
RD21	*cfs1-3*	0.818	1.050	1.349
RD21	Col-0	0.861	1.000	1.161
RNS3	*cfs1-2*	2.275	4.083	7.327
RNS3	*cfs1-3*	2.048	2.981	4.337
RNS3	Col-0	0.725	1.000	1.379
UGT87E2	*cfs1-2*	1.271	1.399	1.540
UGT87E2	*cfs1-3*	1.536	1.644	1.759
UGT87E2	Col-0	0.937	1.000	1.068

Appendix F   Analysis of pavement cell complexity

Circularity of each measured pavement cells are listed in Table values from each technical and biological replicates are listed in Table F.1. All statistical analyses were performed using the functions described in Appendices C and E.

Appendix F.1: Circularity of Col-0, *cfs1-2* and *cfs1-3* pavement cells

Col-0	cfs1-2	cfs1-3
0.243	0.264	0.355
0.308	0.274	0.266
0.265	0.389	0.367
0.344	0.267	0.236
0.297	0.26	0.319
0.199	0.336	0.291
0.439	0.42	0.172
0.259	0.467	0.338
0.359	0.51	0.236
0.408	0.322	0.231
0.263	0.239	0.245
0.276	0.351	0.231
0.329	0.231	0.176
0.312	0.321	0.366
0.437	0.255	0.399
0.257	0.311	0.276
0.298	0.272	0.541
0.229	0.303	0.296
0.488	0.261	0.191
0.203	0.251	0.331

Summary of descriptive statistics for Col-0:

n=20; $\overline{x} \pm sd = 0.31065 \pm 0.080756$,

min = 0.199; $Q_1 = 0.2585$; *median = 0.2975*; $Q_3 = 0.34775$; *max = 0.488*

Summary of descriptive statistics for *cfs1-2*:

n=20; $\overline{x} \pm sd = 0.3152 \pm 0.07763$,

min = 0.231; $Q_1 = 0.2608$; *median = 0.2885*; $Q_3 = 0.3398$; *max = 0.51*

Summary of descriptive statistics for *cfs1-3*:

n=20; $\overline{x} \pm sd = 0.29315 \pm 0.08819$, *min = 0.172*; $Q_1 = 0.2348$; *median = 0.2835*; $Q_3 = 0.3423$; *max = 0.541*

Shapiro-Wilk normality test: normality rejected (W = 0.9404, p-value = 0.005644)

Kruskal-Wallis rank sum test: chi-squared = 0.8476, df = 2, p-value = 0.6546

Appendix G   Analysis of lesion formation in *cfs1 escrt* mutants

Appendix G.1: Number of true leaf and true leaf showing lesions in *cfs1* mutant, *cfs1 escrt-i* double mutants, *escrt-i* mutants and their corresponding background

ID	DAS Genotype	20 all	20 le	25 all	25 le	30 all	30 le
1	*cfs1-2*	2	7	2	8	5	12
2	*elch*	0	5	0	7	0	9
3	*vps28.2*	0	6	0	9	0	13
4	*elch*	0	6	0	9	0	9
5	*cfs1-2 vps28.2*	2	7	2	10	4	12
6	*cfs1-2 vps28.2*	2	7	2	11	5	13
7	*cfs1-2 elch*	0	4	0	6	4	9
8	*cfs1-2*	2	7	2	9	5	12
9	*vps28.2*	0	6	0	11	0	11
10	*cfs1-2 vps28.2*	2	8	2	11	6	14
11	Ws-2	0	9	0	11	0	11
13	*cfs1-2 elch*	0	5	2	9	5	11
14	*cfs1-2 vps28.2*	2	6	3	10	6	11
15	*vps37.1*	0	6	0	11	0	14
16	*cfs1-2*	0	6	2	11	4	13
18	*vps37.1*	0	6	0	12	0	13
19	Ws-2	0	7	0	10	0	10
20	*cfs1-2*	2	7	2	11	5	12
21	*cfs1-2 vps37.1*	0	6	2	11	5	11
22	*Col-0*	0	5	0	8	0	11
23	*Col-0*	0	6	0	11	0	11
24	*Col-0*	0	7	0	12	0	12
25	Ws-2	0	6	0	8	0	8

Continued on next page

Appendix G.1: Number of true leaf and true leaf showing lesions in *cfs1* mutant, *cfs1 escrt-i* double mutants, *escrt-i* mutant and their corresponding background –*continued from previous page*

ID	DAS Genotype	20 all	20 le	25 all	25 le	30 all	30 le
26	*cfs1-2 elch*	0	5	2	8	5	12
27	*Col-0*	0	7	0	10	0	13
28	*cfs1-2 elch*	0	5	2	7	4	8
29	*cfs1-2 vps37.1*	0	6	2	11	5	14
30	*Col-0*	0	7	0	11	0	12
31	*cfs1-2 vps37.1*	2	6	2	11	5	12
32	Ws-2	0	7	0	10	0	10
33	*cfs1-2 vps37.1*	0	6	3	9	4	12
34	Ws-2	0	7	0	7	0	7
35	*elch*	0	3	0	6	0	8
36	*cfs1-2 elch*	0	5	0	8	0	11
37	*elch*	0	4	0	8	0	10
38	*cfs1-2*	2	6	2	11	5	13
39	*vps28.2*	0	6	0	9	0	11
40	*cfs1-2 vps37.1*	2	6	2	9	5	12
41	*cfs1-2 vps37.1*	2	6	2	9	5	13
42	*vps37.1*	0	6	0	9	0	12
43	*cfs1-2 vps28.2*	0	6	2	11	5	12
44	*vps37.1*	0	7	0	11	0	12
45	Ws-2	0	8	0	11	0	11
46	*cfs1-2 vps28.2*	0	6	2	10	6	14
47	*cfs1-2 vps37.1*	0	6	2	11	4	12
48	Ws-2	0	6	0	9	0	8
49	*Col-0*	0	6	0	11	0	11
50	*vps37.1*	0	5	0	9	0	11
51	*cfs1-2*	0	4	0	9	7	12
52	*vps28.2*	0	4	0	9	0	11
53	*Col-0*	0	6	0	9	0	11

Continued on next page

Appendix G.1: Number of true leaf and true leaf showing lesions in *cfs1* mutant, *cfs1 escrt-i* double mutants, *escrt-i* mutant and their corresponding background –*continued from previous page*

ID	DAS Genotype	20		25		30	
		all	le	all	le	all	le
54	*vps37.1*	0	7	0	12	0	12
55	*vps28.2*	0	6	0	9	0	10
56	*Col-0*	0	5	0	9	0	12
57	*cfs1-2*	0	6	2	10	6	12
58	*cfs1-2 vps28.2*	1	5	2	10	6	13
59	*vps37.1*	0	6	0	11	0	12
60	*vps28.2*	0	6	0	10	0	11
61	*cfs1-2 elch*	0	5	0	7	4	8
62	*cfs1-2 vps28.2*	2	6	2	10	6	13
63	*vps28.2*	0	7	0	10	0	13
64	*cfs1-2 elch*	0	5	0	8	4	11
65	*Ws-2*	0	7	0	11	0	11
66	*cfs1-2 vps28.2*	0	5	2	11	4	12
67	*cfs1-2 elch*	0	5	0	8	5	12
68	*cfs1-2 elch*	0	2	0	6	0	9
69	*cfs1-2 vps37.1*	2	6	2	11	5	11
70	*cfs1-2*	0	2	0	4	0	6
71	*Ws-2*	0	6	0	8	0	8
72	*cfs1-2 vps37.1*	0	6	2	10	3	12
73	*elch*	0	4	0	8	0	10
74	*vps37.1*	0	6	0	11	0	13
77	*vps28.2*	0	6	0	10	0	12
78	*elch*	0	5	0	9	0	9
79	*vps28.2*	0	6	0	9	0	12
80	*vps28.2*	0	5	0	9	0	9
81	*elch*	0	5	0	7	0	8
82	*cfs1-2 vps37.1*	0	6	2	10	6	13
83	*cfs1-2 vps28.2*	0	6	2	10	6	12

Continued on next page

Appendix G.1: Number of true leaf and true leaf showing lesions in *cfs1* mutant, *cfs1 escrt-i* double mutants, *escrt-i* mutant and their corresponding background –*continued from previous page*

ID	DAS Genotype	20 all	20 le	25 all	25 le	30 all	30 le
84	*cfs1-2 elch*	0	5	0	8	3	8
85	Ws-2	0	7	0	8	0	8
86	*cfs1-2 elch*	0	6	2	9	6	8
87	*vps37.1*	0	6	0	10	0	12
88	*elch*	0	5	0	9	0	9
89	*cfs1-2 vps28.2*	0	7	2	10	7	12
90	Ws-2	0	7	0	10	0	10
91	Ws-2	0	7	0	8	0	8
92	*cfs1-2 elch*	0	5	0	9	5	11
93	*cfs1-2*	2	6	2	11	6	11
94	*cfs1-2 vps37.1*	2	6	3	10	6	14
95	Ws-2	0	6	0	8	0	8
96	Ws-2	0	6	0	7	0	7
97	*cfs1-2 elch*	0	5	2	7	3	9
98	*cfs1-2 vps37.1*	0	6	2	10	6	12
99	*vps37.1*	0	6	0	9	0	13
100	*cfs1-2 vps28.2*	0	7	3	11	7	10
101	*Col-0*	0	7	0	11	0	12
102	*vps28.2*	0	7	0	11	0	13
103	*vps37.1*	0	7	0	11	0	15
104	*cfs1-2*	0	6	2	11	4	12
105	*Col-0*	0	7	0	9	0	10
106	*Col-0*	0	6	0	9	0	12
107	*Col-0*	0	7	0	11	0	11
108	*cfs1-2*	2	7	2	11	6	12
109	*vps37.1*	0	7	0	11	0	12
110	*vps28.2*	0	0	0	11	0	10
111	*cfs1-2 vps37.1*	0	7	2	11	6	14

Continued on next page

Appendix G.1: Number of true leaf and true leaf showing lesions in *cfs1* mutant, *cfs1 escrt-i* double mutants, *escrt-i* mutant and their corresponding background –*continued from previous page*

ID	DAS Genotype	20 all	20 le	25 all	25 le	30 all	30 le
112	*cfs1-2*	2	6	2	11	7	13
114	*cfs1-2 elch*	0	5	0	8	4	10
115	*cfs1-2 vps28.2*	2	6	2	10	6	13
116	*cfs1-2 vps28.2*	0	7	2	9	5	11
117	*cfs1-2 vps28.2*	2	6	2	9	6	12
118	*Col-0*	0	7	0	11	0	12
119	*cfs1-2 vps37.1*	2	6	2	11	6	14
120	*elch*	0	5	0	8	0	8
121	*cfs1-2 elch*	0	5	2	10	6	12
122	*vps28.2*	0	6	0	11	0	14
123	*cfs1-2*	2	6	2	11	6	14
124	*vps28.2*	0	7	0	10	0	11
125	*cfs1-2 elch*	0	6	0	9	6	11
126	*cfs1-2 vps28.2*	2	6	2	11	5	14
127	*Ws-2*	0	8	0	11	0	10
128	*vps37.1*	0	6	0	13	0	12
129	*cfs1-2*	0	7	3	11	6	13
130	*Col-0*	0	7	0	12	0	11
131	*cfs1-2*	2	7	3	14	5	12
132	*cfs1-2 vps28.2*	2	6	2	11	5	13
133	*elch*	0	5	0	10	0	10
134	*vps28.2*	0	5	0	10	0	12
136	*elch*	0	6	0	9	0	9
137	*Ws-2*	0	7	0	11	0	11
138	*cfs1-2 vps37.1*	2	7	2	12	5	14
139	*vps37.1*	0	7	0	12	0	12
140	*Ws-2*	0	7	0	8	0	8
141	*vps37.1*	0	6	0	11	0	13

Continued on next page

Appendix G.1: Number of true leaf and true leaf showing lesions in *cfs1* mutant, *cfs1 escrt-i* double mutants, *escrt-i* mutant and their corresponding background –*continued from previous page*

ID	DAS Genotype	20 all	20 le	25 all	25 le	30 all	30 le
142	*vps28.2*	0	7	0	11	0	10
143	*cfs1-2 vps37.1*	2	7	3	12	5	11
144	*cfs1-2*	0	7	2	8	4	11
145	*elch*	0	6	0	9	0	9
146	*cfs1-2 vps28.2*	2	7	3	12	7	14
147	*cfs1-2 vps37.1*	2	7	2	12	4	13
148	*cfs1-2 elch*	0	5	0	9	4	10
149	*cfs1-2 elch*	0	5	0	8	4	10
150	*Col-0*	0	6	0	11	0	11
151	*cfs1-2 vps37.1*	2	7	3	12	5	13
152	Ws-2	0	8	0	11	0	10
153	*Col-0*	0	6	0	11	0	11
154	*vps37.1*	0	7	0	12	0	13
155	*cfs1-2 vps37.1*	0	6	2	9	6	11
156	*cfs1-2 vps37.1*	0	6	2	11	4	12
157	*vps28.2*	0	6	0	11	0	11
158	*cfs1-2 elch*	0	6	2	9	4	12
159	*cfs1-2*	1	6	2	11	6	12
160	*vps37.1*	0	7	0	12	0	11
161	*vps37.1*	0	7	0	12	0	13
162	*cfs1-2 vps37.1*	0	7	2	10	5	12
163	*elch*	0	6	0	8	0	9
164	*cfs1-2 elch*	0	5	1	8	0	10
165	*cfs1-2*	2	8	2	10	6	12
166	*vps37.1*	0	7	0	11	0	14
167	*cfs1-2 vps28.2*	2	7	3	11	5	12
168	*elch*	0	6	0	8	0	8
170	*Col-0*	0	8	0	11	0	12

Continued on next page

Appendix G.1: Number of true leaf and true leaf showing lesions in *cfs1* mutant, *cfs1 escrt-i* double mutants, *escrt-i* mutant and their corresponding background –*continued from previous page*

ID	DAS Genotype	20 all	20 le	25 all	25 le	30 all	30 le
171	*vps37.1*	0	6	0	10	0	13
172	*vps28.2*	0	6	0	11	0	13
173	*elch*	0	5	0	8	0	8
175	*Col-0*	0	6	0	13	0	12
176	*cfs1-2 vps37.1*	0	5	2	11	4	11
177	*cfs1-2 elch*	0	6	0	9	4	11
178	*elch*	0	5	0	8	0	8
179	*cfs1-2 elch*	0	6	0	10	5	10
180	*vps37.1*	0	7	0	10	0	12
181	*Col-0*	0	8	0	11	0	12
182	*cfs1-2*	2	6	2	10	5	11
183	*cfs1-2*	0	5	2	11	6	13
184	*Ws-2*	0	6	0	11	0	10
185	*vps28.2*	0	5	0	11	0	12
186	*Ws-2*	0	6	0	7	0	8
187	*cfs1-2*	2	7	2	11	4	11
188	*cfs1-2 vps28.2*	2	6	2	11	4	11
189	*cfs1-2 vps28.2*	2	7	2	12	4	14
190	*Ws-2*	0	8	0	12	0	12
191	*Col-0*	0	7	0	10	0	12
192	*cfs1-2 vps28.2*	0	7	2	12	6	12
194	*Col-0*	0	7	0	12	0	12
195	*cfs1-2 elch*	0	6	2	9	4	12
197	*Col-0*	0	5	0	10	0	11
198	*Ws-2*	0	6	0	8	0	8
199	*Col-0*	0	7	0	12	0	12
200	*cfs1-2 vps28.2*	2	6	2	11	5	12
201	*cfs1-2 vps37.1*	1	6	2	11	4	12

Continued on next page

Appendix G.1: Number of true leaf and true leaf showing lesions in *cfs1* mutant, *cfs1 escrt-i* double mutants, *escrt-i* mutant and their corresponding background –*continued from previous page*

ID	DAS Genotype	20 all	20 le	25 all	25 le	30 all	30 le
202	*cfs1-2 vps37.1*	2	6	2	11	5	14
203	*cfs1-2 vps28.2*	0	6	3	11	5	11
204	*vps28.2*	0	6	0	10	0	12
205	*cfs1-2 vps37.1*	0	6	2	11	5	13
206	*Col-0*	0	6	0	10	0	11
207	*cfs1-2*	2	7	2	11	6	13
208	*cfs1-2 vps37.1*	0	7	2	10	4	11
209	*cfs1-2 vps28.2*	2	7	2	11	7	11
210	*cfs1-2*	0	6	2	11	6	12
211	*cfs1-2*	0	6	2	11	5	11
212	*cfs1-2 elch*	0	6	0	10	4	12
213	Ws-2	0	8	0	12	0	12
214	*vps37.1*	0	7	0	11	0	13
215	Ws-2	0	6	0	9	0	9
216	*elch*	0	5	0	9	0	9
217	*vps28.2*	0	6	0	11	0	13
218	*cfs1-2 elch*	0	6	0	9	6	11
219	*elch*	0	6	0	9	0	10
220	*vps37.1*	0	6	0	11	0	14
221	*elch*	0	6	0	10	0	9
222	*vps28.2*	0	6	0	11	0	12
223	*cfs1-2*	2	8	3	12	5	12
224	*cfs1-2 vps28.2*	2	6	2	11	4	12
225	*cfs1-2 elch*	0	5	0	8	0	9
226	Ws-2	0	8	0	11	0	11
227	Ws-2	0	6	0	11	0	9
228	*cfs1-2 elch*	0	3	0	5	0	11
229	Ws-2	0	7	0	12	0	12

Continued on next page

Appendix G.1: Number of true leaf and true leaf showing lesions in *cfs1* mutant, *cfs1 escrt-i* double mutants, *escrt-i* mutant and their corresponding background –*continued from previous page*

ID	DAS Genotype	20 all	20 le	25 all	25 le	30 all	30 le
230	*vps28.2*	0	6	0	10	0	11
232	*Col-0*	0	6	0	10	0	11
233	*cfs1-2 vps28.2*	2	6	0	10	4	12
234	*vps28.2*	0	6	0	9	0	11
235	*cfs1-2*	2	6	2	9	4	12
236	*elch*	0	2	0	6	0	6
237	*cfs1-2 elch*	0	5	2	8	4	10
238	*cfs1-2 vps28.2*	2	7	2	11	5	12
239	*vps28.2*	0	5	0	9	0	11
240	*elch*	0	6	0	9	0	9
241	*vps28.2*	0	6	0	9	0	11
242	Ws-2	0	7	0	7	0	7
243	*vps28.2*	0	5	0	9	0	10
244	*cfs1-2 vps28.2*	2	6	3	9	6	11
246	Ws-2	0	6	0	8	0	8
247	*vps37.1*	0	6	0	9	0	11
248	*cfs1-2 elch*	0	5	2	8	4	9
249	*cfs1-2 vps28.2*	0	6	3	9	6	11
250	*cfs1-2 vps37.1*	2	6	2	9	4	12
251	*cfs1-2*	0	6	2	9	4	12
252	Ws-2	0	5	0	7	0	7
253	*vps28.2*	0	5	0	10	0	12
254	Ws-2	0	6	0	7	0	7
255	*cfs1-2 elch*	0	6	2	8	5	10
256	*elch*	0	4	0	7	0	8
257	*cfs1-2 elch*	0	4	2	6	5	11
258	*vps37.1*	0	5	0	9	0	12
259	*Col-0*	0	5	0	9	0	12

Continued on next page

Appendix G.1: Number of true leaf and true leaf showing lesions in *cfs1* mutant, *cfs1 escrt-i* double mutants, *escrt-i* mutant and their corresponding background –*continued from previous page*

ID	DAS Genotype	20 all	20 le	25 all	25 le	30 all	30 le
260	*vps28.2*	0	4	0	7	0	10
261	*cfs1-2 vps37.1*	2	6	2	9	5	14
262	*vps28.2*	0	6	0	9	0	12
263	*cfs1-2 elch*	0	5	0	8	4	11
264	*cfs1-2 vps37.1*	2	6	2	10	5	12
265	*cfs1-2 elch*	0	5	2	8	0	12
266	*vps37.1*	0	6	0	9	0	10
267	*cfs1-2 elch*	0	5	0	9	6	11
268	*cfs1-2*	0	5	2	9	0	11
269	Col-0	0	6	0	9	0	11
270	Col-0	0	6	0	9	0	11
271	Col-0	0	4	0	6	0	9
272	*cfs1-2*	2	6	2	9	5	12
273	*cfs1-2*	2	5	2	9	5	11
274	*cfs1-2 vps28.2*	2	6	2	10	4	11
275	*elch*	0	6	0	8	0	8
276	*cfs1-2 vps28.2*	0	6	2	9	4	12
277	Ws-2	0	5	0	7	0	7
279	*cfs1-2 vps37.1*	2	6	2	9	4	11
280	*vps37.1*	0	5	0	9	0	11
281	Col-0	0	5	0	10	0	10
282	*cfs1-2 vps28.2*	2	6	2	10	6	11
283	Ws-2	0	6	0	7	0	7
284	*elch*	0	4	0	8	0	7
285	*cfs1-2*	2	6	0	8	6	12
286	Ws-2	0	6	0	8	0	9
287	*vps37.1*	0	5	0	9	0	10
289	*cfs1-2*	1	5	1	8	4	11

Continued on next page

Appendix G.1: Number of true leaf and true leaf showing lesions in *cfs1* mutant, *cfs1 escrt-i* double mutants, *escrt-i* mutant and their corresponding background –*continued from previous page*

ID	DAS Genotype	20 all	20 le	25 all	25 le	30 all	30 le
290	*vps37.1*	0	6	0	10	0	11
291	*vps37.1*	0	6	0	8	0	11
292	*cfs1-2 elch*	0	5	2	7	6	10
293	*elch*	0	5	0	7	0	8
294	*Col-0*	0	4	0	8	0	10
296	*elch*	0	5	0	8	0	8
297	Ws-2	0	6	0	8	0	8
298	*Col-0*	0	6	0	9	0	12
299	*cfs1-2*	2	5	2	9	6	11
300	*cfs1-2 vps28.2*	0	6	2	9	4	12
301	*cfs1-2 vps28.2*	0	5	2	8	5	12
302	*vps28.2*	0	6	0	9	0	11
303	*cfs1-2 vps37.1*	0	6	1	9	0	10
304	*cfs1-2 vps37.1*	2	6	2	9	2	11
305	Ws-2	0	6	0	8	0	8
306	*cfs1-2 vps37.1*	0	5	1	8	4	11
307	*vps37.1*	0	6	0	10	0	12
308	*cfs1-2 vps37.1*	2	5	1	9	4	11

DAS: date after sowing

all: number of true leaf

les: number of true leaf showing lesions

The number of individuals showing lesions from Table G.1 is summarized in Table G.2.

Appendix G.2: Summary of the number *cfs1* mutant, *cfs1 escrt-i* double mutants, *escrt-i* mutants and their corresponding background showing spontaneous lesion formation

Genotype	DAS	avg. total lf no.	avg. total le no.	N_{lesion}	N_{all}	%phenotype
cfs1-2	20	6.1	1.2	21	33	63.64
	25	10.0	1.9	30	33	90.91
	30	11.8	5.0	31	33	93.94
cfs1-2 elch	20	5.1	0.0	0	35	0.00
	25	8.1	0.8	15	35	42.86
	30	10.3	3.8	29	35	82.86
cfs1-2 vps28.2	20	6.3	1.2	22	35	62.86
	25	10.3	2.1	34	35	97.14
	30	12.1	5.3	35	35	100.00
cfs1-2 vps37.1	20	6.1	1.0	18	34	52.94
	25	10.2	2.0	34	34	100.00
	30	12.2	4.6	34	34	100.00
Col-0	20	6.2	0.0	0	32	0.00
	25	10.2	0.0	0	32	0.00
	30	11.3	0.0	0	32	0.00
elch	20	5.0	0.0	0	26	0.00
	25	8.2	0.0	0	26	0.00
	30	8.6	0.0	0	26	0.00
vps28.2	20	5.6	0.0	0	31	0.00
	25	9.9	0.0	0	32	0.00
	30	11.5	0.0	0	31	0.00
vps37.1	20	6.2	0.0	0	31	0.00
	25	10.5	0.0	0	31	0.00
	30	12.2	0.0	0	31	0.00
Ws-2	20	6.7	0.0	0	36	0.00

Continued on next page

Appendix G.2: Summary of the number *cfs1* mutant, *cfs1 escrt-i* double mutants, *escrt-i* mutants and their corresponding backgroundshowing spontaneous lesion formation –*continued from previous page*

Genotype	DAS	avg. total lf no.	avg. total le no	N_{lesion}	N_{all}	%phenotype
	25	9.1	0.0	0	36	0.00
	30	9.0	0.0	0	36	0.00

DAS: Day after sowing

avg. total lf no.: Average total leaf number per plant

avg. total lf no.: Average total leaf number showing lesions per plant

N_{lesion}: Number of individuals showing lesions

N_{all} : Number of individuals observed

Fisher's exact test was performed using *fisher.test* function, and Pearson's χ^2 test of independence was performed using *prop.test* function without continuity correction.

Comparison of **cfs1-2** and **cfs1-2 elch**:
at **20 DAS**:
two-sided Fisher's Exact test:
p-value =4.904e-06
95 percent confidence interval: 4.905975, Inf
sample estimates: odds ratio Inf

two-sided Pearson's χ^2 test:
χ^2 =32.224, df = 1, p-value = 1.374e-08
95 percent confidence interval:0.4722376, 0.8004897
sample estimates: prop 1 = 0.6363636; prop 2 = 0.0000000

at **25 DAS**:
two-sided Fisher's Exact test:
p-value = 0.0813
95 percent confidence interval: 0.9093774, 5.0253256
sample estimates: odds ratio 2.107019

two-sided Pearson's χ^2 test:

χ^2 =17.522, df = 1, p-value = 2.841e-05

95 percent confidence interval: 0.2894711, 0.6715679

sample estimates: prop 1 = 0.9090909; prop 2 = 0.4285714

at **30 DAS**:

two-sided Fisher's Exact test:

p-value = 0.8595

95 percent confidence interval: 0.5343935, 2.4066953

sample estimates: odds ratio 1.132637

two-sided Pearson's χ^2 test:

χ^2 =2.0096, df = 1, p-value = 0.1563

95 percent confidence interval: -0.03823208, 0.25987710

sample estimates: prop 1 = 0.9393939; prop 2 = 0.8285714

Comparison of *cfs1-2* and *cfs1-2 vps28.2*:

at **20 DAS**:

two-sided Fisher's Exact test:

p-value =1

95 percent confidence interval: 0.4394925, 2.3294577

sample estimates: 1.012286

two-sided Pearson's χ^2 test:

χ^2 = 0.0044361, df = 1, p-value = 0.9469

95 percent confidence interval: -0.2214719, 0.2370563

sample estimates: prop 1 = 0.6363636; prop 2 = 0.6285714

at **25 DAS**:

two-sided Fisher's Exact test:

p-value = 0.8634

95 percent confidence interval: 0.4466068, 1.9600381

sample estimates: odds ratio 0.9363062

two-sided Pearson's χ^2 test:

χ^2 =1.1922, df = 1, p-value = 0.2749

95 percent confidence interval: -0.17488441, 0.05020909

sample estimates: prop 1 = 0.9090909; prop 2 = 0.9714286

at **30 DAS**:

two-sided Fisher's Exact test:

p-value = 0.8646

95 percent confidence interval: 0.4511315, 1.9553742

sample estimates: odds ratio 0.9398441

two-sided Pearson's χ^2 test:

χ^2 =2.1855, df = 1, p-value = 0.1393

95 percent confidence interval: -0.14201517, 0.02080305

sample estimates: prop 1 = 0.9393939; prop 2 = 1.0000000

Comparison of *cfs1-2* and *cfs1-2 vps37.1*:

at **20 DAS**:

two-sided Fisher's Exact test:

p-value =0.6906

95 percent confidence interval: 0.5065422, 2.8627941

sample estimates: 1.199929

two-sided Pearson's χ^2 test:

χ^2 = 0.78745, df = 1, p-value = 0.3749

95 percent confidence interval:-0.1277514, 0.3416552

sample estimates: prop 1 = 0.6363636; prop 2 = 0.5294118

at **25 DAS**:

two-sided Fisher's Exact test:

p-value = 0.8616

95 percent confidence interval: 0.4326427, 1.9091986

sample estimates: odds ratio 0.9097537

two-sided Pearson's χ^2 test:

χ^2 =3.2358, df = 1, p-value = 0.07205

95 percent confidence interval: -0.188993151, 0.007174969

sample estimates: prop 1 = 0.9090909; prop 2 = 1.0000000

at **30 DAS**:

two-sided Fisher's Exact test:

p-value = 1

95 percent confidence interval: 0.460948, 2.031717

sample estimates: odds ratio 0.9680871

two-sided Pearson's χ^2 test:

χ^2 =0.38099, df = 1, p-value = 0.5371

95 percent confidence interval: -0.13045541, 0.06806681

sample estimates: prop 1 = 0.9393939; prop 2 = 0.9705882

Appendix H   Analysis of *elch*-trichome

The number of wild-type and *elch*-trichome in leaf 3 and leaf 4 and listed in Table H.1.

Appendix H.1: Number of wild-type and *elch*-trichome

Genotype	Leaf number	Wild-type trichome	*elch* trichome	All trichome
cfs1-2	3	104	0	104
cfs1-2	4	120	0	120
cfs1-2	3	165	0	165
cfs1-2	4	175	0	175
cfs1-2	3	133	0	133
cfs1-2	4	119	0	119
cfs1-2	3	90	0	90
cfs1-2	4	114	0	114
cfs1-2	3	84	0	84
cfs1-2	4	77	0	77
cfs1-2	3	81	0	81
cfs1-2	4	77	0	77
cfs1-2	3	137	0	137
cfs1-2	4	218	0	218
cfs1-2	3	118	0	118
cfs1-2	4	122	0	122
cfs1-2	3	87	0	87
cfs1-2	4	102	0	102
cfs1-2	3	94	0	94
cfs1-2	4	108	0	108
cfs1-2	3	77	0	77
cfs1-2	4	103	0	103
cfs1-2	3	54	0	54
cfs1-2	4	74	0	74
Col-0	3	86	0	86
Col-0	4	119	0	119
Col-0	3	83	0	83

Continued on next page

Appendix H.1: Number of wild-type and *elch*-trichome *–continued from previous page*

Genotype	Leaf number	Wild-type trichome	*elch* trichome	All trichome
Col-0	4	112	0	112
Col-0	3	74	0	74
Col-0	4	96	0	96
Col-0	3	86	0	86
Col-0	4	97	0	97
Col-0	3	78	0	78
Col-0	4	157	0	157
Col-0	3	130	0	130
Col-0	4	156	0	156
Col-0	3	101	0	101
Col-0	4	117	0	117
Col-0	3	95	0	95
Col-0	4	142	0	142
Col-0	3	92	0	92
Col-0	4	127	0	127
Col-0	3	87	0	87
Col-0	4	145	0	145
Col-0	3	72	0	72
Col-0	4	101	0	101
cfs1-2 elch	3	147	0	147
cfs1-2 elch	4	138	0	138
cfs1-2 elch	3	56	0	56
cfs1-2 elch	4	82	0	82
cfs1-2 elch	3	7	0	7
cfs1-2 elch	4	185	1	186
cfs1-2 elch	3	79	0	79
cfs1-2 elch	4	100	2	102
cfs1-2 elch	3	88	1	89
cfs1-2 elch	4	131	2	133
cfs1-2 elch	3	80	0	80

Appendix H.1: Number of wild-type and *elch*-trichome –*continued from previous page*

Genotype	Leaf number	Wild-type trichome	*elch* trichome	All trichome
cfs1-2 elch	4	97	0	97
cfs1-2 elch	3	128	0	128
cfs1-2 elch	4	176	2	178
cfs1-2 elch	3	102	1	103
cfs1-2 elch	4	137	1	138
cfs1-2 elch	3	100	0	100
cfs1-2 elch	4	99	0	99
cfs1-2 elch	3	89	0	89
cfs1-2 elch	4	92	0	92
cfs1-2 elch	3	91	0	91
cfs1-2 elch	4	112	0	112
cfs1-2 elch	3	118	0	118
cfs1-2 elch	4	159	0	159
cfs1-2 elch	3	116	1	117
cfs1-2 elch	4	260	2	262
cfs1-2 elch	3	91	1	92
cfs1-2 elch	4	120	0	120
cfs1-2 elch	3	87	0	87
cfs1-2 elch	4	104	0	104
cfs1-2 elch	3	59	0	59
cfs1-2 elch	4	67	1	68
cfs1-2 elch	3	76	0	76
cfs1-2 elch	4	110	1	111
cfs1-2 elch	3	48	0	48
cfs1-2 elch	4	88	0	88
elch	3	135	2	137
elch	4	146	0	146
elch	3	130	3	133
elch	4	139	2	141
elch	3	117	2	119

Continued on next page

Appendix H.1: Number of wild-type and *elch*-trichome *–continued from previous page*

Genotype	Leaf number	Wild-type trichome	*elch* trichome	All trichome
elch	4	159	2	161
elch	3	101	1	102
elch	4	132	3	135
elch	3	151	7	158
elch	4	190	5	195
elch	3	176	1	177
elch	4	156	0	156
elch	3	134	3	137
elch	4	128	2	130
elch	3	109	0	109
elch	4	120	2	122
elch	3	165	1	166
elch	4	155	2	157
elch	3	181	2	183
elch	4	170	2	172
elch	3	99	0	99
elch	4	118	1	119
elch	3	113	0	113
elch	4	116	0	116
elch	3	108	1	109
elch	4	185	0	185
elch	3	86	0	86
elch	4	101	2	103
elch	3	87	1	88
elch	4	107	0	107
Ws-2	3	83	0	83
Ws-2	4	123	0	123
Ws-2	3	111	0	111
Ws-2	4	120	0	120
Ws-2	3	132	0	132

Continued on next page

Appendix H.1: Number of wild-type and *elch*-trichome –*continued from previous page*

Genotype	Leaf number	Wild-type trichome	*elch* trichome	All trichome
Ws-2	4	147	0	147
Ws-2	3	139	0	139
Ws-2	4	160	0	160
Ws-2	3	141	0	141
Ws-2	4	151	0	151
Ws-2	3	146	0	146
Ws-2	4	129	0	129
Ws-2	3	45	0	45
Ws-2	4	106	0	106

The number of wild-type and *elch* trichomes shown in Table H.1 is summarized in Table H.2

Appendix H.2: Summary of wild-type and *elch* trichome number in Col-0, *cfs1-2*, *cfs1-2 elch*, *elch* and Ws-2

Leaf number	Genotype	Wild-type	*elch*	All	%*elch*	N_{WT}	N_{elch}	N_{all}
3	Col-0	984	0	984	0.000	11	0	11
4	Col-0	1369	0	1369	0.000	11	0	11
	Σ	2353	0	2353	0.000	22	0	22
3	*cfs1-2*	1224	0	1224	0.000	12	0	12
4	*cfs1-2*	1409	0	1409	0.000	12	0	12
	Σ	2633	0	2633	0.000	24	0	24
3	*cfs1-2 elch*	1562	4	1566	0.255	18	4	18
4	*cfs1-2 elch*	2257	12	2269	0.529	18	8	18
	Σ	3819	16	3835	0.417	36	12	36
3	*elch*	1892	24	1916	1.253	15	11	15
4	*elch*	2122	23	2145	1.072	15	10	15
	Σ	4014	47	4061	1.157	30	21	30
3	Ws-2	797	0	797	0.000	7	0	7
4	Ws-2	936	0	936	0.000	7	0	7
	Σ	1733	0	1733	0.000	14	0	14

%*elch*: Percentage of *elch* trichome number to total trichome number
N_{WT}: Number of leaves showing wild-type trichome
N_{elch}: Number of leaves showing *elch* trichome
N_{all}: Number of all leaves counted

Fisher's exact test was performed using *fisher.test* function. The results were as follows:

For **leaf number 3**:

two-sided test:

p-value = 0.0009012

sample estimates: odds ratio 0.2039913

Test if *elch* trichome in *cfs1-2 elch* is less than in *elch*:

p-value = 0.0006384

sample estimates: odds ratio 0.2039913

For **leaf number 4**:

two-sided test:

p-value = 0.06037

sample estimates: odds ratio 0.4933059

Test if *elch* trichome in *cfs1-2 elch* is less than in *elch*:

p-value = 0.03176

sample estimates: odds ratio 0.4933059

For **both leaf number**:

two-sided test:

p-value = 3.666e-05

sample estimates: odds ratio 0.3212671

Test if *elch* trichome in *cfs1-2 elch* is less than in *elch*:

p-value = 2.428e-05

sample estimates: odds ratio 0.3212671

Pearson's χ^2 test of independence was performed using *prop.test* function without continuity correction.

For **leaf number 3**:

two-sided test:

χ^2 =10.742, df = 1, p-value = 0.001047

Test if *elch* trichome in *elch* is greater than in *elch*:

χ^2 =10.742, df = 1, p-value = 0.001047

For **leaf number 3**:

two-sided test:

χ^2 =10.742, df = 1, p-value = 0.001047

Test if *elch* trichome in *elch* is greater than in *elch*:

χ^2 =10.742, df = 1, p-value = 0.0005237

For **leaf number 4**:

two-sided test:

χ^2 = 4.1389, df = 1, p-value = 0.041911

Test if *elch* trichome in *elch* is greater than in *elch*:

χ^2 = 4.1389, df = 1, p-value = 0.02095

For **both leaf number**:

two-sided test:

χ^2 = 13.628, df = 1, p-value = 0.0002228

Test if *elch* trichome in *elch* is greater than in *elch*:

χ^2 = 13.628, df = 1, p-value = 0.0001114

Appendix I Accumulation of ubiquitinated proteins
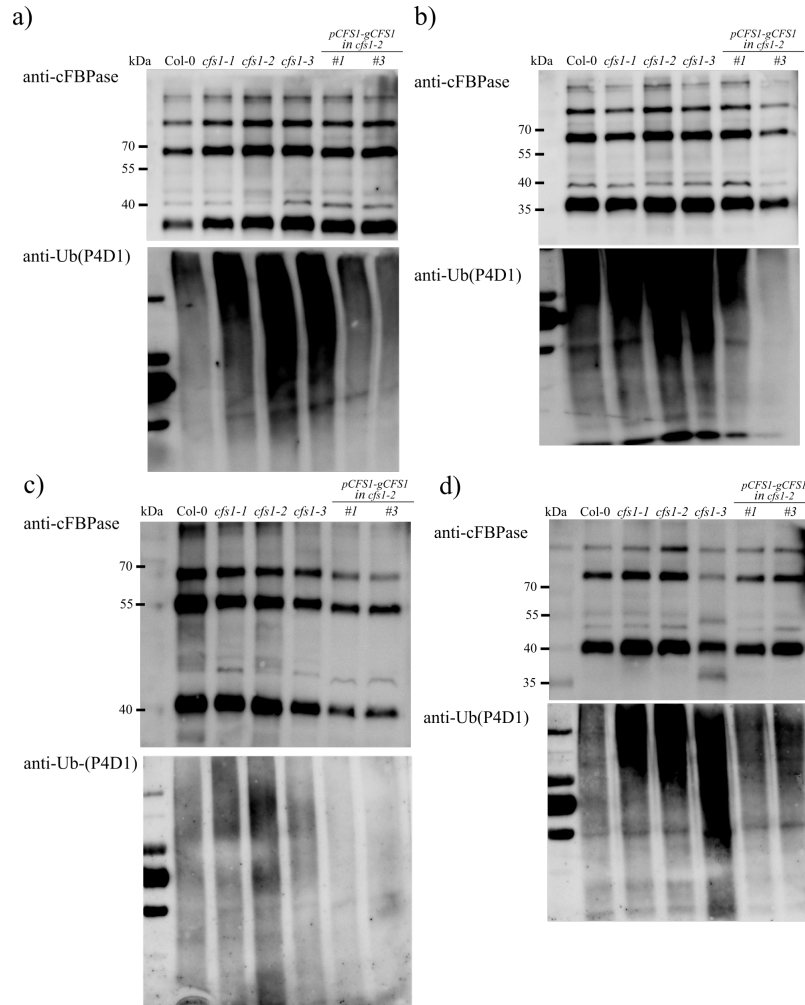
Figure I.1: **Accumulation of ubiquitinated proteins in mature plants** - Crude extract of *cfs1* leaves showing lesions and the other of the same age were probed with anti-Ub(P4D1) to detect accumulation of ubiquitinated proteins. Anti-cFBPase was used as a loading control. The experiments was repeated with four biological replicates (a-d)
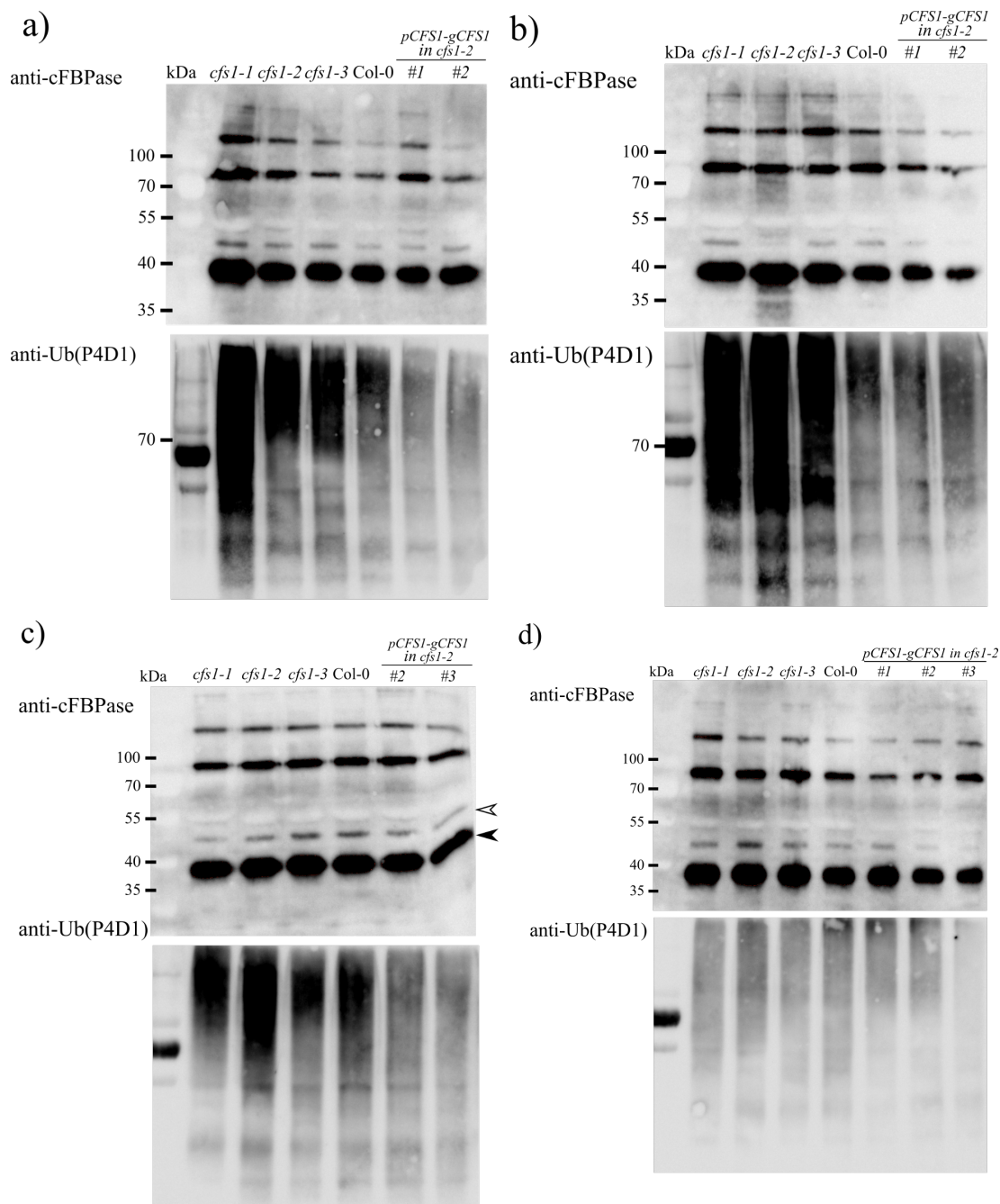
Figure I.2: **Accumulation of ubiquitinated proteins in growing plants** - Crude extract from growing plants without lesions was probed with anti-Ub(P4D1) to detect accumulation of ubiquitinated proteins. Anti-cFBPase was used as a loading control. The experiments was repeated with four biological replicates (a-d)
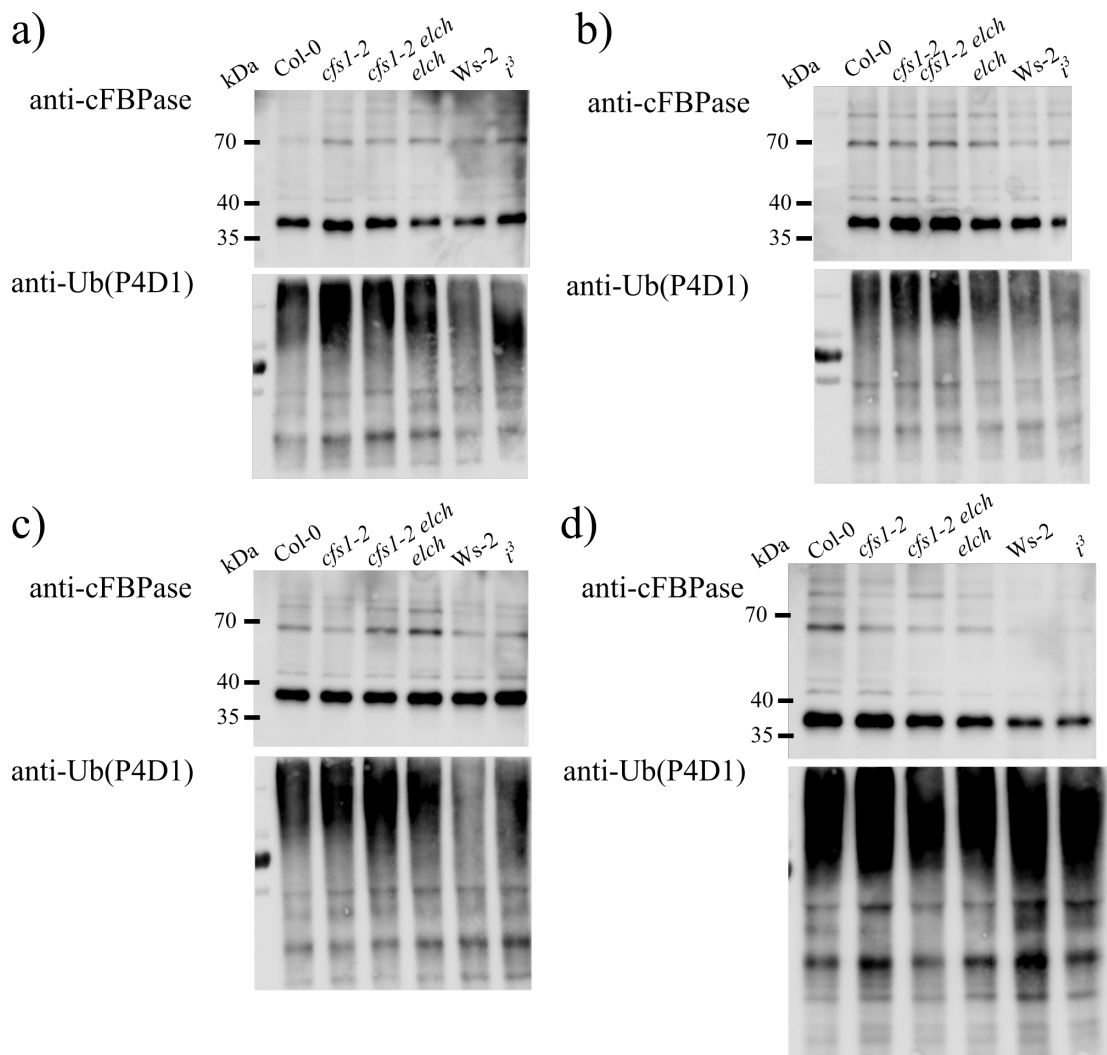
Figure I.3: **Accumulation of ubiquitinated proteins in *cfs1-2* and *cfs1-2 elch*** - Crude extract from *cfs1-2* and *cfs1-2 elch* leaves without lesions were probed with anti-Ub(P4D1) to detect accumulation of ubiquitinated proteins. Anti-cFBPase was used as a loading control. The experiments was repeated with four biological replicates (a-d)

Appendix J   Accumulation of autophagosomes

For the calculation purpose, samples probed with anti-cFBPase were used as a loading control and were relatively adjusted (Relative density) by comparing the difference of band intensity (Area) between samples loaded and blotted onto the same membrane. %Peak referred to the transformed value of Area as percentage obtained from Fiji/ImageJ. The extent of ATG8a and NBR1 accumulation (Adjusted density, AD) was calculated by dividing the %Peak adjusted with the relative density of the loading control of the corresponding samples. Relative ATG8a and NBR1 accmulation (Relative AD) was calculated by dividing AD with that of the corresponding ecotype background.

For mature plants, samples were grown in soil for 24-30 days (approximately 8-leaf stage), and leaves showing lesion were collected. The experiments were repeated with four biological replicates (Figures J.1 to J.4).

For growing plants, samples were grown in soil for 14-16 days and collected at 4-leaf stage. The experiment was repeated with four biological replicates (Figures J.5 to J.8).

Samples used for young seedlings were grown in half-strength MS medium plates for 7-10 days. This experiment was repeated with three biological replicates (Figures J.9 to J.11).

For *escrt* mutant and *cfs1-2 elch* double mutants, plants were grown on soil for approximately 14 days and collected at 4-leaf stage. The extent of accumulation in *elch* was in relative to Ws-2 and in i^3 relative to *elch*. This experiment was repeated with four biological replicates (Figures J.12 to J.15).

For *cfs1-2* mutant and *cfs1-2 eds1-2* double mutants, plants were grown on soil and collected at 4-leaf stage. This experiment was repeated with four biological replicates (Figures J.16 to J.19).

a)

Sample	Area	%Peak	Relative density
Col-0	31707.5	10.386	0.53
cfs1-1	47476	15.551	0.79
cfs1-2	55577.5	18.205	0.93
cfs1-3	59873.8	19.612	1.00
rescue#1	55300.1	18.114	0.92
rescue#3	55359.1	18.133	0.92

b)

Sample	Area	%Peak	AD	Relative AD
Col-0	8320.39	2.859	5.40	1
cfs1-1	95322.1	32.749	41.30	7.65
cfs1-2	87925.7	30.208	32.54	6.03
cfs1-3	83687.4	28.752	28.75	5.33
rescue#1	8180.73	2.811	3.04	0.56
rescue#3	7631.22	2.622	2.84	0.53

c)

Sample	Area	%Peak	AD	Relative AD
Col-0	3205.66	3.691	6.97	1
cfs1-1	53112.4	61.146	77.11	11.06
cfs1-2	3394.56	3.908	4.21	0.60
cfs1-3	16803	19.345	19.35	2.78
rescue#1	7292.34	8.395	9.09	1.30
rescue#3	3053.27	3.515	3.80	0.55

Figure J.1: **Accumulation of autophagosomes in mature plants from leaves showing lesions: the first biological replicates** - Crude extract was probed with **a)** anti-cFBPase, **b)** anti-ATG8a and **c)** anti-NBR1. Arrowhead denotes expected protein size. Filled arrowhead indicates bands used for intensity calculation.

a)

Sample	Area	%Peak	Relative density
Col-0	60725.3	17.465	0.90
cfs1-1	53435	15.368	0.80
cfs1-2	68017	19.562	1.01
cfs1-3	67137	19.309	1.00
rescue#1	56185	16.159	0.84
rescue#3	42204.2	12.138	0.63

b)

Sample	Area	%Peak	AD	Relative AD
Col-0	3049.76	1.986	2.20	1
cfs1-1	44082.4	28.7	36.06	16.42
cfs1-2	42200.6	27.475	27.12	12.35
cfs1-3	56762.8	36.956	36.96	16.83
rescue#1	6715.16	4.372	5.22	2.38
rescue#3	785.092	0.511	0.81	0.37

c)

Sample	Area	%Peak	AD	Relative AD
Col-0	43473.7	18.572	20.53	1
cfs1-1	64875.2	27.714	34.82	1.70
cfs1-2	48131.9	20.561	20.30	0.99
cfs1-3	49332.8	21.074	21.07	1.03
rescue#1	21212.1	9.062	10.83	0.53
rescue#3	7062.61	3.017	4.80	0.23

Figure J.2: **Accumulation of autophagosomes in mature plants from leaves showing lesions: the second biological replicates** - Crude extract was probed with **a)** anti-cFBPase, **b)** anti-ATG8a and **c)** anti-NBR1. Arrowhead denotes expected protein size. Filled arrowhead indicates bands used for intensity calculation.

a)

Sample	Area	%Peak	Relative density
Col-0	69901.6	22.027	1.00
cfs1-1	65444.4	20.623	0.94
cfs1-2	66226.7	20.869	0.95
cfs1-3	51349.7	16.181	0.73
rescue#1	30323.6	9.555	0.43
rescue#3	34096.5	10.744	0.49

b)

Sample	Area	%Peak	AD	Relative AD
Col-0	4245.76	2.202	2.20	1
cfs1-1	54038	28.025	29.93	13.59
cfs1-2	66583.5	34.532	36.45	16.55
cfs1-3	63775.2	33.075	45.02	20.45
rescue#1	2352.06	1.22	2.81	1.28
rescue#3	1822.65	0.945	1.94	0.88

c)

Sample	Area	%Peak	AD	Relative AD
Col-0	4560.1	1.63	1.63	1
cfs1-1	60217.3	21.522	22.99	14.10
cfs1-2	10978.1	3.924	4.14	2.54
cfs1-3	75534	26.997	36.75	22.54
rescue#1	33698.1	12.044	27.76	17.03
rescue#3	19268.4	6.887	14.12	8.66

Figure J.3: **Accumulation of autophagosomes in mature plants from leaves showing lesions: the third biological replicates** - Crude extract was probed with **a)** anti-cFBPase, **b)** anti-ATG8a and **c)** anti-NBR1. Arrowhead denotes expected protein size. Filled arrowhead indicates bands used for intensity calculation.

a)

Sample	Area	%Peak	Relative density
Col-0	66439.4	16.331	0.80
cfs1-1	83405.1	20.501	1.00
cfs1-2	76479	18.799	0.92
cfs1-3	51167.8	12.577	0.61
rescue#1	60076.1	14.767	0.72
rescue#3	69266.8	17.026	0.83

b)

Sample	Area	%Peak	AD	Relative AD
Col-0	1941.69	1.14	1.43	1
cfs1-1	44107.7	25.887	25.89	18.09
cfs1-2	53028.9	31.122	33.94	23.72
cfs1-3	67635.1	39.695	64.70	45.21
rescue#1	1703.41	1	1.39	0.97
rescue#3	1971.55	1.157	1.39	0.97

c)

Sample	Area	%Peak	AD	Relative AD
Col-0	17407.7	7.703	9.67	1
cfs1-1	55667.9	24.635	24.64	2.55
cfs1-2	64174.9	28.399	30.97	3.20
cfs1-3	768.506	0.34	0.55	0.06
rescue#1	47888.3	21.192	29.42	3.04
rescue#3	40065.9	17.73	21.35	2.21

Figure J.4: **Accumulation of autophagosomes in mature plants from leaves showing lesions: the fourth biological replicates** - Crude extract was probed with **a)** anti-cFBPase, **b)** anti-ATG8a and **c)** anti-NBR1. Arrowhead denotes expected protein size. Filled arrowhead indicates bands used for intensity calculation.
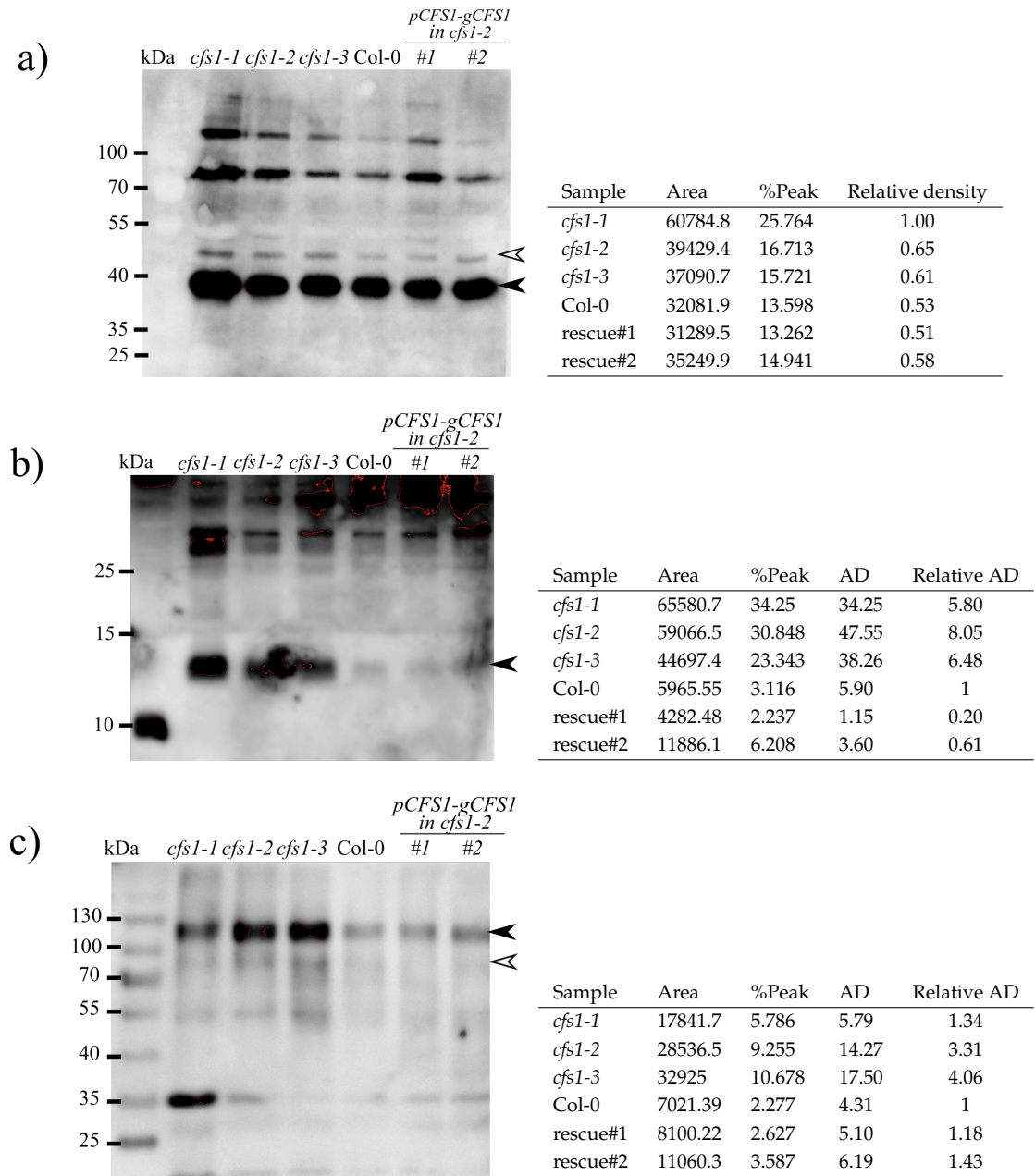
Figure J.5: **Accumulation of autophagosomes in growing plants: the first biological replicates** - Crude extract from growing plant was probed with **a)** anti-cFBPase, **b)** anti-ATG8a and **c)** anti-NBR1. Arrowhead denotes expected protein size. Filled arrowhead indicates bands used for intensity calculation.

a)

Sample	Area	%Peak	Relative density
cfs1-1	38642	23.436	1.00
cfs1-2	39882.9	24.188	1.03
cfs1-3	33551.6	20.349	0.87
Col-0	23708.8	14.379	0.61
rescue#1	17879.6	10.844	0.46
rescue#3	11219.5	6.804	0.29

b)

Sample	Area	%Peak	AD	Relative AD
cfs1-1	41311.2	27.024	27.02	3.43
cfs1-2	54276.9	35.506	34.40	4.37
cfs1-3	44282.7	28.968	33.36	4.23
Col-0	7392.26	4.836	7.88	1
rescue#1	1783.38	1.167	2.52	0.32
rescue#3	3822.65	2.501	8.61	1.09

c)

Sample	Area	%Peak	AD	Relative AD
cfs1-1	31890.6	34.531	34.53	2.52
cfs1-2	3011.69	3.261	3.16	0.17
cfs1-3	22899.6	24.795	28.56	1.96
Col-0	7650.92	8.284	13.50	1
rescue#1	13789.6	14.931	32.27	2.34
rescue#3	13111.5	14.197	48.90	3.33

Figure J.6: **Accumulation of autophagosomes in growing plants: the second biological replicates** - Crude extract from growing plants was probed with **a)** anti-cFBPase, **b)** anti-ATG8a and **c)** anti-NBR1. Arrowhead denotes expected protein size. Filled arrowhead indicates bands used for intensity calculation.
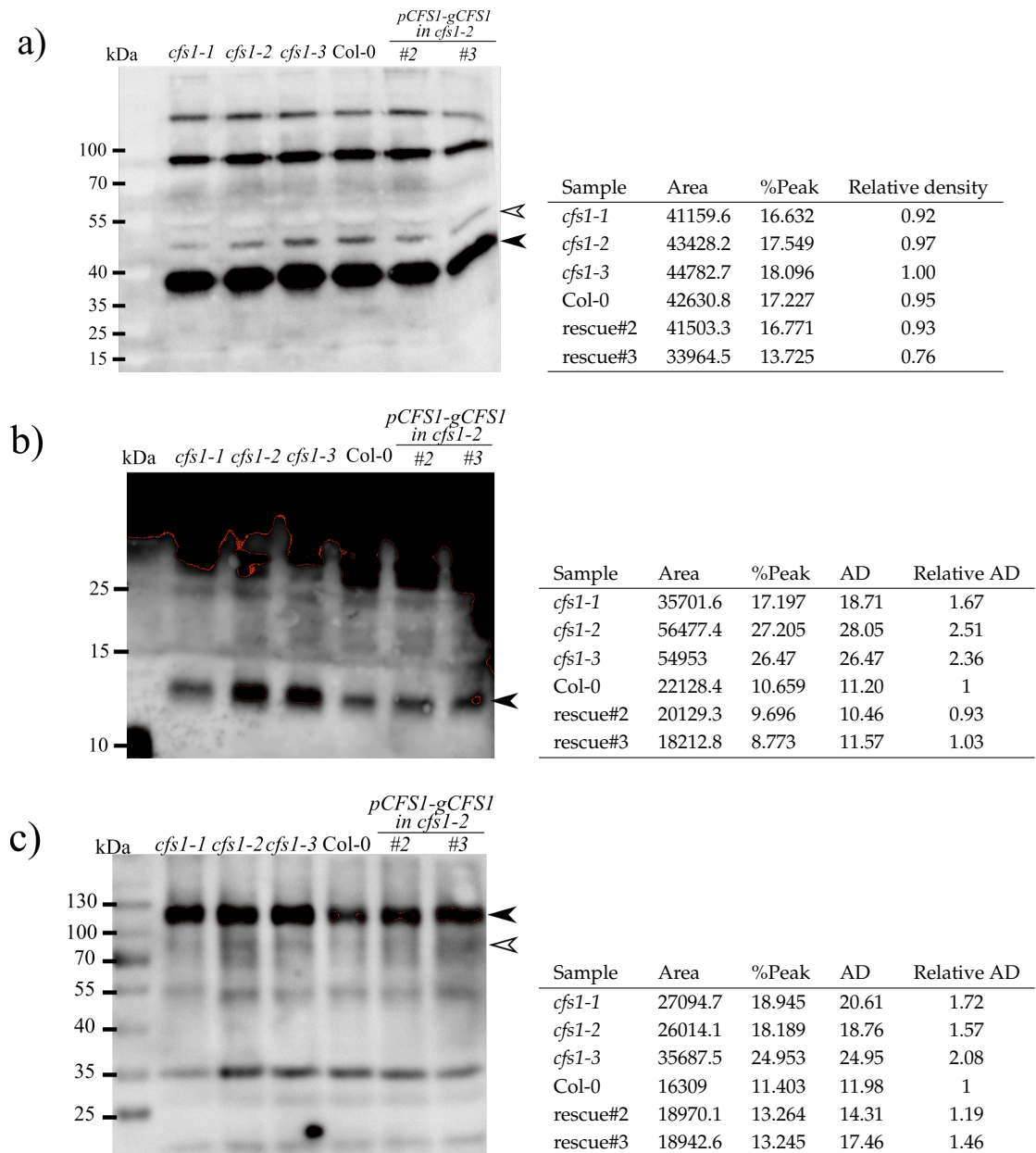
Figure J.7: **Accumulation of autophagosomes in growing plants: the third biological replicates** - Crude extract from growing plants probed with **a)** anti-cFBPase, **b)** anti-ATG8a and **c)** anti-NBR1. Arrowhead denotes expected protein size. Filled arrowhead indicates bands used for intensity calculation.

a)

Sample	Area	%Peak	Relative density
cfs1-1	41159.6	16.632	0.92
cfs1-2	43428.2	17.549	0.97
cfs1-3	44782.7	18.096	1.00
Col-0	42630.8	17.227	0.95
rescue#2	41503.3	16.771	0.93
rescue#3	33964.5	13.725	0.76

b)

Sample	Area	%Peak	AD	Relative AD
cfs1-1	35701.6	17.197	18.71	1.67
cfs1-2	56477.4	27.205	28.05	2.51
cfs1-3	54953	26.47	26.47	2.36
Col-0	22128.4	10.659	11.20	1
rescue#2	20129.3	9.696	10.46	0.93
rescue#3	18212.8	8.773	11.57	1.03

c)

Sample	Area	%Peak	AD	Relative AD
cfs1-1	27094.7	18.945	20.61	1.72
cfs1-2	26014.1	18.189	18.76	1.57
cfs1-3	35687.5	24.953	24.95	2.08
Col-0	16309	11.403	11.98	1
rescue#2	18970.1	13.264	14.31	1.19
rescue#3	18942.6	13.245	17.46	1.46

Sample	Area	%Peak	Relative density
cfs1-1	52470.9	17.616	1.00
cfs1-2	48479.3	16.276	0.92
cfs1-3	49231.9	16.528	0.94
Col-0	41166.4	13.821	0.78
rescue#1	43165.4	14.492	0.82
rescue#2	34903.4	11.718	0.67
rescue#3	28444.5	9.55	0.54

Sample	Area	%Peak	AD	Relative AD
cfs1-1	36805.5	23.425	23.43	2.97
cfs1-2	54877.2	34.926	37.80	4.79
cfs1-3	31469.5	20.029	21.35	2.70
Col-0	9737.6	6.197	7.90	1
rescue#1	5914	3.764	4.58	0.58
rescue#2	9915.73	6.311	9.49	1.20
rescue#3	8404.08	5.349	9.87	1.25

Sample	Area	%Peak	AD	Relative AD
cfs1-1	32892.8	25.398	25.40	4.16
cfs1-2	30952.1	23.9	25.87	4.24
cfs1-3	28668.3	22.136	23.59	3.87
Col-0	6202.59	4.789	6.10	1
rescue#1	9087.95	7.017	8.53	1.40
rescue#2	9680.67	7.475	11.24	1.84
rescue#3	12023.3	9.284	17.13	2.81

Figure J.8: **Accumulation of autophagosomes in growing plants: the fourth biological replicates** - Crude extract from growing plants probed with **a)** anti-cFBPase, **b)** anti-ATG8a and **c)** anti-NBR1. Arrowhead denotes expected protein size. Filled arrowhead indicates bands used for intensity calculation.

a)

Sample	Area	%Peak	Relative density
cfs1-1	13127.72	11.20	0.61
cfs1-2	21784.79	18.58	1.02
cfs1-3	21387.31	18.24	1.00
Col-0	12812.17	10.93	0.60
rescue#1	21427.89	18.28	1.00
rescue#2	12452.65	10.62	0.58
rescue#3	14258.84	12.16	1.15

b)

Sample	Area	%Peak	AD	Relative AD
cfs1-1	7500.187	26.335	42.9061	13.74
cfs1-2	6768.338	23.765	23.3314	7.33
cfs1-3	9821.602	34.486	34.486	10.83
Col-0	543.263	1.908	3.185122	1
rescue#1	1449.941	5.091	5.100489	1.60
rescue#2	734.263	2.578	1.500924	0.47
rescue#3	1662.406	5.837	5.097355	1.60

c)

Sample	Area	%Peak	AD	Relative AD
cfs1-1	16922.82	27.233	44.36916	2.03
cfs1-2	15113.24	24.321	23.87725	1.09
cfs1-3	10119.17	16.284	16.284	0.74
Col-0	8137.631	13.095	21.86015	1
rescue#1	3956.004	6.366	6.354156	0.29
rescue#2	5180.66	8.337	14.3197	0.66
rescue#3	2712.154	4.364	3.811009	0.17

Figure J.9: **Accumulation of autophagosomes in young seedlings: the first biological replicates** - Crude extract from young seedlings probed with **a)** anti-cFBPase, **b)** anti-ATG8a and **c)** anti-NBR1. Arrowhead denotes expected protein size. Filled arrowhead indicates bands used for intensity calculation.

a)

Sample	Area	%Peak	Relative density
cfs1-1	33145.82	20.45	1.00
cfs1-2	26673.69	16.46	0.80
cfs1-3	21908.09	13.52	0.66
Col-0	32174.52	19.85	0.97
rescue#1	25141.57	15.51	0.76
rescue#2	12736.43	7.86	0.38
rescue#4	10299.38	6.36	0.31

b)

Sample	Area	%Peak	AD	Relative AD
cfs1-1	19206.37	21.44	21.44	1.39
cfs1-2	14581.16	16.28	20.23	1.32
cfs1-3	11296.36	12.61	19.08	1.24
Col-0	13368.38	14.92	15.37	1
rescue#1	6150.296	6.87	9.05	0.59
rescue#2	15654.3	17.48	45.48	2.96
rescue#4	9321.146	10.41	33.49	2.18

c)

Sample	Area	%Peak	AD	Relative AD
cfs1-1	15881.53	23.47	23.47	2.86
cfs1-2	16581.85	24.51	30.45	3.71
cfs1-3	16459.78	24.33	36.80	4.49
Col-0	5385.024	7.96	8.20	1
rescue#1	7111.56	10.51	13.86	1.69
rescue#2	2492.104	3.68	9.58	1.17
rescue#4	3752.347	5.55	17.85	2.18

Figure J.10: **Accumulation of autophagosomes in young seedlings: the second biological replicates** - Crude extract from young seedlings probed with **a)** anti-cFBPase, **b)** anti-ATG8a and **c)** anti-NBR1. Arrowhead denotes expected protein size. Filled arrowhead indicates bands used for intensity calculation.

a)

Sample	Area	%Peak	Relative density
cfs1-1	9864.359	9.41	0.35
cfs1-2	17360.67	16.57	0.62
cfs1-3	27806.33	26.54	1.00
Col-0	25503.55	24.34	0.92
rescue#1	19911.89	19.00	0.72
rescue#2	4337.782	4.14	0.16

b)

Sample	Area	%Peak	AD	Relative AD
cfs1-1	3839.033	7.58	21.37	0.96
cfs1-2	10305.97	20.36	32.60	1.46
cfs1-3	19178.3	37.88	37.88	1.69
Col-0	10389.09	20.52	22.37	1
rescue#1	4269.033	8.43	11.77	0.53
rescue#2	2650.648	5.24	33.56	1.50

c)

Sample	Area	%Peak	AD	Relative AD
cfs1-1	9137.439	18.58	52.39	6.07
cfs1-2	13881.8	28.23	45.22	5.24
cfs1-3	18953.05	38.55	38.55	4.47
Col-0	3891.368	7.91	8.63	1
rescue#1	2173.225	4.42	6.17	0.72
rescue#2	1131.368	2.30	14.75	1.71

Figure J.11: **Accumulation of autophagosomes in young seedlings: the third biological replicates** - Crude extract from young seedlings probed with **a)** anti-cFBPase, **b)** anti-ATG8a and **c)** anti-NBR1. Arrowhead denotes expected protein size. Filled arrowhead indicates bands used for intensity calculation.

a)

Sample	Area	%Peak	Relative density
Col-0	54485.1	18.031	0.93
cfs1-2	58150.5	19.244	1.00
cfs1-2 elch	58383.8	19.321	1.00
elch	44506.8	14.728	0.82
Ws-2	42807.4	14.166	0.73
i³	43848.3	14.511	0.75

b)

Sample	Area	%Peak	AD	Relative AD
Col-0	10660.6	5.553	5.95	1
cfs1-2	52170.8	27.178	27.29	4.59
cfs1-2 elch	61420.7	31.996	32.00	5.38
elch	41702.9	21.724	26.60	4.27
Ws-2	16297.1	8.49	6.22	1
i³	9710.87	5.059	3.80	0.14

c)

Sample	Area	%Peak	AD	Relative AD
Col-0	23859.1	16.559	17.74	1
cfs1-2	40717	28.26	28.37	1.60
cfs1-2 elch	27987.5	19.425	19.43	1.09
elch	13761.8	9.551	11.69	2.40
Ws-2	5138.83	3.567	4.87	1
i³	32617	22.638	30.14	2.58

Figure J.12: **Accumulation of autophagosomes in *elch* and *cfs1-2 elch* mutants: the first biological replicates** - Crude extract was probed with **a)** anti-cFBPase, **b)** anti-ATG8a and **c)** anti-NBR1. Arrowhead denotes expected protein size. Filled arrowhead indicates bands used for intensity calculation.
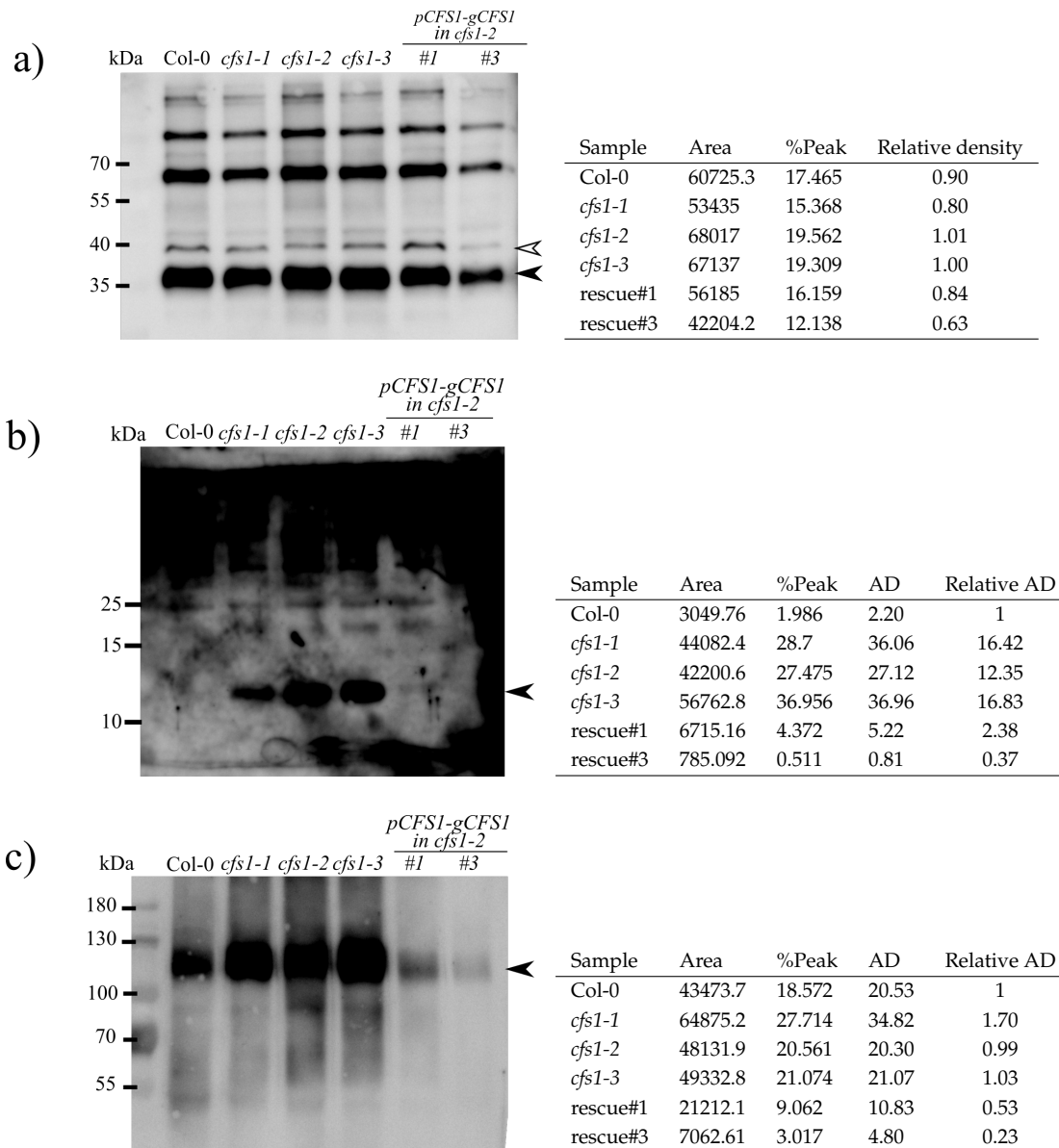
a)

Sample	Area	%Peak	Relative density
Col-0	56883.1	16.471	0.91
cfs1-2	67560.8	19.562	1.08
cfs1-2 elch	61643.3	17.849	0.99
elch	62491.9	18.095	1.00
Ws-2	59766	17.305	0.96
i³	37017.1	10.718	0.59

b)

Sample	Area	%Peak	AD	Relative AD
Col-0	17873.9	9.165	10.07	1
cfs1-2	65863.3	33.774	31.24	3.10
cfs1-2 elch	51250.8	26.281	26.64	2.65
elch	22912.5	11.749	11.75	0.95
Ws-2	23041.4	11.815	12.35	1
i³	14072	7.216	12.18	1.04

c)

Sample	Area	%Peak	AD	Relative AD
Col-0	21396.1	9.717	10.68	1
cfs1-2	55688.9	25.291	23.39	2.19
cfs1-2 elch	53255.6	24.186	24.52	2.30
elch	29830.6	13.548	13.55	0.88
Ws-2	32357	14.695	15.37	1
i³	27664.2	12.564	21.21	1.57

Figure J.13: **Accumulation of autophagosomes in *elch* and *cfs1-2 elch*: the second biological replicates** - Crude extract was probed with **a)** anti-cFBPase, **b)** anti-ATG8a and **c)** anti-NBR1. Arrowhead denotes expected protein size. Filled arrowhead indicates bands used for intensity calculation.
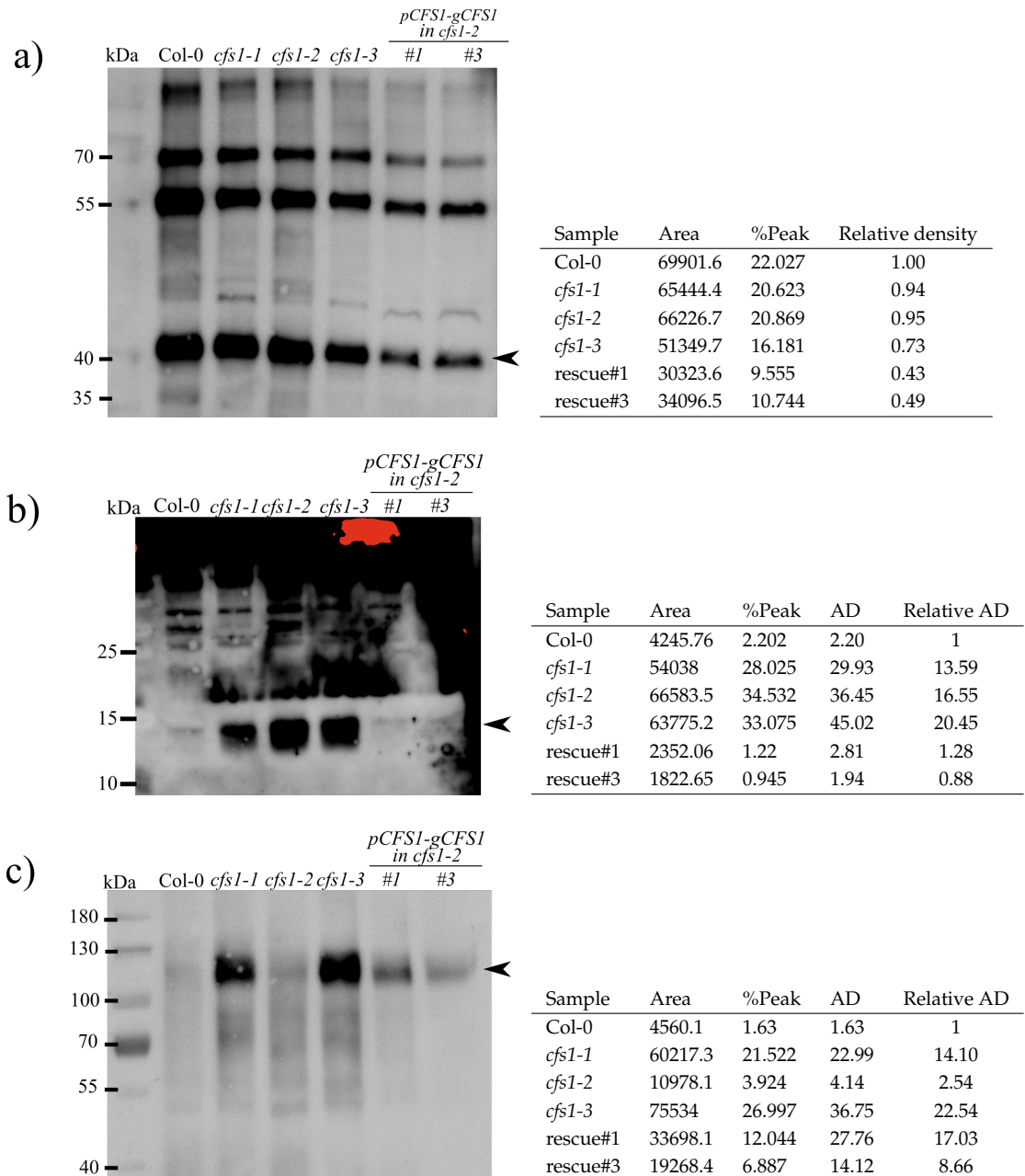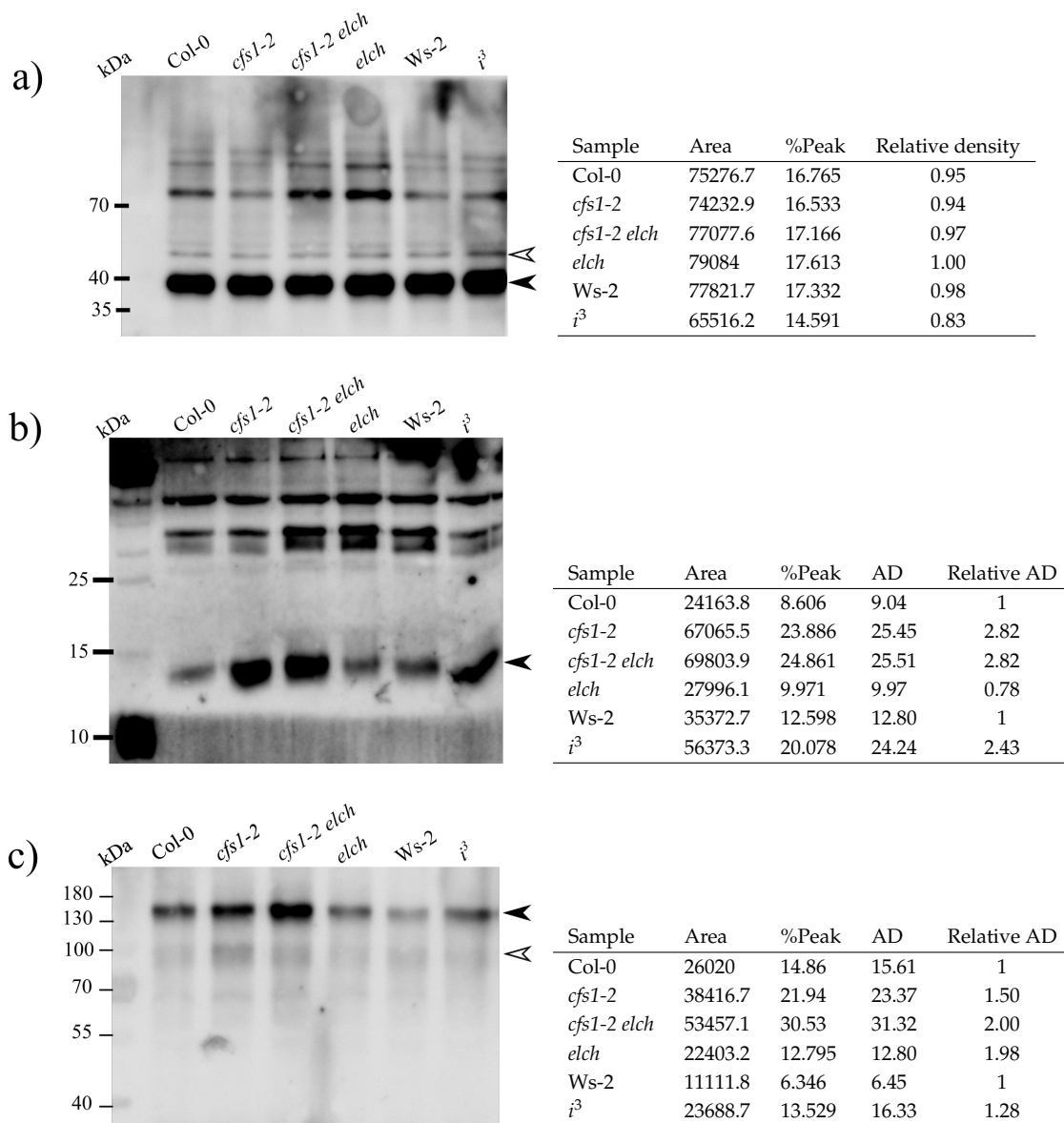
Figure J.14: **Accumulation of autophagosomes in** *elch* **and** *cfs1-2 elch*: **the third biological replicates** - Crude extract was probed with **a)** anti-cFBPase, **b)** anti-ATG8a and **c)** anti-NBR1. Arrowhead denotes expected protein size. Filled arrowhead indicates bands used for intensity calculation.
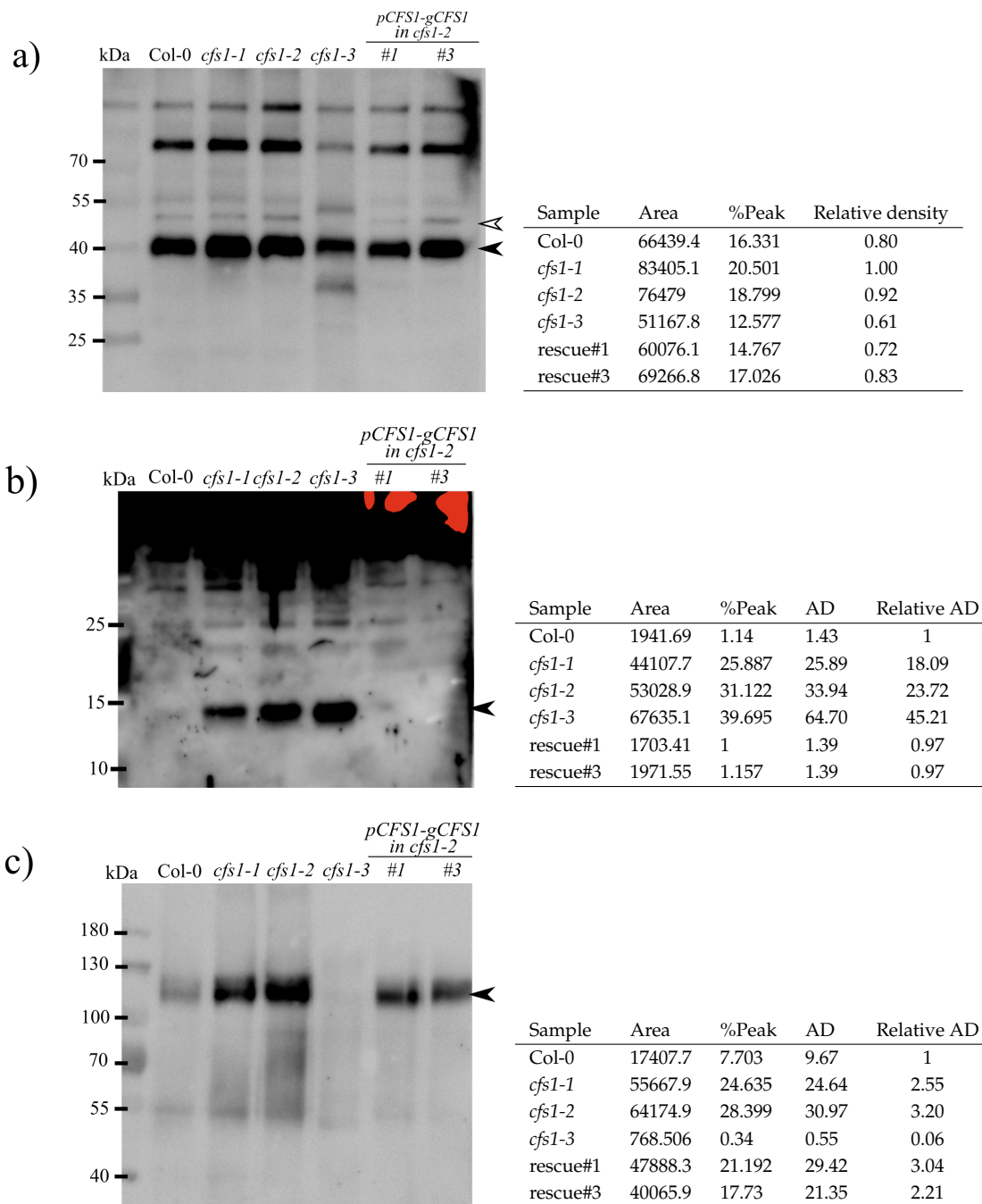
a)

Sample	Area	%Peak	Relative density
Col-0	71997.8	19.981	1.00
cfs1-2	72226.5	20.044	1.00
cfs1-2 elch	65826.6	18.268	0.91
elch	59872.3	16.615	0.83
Ws-2	50339.9	13.97	0.70
i³	40077	11.122	0.56

b)

Sample	Area	%Peak	AD	Relative AD
Col-0	43925.7	14.239	14.24	1
cfs1-2	92224.3	29.896	29.80	2.09
cfs1-2 elch	79857.6	25.887	28.31	1.99
elch	41337.8	13.4	16.11	1.10
Ws-2	31503.1	10.212	14.61	1
i³	19637.5	6.366	11.44	0.71

c)

Sample	Area	%Peak	AD	Relative AD
Col-0	21808.3	14.143	14.14	1
cfs1-2	28673.9	18.595	18.54	1.31
cfs1-2 elch	28361.7	18.392	20.12	1.42
elch	31468	20.407	24.54	6.29
Ws-2	4207.79	2.729	3.90	1
i³	39683.4	25.735	46.23	1.88

Figure J.15: **Accumulation of autophagosomes in *elch* and *cfs1-2 elch*: the fourth biological replicates** - Crude extract was probed with **a)** anti-cFBPase, **b)** anti-ATG8a and **c)** anti-NBR1. Arrowhead denotes expected protein size. Filled arrowhead indicates bands used for intensity calculation.
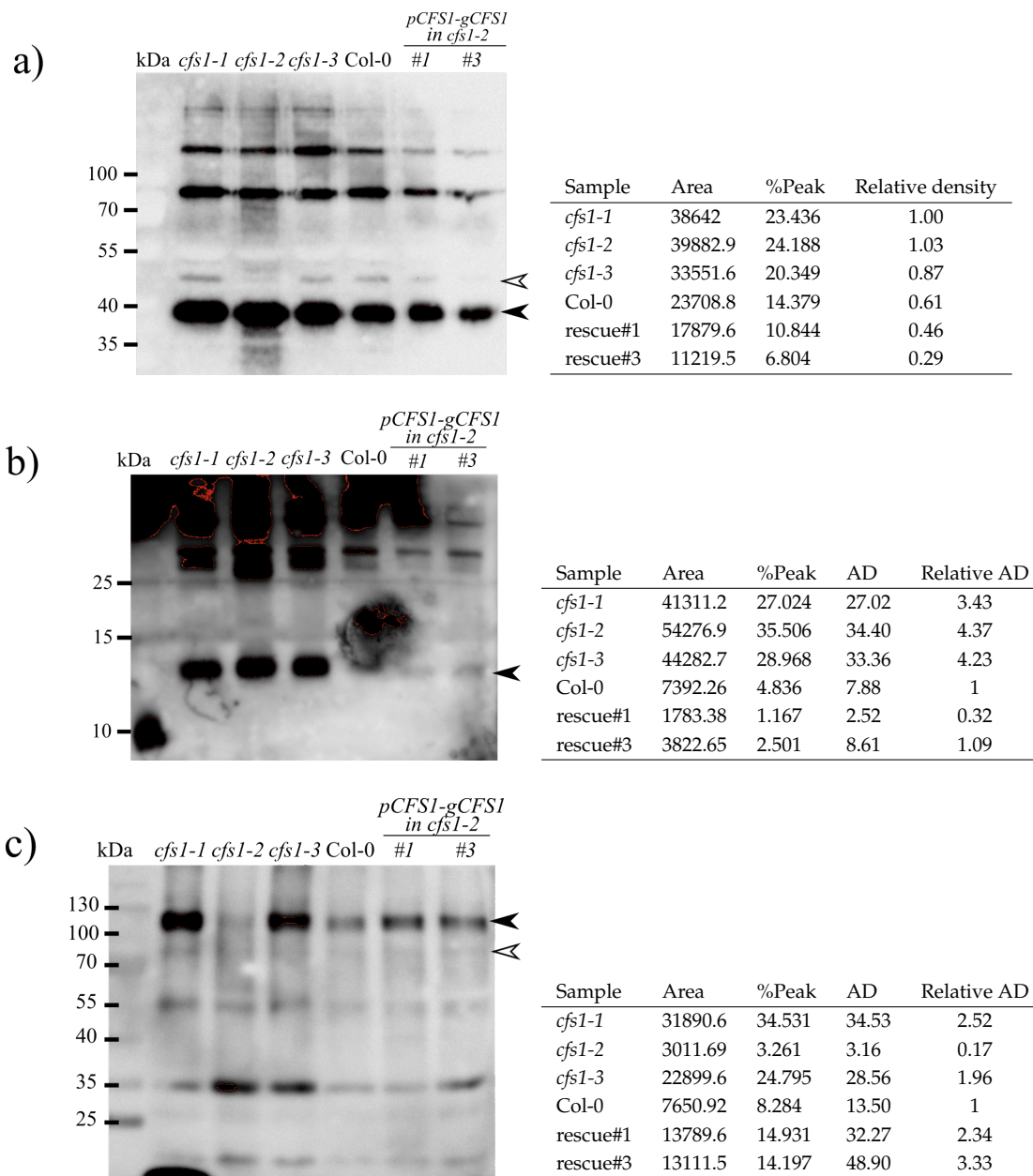
a)

| Sample	Area	%Peak	Relative density
Col-0	43830.6	25.668	1.00
eds1-2	41433.2	24.264	0.95
cfs1-2	43669.1	25.573	1.00
cfs1-2 eds1-2	41829.5	24.496	0.95

b)

Sample	Area	%Peak	AD	Relative AD
Col-0	22310.2	8.614	8.58	1
eds1-2	62802.8	24.249	25.56	2.98
cfs1-2	83819	32.364	32.36	3.77
cfs1-2 eds1-2	90055.7	34.772	36.44	4.25

c)

Sample	Area	%Peak	AD	Relative AD
Col-0	36141.2	16.662	16.60	1
eds1-2	30720	14.162	14.93	0.90
cfs1-2	68056.9	31.375	31.38	1.89
cfs1-2 eds1-2	81995.4	37.801	39.61	2.39

Figure J.16: **Accumulation of autophagosomes in *cfs1-2* and *cfs1-2 eds1-2* mutants: the first biological replicates** - Crude extract was probed with **a)** anti-cFBPase, **b)** anti-ATG8a and **c)** anti-NBR1. Arrowhead denotes expected protein size. Filled arrowhead indicates bands used for intensity calculation.
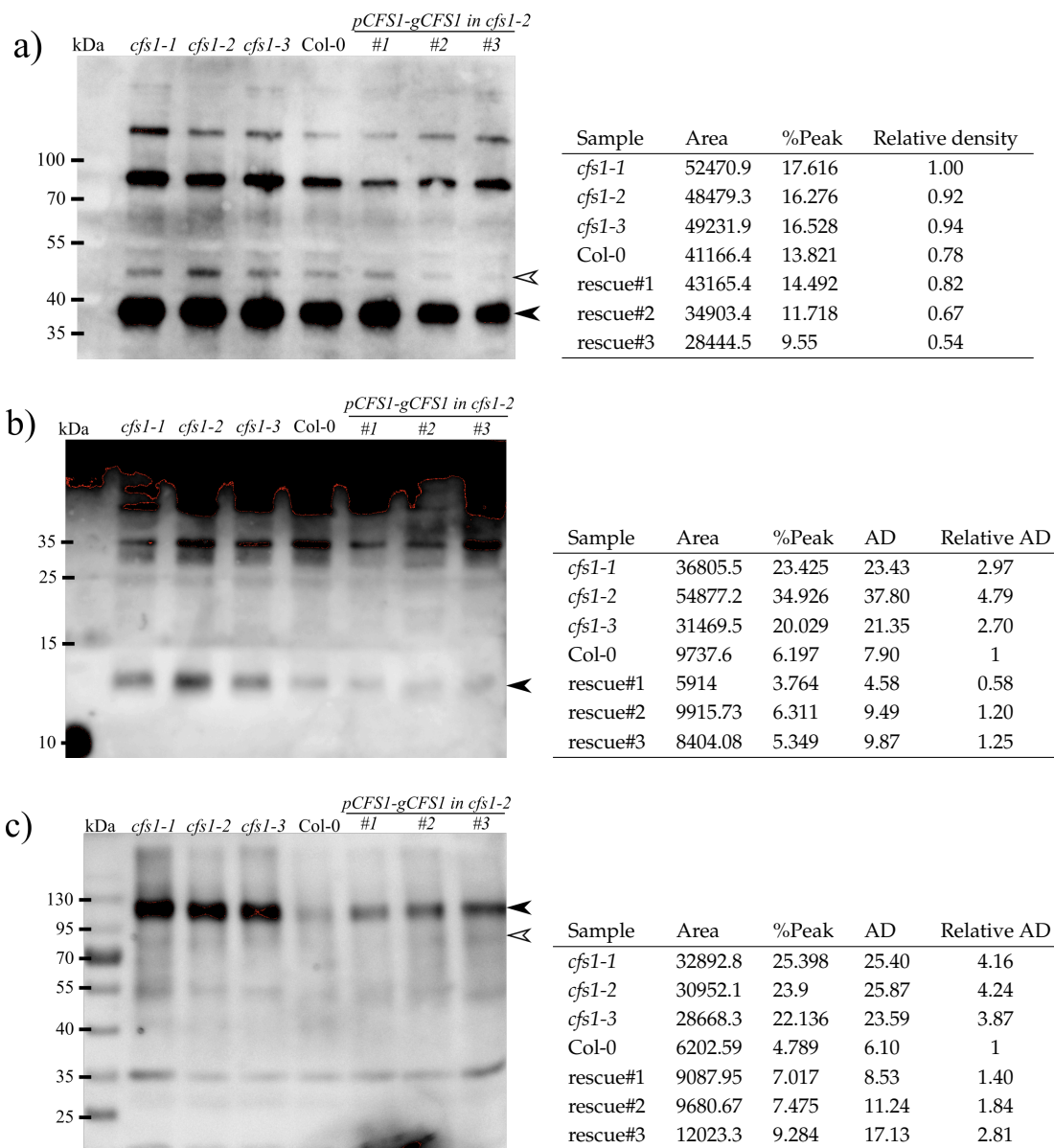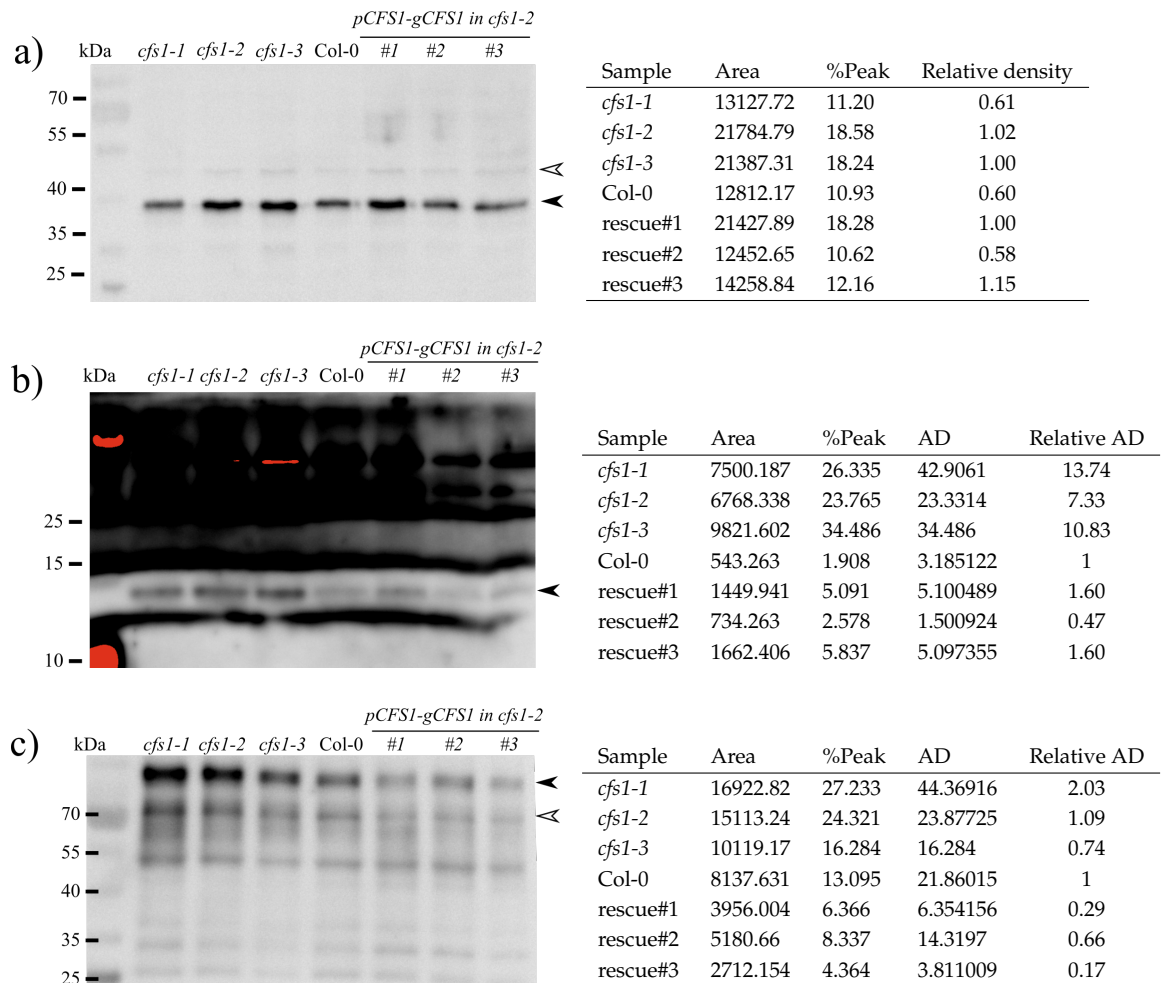
a)

Sample	Area	%Peak	Relative density
Col-0	51511	24.895	0.94
eds1-2	55085.4	26.622	1.00
cfs1-2	52153.1	25.205	0.95
cfs1-2 eds1-2	48165	23.278	0.87

b)

Sample	Area	%Peak	AD	Relative AD
Col-0	36027.9	15.183	16.24	1
eds1-2	45272.6	19.08	19.08	1.18
cfs1-2	76582.3	32.275	34.09	2.10
cfs1-2 eds1-2	79400.5	33.462	38.27	2.36

c)

Sample	Area	%Peak	AD	Relative AD
Col-0	28505.8	16.136	17.26	1
eds1-2	24833.6	14.058	14.06	0.81
cfs1-2	59322.4	33.581	35.47	2.06
cfs1-2 eds1-2	63993.3	36.225	41.43	2.40

Figure J.17: **Accumulation of autophagosomes in *cfs1-2* and *cfs1-2 eds1-2*: the second biological replicates** - Crude extract was probed with **a)** anti-cFBPase, **b)** anti-ATG8a and **c)** anti-NBR1. Arrowhead denotes expected protein size. Filled arrowhead indicates bands used for intensity calculation.
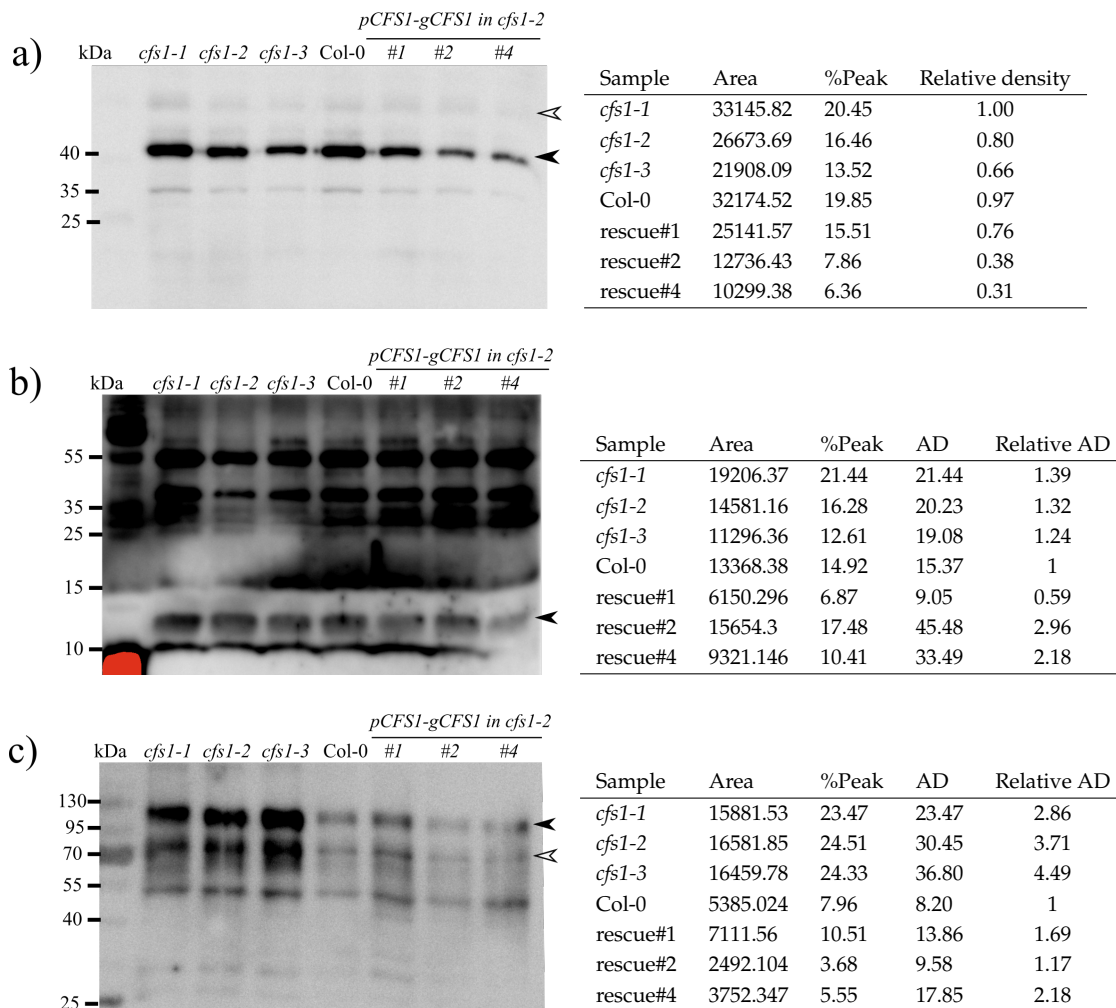
a)

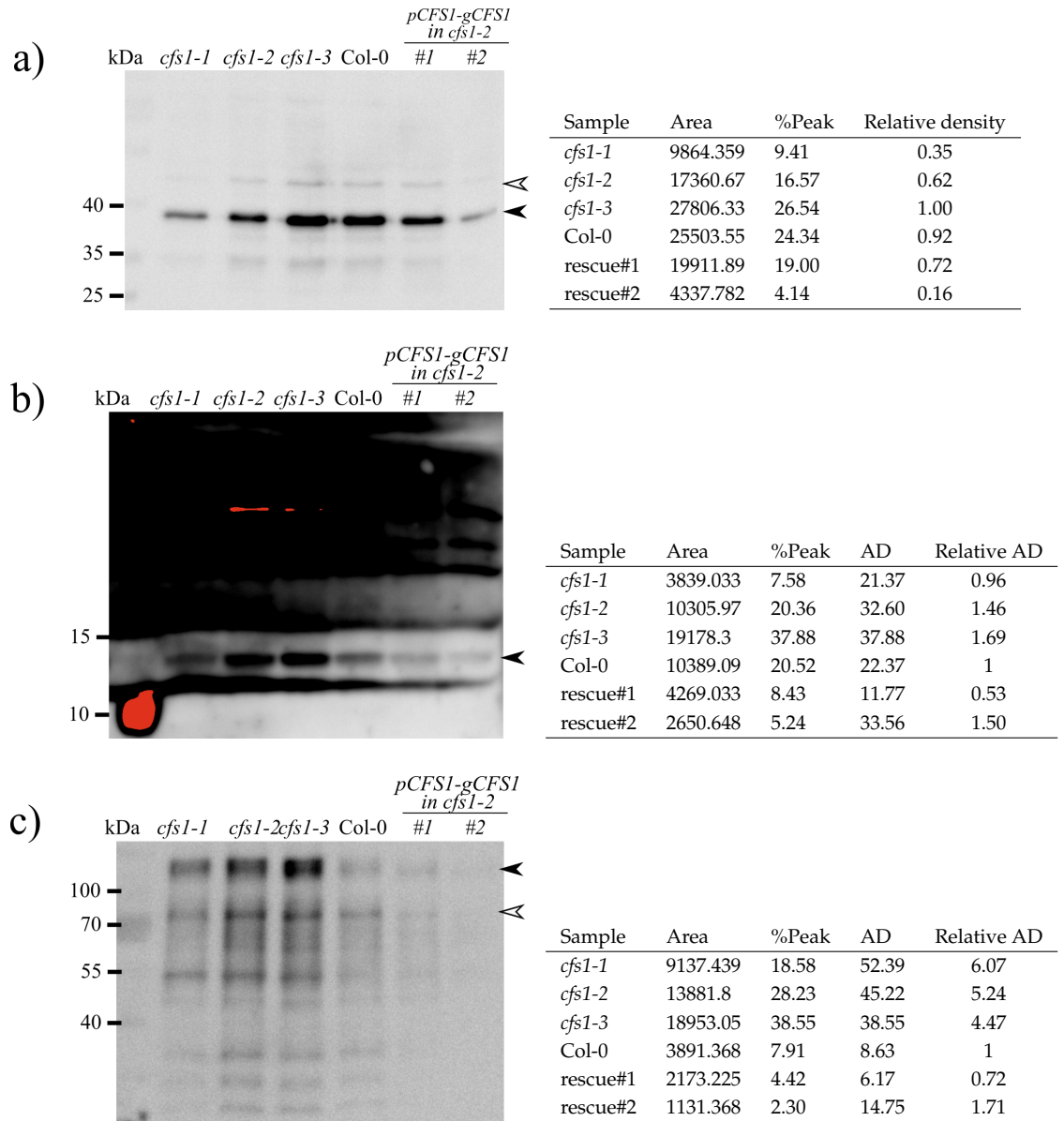| Sample	Area	%Peak	Relative density
Col-0	55441	26.384	1.00
eds1-2	50545.2	24.054	0.91
cfs1-2	51450.9	24.485	0.93
cfs1-2 eds1-2	52697.1	25.078	0.95

b)

Sample	Area	%Peak	AD	Relative AD
Col-0	19587.7	11.332	11.33	1
eds1-2	34979.6	20.236	22.20	1.96
cfs1-2	56667.1	32.783	35.33	3.12
cfs1-2 eds1-2	61621.7	35.649	37.51	3.31

c)

Sample	Area	%Peak	AD	Relative AD
Col-0	37496.3	22.065	22.07	1.
eds1-2	39121.2	23.021	25.25	1.14
cfs1-2	42913.3	25.253	27.21	1.23
cfs1-2 eds1-2	50404.3	29.661	31.21	1.41

Figure J.18: **Accumulation of autophagosomes in *cfs1-2* and *cfs1-2 eds1-2*: the third biological replicates** - Crude extract was probed with **a)** anti-cFBPase, **b)** anti-ATG8a and **c)** anti-NBR1. Arrowhead denotes expected protein size. Filled arrowhead indicates bands used for intensity calculation.
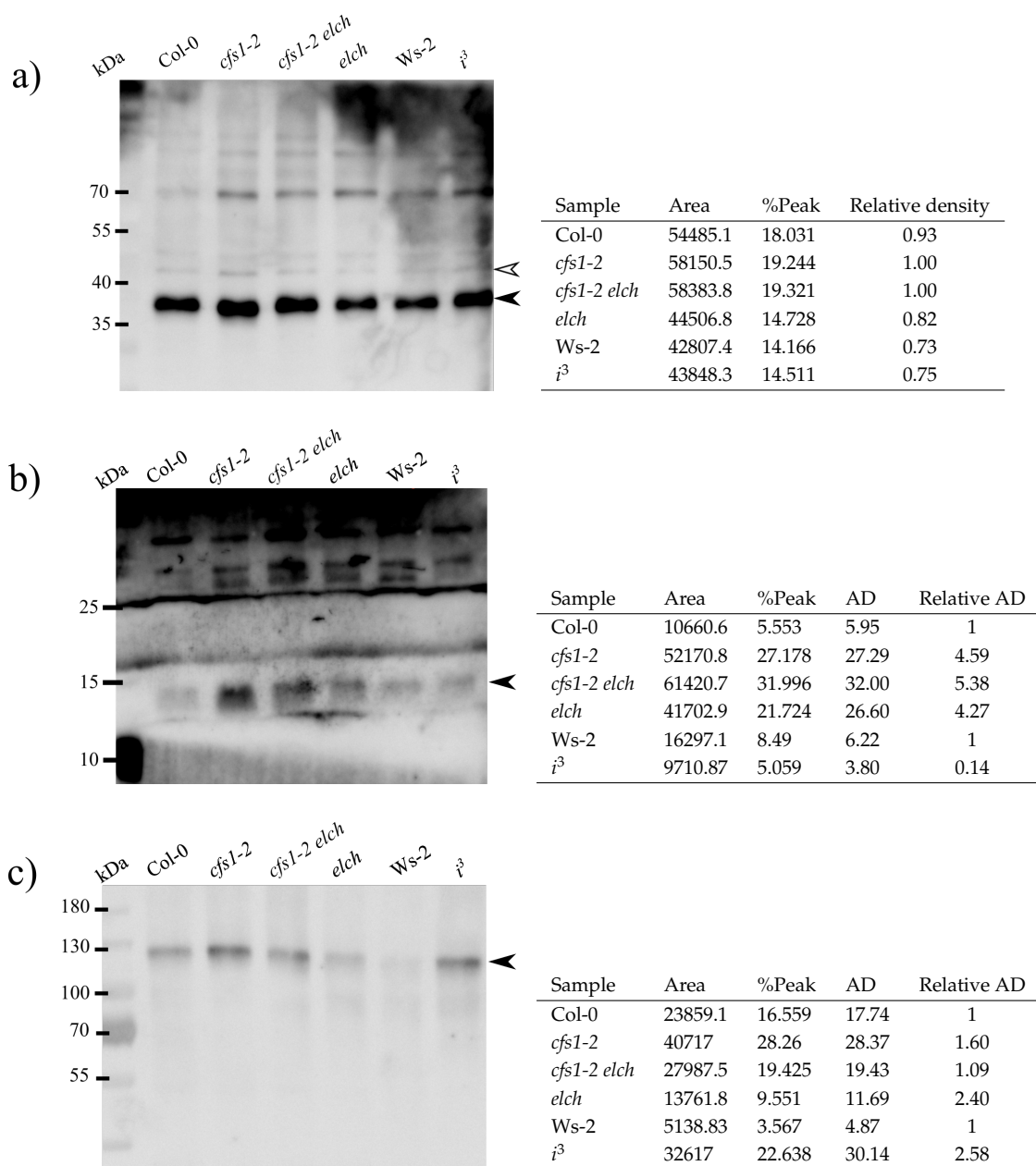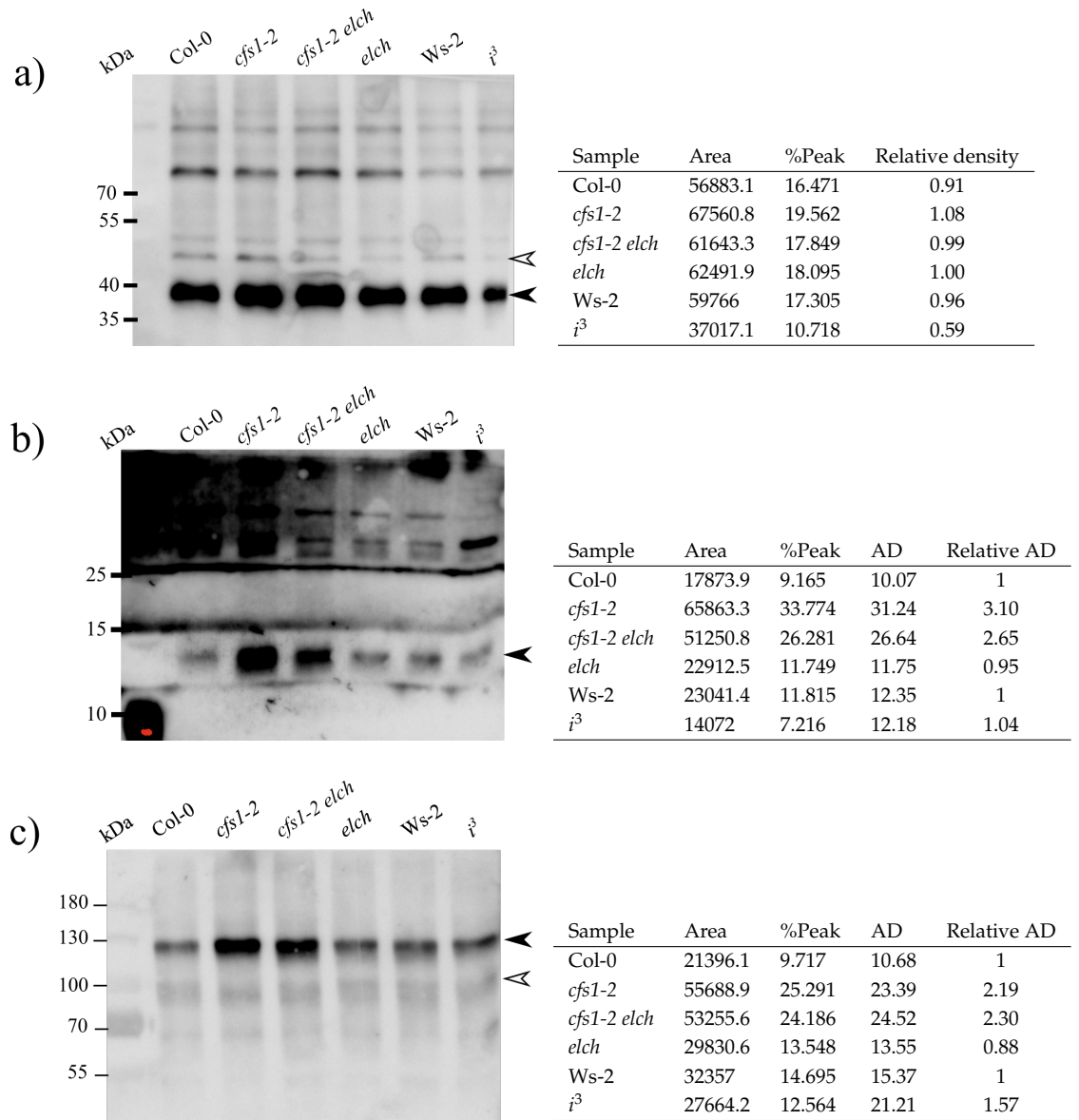
a)

Sample	Area	%Peak	Relative density
Col-0	43292.7	23.829	0.88
eds1-2	41683.7	22.943	0.85
cfs1-2	48972.2	26.955	1.00
cfs1-2 eds1-2	47732.2	26.273	0.97

b)

Sample	Area	%Peak	AD	Relative AD
Col-0	32511.8	14.511	16.41	1
eds1-2	33580.9	14.988	17.61	1.07
cfs1-2	86494.4	38.606	38.61	2.35
cfs1-2 eds1-2	71458.3	31.895	32.72	1.99

c)

Sample	Area	%Peak	AD	Relative AD
Col-0	37496.3	22.065	24.96	1
eds1-2	39121.2	23.021	27.05	1.08
cfs1-2	42913.3	25.253	25.25	1.01
cfs1-2 eds1-2	50404.3	29.661	30.43	1.22
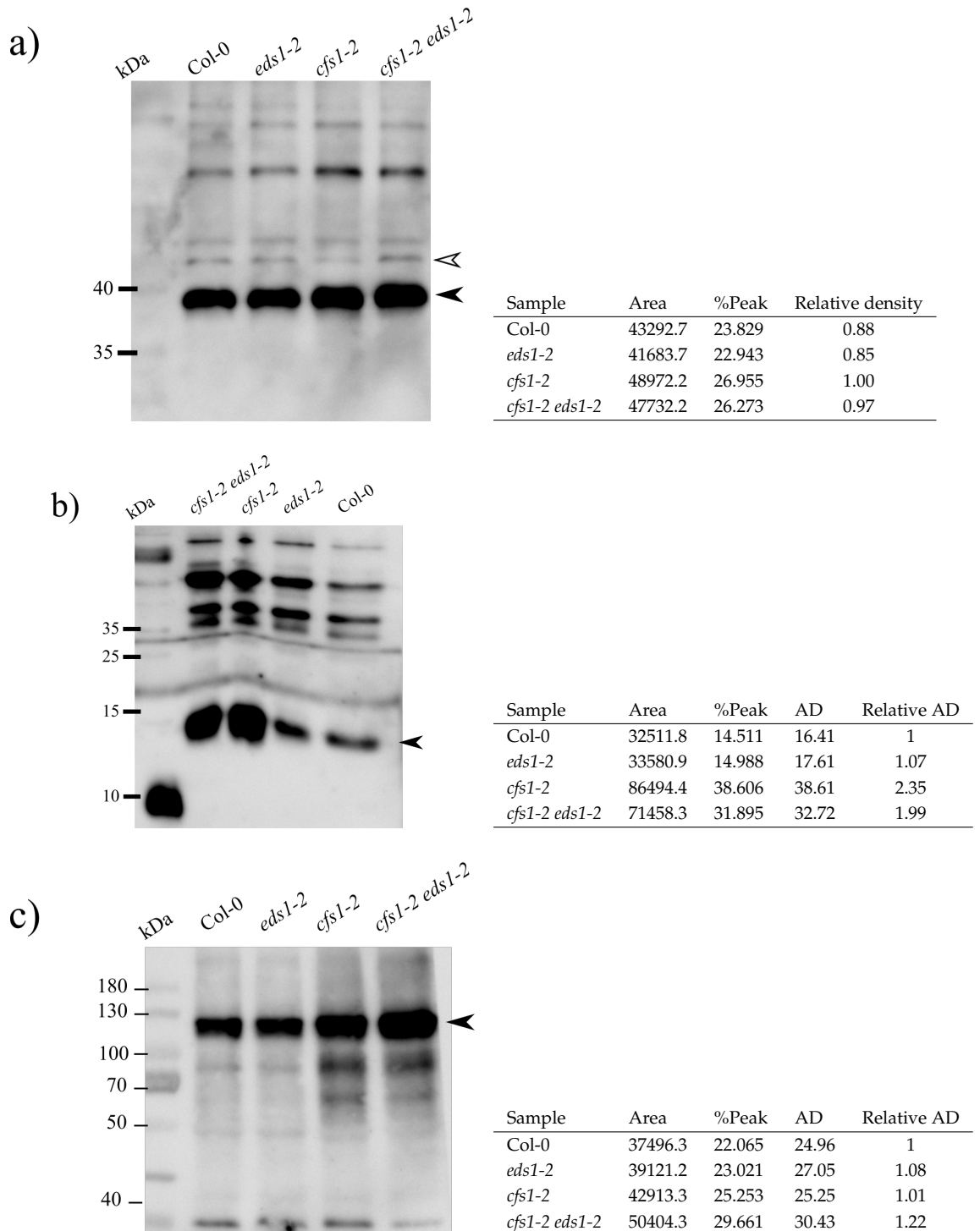
Figure J.19: **Accumulation of autophagosomes in *cfs1-2* and *cfs1-2 eds1-2*: the fourth biological replicates** - Crude extract was probed with **a)** anti-cFBPase, **b)** anti-ATG8a and **c)** anti-NBR1. Arrowhead denotes expected protein size. Filled arrowhead indicates bands used for intensity calculation.
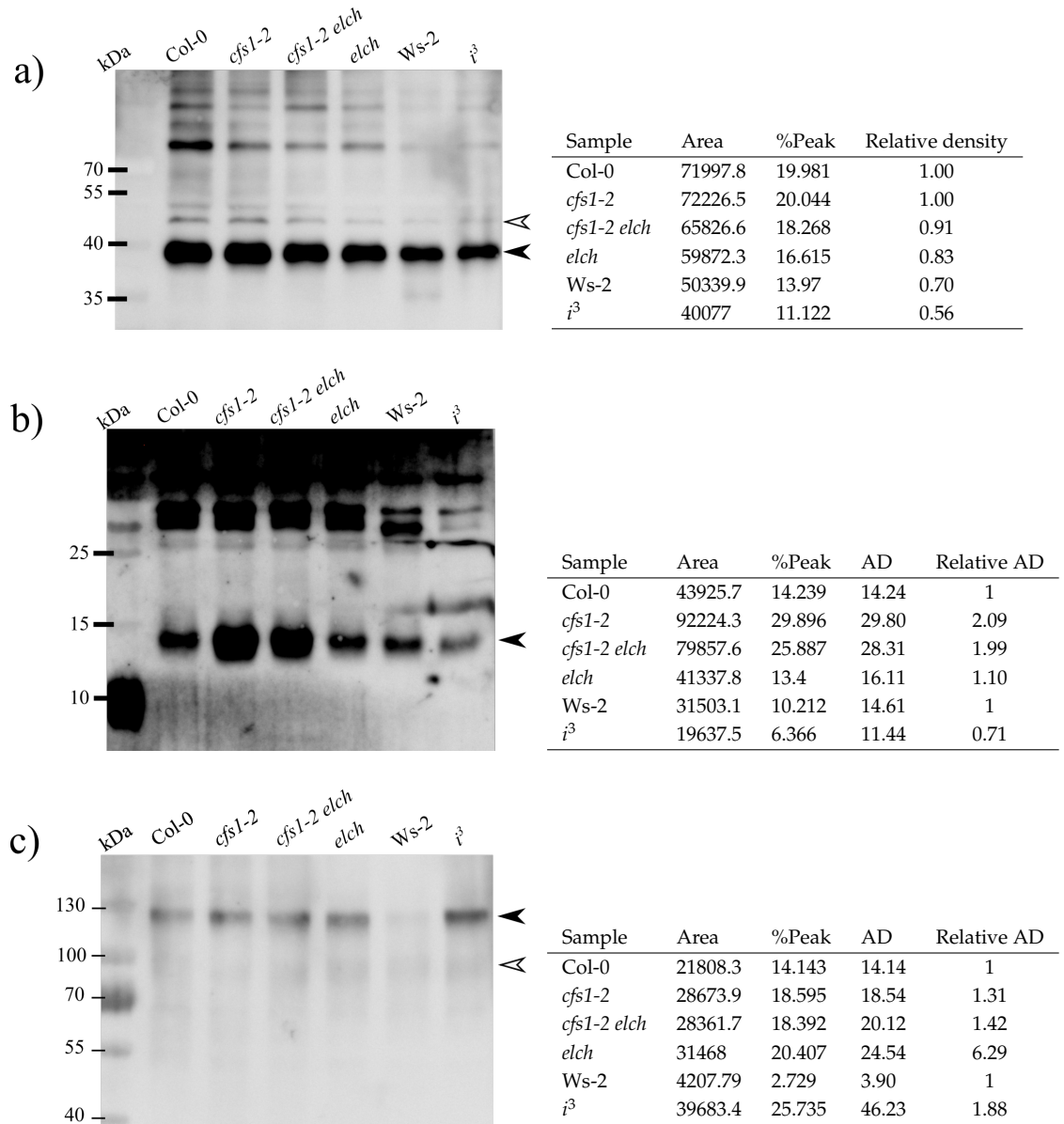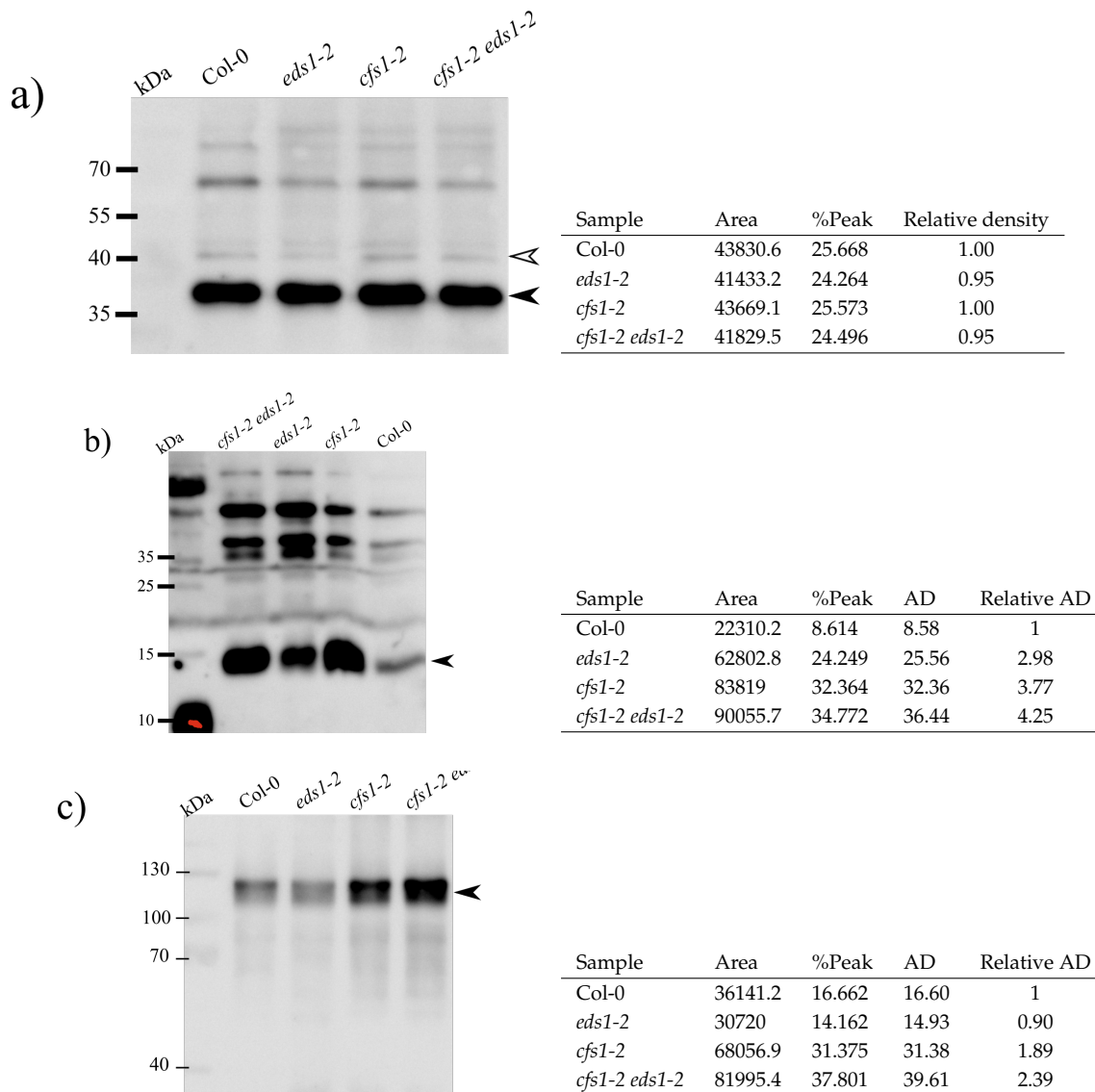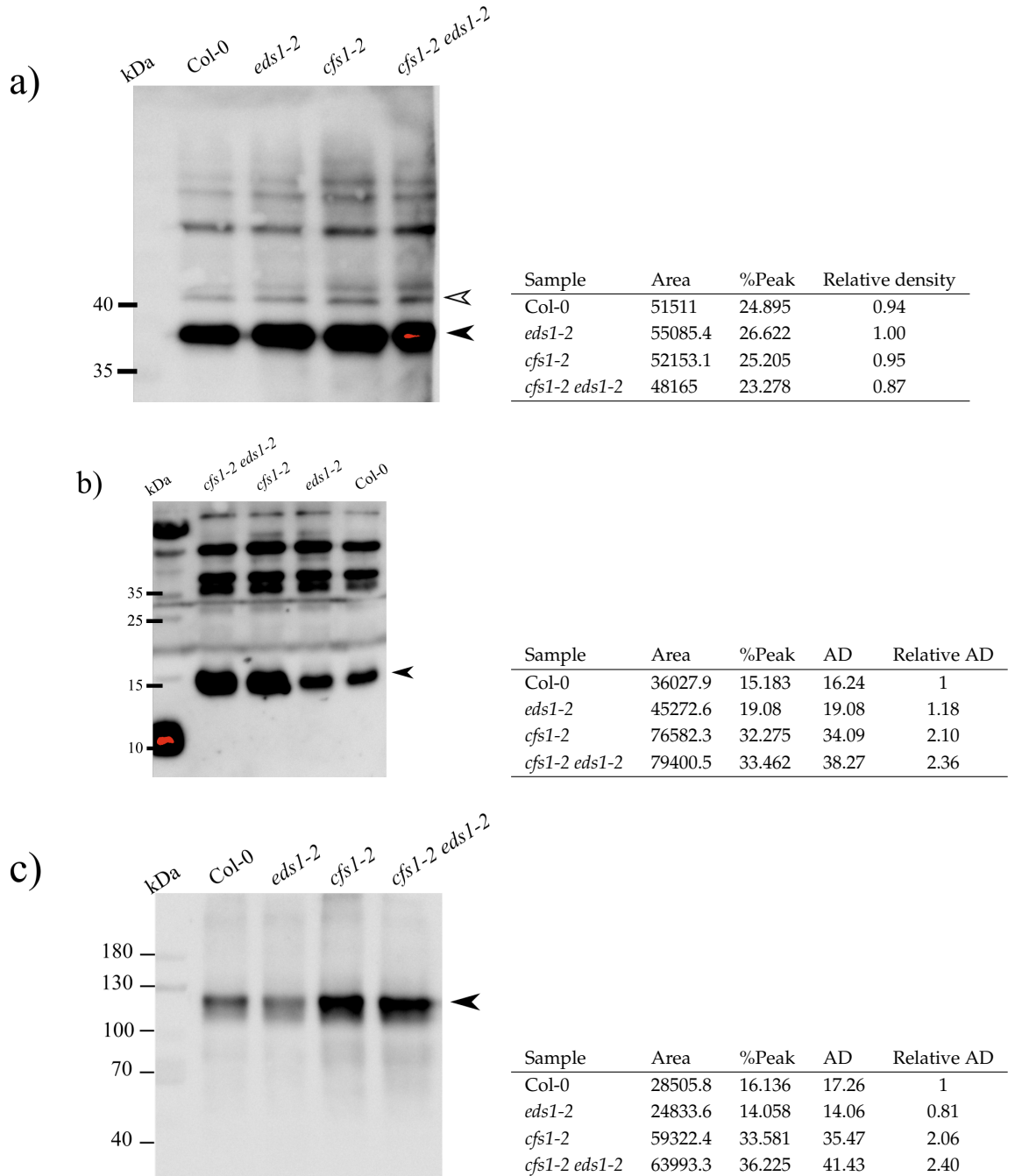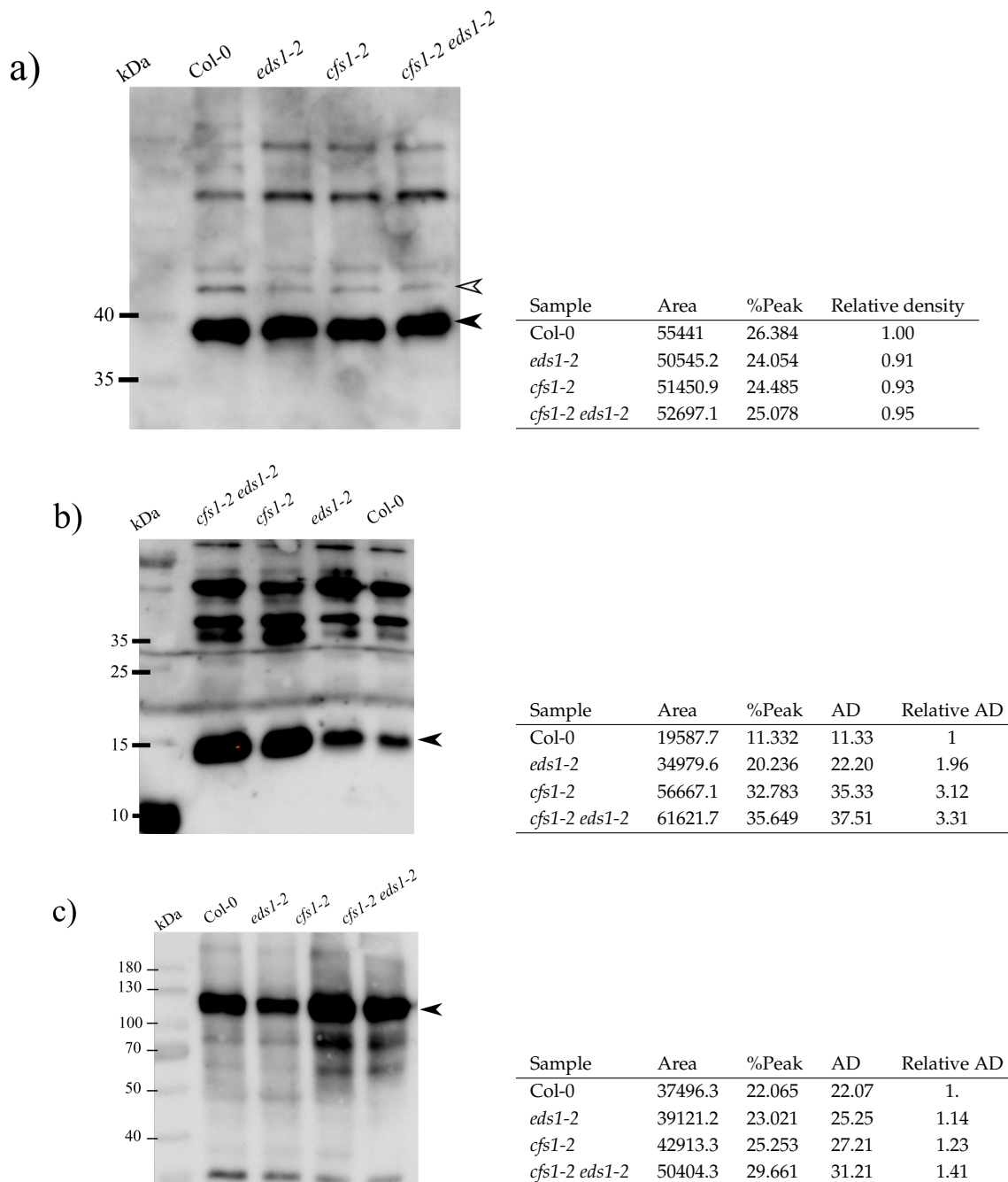
Appendix K Analysis of *ATG8* genes and *NBR1* transcripts

Ct values from each technical and biological replicates are listed in Table K.1.

Appendix K.1: Ct values of *EFα1*, *ATG8* and *NBR1* transcripts

Replication		Target	Samples			
biological	technical		cfs1-3	Col-0	cfs1-2	water
1	1	*EFalpha1*	20.231	19.91	19.44	NA
1	2	*EFalpha1*	20.216	19.981	19.436	NA
1	1	*ATG8a*	22.536	23.159	23.347	NA
1	2	*ATG8a*	22.367	23.001	22.225	33.904
1	1	*ATG8b*	23.939	23.806	23.644	NA
1	2	*ATG8b*	23.976	23.739	23.659	NA
1	1	*ATG8c*	23.774	23.555	23.187	NA
1	2	*ATG8c*	23.681	23.584	23.16	NA
2	1	*ATG8a*	22.326	23.009	22.182	NA
2	2	*EFalpha1*	19.116	19.723	19.331	NA
2	2	*ATG8a*	21.883	23.059	22.063	NA
2	1	*EFalpha1*	19.085	19.936	19.304	30.189
2	1	*ATG8b*	23.87	23.712	23.529	NA
2	2	*ATG8*b	23.666	23.551	23.036	NA
2	1	*ATG8c*	23.051	23.629	23.017	NA
2	2	*ATG8c*	23.119	23.676	23.072	NA
3	1	*ATG8a*	23.573	22.447	22.138	NA
3	2	*ATG8a*	23.567	22.645	21.693	NA
3	1	*ATG8b*	24.539	23.481	23.41	NA
3	2	*ATG8b*	24.465	23.108	23.024	NA
3	1	*ATG8c*	24.266	23.225	23.181	NA
3	2	*ATG8c*	24.555	23.358	23.088	NA
3	1	*EFalpha1*	21.211	19.241	19.337	NA
3	2	*EFalpha1*	21.098	19.199	19.219	32.679
1	1	*ATG8e*	23.0527	24.203	24.4757	NA

Continued on next page

Appendix K.1: Ct values of *ATG8* genes and *NBR1* transcripts *–continued from previous page*

Replication		Target	Samples			
biological	technical		*cfs1-3*	Col-0	*cfs1-2*	water
1	2	*ATG8e*	23.2513	23.3684	24.4425	38.2188
1	3	*ATG8e*	23.2665	22.5278	24.3423	34.9291
1	1	*ATG8f*	22.1954	23.8134	23.5868	NA
1	2	*ATG8f*	22.0132	22.6754	23.4741	NA
1	3	*ATG8f*	22.4408	21.7444	23.4405	NA
1	1	*ATG8g*	26.9099	NA	28.7098	NA
1	2	*ATG8g*	28.7001	27.2841	27.134	NA
1	3	*ATG8g*	27.0285	26.3096	27.8434	NA
1	1	*ATG8h*	26.2864	26.4601	26.5358	NA
1	2	*ATG8h*	25.9632	25.2746	26.5544	NA
1	3	*ATG8h*	26.0016	24.8755	26.4914	NA
1	1	*ATG8i*	22.7353	24.3693	23.8491	NA
1	2	*ATG8i*	22.8391	23.2206	23.4964	NA
1	3	*ATG8i*	22.7984	23.1924	23.6987	NA
1	1	*EFalpha1*	20.0793	21.2823	20.6891	NA
1	2	*EFalpha1*	19.3508	20.6404	22.0788	NA
1	3	*EFalpha1*	19.2878	19.7239	20.3502	NA
1	1	*NBR1*	20.0009	21.4	21.2178	NA
1	2	*NBR1*	19.5178	21.3115	21.2632	31.1971
1	3	*NBR1*	20.0963	19.563	22.0233	NA
2	1	*ATG8e*	22.1831	22.7255	23.1337	35.0516
2	2	*ATG8e*	22.0992	22.5457	22.7287	35.2031
2	3	*ATG8*e	21.875	22.6247	23.1182	39.9897
2	1	*ATG8f*	21.943	21.6765	22.9157	NA
2	2	*ATG8f*	21.9885	21.975	22.3119	NA
2	3	*ATG8f*	22.0903	21.9526	22.4898	NA
2	1	*ATG8g*	26.1112	26.9017	27.6924	NA
2	2	*ATG8g*	26.1651	26.0184	27.3153	NA
2	3	*ATG8g*	26.5068	26.5355	27.3728	NA

Continued on next page

Appendix K.1: Ct values of *ATG8* genes and *NBR1* transcripts –*continued from previous page*

| Replication | | Target | Samples | | | |
biological	technical		*cfs1-3*	Col-0	*cfs1-2*	water
2	1	*ATG8*h	25.2115	25.4319	26.3755	NA
2	2	*ATG8h*	24.926	26.3949	26.1317	NA
2	3	*ATG8h*	25.3709	25.6541	26.1477	NA
2	1	*ATG8i*	22.3961	22.7605	23.0552	NA
2	2	*ATG8i*	22.4567	22.4152	23.3955	NA
2	3	*ATG8i*	22.2593	22.6049	23.2128	NA
2	1	*EFalpha1*	19.7775	19.7331	19.8446	35.771
2	2	*EFalpha1*	19.1159	20.0141	19.6151	37.3649
2	3	*EFalpha1*	19.242	18.5658	19.9917	NA
2	1	*NBR1*	19.6409	19.7376	20.6459	NA
2	2	*NBR1*	20.0556	19.4463	20.7591	32.967
2	3	*NBR1*	19.3492	20.1551	21.0471	NA
3	1	*ATG8e*	21.8051	23.3547	22.3292	37.2633
3	2	*ATG8e*	21.5194	23.0481	22.2287	39.3599
3	3	*ATG8e*	21.9835	23.2505	22.4528	NA
3	1	*ATG8f*	21.4275	22.9242	21.5239	NA
3	2	*ATG8f*	21.9246	23.1596	21.7858	NA
3	3	*ATG8f*	21.8105	23.0142	21.7949	NA
3	1	*ATG8g*	25.4308	26.3155	25.491	NA
3	2	*ATG8g*	25.474	27.3102	26.2934	NA
3	3	*ATG8g*	26.0749	27.0789	26.3211	NA
3	1	*ATG8h*	24.1947	26.5988	26.1517	NA
3	2	*ATG8h*	24.1138	26.7991	26.0693	NA
3	3	*ATG8h*	24.138	26.9758	26.1907	NA
3	1	*ATG8i*	22.0733	23.2695	22.327	38.702
3	2	*ATG8i*	22.0672	23.2651	22.4367	38.3469
3	3	*ATG8i*	21.9687	23.1862	22.3388	NA
3	1	*EFalpha1*	19.2975	20.7927	18.7061	NA
3	2	*EFalpha1*	19.0026	20.4141	18.6272	NA

Continued on next page

Appendix K.1: Ct values of *ATG8* genes and *NBR1* transcripts *–continued from previous page*

Replication		Target	Samples			
biological	technical		*cfs1-3*	**Col-0**	*cfs1-2*	**water**
3	3	*EFalpha1*	20.0214	21.1516	19.0792	NA
3	1	*NBR1*	19.1534	19.9541	19.7203	35.627
3	2	*NBR1*	19.3524	20.2245	19.7769	32.6475
3	3	*NBR1*	19.0096	19.8826	19.6051	NA

NA: undetected

All statistical analyses were performed using the functions described in Appendices C and E. ΔC_t values were subjected to statistical test as follows:

For *ATG8a*:

Shapiro-Wilk normality test: normality accepted

(W = 0.9243, p-value = 0.429)

ANOVA:

	Df	Sum Sq	Mean Sq	F Value	Pr($>$ *F*)
genotype	2	0.6824	0.3412	3.28	0.109
Residuals	6	0.6226	0.1038		

Signif. codes: 0 *** 0.001 ** 0.01 * 0.05 . 0.1 1

For *ATG8b*:

Shapiro-Wilk normality test: normality accepted

(W = 0.95469, p-value = 0.7415)

ANOVA:

	Df	Sum Sq	Mean Sq	F Value	Pr($>$ *F*)
genotype	2	0.0344	0.01718	0.102	0.905
Residuals	6	1.0124	0.16873		

Signif. codes: 0 *** 0.001 ** 0.01 * 0.05 . 0.1 1

For *ATG8c*:

Shapiro-Wilk normality test: normality accepted

(W = 0.96863, p-value = 0.8828)

ANOVA:

	Df	Sum Sq	Mean Sq	F Value	Pr(> F)
genotype	2	0.1077	0.05383	0.838	0.478
Residuals	6	0.3854	0.06423		

—

Signif. codes: 0 *** 0.001 ** 0.01 * 0.05 . 0.1 1

For *ATG8e*:

Shapiro-Wilk normality test: normality accepted

(W = 0.93221, p-value = 0.5026)

ANOVA:

	Df	Sum Sq	Mean Sq	F Value	Pr(> F)
genotype	2	0.5447	0.2723	1.313	0.337
Residuals	6	1.2449	0.2075		

—

Signif. codes: 0 *** 0.001 ** 0.01 * 0.05 . 0.1 1

For *ATG8f*:

Shapiro-Wilk normality test: normality accepted

(W = 0.94884, p-value = 0.6773)

ANOVA:

	Df	Sum Sq	Mean Sq	F Value	Pr(> F)	
genotype	2	0.2576	0.12881	3.61	0.0935	.
Residuals	6	0.2141	0.03569			

—

Signif. codes: 0 *** 0.001 ** 0.01 * 0.05 . 0.1 1

For *ATG8g*:

Shapiro-Wilk normality test: normality accepted

(W = 0.93621, p-value = 0.5426)

ANOVA:

	Df	Sum Sq	Mean Sq	F Value	Pr(> F)
genotype	2	0.9533	0.4767	1.198	0.365
Residuals	6	2.3872	0.3979		

—

Signif. codes: 0 *** 0.001 ** 0.01 * 0.05 . 0.1 1

For *ATG8h*:

Shapiro-Wilk normality test: normality accepted

(W = 0.97212, p-value = 0.9123)

ANOVA:

	Df	Sum Sq	Mean Sq	F Value	Pr($> F$)
genotype	2	0.935	0.4675	0.638	0.561
Residuals	6	4.398	0.7330		

—

Signif. codes: 0 *** 0.001 ** 0.01 * 0.05 . 0.1   1

For *ATG8i*:

Shapiro-Wilk normality test: normality accepted

(W = 0.95457, p-value = 0.7401)

ANOVA:

	Df	Sum Sq	Mean Sq	F Value	Pr($> F$)
genotype	2	0.1753	0.08767	0.543	0.607
Residuals	6	0.9682	0.16136		

—

Signif. codes: 0 *** 0.001 ** 0.01 * 0.05 . 0.1   1

For *NBR1*:

Shapiro-Wilk normality test: normality accepted

(W = 0.92699, p-value = 0.4532)

ANOVA:

	Df	Sum Sq	Mean Sq	F Value	Pr($> F$)
genotype	2	1.225	0.6124	3.306	0.108
Residuals	6	1.111	0.1852		

—

Signif. codes: 0 *** 0.001 ** 0.01 * 0.05 . 0.1   1

Fold change in relative to Col-0 and its corresponding minimum and maximum fold change is listed in Table K.2 .

Appendix K.2: Fold change in expression of *ATG8* genes and *NBR1*

Target	Genotype	Fold change		
		maximum	average	minimum
ATG8a	*cfs1-2*	0.867	1.224	1.728
ATG8a	*cfs1-3*	1.388	1.594	1.830
ATG8a	Col-0	0.907	1.000	1.102
ATG8b	*cfs1-2*	0.759	0.909	1.089
ATG8b	*cfs1-3*	0.922	0.990	1.062
ATG8b	Col-0	0.875	1.000	1.143
ATG8c	*cfs1-2*	1.000	1.047	1.097
ATG8c	*cfs1-3*	1.088	1.196	1.314
ATG8c	Col-0	0.926	1.000	1.079
ATG8e	*cfs1-2*	1.026	1.404	1.921
ATG8e	*cfs1-3*	0.863	1.463	2.479
ATG8e	Col-0	0.672	1.000	1.488
ATG8f	*cfs1-2*	0.827	1.138	1.567
ATG8f	*cfs1-3*	0.744	1.332	2.385
ATG8f	Col-0	0.665	1.000	1.504
ATG8g	*cfs1-2*	0.691	1.163	1.959
ATG8g	*cfs1-3*	0.978	1.709	2.987
ATG8g	Col-0	0.584	1.000	1.711
ATG8h	*cfs1-2*	1.222	1.667	2.274
ATG8h	*cfs1-3*	0.872	1.530	2.684
ATG8h	Col-0	0.678	1.000	1.474
ATG8i	*cfs1-2*	0.911	1.204	1.591
ATG8i	*cfs1-3*	0.799	1.247	1.944
ATG8i	Col-0	0.675	1.000	1.480
EFalpha1	*cfs1-2*	0.660	1.000	1.514
EFalpha1	*cfs1-3*	0.560	1.000	1.787
EFalpha1	Col-0	0.577	1.000	1.732
NBR1	*cfs1-2*	1.137	1.597	2.242
NBR1	*cfs1-3*	1.032	1.812	3.184

Continued on next page

Appendix K.2: Fold change in expression of *ATG8* genes and *NBR1* –*continued from previous page*

Target	Genotype	Fold change		
		maximum	**average**	**minimum**
NBR1	Col-0	0.651	1.000	1.537

Appendix L   Analysis of ER-stress marker genes

Ct values from each technical and biological replicates are listed in Table L.1.

Appendix L.1: Ct values of *EFα1* and ER-stress marker genes

| Replication | | Target | Samples | | |
biological	technical		*cfs1-3*	Col-0	*cfs1-2*
1	2	*BIP1.1*	24.41	23.492	24.35
1	1	*BIP1.1*	25.259	23.183	25.239
2	2	*BIP1.1*	23.659	24.976	24.284
2	1	*BIP1.1*	24.588	25.469	24.142
3	2	*BIP1.1*	26.555	24.375	24.311
3	1	*BIP1.1*	26.483	24.851	24.609
1	2	*BIP2.1*	23.089	22.28	23.323
1	1	*BIP2.1*	23.213	22.283	23.501
2	2	*BIP2.1*	23.008	23.647	23.632
2	1	*BIP2.1*	23.155	23.802	23.93
3	2	*BIP2.1*	24.045	23.489	23.009
3	1	*BIP2.1*	24.304	23.599	22.882
1	1	*BIP3.1*	32.838	34.151	35.03
1	2	*BIP3.1*	33.089	35.251	37.191
2	1	*BIP3.1*	34.837	40	36.129
2	2	*BIP3.1*	36.58	39.418	37.667
3	1	*BIP3.1*	35.322	36.113	34.208
3	2	*BIP3.1*	38.156	38.378	36.198
1	1	*bZIP60s*	33.626	32.438	32.333
1	2	*bZIP60s*	33.478	31.706	32.475
2	1	*bZIP60s*	33.013	33.332	33.256
2	2	*bZIP60s*	34.142	33.971	32.964
3	1	*bZIP60s*	35.429	33.137	35.042
3	2	*bZIP60s*	33.435	33.257	32.966
1	2	*bZIP60u*	23.151	23.6	22.85
1	1	*bZIP60u*	23.184	23.014	22.411
2	2	*bZIP60u*	23.049	23.241	23.457

Continued on next page

Appendix L.1: Ct values of ER-stress marker gene –*continued from previous page*

Replication		Target	Samples		
biological	technical		*cfs1-3*	Col-0	*cfs1-2*
2	1	*bZIP60u*	23.257	23.511	23.446
3	2	*bZIP60u*	25.435	24.076	25.07
3	1	*bZIP60u*	23.994	23.853	23.572
1	2	*EF1alpha*	20.362	20.105	19.721
1	1	*EF1alpha*	20.689	20.173	19.414
2	2	*EF1alpha*	19.173	20.015	19.383
2	1	*EF1alpha*	19.381	20.032	19.651
3	2	*EF1alpha*	20.519	19.45	19.569
3	1	*EF1alpha*	21.417	19.232	19.234

All statistical analyses were performed using the functions described in Appendices C and E. ΔC_t values were subjected to statistical tests as follows:

For *BIP1.1*:

Shapiro-Wilk normality test: normality accepted

(W = 0.86768, p-value = 0.1161)

ANOVA:

	Df	Sum Sq	Mean Sq	F Value	Pr($>$ *F*)
genotype	2	0.2942	0.1471	0.279	0.766
Residuals	6	3.1602	0.5267		

Signif. codes: 0 *** 0.001 ** 0.01 * 0.05 . 0.1   1

For *BIP2.1*:

Shapiro-Wilk normality test: normality accepted

(W = 0.92881, p-value = 0.4701)

ANOVA:

	Df	Sum Sq	Mean Sq	F Value	Pr($>$ *F*)
genotype	2	0.705	0.3526	0.65	0.555
Residuals	6	3.255	0.5425		

Signif. codes: 0 *** 0.001 ** 0.01 * 0.05 . 0.1   1

For *BIP3.1*:

Shapiro-Wilk normality test: normality accepted

(W = 0.98017, p-value = 0.9652)

ANOVA:

	Df	Sum Sq	Mean Sq	F Value	Pr(> F)
genotype	2	8.166	4.083	1.542	0.288
Residuals	6	15.884	2.647		

Signif. codes: 0 *** 0.001 ** 0.01 * 0.05 . 0.1   1

For *bZIP60s*:

Shapiro-Wilk normality test: normality accepted

(W = 0.94826, p-value = 0.671)

ANOVA:

	Df	Sum Sq	Mean Sq	F Value	Pr(> F)
genotype	2	0.451	0.2257	0.292	0.757
Residuals	6	4.641	0.7735		

Signif. codes: 0 *** 0.001 ** 0.01 * 0.05 . 0.1   1

For *bZIP60u*:

Shapiro-Wilk normality test: normality accepted

(W = 0.92786, p-value = 0.4612)

ANOVA:

	Df	Sum Sq	Mean Sq	F Value	Pr(> F)
genotype	2	0.612	0.3058	0.496	0.632
Residuals	6	3.698	0.6163		

Signif. codes: 0 *** 0.001 ** 0.01 * 0.05 . 0.1   1

Fold change in relative to Col-0 and its corresponding minimum and maximum fold change is listed in Table L.2.

Appendix L.2: Fold change in expression of ER-stress marker genes

Target	Genotype	Fold change		
		maximum	average	minimum
BIP1.1	Col-0	0.809	1.000	1.237
BIP1.1	*cfs1-2*	0.549	0.762	1.057
BIP1.1	*cfs1-3*	0.548	0.772	1.087
BIP2.1	Col-0	0.914	1.000	1.094
BIP2.1	*cfs1-2*	0.58	0.674	0.782
BIP2.1	*cfs1-3*	0.829	1.032	1.284
BIP3.1	Col-0	0.441	1.000	2.266
BIP3.1	*cfs1-2*	0.769	1.564	3.182
BIP3.1	*cfs1-3*	2.133	4.805	10.824
bZIP60s	Col-0	0.738	1.000	1.356
bZIP60s	*cfs1-2*	0.418	0.685	1.122
bZIP60s	*cfs1-3*	0.482	0.856	1.52
bZIP60u	Col-0	0.78	1.000	1.282
bZIP60u	*cfs1-2*	0.624	0.900	1.298
bZIP60u	*cfs1-3*	0.853	1.377	2.222
EF1alpha	Col-0	0.935	1.000	1.069
EF1alpha	*cfs1-2*	0.852	1.000	1.173
EF1alpha	*cfs1-3*	0.746	1.000	1.34

Appendix M Analysis of YPF-ATG8a punctate structure

All Z-slices of the image were combined to generate image showing maximum projection. Images were manually thresholded and then subjected to particle analysis function. Result of the analysis of an individual sample is displayed in Table M.1 and M.2. The number of YFP-ATG8a punctate structure (Count) were used for subsequent statistical analysis.

To test for significant difference between two groups, the data tested for normality using Shapiro-Wilk's test for normality (W = 0.76276, p-value = 6.889e-09). As normality was rejected, Wilcoxon rank sum test with continuity correction was applied (W = 265, p-value = 0.0005894).

Appendix M.1: Particle analysis of YFP-ATG8a transiently expressed in Col-0

Slice	Count	Total Area	Average Size	%Area
MAX_YFP-ATG8a in Col.lif - Series030 - C=1	5	0.433	0.087	0.003
MAX_YFP-ATG8a in Col.lif - Series025 - C=1	14	10.497	0.75	0.053
MAX_YFP-ATG8a in Col.lif - Series020 - C=1	24	4.718	0.197	0.088
MAX_YFP-ATG8a in Col.lif - Series018 - C=1	93	16.221	0.174	0.161
MAX_YFP-ATG8a in Col.lif - Series009 - C=2	18	0.71	0.039	0.007
MAX_YFP-ATG8a in Col.lif - Series010 - C=1	17	0.257	0.015	0.003
MAX_YFP-ATG8a in Col.lif - Series041 - C=1	20	8.358	0.418	0.04
MAX_YFP-ATG8a in Col.lif - Series039 - C=1	11	9.263	0.842	0.053
MAX_YFP-ATG8a in Col.lif - Series036 - C=1	60	153.517	2.559	0.049
MAX_YFP-ATG8a in Col.lif - Series034 - C=1	22	9.43	0.429	0.052
MAX_YFP-ATG8a in Col.lif - Series032 - C=1	11	6.316	0.574	0.048
MAX_YFP-ATG8a in Col.lif - Series045 - C=1	37	12.052	0.326	0.091
MAX_YFP-ATG8a in Col.lif - Series043 - C=1	20	1.501	0.075	0.012
MAX_YFP-ATG8Col1.lif - Series009 - C=0	7	0.819	0.117	0.007
MAX_YFP-ATG8Col1.lif - Series006 - C=0	11	0.431	0.039	0.012
MAX_YFP-ATG8Col1.lif - Series004 - C=0	6	9.192	1.532	0.035
MAX_YFP-ATG8Col1.lif - Series002 - C=0	6	0.092	0.015	7.63E-04
MAX_YFP-ATG8Col1.lif - Series019 - C=0	3	0.014	0.005	2.86E-04
MAX_YFP-ATG8Col1.lif - Series017 - C=0	27	2.725	0.101	0.071
MAX_YFP-ATG8Col1.lif - Series014 - C=0	18	12.844	0.714	0.09
MAX_YFP-ATG8Col1.lif - Series002 - C=0	4	0.069	0.017	5.72E-04
MAX_YFP-ATG8Col2.lif - Series013 - C=0	0	0	NaN	0
MAX_YFP-ATG8Col2.lif - Series011 - C=0	8	4.252	0.532	0.011
MAX_YFP-ATG8Col2.lif - Series005 - C=0	0	0	NaN	0
MAX_YFP-ATG8Col2.lif - Series003 - C=0	39	0.392	0.01	0.006
MAX_YFP-ATG8Col2.lif - Series001 - C=0	6	2.742	0.457	0.018
MAX_YFP-ATG8Col2.lif - Series028 - C=0	2	3.334	1.667	0.01
MAX_YFP-ATG8Col2.lif - Series023 - C=0	1	0.011	0.011	9.54E-05
MAX_YFP-ATG8Col2.lif - Series020 - C=0	9	1.468	0.163	0.017
MAX_YFP-ATG8Col2.lif - Series017 - C=0	0	0	NaN	0
MAX_YFP-ATG8Col2.lif - Series015 - C=0	3	1.062	0.354	0.002

NaN : no calculation possible (YFP signal was cytoplasmic).

Summary of descriptive statistics: $n=31$; $\bar{x} \pm sd = 16.1936 \pm 19.5455$, $min = 0$; $Q_1 = 4.5$; $median = 11$; $Q_3 = 20$; $max = 93$

Appendix M.2: Particle analysis of YFP-ATG8a transiently expressed in *cfs1-2*

Slice	Count	Total Area	Average Size	%Area
MAX_YFP-ATG82-2_1.lif - C=0	9	0.643	0.071	0.013
MAX_YFP-ATG82-2_2.lif - Series011 - C=0	36	61.448	1.707	0.02
MAX_YFP-ATG82-2_2.lif - Series009 - C=0	17	12.333	0.725	1.60E-02
MAX_YFP-ATG82-2_2.lif - Series007 - C=0	8	4.341	0.543	0.054
MAX_Atg8 in 2-2.lif - Series022 - C=0	24	7.043	0.293	0.05
MAX_Atg8 in 2-2.lif - Series018 - C=0	43	5.576	0.13	0.036
MAX_Atg8 in 2-2.lif - Series012 - C=0	40	36.23	0.906	0.101
MAX_Atg8 in 2-2.lif - Series008 - C=0	9	5.914	0.657	0.008
MAX_Atg8 in 2-2.lif - Series005 - C=0	12	19.617	1.635	0.006
MAX_Atg8 in 2-2.lif - Series060 - C=0	19	2.687	0.141	2.00E-02
MAX_Atg8 in 2-2.lif - Series057 - C=0	120	31.445	0.262	0.282
MAX_Atg8 in 2-2.lif - Series055 - C=0	29	7.947	0.274	0.055
MAX_Atg8 in 2-2.lif - Series046 - C=0	7	1.89	0.27	0.005
MAX_Atg8 in 2-2.lif - Series042 - C=0	26	25.315	0.974	0.033
MAX_Atg8 in 2-2.lif - Series040 - C=0	13	7.919	0.609	0.029
MAX_Atg8 in 2-2.lif - Series037 - C=0	6	4.722	0.787	0.014
MAX_Atg8 in 2-2.lif - Series035 - C=0	13	1.824	0.14	0.012
MAX_Atg8 in 2-2.lif - Series033 - C=0	13	2.03	0.156	0.015
MAX_Atg8 in 2-2.lif - Series031 - C=0	11	3.617	0.329	0.02
MAX_Atg8 in 2-2.lif - Series026 - C=0	53	9.232	0.174	0.049
MAX_Atg8 in 2-2.lif - Series005 - C=0	33	90.873	2.754	0.03
MAX_YFP-ATG8a in 2-2.lif - Series014 - C=1	43	10.456	0.243	0.055
MAX_YFP-ATG8a in 2-2.lif - Series012 - C=1	59	1.246	0.021	0.013
MAX_YFP-ATG8a in 2-2.lif - Series010 - C=1	132	9.026	0.068	0.071
MAX_YFP-ATG8a in 2-2.lif - Series008 - C=1	77	30.78	0.4	0.134
MAX_YFP-ATG8a in 2-2.lif - Series003 - C=1	1	0.01	0.01	9.54E-05
MAX_YFP-ATG8a in 2-2.lif - Series024 - C=1	53	8.967	0.169	0.055
MAX_YFP-ATG8a in 2-2.lif - Series022 - C=1	9	44.96	4.996	0.081
MAX_YFP-ATG8a in 2-2.lif - Series020 - C=1	63	11.511	0.183	0.041
MAX_YFP-ATG8a in 2-2.lif - Series018 - C=1	96	47.268	0.492	0.156
MAX_YFP-ATG8a in 2-2.lif - Series016 - C=1	157	25.748	0.164	0.247
MAX_YFP-ATG8a in 2-2.lif - Series034 - C=1	46	2.06	0.045	0.027
MAX_YFP-ATG8a in 2-2.lif - Series032 - C=1	28	7.48	0.267	0.064
MAX_YFP-ATG8a in 2-2.lif - Series029 - C=1	53	26.449	0.499	0.087

Summary of descriptive statistics: *n=34*; $\overline{x} \pm sd = 39.9412 \pm 38.037$; *min* = 1; $Q_1 = 12.25$; *median* = 28.5; $Q_3 = 53$; *max* = 157

Erklärung

Ich versichere, dass ich die von mir vorgelegte Dissertation selbständig angefertigt, die benutzten Quellen und Hilfsmittel vollständig angegeben und die Stellen der Arbeit einschlielich Tabellen, Karten und Abbildungen , die anderen Werken im Wortlaut oder dem Sinn nach entnommen sind, in jedem Einzelfall als Entlehnung kenntlich gemacht habe; dass diese Dissertation noch keiner anderen Fakultät oder Universität zur Prüfung vorgelegen hat; dass sie abgesehen von unten angegebenen Teilpublikationen noch nicht veröfentlicht worden ist, sowie, dass ich eine solche Veröffentlichung vor Abschluss des Promotionsverfahrens nicht vornehmen werde. Die Bestimmungen der Promotionsordnung sind mir bekannt. Die von mir vorgelegte Dissertation ist von Prof. Dr. Martin Hülskamp betreut worden.

Köln, den 15 October 2015

Lebenslauf

Persönliche Daten

Name:	Sutipatanasomboon
Vorname:	Arpaporn
Geburtsdatum:	25 Januar 1988
Geburtsort:	Bangkok
Staatsangehörigkeit:	Thailand
E-mail:	asutipat@smail.uni-koeln.de

Ausbildung

Studienverlauf

seit Oktober 2012   Promotionstudium am Botanisches Institut III

Universität zu Köln

Oktober 2010 - September 2012   Master of Science (Biological Sciences)

Universität zu Köln

Juni 2006 - März 2010   Bachelor of Science (Plant Sciences)

with *First Class Honors*

Mahidol University, Thailand

Schulbildung

Juni 2000 - März 2006   Sekundarstufe I und II

Bodindecha (Sing Singhaseni) School

Juni 1994 - März 2000   Grundschule

Anubanphibunwes School